



The University of
Nottingham

UNITED KINGDOM · CHINA · MALAYSIA

Faculty of Engineering – Civil Engineering

Effect of air voids on pavement thermal properties

By

Abdushafi Alhashmi Hassn

Thesis submitted to the University of Nottingham

for the degree of Doctor of Philosophy

October 2017

ABSTRACT

Harvesting Energy stands as one of the most promising techniques for approaching the global energy problem without depleting natural resources. Pavement solar energy harvesting (PSEH) technology is one of these techniques and it is considered as a new research area and currently under development which aims to enhance pavements for capture, and storage of thermal energy.

To advance the study of PSEH, a study was made of the influence of moisture inside asphalt on its energy transport and storage abilities. Measurements of almost all the key thermal properties of asphalt are reported for a range of mixtures with various air void contents ranging from 4.5% to 30%.

On the basis of this study it is concluded that, under dry conditions, asphalt mixtures with low air voids content have higher thermo-physical properties (i.e. density, thermal conductivity, specific heat capacity, thermal diffusivity and thermal effusivity) than asphalt mixtures with higher air voids content. Therefore, heating and cooling rates of dense asphalt mixtures were higher than those from porous asphalt mixtures. The total amount of energy accumulated in asphalt mixtures with different air voids content, but with the same constitutive materials, during heating and cooling depends only on the density of the mixtures. In addition, results indicate that asphalt mixtures with high air voids content accumulate less energy than asphalt mixtures with lower air voids content. It is concluded that mixtures with high air voids content are recommended to alleviate the urban heat island effect while mixtures with low air voids content are recommended for harvesting solar heat from pavements.

It is concluded that under wet conditions, a relationship exists between the evaporation rate, the heat flux, and the surface temperature during water evaporation. In addition, the evaporation rate has been related to air voids parameters such as air voids content and diameter, tortuosity, or the Euler number.

The study also investigated the feasibility of harvesting heat from asphalt concrete mixtures by Thermoelectric Power Generators (TEG) and how the air voids content can affect the recovery of this heat. It was found that increasing and/or maintaining the temperature difference between the hot side and cold side of a TEG is considered to be the most important factor in energy recovery application from asphalt pavement. It is concluded that maintaining the temperature gradient between the asphalt pavement and the subgrade could provide a potential of converting heat energy to electrical energy through the use of Thermoelectric Power generators

PUBLICATIONS

These are a list of the papers that have been published by the author during the research period of time:

- **Hassn, A.**, Chiarelli, A., Dawson, A. and Garcia, A., 2016. Thermal properties of asphalt pavements under dry and wet conditions: Materials & Design. 91, 432-439.
- **Hassn, A.**, Garcia, A., Chiarelli, A. and Dawson, A., 2015. Multivariable analysis of potential evaporation from moist asphalt mixture: Construction and Building Materials. 98, 80-88.
- **Hassn, A.**, M. Aboufoul, Y. Wu, A. Dawson, A. Garcia, 2016. Effect of air voids content on thermal properties of asphalt mixtures: Construction and Building Materials. 115, 327-335.
- **Hassn, A., Garcia, A., Chiarelli, A. and Dawson, A., 2015.** Water evaporation dynamics in moist asphalt samples with various air voids contents: 9th International Conference on Road and Airfield Pavement Technology (9th ICPT, 2015), China.

DECLARATION

The research described in this thesis was conducted at the University of Nottingham, Department of Civil Engineering between January 2014 and June 2017. I declare that the work is my own and has not been submitted for a degree of another university.

Abdushafi Alhashmi Hassn

University of Nottingham

October 2017

ACKNOWLEDGEMENTS

This thesis would not have been possible without the assistance, support, and help of many people that I am very grateful to.

Firstly, I would like to express my appreciations to my supervisors, Andrew Dawson and Alvaro Garcia for their continuous invaluable advice, guidance, motivation, and continuous support throughout the research period despite their heavy work load.

I would also like to thank all the academic staff in Nottingham Transportation Engineering Centre (NTEC), particularly Prof. Gordon Airey for providing all the required facilities. My thanks also given to the team of technicians in the laboratory for their tremendous efforts in preparing specimens and setting up experiments.

Finally, and most importantly, I am extremely grateful to my lovely wife, Sakina, my kids, Nusaiba, Fatma, Ahmed, Sara and my parents, my brothers my sisters and my in laws for their patient, continuous support and encouragements throughout the research period.

TABLE OF CONTENTS

ABSTRACT.....	i
PUBLICATIONS	v
DECLARATION	vi
ACKNOWLEDGEMENTS.....	vii
TABLE OF CONTENTS	viii
LIST OF FIGURES	xv
LIST OF TABLES.....	xx
LIST OF ABBREVIATIONS	xxi
LIST OF SYMBOLS.....	xxii
1. Introduction.....	1
1.1 Research Aims and Objectives	4
1.1.1 Research Aims	4
1.1.2 Research Objectives	4
1.1.3 Research Methodology	5
1.2 Research Layout.....	8
2. Literature Review.....	10

2.1 Introduction	10
2.2 Heat Transfer Mechanisms (Modes)	11
2.2.1 Conduction	11
2.2.2 Radiation	12
2.2.2.1 Thermal (Emitted) Radiation.....	14
2.2.2.2 Solar (Absorbed) Radiation	16
2.2.3 Convection.....	16
2.3 Factors Affecting Heat Transfer Properties of Asphalt Mixtures.....	17
2.3.1 Thermo-Physical Properties of Asphalt Mixtures.....	18
2.3.1.1 Thermal Conductivity	19
2.3.1.2 Specific Heat Capacity	30
2.3.1.3 Thermal Diffusivity	34
2.3.1.4 Thermal Effusivity	35
2.3.2 Surface Properties of Asphalt Mixtures.....	36
2.3.2.1 Albedo	36
2.3.2.2 Emissivity	38
2.3.2.3 Absorptivity.....	38
2.3.3 Weather Condition.....	39
2.3.3.1 Solar Irradiation	40
2.3.3.2 Air Temperature.....	41
2.3.3.3 Wind Velocity	42
2.3.3.4 Rain	43

2.4 Pavement Energy Harvesting Applications	44
2.4.1 Conversion of Kinetic Energy into Electrical Energy	46
2.4.2 Conversion of Solar Energy into Thermal Energy.....	49
2.4.3 Conversion of Solar Energy into Electrical Energy	51
2.5 Summary.....	54
3. Effect of Air Voids Content on Thermal Properties of Asphalt Mixtures under Dry Condition	57
3.1 Introduction	57
3.2 Material Selection.....	58
3.2.1 Bitumen	58
3.2.2 Aggregate.....	58
3.3 Material Preparation	59
3.3.1 Aggregate Gradation.....	59
3.3.2 Test Sample Preparation.....	60
3.4 Test Sample Density	61
3.4.1 Maximum Density	61
3.4.2 Bulk Density	61
3.5 Test Sample Air Voids Content	63
3.6 Experimental Program and Measurements.....	63
3.6.1 Experimental Setup.....	64
3.6.2 Experimental Measurements.....	67

3.6.2.1 Light Intensity Measurements	67
3.6.2.2 Temperature Profile.....	68
3.6.2.3 Data Acquisition System	69
3.6.2.4 Thermal Conductivity	69
3.6.2.5 Emissivity Measurements	71
3.6.2.6 Heat Accumulation in Asphalt Mixture.....	72
3.6.2.7 Computed Tomography Scans	73
3.7 Test Results.....	73
3.7.1 Thermal Conductivity	73
3.7.2 Specific Heat Capacity.....	74
3.7.3 Thermal Emissivity	75
3.7.4 Thermal Diffusivity	77
3.7.5 Evolution of temperature under infrared heating and cooling ..	78
3.8 Discussion.....	81
3.9 Summary	89

4. Multivariable analysis of water evaporation from moist asphalt mixture..... 91

4.1 Introduction	91
4.2 Description of Materials.....	93
4.3 Density of Test Samples	94
4.4 Air Voids Content	94

4.5	Experimental Setup	94
4.6	Heat Flux and Temperature Measurements	96
4.7	X-ray Computed Tomography (CT scans)	97
4.8	Topology of Air Voids	98
4.9	Statistics.....	100
4.10	Experimental Results	100
4.10.1	Thermo-physical properties of asphalt slabs	100
4.10.2	Air voids characteristics	101
4.10.3	Evolution of surface temperature with time.....	105
4.10.4	Mass loss and evaporation rate with time	106
4.10.5	Heat flux evolution with time	109
4.11	Discussion.....	111
4.11.1	Stages of water evaporation	111
4.11.2	Determination of the onset of Stage 2	117
4.12	Summary	120
5.	Thermal properties of asphalt mixture under dry and wet conditions.....	122
5.1	Introduction	122
5.2	Experimental Method.....	123
5.2.1	Material Description.....	123
5.2.2	Density and Air Voids Content	124

5.2.3 Experimental Setup and Measurements	124
5.2.4 X-ray Computed Tomography	124
5.3 Experimental Results	126
5.3.1 Evolution of Surface Temperature with Time.....	126
5.3.2 Evolution of Bottom Temperature with Time	128
5.3.3 Heat Flux Evolution with Time.....	130
5.3.4 Thermal Conductivity Evolution with Time	132
5.4 Discussion.....	134
5.5 Summary.....	139

6. Harvesting heat from pavement by thermoelectric power generators **141**

6.1 Introduction	141
6.2 Background.....	142
6.3 Experimental Method.....	145
6.3.1 Material Description.....	145
6.3.2 Density and Air Voids Content	146
6.3.3 Experimental Setup	147
6.3.4 Thermoelectric Power Generator Measurements	150
6.3.5 Light Intensity Measurements.....	151
6.3.6 Temperature Measurements	152
6.4 Results and Discussion.....	153

6.4.1 Asphalt Temperature Profile.....	153
6.4.2 Soil Temperature Profile.....	155
6.4.3 Temperature Difference between Hot and Cold Junction	157
6.4.4 Output Voltage.....	161
6.4.5 Output Voltage against ΔT	164
6.4.6 Output power	166
6.5 Summary.....	168
7. Conclusions and Recommendations	171
7.1 Overall Discussion.....	172
7.1.1 Effect of air voids content on thermal properties of asphalt mixtures under dry condition	172
7.1.2 Water evaporation dynamics of moist porous asphalt concrete mixtures.....	173
7.1.3 Thermal properties of asphalt mixtures under dry and wet conditions.....	175
7.1.4 Harvesting heat from pavement material by using Thermoelectric Power Generators.....	177
7.2 Recommendations	178
8. References	180
9. Appendix A	194
10. Appendix B.....	195

LIST OF FIGURES

Figure 1-1 Thesis Structure	9
Figure 2-1 Solar Radiation Balance (Russell, 2007).....	11
Figure 2-2 Heat conduction through a section of thickness Δx and area A.....	12
Figure 2-3 Heat transfer by radiation.....	14
Figure 2-4 Electromagnetic Wave Spectrum (PTB, 2010)	15
Figure 2-5 Factors affects heat transfer properties of asphalt mixture	18
Figure 2-6 Heat Flow Meter (Hilton Ltd, 1994)	22
Figure 2-7 Transient Plane Source (Chen, 2010)	23
Figure 2-8 Asphalt Concrete Surface Properties	Error! Bookmark not defined.
Figure 2-9 Albedometers and Pyranometer respectively (KIPP and ZONEN, 2003)	37
Figure 2-10 World Average Annual Temperature (World-Climate-Map, 2007)	41
Figure 2-11 The average air, ground and asphalt temperature variations (Trafikverket, 2010, RETScreen, 2005)	42
Figure 2-12 Total Annual Rainfall (World-Climate-Map, 2007)	44
Figure 2-13 Pavement Energy Harvesting Applications	46
Figure 2-14 Pavegen System (Pavegen, 2012)	48
Figure 2-15 Waynergy System (Waydip, 2012)	48

Figure 2-16 INNOWATTECH Company IPEGTM Piezoelectric System (Edery-Azulay, 2010).....	48
Figure 2-17 Road Energy System invent by Ooms Avenhorn Holding (De Bondt, 2003)	51
Figure 2-18 ICAX™ Asphalt Solar Collector System (ICAX, 2012)	51
Figure 2-19 Solar Roadway System (SR, 2012)	52
Figure 2-20 Schematic Diagram of Thermoelectric Power Generator	54
Figure 3-1 Composition of asphalt mixtures	60
Figure 3-2 Experimental setup schematic diagram	66
Figure 3-3 Laboratory Experimental Setup.....	66
Figure 3-4 Test sample preparation	67
Figure 3-5 Irradiation intensity measurements	68
Figure 3-6 Schematic temperature evolution of the test samples.....	69
Figure 3-7 Thermal Conductivity Measurements by Heat Flow Meter	70
Figure 3-8 Emissivity Measurements by Infrared Camera and using ALTAIR Software.....	72
Figure 3-9 Thermal Conductivity Results.....	74
Figure 3-10 Specific Heat Capacity Results	75
Figure 3-11 Emissivity results of the test samples	76
Figure 3-12 Maximum surface and bottom temperature at the steady state condition for all the test samples	79

Figure 3-13 Increments and decrements of temperature after 1 hour heating and cooling	80
Figure 3-14 Air voids connected to the surface of tests specimens with (a) 5.0% air voids content and (b) 25.3% air voids content.....	83
Figure 3-15 Ratio of air voids area versus air voids content	84
Figure 3-16 Difference between surface and bottom temperature for all test slabs	85
Figure 3-17 (a) Average temperature of the test samples. (b) Total accumulated heat in the test samples.....	85
Figure 3-18 Dimensionless total heat versus dimensionless density in the test samples studied.....	87
Figure 3-19 Effect of various thermal properties on the temperature evolution of asphalt mixture under infrared heating	88
Figure 4-1 Experimental setup.....	95
Figure 4-2 ITI model GHT-2c Geothermal Heat Flux Transducer	96
Figure 4-3 Position of Heat Flux Transducer	97
Figure 4-4 Vertical distribution of macroporosity in the ROI against average diameter of air voids	102
Figure 4-5 Vertical distribution of macroporosity in the ROI against Area Percentage	102
Figure 4-6 Largest connected air voids network for the test samples studied	104
Figure 4-7 Surface temperature versus time	106

Figure 4-8 Mass Loss of saturated samples versus time	108
Figure 4-9 Evaporation rate versus time	108
Figure 4-10 Heat flux versus time.....	109
Figure 4-11: Scheme of water evaporation in asphalt mixture.....	110
Figure 4-12 Reference points in the evolution of the physical parameters.....	112
Figure 4-13 Evaporation rate versus temperature.....	116
Figure 4-14 First derivative of evaporation rate versus time	119
Figure 5-1: Reconstructed air voids in the test samples studied (a) 5%, (b) 13.2%, (c) 17.4%, (d) 21.5%, (e) 25.3%.....	125
Figure 5-2: Evolution of the surface temperature (a) in dry conditions. (b) in wet conditions.	127
Figure 5-3: Evolution of the bottom temperature (a) in dry conditions. (b) in wet conditions.	129
Figure 5-4: Heat flux versus time (a) in dry conditions. (b) in wet conditions.	131
Figure 5-5: Thermal conductivity versus time for samples containing 5% and 26% air voids (a) in dry conditions. (b) in wet conditions.	133
Figure 5-6: Biggest connected air voids skeleton for reconstructed test samples in Figure 2. (a) 5%, (b) 13.2%, (c) 17.4%, (d) 21.5%, (e) 25.3%.	138
Figure 6-1 Schematic Diagram of Thermoelectric Power Generator	143
Figure 6-2 Composition of asphalt mixtures.....	146
Figure 6-3 Experimental setup schematic diagram	148
Figure 6-4 Laboratory experimental setup.....	149

Figure 6-5 Experimental setup configuration	150
Figure 6-6 Experimental test preparation	150
Figure 6-7 Asphalt surface and bottom temperature profile	154
Figure 6-8 Soil temperature profile versus time	156
Figure 6-9 Pavement temperature profile (Ongel and Harvey, 2004)	156
Figure 6-10 Temperature difference between hot and cold junction (Configuration 1)	158
Figure 6-11 Temperature difference between hot and cold Junction (Configuration 2).....	159
Figure 6-12 Temperature Difference between Hot and Cold Junction (Configuration 3).....	161
Figure 6-13 Output Voltage (Configuration 1).....	162
Figure 6-14 Output Voltage (Configuration 2)	163
Figure 6-15 Output Voltage (Configuration 3)	164
Figure 6-16 Output Voltage against ΔT (Configuration 1)	165
Figure 6-17 Output Voltage against ΔT (Configuration 2)	165
Figure 6-18 Output Voltage against ΔT (Configuration 3).....	166
Figure 6-19 Maximum Output Power	167

LIST OF TABLES

Table 2-1 Thermal conductivity of pavement constituents (Sundberg, 1988, Somerton, 1992, Read and Whiteoak, 2003, Banks, 2012).....	25
Table 2-2 Specific Heat Capacity of Pavement Constituents (Sundberg, 1988, Somerton, 1992, Read and Whiteoak, 2003, Banks, 2012, Busby et al., 2009)	33
Table 2-3 Mean values of dry-state specific heat capacity of pavement components (Max variation of $\pm 7\%$) (Dehdezi, 2012)	33
Table 3-1 Specification for 0/20 mm size dense binder course (BS 4987 part 1, 2005)	60
Table 3-2 Test sample maximum density, bulk density and air voids content	64
Table 3-3 Main parameters of the asphalt mixtures results	77
Table 4-1 Composition of asphalt mixture.....	94
Table 4-2 Topological constants	103
Table 4-3 Pearson’s correlation between all the parameters studied	105
Table 6-1 Performance Parameters.....	151
Table 6-2 Experimental results.....	155

LIST OF ABBREVIATIONS

PSEH Pavement Solar Energy Harvesting

UHI Urban Heat Island Effect

TRL Transport Research Laboratory

ROI Region of Interest

LIST OF SYMBOLS

Q_x	Rate of Conductive Heat Transfer (W)
k	Transport Property known as Thermal Conductivity of the
A	Surface Area (m ²)
$\frac{\Delta T}{\Delta X}$	Temperature Gradient in the Direction of Heat Flow for one
T_1	Temperature at depth (K)
T_2	Surface Temperature (K)
$Q_{Convection}$	Rate of Convection Heat Transfer (W)
h_c	Heat Transfer Coefficient (w/m ² K)
T_s	Surface Temperature (K)
T_f	Fluid Temperature (K)
$Q_{Thermal}$	Rate of Heat Radiated (W)
σ	Stefan-Boltzman Constant = $5.67 \times 10^{-8} \text{ W/m}^2\text{k}^4$
ε	Emissivity
$Q_{Absorbed}$	Absorbed Radiation Flux (W)
α	Surface Absorptivity ($0 < \alpha \leq 1$)
$Q_{incident}$	Incident Solar Radiation (W/m ²)
q	Quantity of heat passing through a unit area of the sample in unit time known as Heat flux (W/m ²)
ΔQ	Heat gain or loss (J)
m	Mass (kg)
c_p	Specific heat capacity (J/kg K)
ΔT	Temperature change (K)
ρ	Density (kg/m ³)

VHC	Volumetric Heat Capacity (J/m ³ K)
c	Specific heat capacity for each constituent (J/kg K)
α	Thermal diffusivity (m ² /s)
Δz	Depth increment (m)
Δt	Time increment (s)
i	Time node
m	Depth node
β	Thermal effusivity (J/s ^{0.5} m ² K)
G	Incident radiation (W)
ρ_m	Theoretical maximum density of the mixture without voids
ρ_b	Bulk density in the mixture (Kg/m ³)
V_m	Air voids content in the mixture (%)
$k_1 - k_6$	Calibration constants of the apparatus determined separately
$\bar{T} = \frac{T_{hot} + T_{cold}}{2}$	Average temperature of hot & cold plate (°C)
HFM	Heat flow meter output (Mv)
l_s	Thickness of the specimen (mm)
ZT	Thermoelectric figure of merit
S	Seebeck coefficient
θ	Electrical conductivity
T	Absolute Temperature
k_n	Thermal Conductivity n-type thermo-element
Kk_p	Thermal Conductivity p-type thermo-element

1. Introduction

In today's climate of growing energy needs and increasing environmental concern, alternatives to the use of non-renewable and polluting fossil fuels have to be investigated (Duffie and Beckman, 2013). One such alternative is solar energy. Solar energy is quite simply the energy produced directly by the sun and collected elsewhere, normally the Earth (Duffie and Beckman, 2013). Approximately half of the world's incoming solar energy is absorbed by the earth's surface (Budikova et al., 2010). Asphalt pavements are the commonest type of road surfacing. They can be heated up to 70°C due to solar irradiation in summer, because of their high heat absorbing property (Shaopeng et al., 2011, Wang et al., 2010). Pavements comprise large areas of our infrastructure and include roads, pedestrian pathways and parking areas. The high temperatures reached by asphalt mixtures are the origin of problems such as the urban heat island effect, which may cause discomfort to urban residents (Wong, 2009) and damage to pavements, such as rutting (Mallick et al., 2009, Brown and Cross, 1992).

The Urban Heat Island (UHI) effect leads to an increase in power consumption for cooling of buildings adjacent to pavements and a deterioration of the air quality (Wong, 2009). Moreover, rutting is a major temperature-related distress in asphalt pavements that occurs as a result of high temperature (Brown and Cross, 1992). However, the high temperatures reached by asphalt surfaces may be used to produce energy, by integrating pipes into the pavement structure, with water or air circulating inside (Carder et al., 2008, Sullivan et al., 2007, Garcia and Partl, 2014). The heat collected from the pavement by

Chapter 1. Introduction

integrating pipes could also reduce the Urban Heat Island (UHI) effect and the rutting potential of the asphalt pavement (Shaopeng et al., 2011, Mallick et al., 2009) by reducing the pavement temperature.

Pavement temperature is an energy balance between irradiation from the heat source (i.e. the Sun) and the heat absorbing, transport and storage properties of the asphalt mixture (i.e. the ability of the material to absorb and conduct heat). Heat transfer or energy transfer can occur by means of conduction, radiation, and convection. Evaluating the thermal behaviour of asphalt pavement mixtures requires understanding the surface and thermo-physical properties that affect transport and storage of heat (Stempihar et al., 2012). There are two distinct categories of these properties: those related to transport of energy through a system and those related to the thermodynamic or equilibrium state of a system (Bergman et al., 2011). Heat transfer properties of asphalt mixture are absorptivity (α), albedo ($1-\alpha$), emissivity (ε) and thermal conductivity (k). Thermodynamic properties of asphalt concrete include density (ρ) and specific heat capacity (c_p) which affect the equilibrium state of the system (Incropera et al., 2013).

Asphalt mixture is a composite material consisting of aggregates, bitumen, and air voids. Depending on the asphalt mixture design, the amount of air voids may vary from 4% to almost 30% of the total volume, thus affecting a number of physical properties, such as the thermal conductivity and the specific heat capacity (Incropera et al., 2013). At the present, it is known that the thermal behaviour of an asphalt mixture is mainly influenced by its air voids content, aggregate type and moisture content, although the interactions between these

Chapter 1. Introduction

factors are mostly unknown and have been studied mainly from on-site observations under diverse climatic conditions, not from controlled laboratory tests (Stempihar et al., 2012). In addition, previous research has attempted to change the factors influencing the thermal properties of asphalt pavements, e.g. the influence of moisture on the temperature of porous and dense asphalt mixture (Stempihar et al., 2012); the thermal conductivity of aggregates, such as graphite, steel fibres or steel particles (Carder et al., 2008, Sullivan et al., 2007, Garcia and Partl, 2014, Dawson et al., 2011); or the surface colour of the pavements (Stempihar et al., 2012); however there is no extensive study about the effect of air voids content on the thermal properties of asphalt mixture under different weather conditions.

As the air voids can be expected to influence the conduction/insulation properties of the asphalt, it is essential to understand the relationship between the porosity and the heat transfer properties (thermo-physical and surface properties). Different weather conditions can be expected to have an effect, as well, due to resulting moisture variations.

Over the last years, although there have been some previous attempts to recover heat energy from pavements, the work has been extremely limited in terms of installation. Incorporating tubes in the asphalt pavement is considered the most available solution, applying a heat exchanger design, with water or air circulating inside. There are major drawbacks to these systems such as the effect of traffic and pavement load on the installed pipes, effect of pipes on pavement performance and pavement maintenance and recycling. In addition, another limitation to these systems is that heat has to be used near a collection

point for heating purposes (Wu et al., 2001, Mallick et al., 2008, Dawson et al., 2011). Therefore, it is desirable to undertake a further experimental investigation on the recovery of solar heat from asphalt concrete pavement materials by converting heat into electricity through thermoelectric generators (TEG).

1.1 Research Aims and Objectives

1.1.1 Research Aims

The overall aim of this project is to study the effect of air voids in asphalt concrete pavement material on its thermo-physical and thermal surface properties, and how that could affect the application of harvesting thermal heat from pavement materials and the urban heat island effect. In order to achieve this, thermo-physical and surface thermal properties of asphalt concrete mixtures with various air void contents under different weather conditions were examined experimentally. In addition, experimental investigation has been undertaken on harvesting thermal heat by Thermoelectric Power Generators (TEG) from asphalt concrete mixtures with various air voids contents.

1.1.2 Research Objectives

The following research objectives have been identified to achieve this aim:

- 1- Studying experimentally the effect of air voids content on thermal properties of asphalt concrete mixtures under different climate conditions (dry and wet conditions). This study includes thermo-physical properties (i.e. density, thermal conductivity, specific heat capacity, thermal diffusivity and

Chapter 1. Introduction

thermal effusivity) and surface thermal properties (i.e. albedo, emissivity and absorptivity).

2- Experimental investigation on the water evaporation dynamics of moist porous asphalt concrete mixtures.

3- Studying experimentally the feasibility of harvesting heat from asphalt concrete mixtures by Thermoelectric Power Generators (TEG) and how the air voids content can affect the recovery of the heat in this form.

1.1.3 Research Methodology

In order to meet the previous mentioned objectives, five tasks have been identified as follows:

(1) Conducting a literature review on:

- Heat transfer mechanisms;
- Factors affecting heat transfer properties of asphalt mixtures, this includes thermo-physical properties (i.e. density, thermal conductivity and specific heat capacity) and surface thermal properties (i.e. Albedo, Emissivity and Absorbtivity); and
- The existing applications of pavement energy harvesting.

(2) An experimental detailed study on the effect of air voids content on heat transfer properties of asphalt concrete mixtures under dry conditions has been undertaken. This study includes the thermo-physical properties (such as thermal conductivity, density, specific heat capacity, thermal diffusivity and

Chapter 1. Introduction

thermal effusivity) and also the surface thermal properties (such as absorptivity, emissivity and albedo). The main aim from this study is to have a deep insight into the effect of the air voids content of asphalt mixture on the temperature evolution, transport and storage of heat in asphalt mixtures under dry conditions. Various measurement techniques have been proposed in this study. With this objective, asphalt mixture slabs with different air voids contents have been constructed and their thermal conductivity, specific heat capacity, light absorptivity and thermal diffusivity related to their temperature evolution were measured when they were exposed to infrared light and during the cooling process.

(3) A detailed experimental study on the evaporation rate process of asphalt concrete mixtures has been undertaken. The motivation for this study is to obtain information on the dynamics of the water evaporation process from an asphalt surface during a continuous drying event. For this purpose, asphalt mixtures with air contents ranging from 4 % to 26 % were manufactured, and observations relating the time dependent evaporation rates of saturated asphalt mixtures were compared to the development of a number of parameters, such as asphalt surface temperature during heating, heat flux, porosity, and thermal conductivity. In addition, the air voids configuration was characterized and their properties, e.g., Euler number, tortuosity, diameter of air voids and macro porosity, were compared to the parameters mentioned above. These results are expected to have a strong impact on the design of asphalt mixtures to minimize the pavement contribution to the urban heat island effect and on the design of new types of asphalt solar energy collectors.

Chapter 1. Introduction

(4) The thermal properties of asphalt concrete mixtures have been studied experimentally under dry and wet conditions undertaken. To achieve this task, dry and saturated asphalt slabs with different air voids contents ranging from 4% to 26% have been exposed to infrared light and the surface and bottom temperature evolution, heat flux and evaporation rate have been measured. The temperatures of dry and saturated asphalt mixtures were compared to one another and related to a number of parameters, such as thermal conductivity and emissivity. This study would be expected to have a strong impact on the design of pavements for different climatic conditions, treatments to reduce the urban heat island effect, such as watering, and techniques to harvest solar energy from pavement layers.

(5) An experimental study has been carried out of the feasibility of recovering solar heat from asphalt concrete pavement materials by converting heat into electricity through Thermoelectric Power Generators (TEG). TEGs are solid state devices that produce direct energy conversion from thermal energy (heat) into electrical energy as a result of temperature difference based on the “Seebeck effect”. In addition, the effect of the air voids content on the recovery of the heat was studied by testing three asphalt concrete slabs with different air voids contents. Furthermore, three experimental configurations of cold junctions (heat sinks) have been studied to investigate the amount of electricity that can be maintained. For this purpose, asphalt mixtures with different air voids contents ranging from 4% to 26% were manufactured and three configurations of cold junction were set up. A number of parameters were observed for comparison purposes, including the asphalt surface and bottom

temperature profile, soil temperature profile at different depths, temperature difference between hot and cold junctions, and output voltage.

1.2 Research Layout

This research is organized in seven chapters see **Figure 1-1** below. **Chapter 2** provides a literature and background review to the project. This includes an understanding of the heat transfer mechanisms and the factors affecting heat transfer properties. This chapter also reviews the effect of porosity on heat transfer properties. Finally, the existing applications of pavement energy harvesting are studied in this chapter. The effect of air voids content on thermal properties of asphalt mixtures under dry conditions is studied in **Chapter 3**. This study includes the thermo-physical properties (such as thermal conductivity, specific heat capacity, density, thermal diffusivity and thermal effusivity) and surface thermal properties (such as albedo, emissivity and absorptivity). Multivariable analysis of potential evaporation from moist asphalt mixture is studied in **Chapter 4**. **Chapter 5** presents and discusses the effect of the air voids content on the thermal properties of asphalt concrete mixtures under different weather conditions (dry and wet conditions). The viability of harvesting heat from asphalt pavements by Thermoelectric Power Generators and the effect of air voids on the heat recovery are examined in **Chapter 6**. Finally, **Chapter 7** draws the conclusions of the research and makes recommendations for further research work.

Chapter 1. Introduction

Chapter 1	<ul style="list-style-type: none">• Introduction• Aims and Objectives• Methodology• Research Layout
Chapter 2	<ul style="list-style-type: none">• Literature Review
Chapter 3	<ul style="list-style-type: none">• Effect of air voids content on thermal properties of asphalt mixtures under dry condition
Chapter 4	<ul style="list-style-type: none">• Multivariable analysis of potential evaporation from moist asphalt mixture
Chapter 5	<ul style="list-style-type: none">• Thermal properties of asphalt mixtures under dry and wet conditions
Chapter 6	<ul style="list-style-type: none">• The viability of harvesting heat from asphalt pavement by Thermoelectric Power Generators
Chapter 7	<ul style="list-style-type: none">• Conclusions and Recommendations

Figure 1-1 Thesis Structure

2. Literature Review

2.1 Introduction

This chapter presents a detailed literature review on solar irradiation principles, heat transfer mechanisms, factors affecting heat transfer properties and existing pavement energy harvesting applications.

Solar irradiation is the energy produced by the Sun in the form of electromagnetic radiation which is perceived by humans as sunlight and warmth, and it is often expressed as kWh/m². The electromagnetic radiation is composed of ultraviolet light, visible light, and infrared energy.

Approximately half of the world's incoming solar energy is absorbed by the earth's surface (Russell, 2007, Budikova et al., 2010) (see **Figure 2-1**). The radiation from the sun reaching the earth generates heat on the ground. By absorbing the incoming solar radiation, the Earth warms up, like a black body and its temperature rises. When this solar energy is absorbed by a pavement, it can be transmitted through, or stored in the pavement materials depending on their properties.

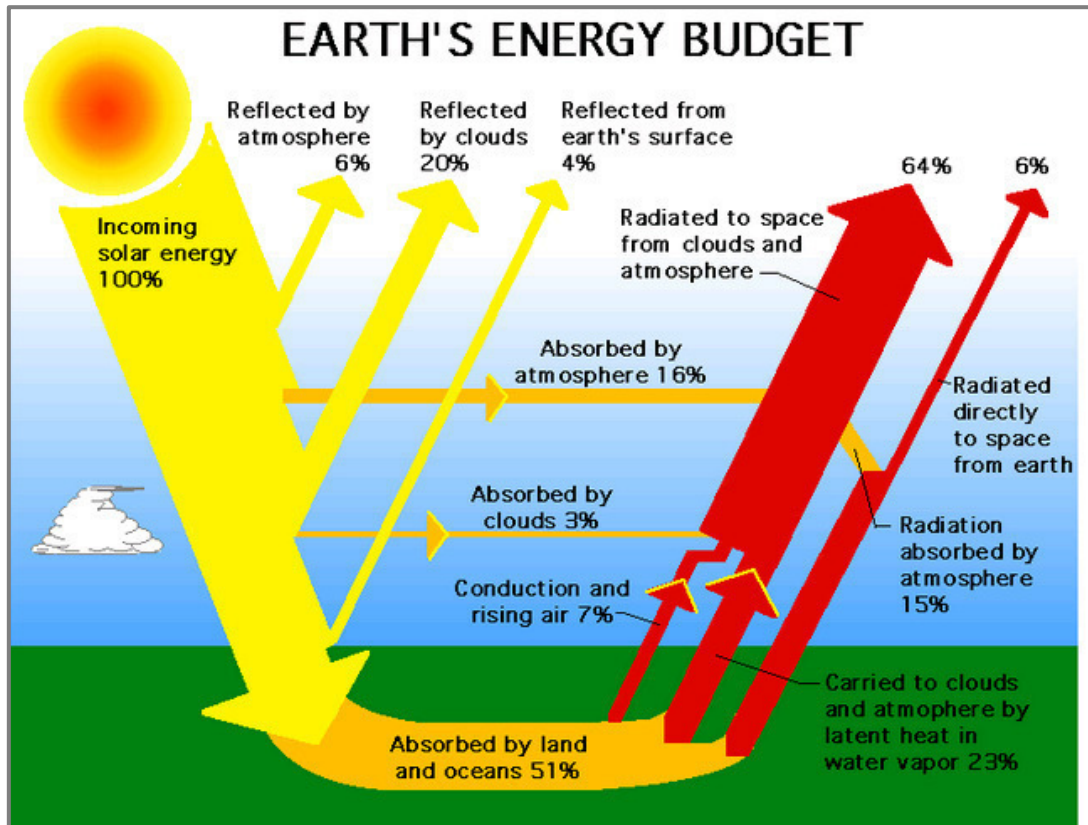


Figure 2-1 Solar Radiation Balance (Russell, 2007)

2.2 Heat Transfer Mechanisms (Modes)

2.2.1 Conduction

Conduction can be defined as “the transfer of energy from the more energetic to the less energetic particles of a substance due to interactions between the particles” (Bergman et al., 2011). Heat transfer by conduction can take place in gases, liquids, and solids. In gases and liquids, conduction is due to the collision and diffusion of the molecules during their random motion, whereas in solids it is due to the combination of vibrations of the molecules in a lattice and the energy transport by free electrons (Cengel, 1998). The geometry of the medium, its thickness, the material properties of the medium, and the temperature difference across the medium are the factors that affect rate of heat conduction.

Chapter 2. Literature Review

The first theory of heat conduction was developed by a French scientist Joseph Fourier. Fourier's theory states that the heat flux in the direction of heat flow is proportional to the temperature gradient in that direction (Das, 2010). **Figure 2-2** illustrates the heat conduction through a section of thickness Δx and area A .

Rate of conduction of heat can be determined through Fourier's law as follows:

$$Q_x = -k A \frac{\Delta T}{\Delta X} = -k A \frac{(T_1 - T_2)}{\Delta X} \quad \text{Eq. 2-1}$$

Where: Q_x is the rate of conductive heat transfer in the x direction, measured in (W), k is the transport property known as thermal conductivity of the medium, measured in (W/m K), A is the surface area measured in (m^2), $\frac{\Delta T}{\Delta X}$ is the temperature gradient in the direction of heat flow for one-dimension (1D), measured in (K/m), T_1 is the temperature at depth, measured in (K), and T_2 is the surface temperature (K).

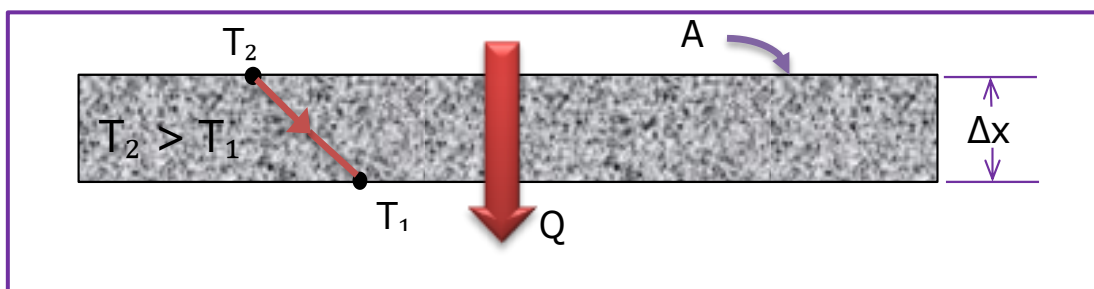


Figure 2-2 Heat conduction through a section of thickness Δx and area A

2.2.2 Radiation

Radiation can be defined as “the energy emitted by matter in the form of electromagnetic waves (or photons) as a result of the changes in the electronic

Chapter 2. Literature Review

configurations of the atoms or molecules” (Cengel, 1998). Transferring energy by radiation does not require the presence of any material medium, as in the case of conduction and convection. Radiation heat transfer occurs in solids, liquids and gases or through vacuums. The energy that reaches the earth from the sun is an example of heat transfer by radiation. Heat transfer by conduction and convection transfers heat from a high temperature medium to a lower temperature one, whereas, heat transfer by radiation can occur even between two bodies separated by a medium colder than both bodies. As an example of that, solar radiation reaches the surface of the earth after passing through extremely cold air layers at high altitudes.

The three important surface material properties that affect heat transfer by radiation are absorptivity, reflectivity (albedo), and emissivity. Absorptivity can be defined as the fraction of the radiation energy incident on a surface that is absorbed by the surface and its value ranges from 0 to 1 (Cengel, 1998). Reflectivity or Albedo is defined as the ratio of reflected solar radiation to the total incident solar radiation, and its value also ranges from 0 to 1 (Das, 2010).

Heat transfer by mode of radiation can be classified into two types; thermal radiation or emitted radiation and solar radiation or absorbed radiation (see **Figure 2-3**).

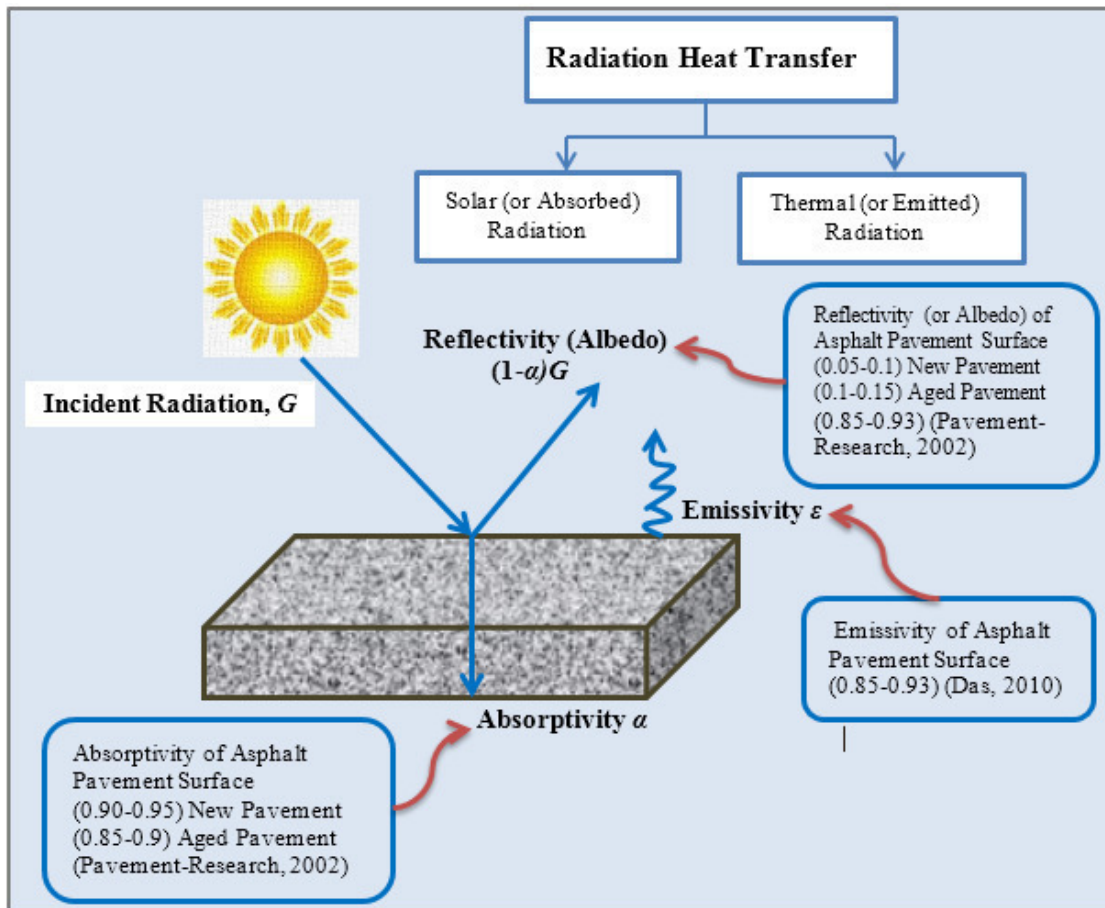


Figure 2-3 Heat transfer by radiation

2.2.2.1 Thermal (Emitted) Radiation

Thermal radiation is defined as “the portion of the electromagnetic spectrum that extends from about 0.1 to 100 μm, since the radiation emitted by bodies because of their temperature falls almost entirely into this wave length range” (Cengel, 1998). From the electromagnetic wave spectrum figure, thermal radiation includes the entire infrared range visible waves and some portion of the ultraviolet wave range (see Figure 2-4). The idealized surface that emits radiation at the maximum rate is called a black-body, which can be determined by the Stefan-Boltzman law as follows:

$$Q_{Thermal} = \sigma A T_S^4 \quad \text{Eq. 2-2}$$

Chapter 2. Literature Review

Where: $Q_{Thermal}$ is the rate of heat radiated, measured in (W), σ is the Stefan-Boltzman Constant = $5.67 \times 10^{-8} \text{ W/m}^2\text{K}^4$, A is the surface area, measured in (m^2), and T_S is the surface temperature (K).

Emissivity is defined as a measure of how closely a surface approximates to a black-body, for which emissivity is equal to 1. Its value ranges from 0 to 1. Therefore, an ideal solar collector has high absorptivity but low emissivity in contrast to a black-body which has values of 1 for both. The radiation emitted by a real surface is less than the radiation emitted by a blackbody. So, Stefan-Boltzman introduced the emissivity term to take account of real surfaces. The emissivity property (ϵ), whose value is in the range 0 to 1, is a measure of how closely a surface approximates to a black-body for which $\epsilon = 1$ (Cengel, 1998). Therefore, the equation will be as follows:

$$Q_{Thermal} = \epsilon \sigma A T_S^4$$

Eq. 2-3

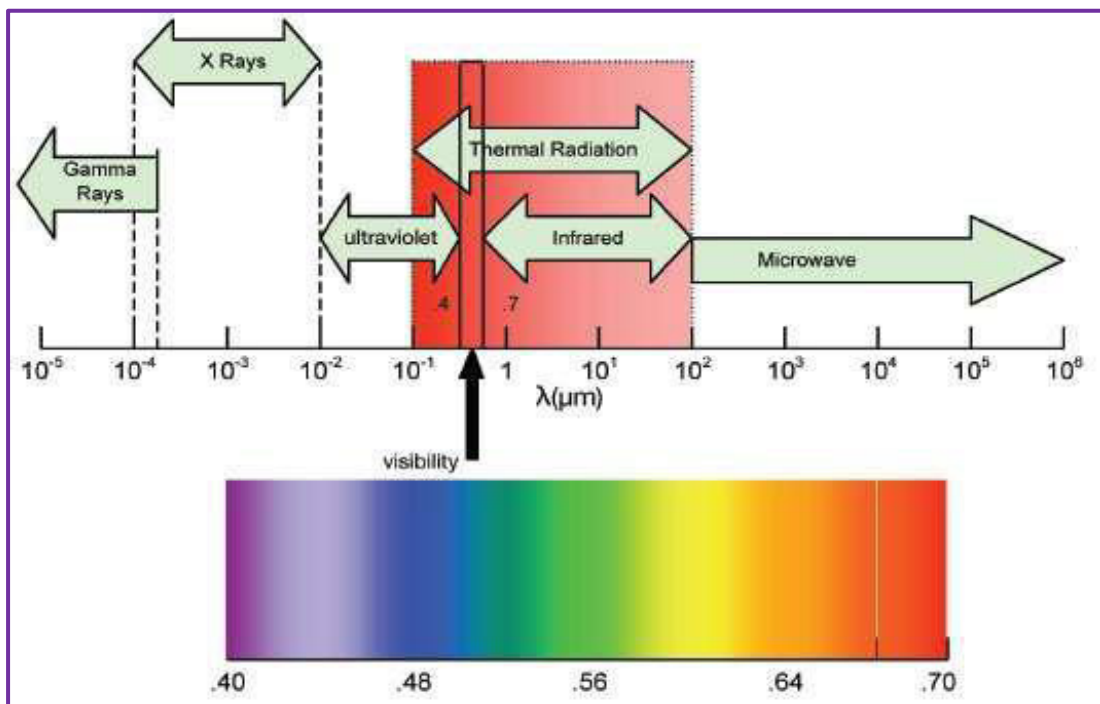


Figure 2-4 Electromagnetic Wave Spectrum (PTB, 2010)

2.2.2.2 Solar (Absorbed) Radiation

Solar radiation is the electromagnetic radiation emitted by the sun with a wavelength band between 0.3 μm and 3 μm . Half of the radiation is in the visible short-wave part of the electromagnetic spectrum and the other half is infrared and ultraviolet. The amount of absorbed radiation can be calculated as follows:

$$Q_{Absorbed} = \alpha A Q_{incident} \quad \text{Eq. 2-4}$$

Where: $Q_{Absorbed}$ is the absorbed radiation flux, measured in (W), α is the surface absorptivity ($0 < \alpha \leq 1$), A is the surface area, measured in (m^2), and $Q_{incident}$ is the incident solar radiation, measured in (W/m^2).

2.2.3 Convection

Convection can be defined as “*the mode of energy transfer between a solid surface and the adjacent liquid or gas that is in motion*” (Cengel, 1998).

Convective heat transfer can be classified by two means according to the nature of the flow; free (or natural) convection and forced convection. Forced convection occurs when the flow is caused by external means, such as fans, pumps or atmospheric wind, whereas, for free (or natural) convection, the flow is induced by forces which are due to density differences caused by temperature variations in the fluid (Incropera et al., 2013). The heat transfer by convection can be determined through Newton’s Law of Cooling as follows:

$$Q_{Convection} = h_c A \Delta T = h_c A (T_s - T_f) \quad \text{Eq. 2-5}$$

Where: $Q_{Convection}$ is the rate of convection heat transfer, measured in (W), h_c is the heat transfer coefficient, measured in ($\text{W}/\text{m}^2 \text{K}$), A is the surface area,

measured in (m²), T_s is the surface temperature (K), and T_f is the fluid temperature (K).

2.3 Factors Affecting Heat Transfer Properties of Asphalt Mixtures

This section will study the main factors that have an effect on the heat transfer properties of asphalt concrete mixtures. This includes the thermo-physical properties such as the thermal conductivity, density, specific heat capacity, thermal diffusivity and thermal effusivity. Furthermore, this study includes the effect of weather conditions on the heat transfer properties of asphalt concrete pavements. **Figure 2-5** illustrates the main factors affects heat transfer properties of asphalt mixture.

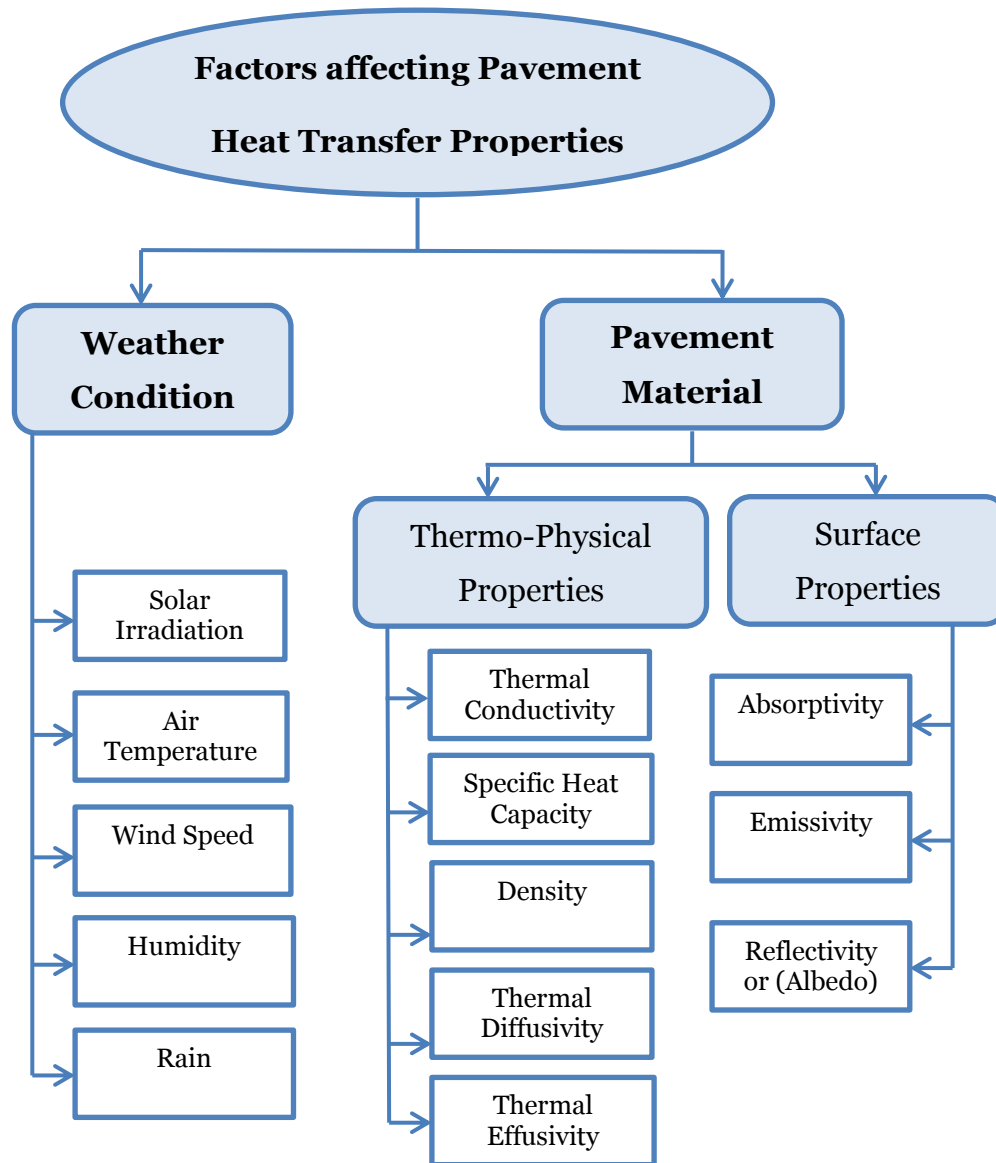


Figure 2-5 Factors affects heat transfer properties of asphalt mixture

2.3.1 Thermo-Physical Properties of Asphalt Mixtures

The thermo-physical properties of material can be defined as the properties affecting the transfer and storage of heat. These includes two distinct categories, transport and thermodynamic properties (Bergman et al., 2011). The transport properties include the diffusion rate coefficients such as thermal conductivity, whereas thermodynamic properties relate to the equilibrium state of a system which affects the ability of a material to store thermal energy, such

Chapter 2. Literature Review

as density and specific heat capacity properties (Das, 2010). In addition, thermal diffusivity which is the ratio of thermal conductivity to the volumetric heat capacity is also considered as an important property in heat transfer. It measures the ability of a material to conduct thermal energy relative to its ability to store thermal energy (Incropera et al., 2013). The next paragraphs overview the influence of pavement thermo-physical properties on heat transfer and storage applications.

2.3.1.1 Thermal Conductivity

Thermal Conductivity is defined as *“The flow of energy (in joules per second, or watts) caused by a 1K (one degree kelvin) temperature difference across a 1m length of material (of 1m² in cross section)”*. Thus, the thermal conductivity unit is W/m K (Thom, 2008). Thermal conductivity of the material describes the ability of this material to conduct heat, and it is considered to be the most important property related to heat conduction. Material with high thermal conductivity will enhance the heat transfer (Conductor Material), while one with a low value will lead to a lower rate of heat transfer (Insulator Material).

This section describes the thermal conductivity measurement methods, factors affecting thermal conductivity, and the effect of thermal conductivity on heat transfer by reviewing previous studies.

◆ Thermal Conductivity Measurement Methods

Based on Fourier’s law (see Eq. 2.1), the measurement of the heat flux and temperature difference always involves measuring thermal conductivity. There are a wide variety of methods and techniques for measuring thermal

Chapter 2. Literature Review

conductivity, each suitable for a limited range of materials, depending on the thermal properties and the temperature of the medium (Kuvandykova, 2011). Generally, methods for measuring thermal conductivity can be classified into two broad categories: steady and transient state heat transfer methods (Mohsenin, 1980). The main difference between these two methods is that the steady-state method performs a measurement when the material is in complete equilibrium which means temperature does not change with time and thermal conductivity is directly computed from Eq.2-1, whereas the transient method performs a measurement during the process of heating up or cooling down and a derivative of Fourier's Law must be used. The next paragraph will outline the main methods used to measure thermal conductivity.

Steady State Method

Reaching the required equilibrium takes a long time and also the difficulty of accurately measuring the heat fluxes are both considered as disadvantages of this technique. Other disadvantages include the requirement that a flat slab specimen with a thickness not exceeding one third of the length of the measured region is required in order to ensure effectively one dimensional heat flow; and it is very difficult to prepare such a specimen in the laboratory (Kuvandykova, 2011). The test using steady-state methods often requires a long time to complete and moisture migration may introduce significant measurement errors (Mohsenin, 1980, Kazarian, 1965, Dutta et al., 1988).

Various laboratory testing methods exist for determining the thermal properties of the material in the steady state method. The guarded hot plate

Chapter 2. Literature Review

method is probably the most common steady state method. From **Eq. 2.1**, thermal conductivity (**k**) in the steady state is defined as:

$$k = \frac{q \cdot \Delta X}{T_1 - T_2} \quad \text{Eq. 2-6}$$

Where: **q** is the quantity of heat passing through a unit area of the sample in unit time known as heat flux, measured in (W/m²)

The quantity of Heat flux (**q**) is given by:

$$q = \frac{Q_x}{A} \quad \text{Eq. 2-7}$$

Where: **Q** is the quantity of heat passing through a base area of the sample, measured in (W) and **A** is the base area of the sample, measured in (m²).

Heat Flow Meter (HFM)

The HFM method measures steady state heat transfer through a material according to ASTM Standard C518, ISO 8301. In this method, a 30.5cm square sample with a thickness of up to 10 cm is placed between a hot plate and a heat flow meter which is attached to a cold plate (see **Figure 2-6**). The two plates are controlled to a specified constant temperature which is measured by thermocouples embedded in the plates.

The heat flow through the specimens can be measured by the heat flux transducers are embedded in each plate. Thermal conductivity will be measured by a set of calibration constants that is derived from testing a known thermal conductivity sample, as well as temperature and heat flow meter outputs. **Hall**

and Allinson (2009) applied this technique to measure the thermal conductivity of pavement materials. The advantage of the HFM method over the conventional steady-state method is that the heat flow through the specimen is measured directly and no estimation of the heat loss/gain is necessary. Therefore, the limits of accuracy of the thermal conductivity values measured by the HFM apparatus are considered to be $\pm 2-3\%$ of the absolute magnitude.

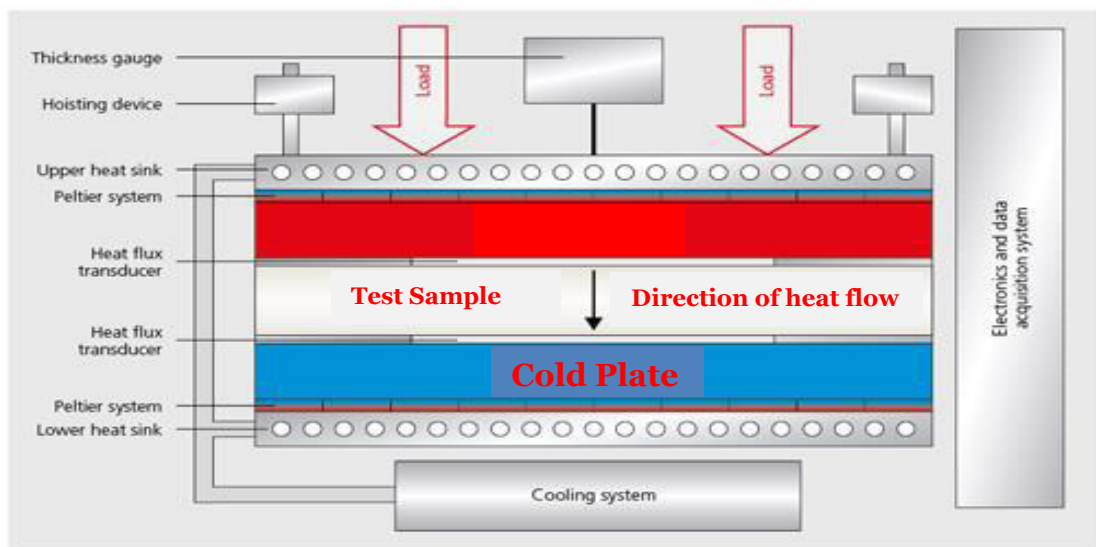


Figure 2-6 Heat Flow Meter (Hilton Ltd, 1994)

Transient Method

This method measures thermal conductivity of a solid in the process of heating up or cooling down. In contrast to steady state procedures, transient methods can determine the thermal conductivity of solid materials like asphalt concrete quicker. Other advantages include the possibility of measuring only one surface of a large specimen, and the feasibility of testing in situ pavements (Kuvandykova, 2011). However, this method has some disadvantages such as the contact resistance problem, especially applications where it is necessary to drill a hole to insert the probe (Somerton, 1992). In addition, transient methods

Chapter 2. Literature Review

have another disadvantage, that it considered unsuitable for non-homogeneous material (Hilton Ltd, 1994).

There are two common transient methods used for measuring thermal conductivity of materials; the Hot Wire Method (HWM) and the Transient Plane Source (TPS) method. The thermal conductivity of concrete has been measured with the HWM by some researchers (Demirboğa and Gül, 2003, Uysal et al., 2004, Demirboğa, 2007). An electrically heated wire is used in the HWM method. The wire is inserted into a material and heat flows out radially from it. The thermal conductivity is then computed from the relationship between the wire temperature and the time since starting. In the TPS method, a circular heating element is placed in contact with the material sample where it serves both as the heat source and as a resistance thermometer, and the temperature is monitored over time (see Figure 2-7).



Figure 2-7 Transient Plane Source (Chen, 2010)

Indirect Method

Thermal conductivity of a material can be indirectly determined if other thermo-physical properties of a material are measured such as specific heat capacity, thermal diffusivity, and density. This can be calculated through the thermo-dynamic equations presented in the following sections.

◆ ***Factors Affecting Thermal Conductivity***

There are several factors that could affect the thermal conductivity of a composite material. The main factors considered are density and moisture content, where increasing these factors will increase thermal conductivity. In asphalt concrete pavement, several factors can affect thermal conductivity such as aggregate type and content, porosity, density and moisture content. In the next paragraphs, these factors will be discussed.

Aggregate Type and Content

Asphalt mixture is a composite material consisting of aggregates, bitumen, and air voids. Therefore, the thermal conductivity of the mix will be dependent on the thermal conductivity of these three constituents. The aggregates total 90 to 95 percent of the total mixture by weight (Thom, 2008); therefore they have a significant effect on the thermal conductivity of pavement mixes. Using high thermal conductivity aggregate will increase the thermal conductivity of the mix. The thermal conductivity of the aggregates that are commonly used in pavement structures (O’Flaherty, 2002) along with other pavement constituents are tabulated in **Table 2-1**.

An experimental study was carried out by Mrawira and Luca (2002) on the influence of aggregate type on thermal properties of asphalt concrete pavement. This experiment showed that the aggregate type has the most significant effect on thermal conductivity, where using high thermal conductivity aggregate such as quartzite will increase the thermal conductivity of the whole mix.

Table 2-1 Thermal conductivity of pavement constituents (Sundberg, 1988, Somerton, 1992, Read and Whiteoak, 2003, Banks, 2012)

Aggregates/Pavement Constituents	Range of Thermal Conductivity (W/m K)
Quartzite	5.5-7.5
Granite	3.0-4.0
Limestone	1.5-3.0
Basalt	1.3-2.3
Bitumen	0.15-0.17
Air	0.024
Water	0.6

There has been an attempt to enhance the thermo-physical properties of asphalt materials for pavement harvesting systems through using different aggregate types (Dawson et al., 2011, Wu et al., 2001, Mallick et al., 2008).

Results of a work carried out by Mallick et al. (2009) showed that the thermal conductivity of the pavement mix can be improved by using aggregates with higher thermal conductivity, such as quartzite (containing high percentage, >90% of quartz).

In addition, Dawson et al. (2011), performed an experimental and numerical simulation model for enhancing thermal properties of asphalt materials for heat storage and transfer application. The study reported that the aggregate type and content has a major influence on the thermal conductivity. In detail, this study illustrated that fully replacing limestone aggregates with quartzite can enhance the thermal conductivity by approximately 135%.

Additions and Mixtures

Several studies have been developed to analyse the influence of increasing the pavement thermal conductivity by adding additive material such as raw iron, graphite powder, steel wool fibres, copper fibres, and powder graphite. Work carried out by [Phillipps \(2007\)](#) illustrated that the addition of raw iron shots in an asphalt mix has no significant effect on the thermal conductivity of the mix. In addition, a similar conclusion was achieved by [Mallick et al. \(2008\)](#) where copper powder was added into the asphalt mixture, and no sign of significant improvement was achieved. The reason was that the copper powder was covered with asphalt during mixing and was partially oxidized during the heating of the aggregates prior to mixing. Therefore there was poor connection between one particle of conductive material and the next, largely obliterating any conductivity benefit that the metal itself provided.

[García et al. \(2013\)](#) investigated the effect of steel wool fibres on the electrical, thermal and induction properties of dense asphalt concrete. The result from this study showed that the thermal conductivity of dense asphalt concrete increases with the volume of steel wool fibres in the mixture. Furthermore, [Dawson et al. \(2011\)](#), developed an experimental and numerical simulation model for enhancing thermal properties of asphalt materials for heat storage and transfer application. The results from this study showed that the addition of copper fibres to the asphalt mixtures improved slightly the thermal conductivity of the asphalt mixture. In these cases, the long nature of the inclusion did enable some conduction but the transfer of energy from one fibre to the next was evidently still problematic.

Chapter 2. Literature Review

Pan et al. (2014) carried out an experimental study on the influence of graphite powder on thermal properties of asphalt binder. The results indicated that the thermal conductivity increased with the increase of graphite content. This increase of thermal conductivity of asphalt binder depends on the amount of graphite particle dispersed in the asphalt. In detail, when the content of graphite increased from 0% to 40%, the thermal conductivity of asphalt binder increased from 0.396 W/m.K to 0.934 W/m.K. In addition, a graphite powder content of 18% by volume in the asphalt binder has been proved to be most appropriate by previous studies, and the content was confirmed by experimental validation (Mingyu et al., 2010). The result from this study showed that, the thermal conductivity of the modified asphalt mixtures (18% of filler graphite powder) was $2.23 \text{ Wm}^{-1}\text{K}^{-1}$, which increased from $1.73 \text{ Wm}^{-1}\text{K}^{-1}$ for a conventional asphalt concrete mixture.

Density and Porosity

Material density can be defined as the mass per unit volume, whereas porosity is the percentage of voids in the material. Porosity can affect the thermal properties of a material due to changes in voids and particle contact. Increasing porosity in the mixture could reduce the weight of the sample which in turn reduces the sample density. Results from previous research illustrated that thermal conductivity of the same material increases with the increase of density and decrease of porosity (Cote and Konrad, 2005, Canakci et al., 2007, Benazzouk et al., 2008). The reason behind that is that by increasing the density of the mix, the contact between particles in the mix would increase and as a result the thermal conductivity of the mix would increase.

Chapter 2. Literature Review

The inner structure of materials is important. Metals and other dense solid materials tend to have high levels of conductivity, whereas materials with very small amounts of solid matter and a large proportion of voids (gas or air bubbles, not large enough to carry heat by convection) have the lowest thermal conductivities (Crompton, 2010).

García et al. (2013) investigated the effect of steel wool fibres on the electrical, thermal and induction properties of dense asphalt concrete. Their results showed that the thermal conductivity of asphalt concrete decreased with the increase of the air voids content in the mixture.

Moisture Content

The thermal conductivity of pavement materials and mixes increases as moisture content increases (Kim et al., 2003, Cote and Konrad, 2005, Canakci et al., 2007, Hall and Allinson, 2009). This can be explained as the air voids in the mix are filled with water, whose thermal conductivity is higher than the thermal conductivity of air. The thermal conductivity of water is 25 times higher than air which allows materials containing voids in a saturated condition to have a higher thermal conductivity than material containing the same voids but in a dry condition (FIP, 1978, Short and Kinniburg, 1978, Asaeda et al., 1996).

According to Becker and Katz (1990), moisture moves from a heated side toward a cooler side, when the specimen is tightly packed and heated; the study found that the thermal conductivity of the cooler side is greater than that of the drier side, while resistance to heat flow is greater in the drier side.

◆ ***Effect of Thermal Conductivity on Heat Transfer***

This section reviews the effect and sensitivities of thermal conductivity on the pavement temperature and heat transfer as found from previous studies.

Gui et al. (2007), investigated the effect of pavement thermo-physical properties on surface temperatures by developing a mathematical model. They concluded that, increasing the thermal conductivity, thermal diffusivity, and volumetric heat capacity would help in mitigating the maximum but not the minimum pavement surface temperature.

Wang et al. (2010), performed a finite element analysis using ANSYS software to investigate the thermal response of heat-conducting asphalt pavements. The result showed that the surface temperature of the pavement decreases when the thermal conductivity increases; however, the pavement's temperature increases at its centre. For example, the surface peak temperature was decreased by 8.83%, and the pavement's mid-depth peak temperature was increased by 13.01% when the thermal conductivity of the asphalt pavement increased from 1.3 W/m.K to 3.0 W/m.K.

Mallick et al. (2008), performed a finite element study to investigate of temperature distributions in small samples, and tested asphalt pavement samples at different size scales. The results of the small-scale testing showed that the use of aggregates with high conductivity can significantly enhance the efficiency of heat capture.

Mingyu et al. (2010), carried out an experimental study on the influence of graphite powder (as a filler) on temperature distribution in asphalt pavements.

They found that the addition of graphite can accelerate the heat transmission from the top to the bottom. As previously mentioned adding graphite powder (as filler) in the asphalt concrete mix will increase the thermal conductivity of the mix which in turn accelerates the heat transfer.

2.3.1.2 Specific Heat Capacity

Specific heat capacity can be defined as “*the energy required to raise the temperature of a unit mass of a substance by one degree*” (Cengel, 1998). Specific heat capacity is considered as one of the thermodynamic properties of asphalt concrete which is concerned with the equilibrium state of the system (Incropera et al., 2013).

The relationship between change in heat content and change in temperature of a body of mass, m (kg) is generally expressed as follows:

$$\Delta Q = mc_p\Delta T \quad \text{Eq. 2-8}$$

Where; ΔQ is the heat gain or loss, measured in (J), m is the mass, measured in (kg), c_p is the specific heat capacity, measured in (J/kg K), ΔT is the temperature change, measured in (K).

Volumetric heat capacity is considered as another expression of specific heat capacity which measures the ability of a material to store thermal energy (Incropera et al., 2013), and it can be expressed as follows:

$$VHC = \rho * c_p \quad \text{Eq. 2-9}$$

Where; ρ is the density, measured in (kg/m^3), and VHC is the volumetric heat capacity, measured in ($\text{J}/\text{m}^3 \text{ K}$).

◆ *Measuring Specific Heat Capacity by Differential Scanning Calorimeter*

The specific heat capacity of pavement materials and mixes can simply be measured by means of a calorimeter and by monitoring heat fluxes and temperature changes (Asaeda et al., 1996).

The specific heat capacity of a material can also be determined from its value of thermal conductivity, thermal diffusivity and density (dos Santos, 2003) based on Eq. 2-10. The accuracy of this method will depend on the methods used to determine the values of other thermal properties.

DSC is a thermal analysis technique that looks at how a material's heat capacity is changed by temperature. The specific heat capacity can also be accurately measured using a Differential Scanning Calorimeter (DSC) (Xu and Chung, 2000, Vosteen and Schellschmidt, 2003). The advantage of this technique is a higher accuracy of determination of the heat capacity of materials (Mehling and Cabeza, 2008). The DSC technique can also determine the temperature-dependent specific heat capacity of materials. However, the DSC method can only be used for a small quantity, and cannot be applied to test the specific heat capacity of solid materials with a large size. As an asphalt mixture is a composite material consisting of aggregates of varied sizes, bitumen, and air voids, the DSC method will not be able to test a whole asphalt slab, though tests can obtain the specific heat capacity of each component of the mixture. But since there are many factors that affect the specific heat capacity of an asphalt mixture, so

averaging the specific heat capacity of each material may not provide the exact value for the mixture as a whole.

The total specific heat capacity of an asphalt concrete mixture can be calculated as the sum of the heat capacities of the constituents parts (aggregate and bitumen) by their relative proportions (Sundberg, 1988, Somerton, 1992, Hall, 2008). Total specific heat capacity can be expressed as follows:

$$c_p = \frac{1}{m_{total}} [m_{Aggregate} * c_{Aggregate} + m_{Bitumen} * c_{Bitumen}] \quad \text{Eq. 2-10}$$

Where; m is the mass of each constituent (kg), c is the specific heat capacity for each constituent (J/kg K), and c_p is the total specific heat capacity (J/kg K).

◆ ***Factors Affecting Specific Heat Capacity***

Aggregate Type and Content

Due to the high percentage of aggregate in the asphalt concrete mix which is around 95% of the total volume, and also because the different aggregate types have different specific heat capacity values (see **Table 2-2**), therefore the aggregate type and content will have a high impact on the specific heat capacity of the mix. Using an aggregate with high specific heat capacity will increase the total specific heat capacity of the mixture.

In addition, specific heat capacity can be affected by temperature variation. Specific heat capacity of the aggregates increases as temperature rises (Somerton, 1992, Dehdezi, 2012) (see **Table 2-3**). Somerton (1992) reported that the specific heat capacity of limestone, due to its calcite content, is higher than that of quartzite which mainly consists of quartz minerals.

Table 2-2 Specific Heat Capacity of Pavement Constituents (Sundberg, 1988, Somerton, 1992, Read and Whiteoak, 2003, Banks, 2012, Busby et al., 2009)

Aggregates/Pavement Constituents	Specific Heat Capacity (J/kg K)
Quartzite	701-800
Granite	790
Limestone	908
Basalt	804
Bitumen	2093

Table 2-3 Mean values of dry-state specific heat capacity of pavement components (Max variation of $\pm 7\%$) (Dehdezi, 2012)

Components	c_p (J/kg K)							
	-10°C	0°C	7°C	17°C	27°C	37°C	47°C	57°C
Limestone	793	838	859	878	892	904	917	931
Quartzite	609	629	642	659	675	693	709	724
Copper slag	628	670	679	691	701	712	723	734
Natural sand	610	637	655	679	698	711	721	734
Lyttag	620	712	741	767	778	787	799	812
Rubber	1194	1292	1326	1369	1406	1444	1485	1523
Hardened Cement Paste	877	1021	1094	1241	1458	1714	1978	2300
Ferag	521	552	562	575	586	589	609	618

Dawson et al. (2011), performed an experimental and numerical simulation of enhancements to the thermal properties of asphalt materials for heat storage and transfer application. The results showed that aggregate type and content has a major influence on the specific heat capacity. For example, the highest total specific heat capacity for a specimen was obtained when using limestone aggregate in the mix.

Porosity

Increasing the percentage of asphalt concrete porosity due to a low percentage of fine aggregate in the mixture will decrease the total weight of the sample which, in turn, will reduce the specific heat capacity of the material.

2.3.1.3 Thermal Diffusivity

Thermal diffusivity (α) is the coefficient that expresses the rapidity of temperature change when a material is exposed to a fluctuating thermal environment and is calculated as:

$$\alpha = \frac{k}{c_p * \rho} \quad \text{Eq. 2-11}$$

Where: α is the Thermal diffusivity, measured in (m²/s), k is the Thermal conductivity, measured in (W/m.K), ρ is the Density, measured in (kg/m³) and c_p is the Specific heat capacity, measured in (J/kg.K).

Thermal diffusivity describes the ability of a material to conduct thermal energy relative to its ability to store thermal energy (Incropera et al., 2007). The higher the thermal diffusivity, the faster is the rate of propagation of heat. A small value of thermal diffusivity (i.e. high volumetric heat capacity and low thermal conductivity) means that a large amount of heat will be absorbed by the material and only a small amount of heat will be conducted further.

◆ *Measuring Thermal Diffusivity*

Asaeda et al. (1996), Mrawira and Luca (2002), applied an experimental setup to measure the thermal diffusivity of pavement mixtures. In this method, at

least three thermocouples are positioned at equal distances. The thermal diffusivity can be determined by applying the heat source and recording the temperature change. The thermal diffusivity can be expressed as follows:

$$\alpha = \frac{(T_m^{i+1} - T_m^i)}{(T_{m+1}^i + T_{m-1}^i - 2 * T_m^i)} * \frac{\Delta z^2}{\Delta t} \quad \text{Eq. 2-12}$$

Where; α is the Thermal diffusivity, measured in (m²/s), Δz is the Depth increment, measured in (m), Δt is the time increment, measured in (s), i is the time node and m is the depth node.

◆ **Factors Affecting Thermal Diffusivity**

It is obvious from **Eq. 2-11** that, three factors can affect the thermal diffusivity; thermal conductivity, specific heat capacity and density. Thermal diffusivity increases with the ability of a body to conduct heat (k), and it decreases with the amount of heat needed to change the temperature of a body (c_p).

2.3.1.4 Thermal Effusivity

Thermal effusivity is a measure of a material ability' to exchange thermal energy with its surroundings ([Incropera et al., 2013](#)) and it is expressed as follows:

$$\beta = \sqrt{k * \rho * c_p} \quad \text{Eq. 2-13}$$

Where; β is the Thermal effusivity, measured in (J/s^{0.5}m²k), k , ρ and C_p are as previously defined.

A large value of thermal effusivity indicates that a large amount of heat can be absorbed by the material and also that a large amount of heat can be conducted further.

2.3.2 Surface Properties of Asphalt Mixtures

The three important surface properties of a material that have an effect on heat transfer are; absorptivity, reflectivity (albedo), and emissivity (see **Figure 2-3**).

2.3.2.1 Albedo

Reflectivity or Albedo is defined as the percentage of incoming radiation reflected from a surface ([Incropera et al., 2013](#)). Albedo values range from 0, for a perfect absorber (known as a black body), to 1, for perfect reflectors. Generally, dark surfaces have a low albedo and light surfaces have a high albedo. The albedo of a surface depends on the surface characteristics as well as the temperature. Due to the black colour of an asphalt concrete pavement, the reflected radiation is low. Asphalt concrete pavement generally has a solar reflectance of approximately 0.05 to 0.1 for a new pavement, and approximately 0.1 to 0.15 for an aged pavement ([Pavement-Research, 2002](#)). The low value of asphalt concrete albedo enhances the pavement material for solar energy harvesting applications as significant heat is going to be absorbed by the surface.

◆ *Measuring Albedo using Albedometers or Inverted Pyranometers*

An Albedometer is a device for measuring both the net global radiation and/or reflected radiation (albedo) over a surface. The albedometer consists of two matched Pyranometers mounted on a rod (see **Figure 2-8**). The top sensor measures the incoming global radiation, while the lower sensor faces down and measures reflected solar radiation. However, for measuring the reflected

radiation only, an inverted Pyranometer can be used, where a Pyranometer is inverted and faced down towards the surface.

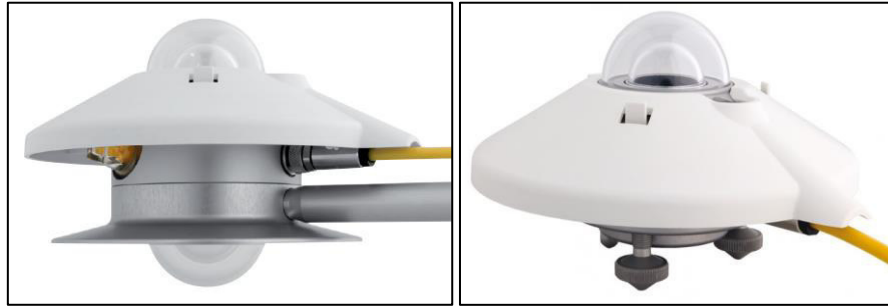


Figure 2-8 Albedometers and Pyranometer respectively (KIPP and ZONEN, 2003)

◆ ***Effect of Albedo on Pavement Temperature***

The surface of the road pavement collects the incident solar radiation. Having a low albedo material (increasing absorptivity), will increase the pavement temperature which in turn leads to more heat energy being harvested. [Gui et al. \(2007\)](#), investigated the effect of pavement thermo-physical properties on surface temperatures by developing a mathematical model. The results indicated that albedo has the highest positive effects on pavement maximum temperatures. A high albedo keeps a pavement cool and this could reduce rutting and the Urban Heat Island Effect; however, this is not ideal for the energy harvesting application.

The efficiency of energy harvesting from a pavement can also be improved by using a reflectivity-reducing and absorptivity-increasing top layer over the pavement. Laboratory results show that the use of black acrylic paint can increase the difference between incoming and outgoing water temperature in asphalt pavements containing pipes for energy harvesting by almost 50% ([Mallick et al., 2009](#)).

2.3.2.2 Emissivity

Emissivity is defined as the ratio of the energy radiated from a material's surface to that radiated from a blackbody (a perfect emitter) at the same temperature and wavelength and under the same viewing conditions (Cengel, 1998, Incropera et al., 2013). It is a dimensionless number between 0 (for a perfect reflector) and 1 (for a perfect emitter). Surface emissivity (ϵ) is a function of temperature, wavelength, and material type (Incropera et al., 2007). The range of typical values of emissivity for an asphalt concrete pavement is from 0.85 to 0.98 (Solaimanian and Kennedy, 1993, CIBSE, 2006, Incropera et al., 2007).

◆ *Measuring Emissivity by Infrared Camera*

Measuring the surface emissivity property of a material by infrared camera can be done through the following procedure:

Firstly, determine the actual temperature of the material using a sensor such as thermocouple or another suitable method. Secondly, measure the object temperature by infrared camera and adjust the emissivity settings until the correct value is reached and that would be the measured emissivity for that material.

2.3.2.3 Absorptivity

Absorptivity can be defined as the fraction of the radiation energy incident on a surface that is absorbed by the surface and its value ranges from 0 (for a perfect reflector) to 1 (for a perfect absorber) (Cengel, 1998, Das, 2010). It is normally a function of wavelength of the incoming radiation, surface colour, wetness, average temperature of pavement, and age of pavement surface

Chapter 2. Literature Review

(Solaimanian and Kennedy, 1993). The range of the typical values of absorptivity for an asphalt concrete pavement is from 0.82 to 0.93 (Solaimanian and Kennedy, 1993, CIBSE, 2006).

The absorptivity of a pavement surface generally decreases during its lifetime as the surface colour becomes lighter, and the reduction is quite marked in asphalt pavements (CIBSE, 2006). This reduction might be due to the high susceptibility of bitumen to aging and/or aggregate polishing under traffic.

Based on Kirchhoff's Law, for a body of any arbitrary material in thermodynamic equilibrium, the emissivity of a surface at a specified wavelength, direction, and temperature is always equal to its absorptivity at the same wavelength, direction, and temperature (Incropera et al., 2007).

2.3.3 Weather Condition

The main weather factors affecting pavement surface temperature are solar radiation, wind speed, humidity, rain and air temperature (Solaimanian and Kennedy, 1993, Hermansson, 2000, Hermansson, 2001, Marshall et al., 2001, Park et al., 2001). Solar radiation, wind and air temperature are climate factors which are of great importance for the temperature of the pavement surface (Hermansson, 2004). These parameters are the result of energy transfer and transformations within the atmosphere at the Earth's surface.

The temperature of road pavement varies due to several climatic factors. Ambient temperature can be considered as the most important factor. The next important factor is considered to be solar radiation. Generally, wind speed and

relative humidity are considered as being of less significance (Diefenderfer, 2002).

2.3.3.1 Solar Irradiation

Solar irradiation depends on the orientation of the Earth (see **Figure 2-9**), where changing the orientation affects the length of the day, angle at which the sunlight hits the surface and the amount of atmosphere the Sun's radiation must penetrate to reach the Earth's surface (Goswami et al., 1999). The availability of energy is affected by location (including latitude and elevation), season, and time of the day.

The greatest factors affecting the available energy are cloud cover and other meteorological conditions which vary with location and time (Goswami et al., 1999). Solar irradiation is considered as the main factor involved in heating up an asphalt pavement (Mallick et al., 2009). The incident irradiation can be measured by the Pyranometer device, see **Figure 2-8**.

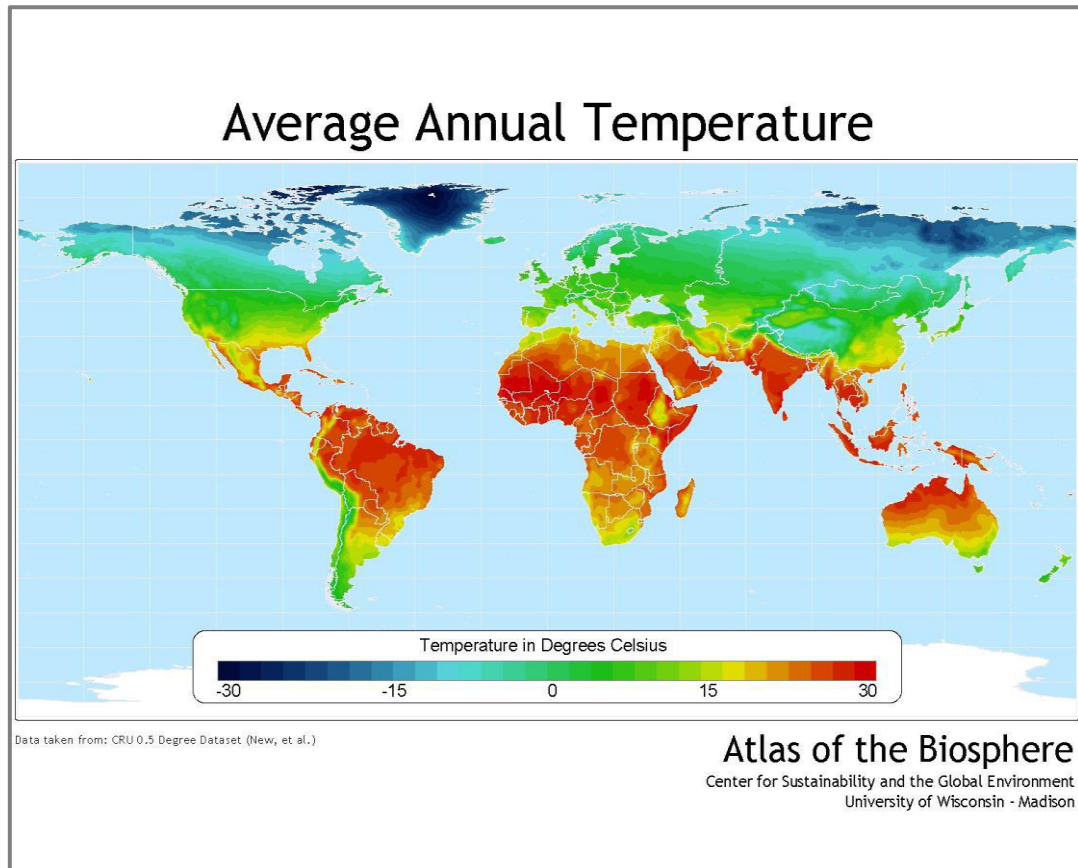


Figure 2-9 World Average Annual Temperature (World-Climate-Map, 2007)

2.3.3.2 Air Temperature

The radiation from the sun reaching the earth through the atmosphere generates heat on the ground. Therefore, air (ambient) temperature starts to increase as the solar radiation comes towards the Earth. The ambient temperature will vary with season and location. The average Earth temperature and pavement temperature at the surface are slightly higher than the average air temperature due to the absorption properties of the Earth and pavement (see **Figure 2-10**). This graph shows that the air temperature is between 14 and 17 °C during the summer, whereas the asphalt pavement temperature reaches 25 °C on average according to the Trafikverket data. As the air

temperature is directly affected by the solar radiation, therefore the factors affecting air temperature are orientation, season, winds, clouds and rain.

In addition, pavement temperature has an effect on air temperature, the radiation from the sun reaching the surface of the pavement making the pavement surface temperature higher than the air temperature due to the high absorptivity of the pavement material. Some of the heat absorbed by the pavement material will be radiated back (emitted) from the pavement surface to the atmosphere (urban heat island effect) and therefore, the near surface air temperature is increased. Air temperature can be measured with thermometers.

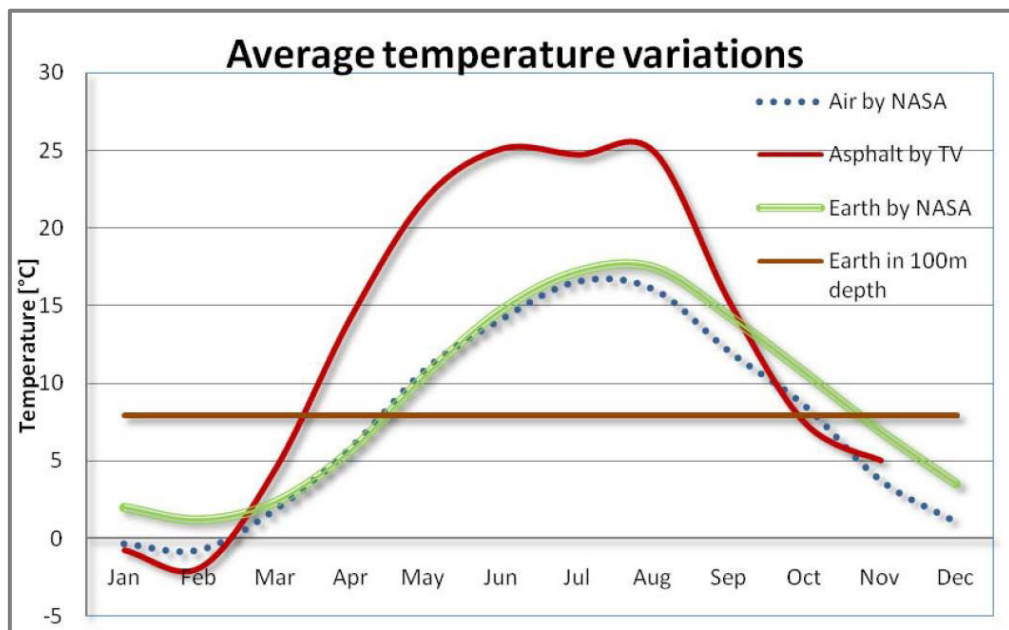


Figure 2-10 The average air, ground and asphalt temperature variations (Trafikverket, 2010, RETScreen, 2005)

2.3.3.3 Wind Velocity

Wind velocity is considered as the most important factor affecting heat transfer through its effect on heat convection. The convection heat flux is a function of fluid velocity and direction, and it is affected primarily by wind velocity and

Chapter 2. Literature Review

direction on the surface (Cenk and Khaled, 2002). Winds can either heat or cool a region by replacing the air in the region with new air from a warmer or colder region up wind depending on the air temperature and humidity (Goswami et al., 1999). Although temperature is the main factor affecting how warm or cold the surface is, the wind can also play an important role, making the surface colder than it would otherwise be. Wind cooling is caused by two factors; 1) the arrival of colder air allowing heat to move from the pavement to the air by convection and 2) due to the arrival of non-saturated air into which water in the pavement can evaporate thereby reducing pavement temperature due to the latent heat of evaporation effect. The higher the wind speed, the more heat is lost from the surface and it therefore becomes colder.

Dehdezi (2012), generated a wind by using two rotary fans to evaluate the performance of the model in windy conditions. The result indicated that the pavement surface temperature reduced by up to 13°C as a result of the wind applied (about 4.2 m/s) on the surface which can be attributed to the fact that surface convection heat transfer plays an important role in near-surface temperature profile. The wind speed can be measured by an Anemometer.

2.3.3.4 Rain

Water that falls from the clouds in the sky to the Earth's surface decreases the surface temperature and cools the surface down because the water coming from a high elevation is cooler than the air and the pavement. Rain intensity is dependent on the orientation and season (see **Figure 2-11**).

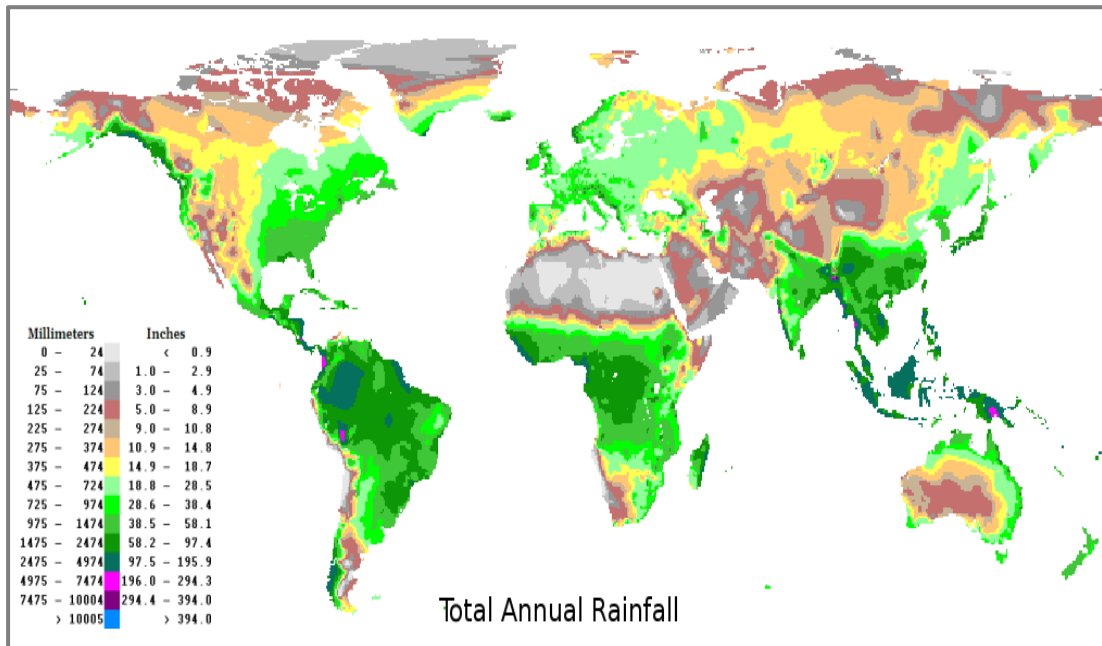


Figure 2-11 Total Annual Rainfall (World-Climate-Map, 2007)

2.4 Pavement Energy Harvesting Applications

Energy harvesting technology refers to applications that capture, gather and exploit the unused energy that comes from energy sources and convert it to a usable source of energy. This section will cover the most well-known existing energy harvesting applications from road pavement. It will not concentrate only on solar energy harvesting, but also other energy sources such as kinetic energy. Although this research covers pavement solar energy harvesting, mention of other energy harvesting applications from road pavements will illustrate the use of the road pavement as an energy harvesting resource.

Developments of new sources of renewable energy has increased greatly in the last few decades due to the increase in energy consumption by people and industries. Another reason behind renewable energy is ensuring a clean energy source that has a lower environmental impact than does a conventional energy source. One of the applications which has gained high attention in recent years

Chapter 2. Literature Review

as a source of renewable energy is harvesting energy from road pavements. Road pavements comprise a high percentage of the land in urban and rural areas which enhances the idea of using them as an energy source.

There are three main existing mechanisms for recovering energy from road pavements (see **Figure 2-12**):

- Converting kinetic energy (either people or vehicle movement) into electrical energy;
- Converting solar energy into thermal energy; and
- Converting solar energy into electrical energy.

Although this thesis concentrates on pavement solar energy harvesting, this section also summarizes some of the other major harvesting techniques that have been conducted in the pavement engineering sector.

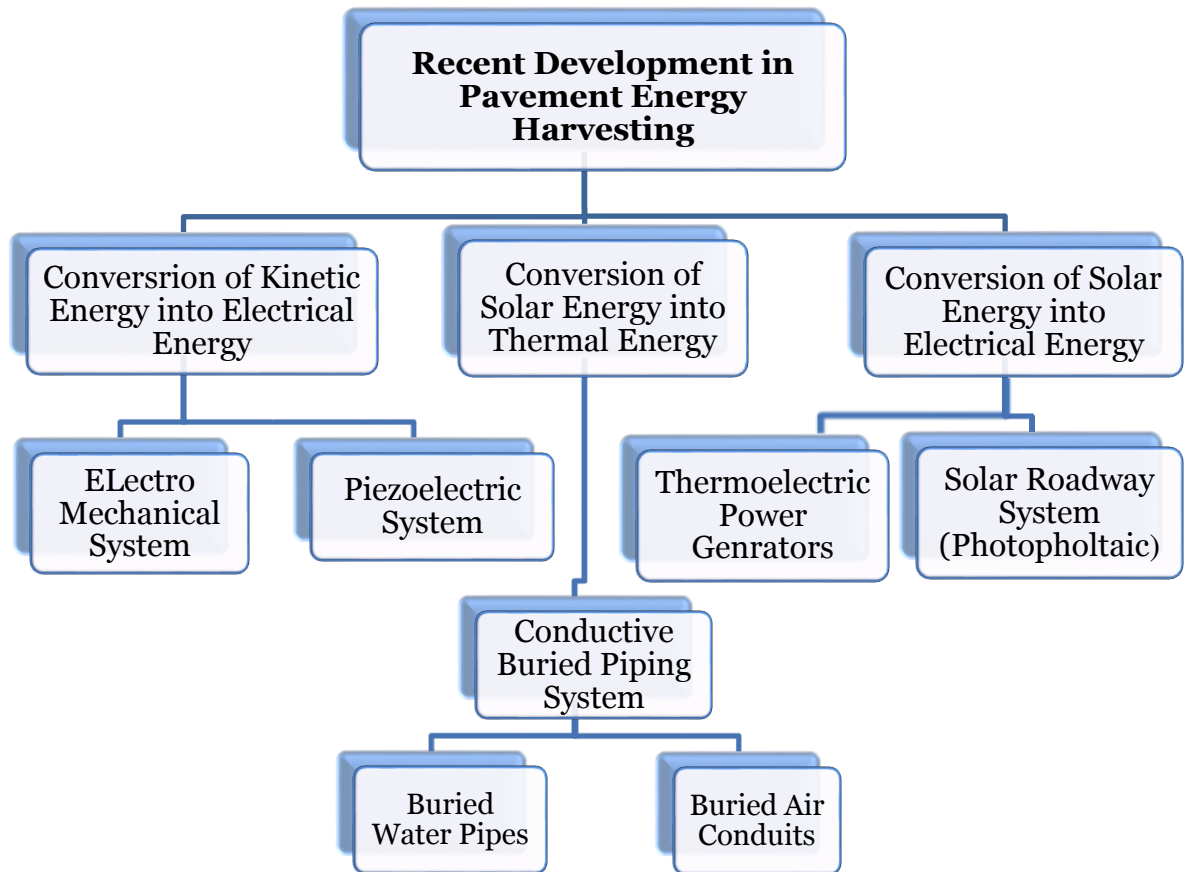


Figure 2-12 Pavement Energy Harvesting Applications

2.4.1 Conversion of Kinetic Energy into Electrical Energy

Over the last year, several attempts have been made to recover energy from pavements through converting mechanical load from vehicle and pedestrian movement into electrical energy, based on piezoelectric elements. A piezoelectric element is a device that generates voltage when subjected to mechanical stress or vibration or both. The next paragraph summarizes the three main well-known applications (Pavegen, Waynergy and Innovaattech Systems) that capture kinetic energy from vehicle and pedestrian movements and convert it into electrical energy.

Chapter 2. Literature Review

The Pavegen system captures kinetic energy from footsteps and converts it into electrical energy (Pavegen, 2012). This system consists of pavement blocks, with piezoelectric elements embedded. These blocks can be built in different dimensions and they can be applied to indoor or outdoor pavements (see **Figure 2-13**). Each time a person steps on a Pavegen slab, a slight displacement is registered on the vertical axis (up to 5mm), which is enough to generate electrical energy (Pavegen, 2012). The best locations for applying this system are busy streets, busy train and bus stations or schools.

The Waynergy system also captures kinetic energy from both people and vehicle movements and converts it into electrical energy (INPI, 2011, Waydip, 2012, WIPO, 2011). This system consists of pavement blocks with an independent power generation mechanism. When a load is applied, a displacement is registered on the vertical axis (1-3mm) which generates electricity (see **Figure 2-14**). Depending on their size, Waynergy blocks can be used for pedestrian $0.5 \times 0.5 \times 0.16 \text{ m}^3$ or for vehicles $3.0 \times 0.5 \times 0.16 \text{ m}^3$ (INPI, 2011, Waydip, 2012, WIPO, 2011).

INNOWAATTECH has developed piezoelectric generators which harvest the mechanical energy imparted to railways, roadways, and pedestrian ways from passing traffic and convert it into electricity (Ederly-Azulay, 2010). They consist of blocks in different shapes with a piezoelectric generator called IPEG™ which generates energy from the displacement on the vertical axis as the vehicle moves over the block area (see **Figure 2-15**).



Figure 2-13 Pavegen System (Pavegen, 2012)

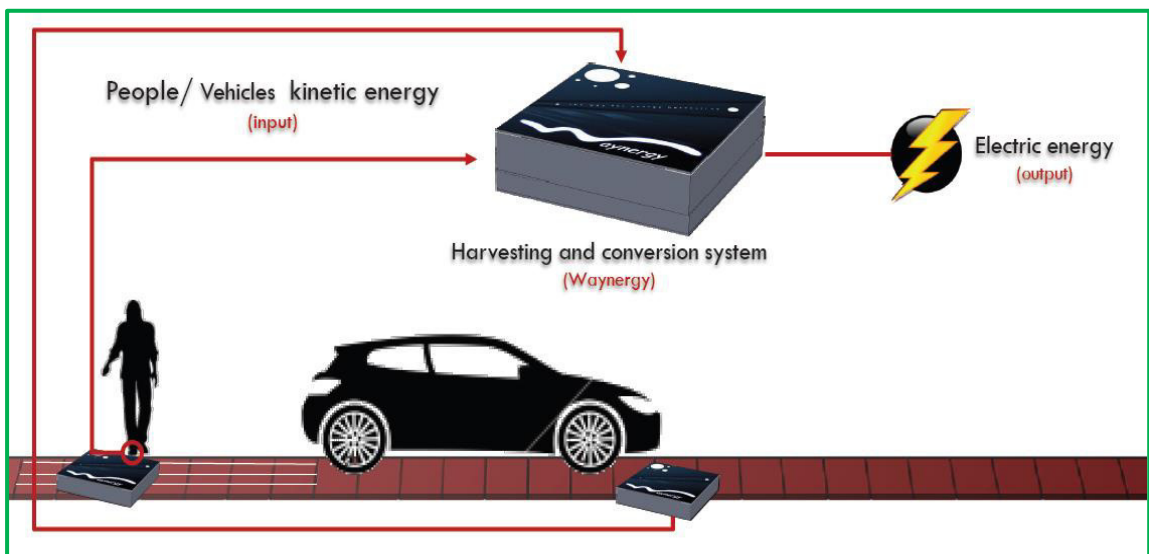


Figure 2-14 Waynergy System (Waydip, 2012)

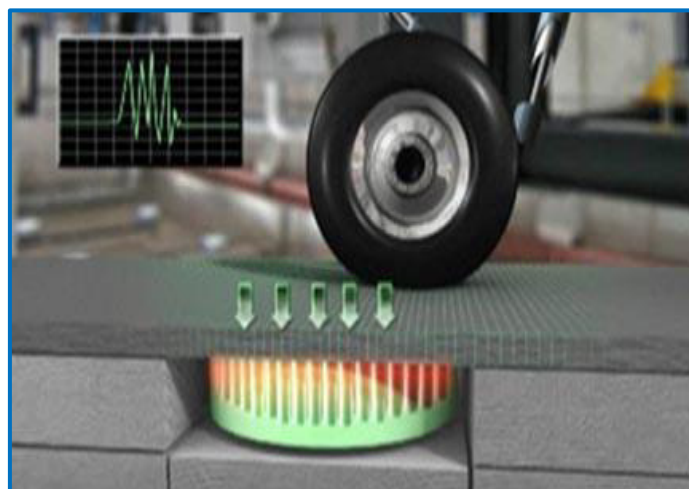


Figure 2-15 INNOWATTECH Company IPEGTM Piezoelectric System (Edery-Azulay, 2010)

2.4.2 Conversion of Solar Energy into Thermal Energy

Pavements cover a large area of our infrastructure including roads, pedestrian pathways, and parking areas (Hall et al., 2012). Asphalt pavements can heat up to reach 70 °C during solar irradiation in summertime because of their excellent heat-absorbing properties (Wang et al., 2010). As summarized by Bijsterveld et al. (2002), there are three potential ways of utilizing heat from pavements. The heat can be used to provide heating energy to buildings; it can be used to melt the snow on pavements in winter and keep its temperature higher than the natural level; or it can be extracted away from pavements during summer to reduce the potential for permanent deformation (or rutting).

Over recent years, although there have been previous attempts to recover heat energy from pavements, this work is still extremely limited in terms of installation. Incorporating tubes in the asphalt pavement is considered the most practical solution, applying a heat exchanger design. On the market, there are two existing systems, one in the Netherland (Ooms) and one in the UK (ICAX^{Ltd}), which both used embedded pipes in the pavement to extract the heat. The Ooms ‘Road Energy System’ (see **Figure 2-16**) is a method for heating and cooling buildings and roads (Sullivan et al., 2007). This method works as follows: in summer, cold water is pumped up from an aquifer and transported through pipes in the upper part of the asphaltic layers of a pavement. Due to the effect of the sun, the water gets warm. Via a heat exchanger, this heat is transported into another underground reservoir and held at this location until required. In winter, the system operates in the opposite way. The previously

Chapter 2. Literature Review

stored heated water flows from the hot storage medium to the road or buildings for heating purposes or for de-icing the pavements (Sullivan et al., 2007).

Another major instrumented trial of solar energy collector and storage techniques was undertaken by Transport Research Laboratory (TRL) in the UK (ICAX^{Ltd}) (Carder et al., 2008). The ICAX^{Ltd} system collects solar heat from the asphalt pavement surface in the summer through embedded pipes and stores it in shallow isolated ground heat storage. The stored heat can be used for ice prevention on the road surface during winter and for building heating (see **Figure 2-17**).

There are other studies on the use of asphalt solar collectors as snow melting systems, such as SERSO (Eugster, 2007) and GAIA (GAIA, 1998). SERSO is a Swiss system, which consists of pipes embedded in a bridge deck, and is used to capture and store the heat in the summer and use this heat later in the winter for de-icing the bridge surface. The GAIA system is also a snow melting system installed in 1995 in Ninohe, Japan, which consists of pipes embedded under the pavement surface.

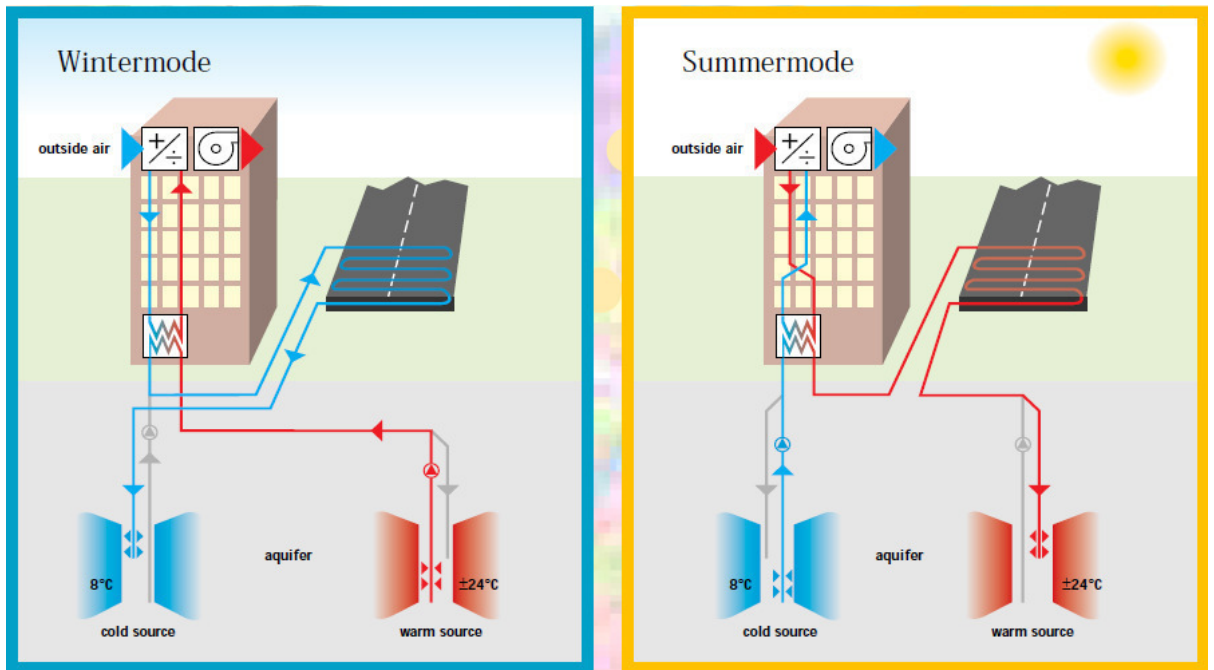


Figure 2-16 Road Energy System invent by Ooms Avenhorn Holding (De Bondt, 2003)

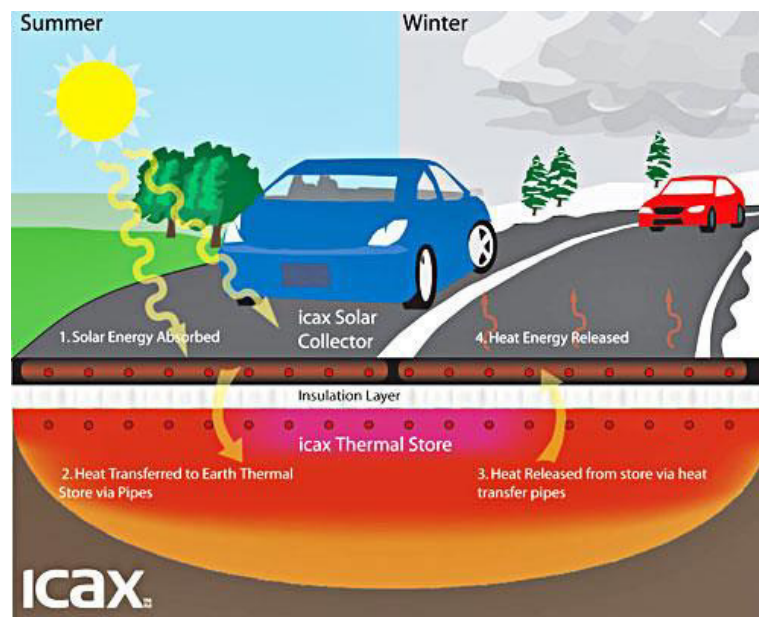


Figure 2-17 ICAX™ Asphalt Solar Collector System (ICAX, 2012)

2.4.3 Conversion of Solar Energy into Electrical Energy

This is similar to the system described in Section 2.4.2 in terms of using the same source of heat which is the heat coming from the sun. This system aims to convert solar heat into electrical energy through replacing all concrete and

Chapter 2. Literature Review

asphalt surfaces that are exposed to the sun with solar road panels. The Solar Roadways System consists of panels, where each individual panel consists of three basic layers; Road Surface Layer, Electronics layer, and Base Plate Layer (see **Figure 2-18**). The road surface layer provides the strength to protect the electronic layers beneath it, works as water proof layer, and lets the sunlight pass through. The electronics layer collects the light that passes the first layer and transforms it into electricity. The base plate layer distributes the power collected from the electronics layer. In addition, it also works as a waterproof layer for the electronic layer (SR, 2012).

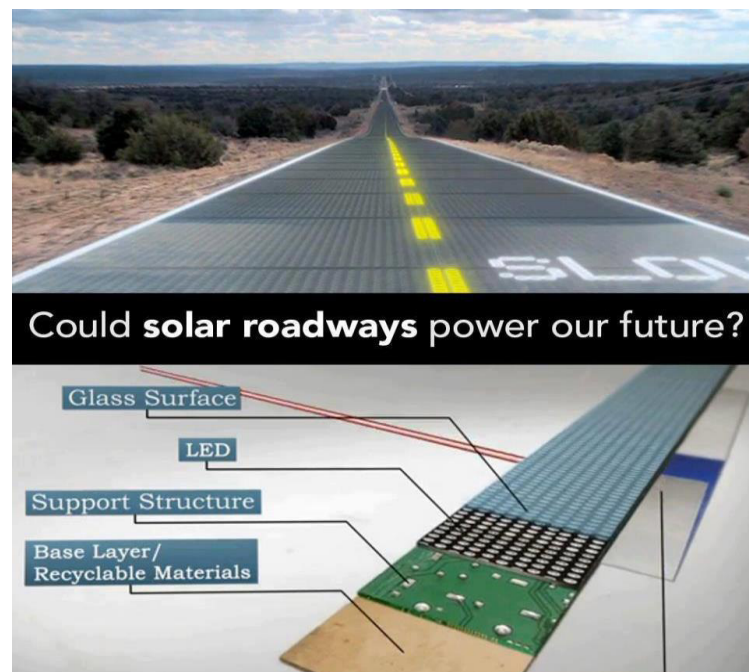


Figure 2-18 Solar Roadway System (SR, 2012)

Another promising technique for beneficially recovering waste heat is the use of Thermoelectric Power Generators (TEG) (Snyder, 2006). A TEG is a solid-state device that provides direct energy conversion from thermal energy (heat) due to a temperature gradient into electrical energy based on the “Seebeck effect”. The Seebeck effect occurs when a temperature difference exists between

Chapter 2. Literature Review

two dissimilar electrical conductors, producing a voltage across two materials. The magnitude of the voltage generated is proportional to the temperature gradient where it increases with the increase in temperature difference. TEG systems have been used widely in industrial manufacture where the temperature difference is high whereas it has not been used much for low temperature applications such as in road pavements. TEGs contain no moving parts and are completely silent unlike traditional dynamic heat engines. The major drawback of TEGs is their relatively low conversion efficiency (typically ~5%) (Nolas et al., 2013) compared to large traditional heat engines. For small applications, TEGs can become competitive because they are compact, simple (inexpensive) and scalable (Liu, 2014). Thermoelectric systems can easily be designed to operate with small heat sources and small temperature differences.

Most of the recent research on thermoelectric power generators applications have been directed towards utilisation of industrial waste heat (Riffat et al., 2003). Vast amounts of heat are rejected from industry, manufacturing plants and power utilities as gases or liquids at temperature which are too low to be used in conventional generating units (<450 K). In particular, the replacement of by-heat boiler and gas turbine by thermoelectric power generators makes it capable of largely reducing capital cost, increasing stability, saving energy source, and protecting environment (Weiling et al., 2004).

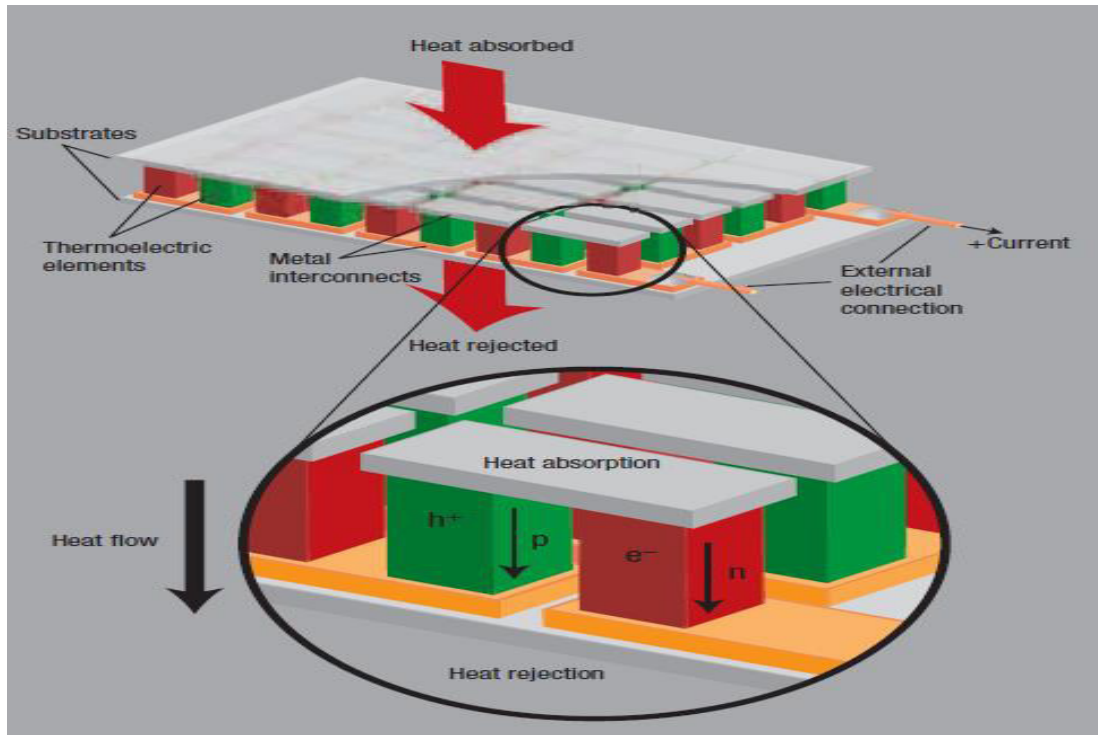


Figure 2-19 Schematic Diagram of Thermoelectric Power Generator

2.5 Summary

The following key summary has been drawn based on the previous review about harvesting solar energy from road pavements:

- The thermal properties of asphalt concrete pavement (the ability of material to absorb and conduct heat) are the most important factors that have an effect on the asphalt mixture temperature profile. Although different studies have been carried out to identify the key factors that can beneficially affect the heat transfer properties of asphalt mixtures, thereby increasing the overall efficiency of solar applications, further research is required to address these factors under different climate conditions.

Chapter 2. Literature Review

- Various previous studies have been carried out to improve the heat transfer and storage properties of asphalt pavement mixture through the use of high thermal conductive aggregate instead of using conventional aggregate. In addition, high thermal additive fillers were used with an aim to increase the thermal conductivity of the asphalt mixture. Furthermore, the surface of the pavement can be painted with a black sealer in order to decrease the albedo and increase the absorptivity of the asphalt concrete material. There is a need to conduct a detailed study on the possibility of identifying techniques that could enhance the thermal properties of asphalt concrete pavements in order to increase the overall efficiency of energy harvesting applications.

- Road pavements could be used as a source of energy harvesting, due to their excellent heat absorbing properties and the large existing areas of infrastructure which include roads, pedestrian pathways and parking areas. In addition, the heat harvested from road pavements could also reduce the Urban Heat Island effect and the rutting potential of asphalt pavements by reducing the pavement temperature.

- The existing application of harvesting solar energy from road pavement is extremely limited especially in terms of installation. Buried tubes with water circulating inside the asphalt pavement are considered the most practical solution for a heat exchanger in terms of installation. Although there is existing research into using buried tubes with air circulating as a heat exchanger design, it is still at the early stage of its development. Therefore, there will be a need for significant research effort to identify

Chapter 2. Literature Review

other heat transfer and exchanger systems and to assess their performance.

- Thermoelectric Power Generators (TEG) are unique devices which convert thermal energy (heat) directly into electrical energy based on the “Seebeck effect”.

3. Effect of Air Voids Content on Thermal Properties of Asphalt Mixtures under Dry Conditions

3.1 Introduction

Evaluating the thermal behaviour of asphalt pavements requires understanding the surface and thermo-physical properties that affect transport and storage of heat (Stempihar et al., 2012). There are two distinct categories of these properties: those related to transport of energy through a system and those related to the thermodynamic or equilibrium state of a system (Incropera et al., 2013). Heat transfer properties of asphalt mixture are absorptivity (α), albedo ($1-\alpha$), emissivity (ϵ) and thermal conductivity (k). Thermodynamic properties of asphalt concrete include density (ρ) and specific heat capacity (c_p) which are related to the equilibrium state of a system (Incropera et al., 2013).

At present, it is known that the thermal behaviour of asphalt mixture is mainly influenced by its air voids content, aggregate type and moisture content, although the interactions between these factors are mostly unknown and have been studied mainly from on-site observations under diverse climatic conditions, not from controlled laboratory tests (Stempihar et al., 2012). In addition, previous research has attempted to change the factors influencing the thermal properties of asphalt pavements, e.g. the influence of moisture on the temperature of porous and dense asphalt mixture (Leong, 1998); the thermal conductivity of aggregates, such as graphite, steel fibres or steel particles (Wu

et al., 2001, Mallick et al., 2008, Dawson et al., 2011); or the surface colour of the pavements (Mallick et al., 2009); but there is no extensive study about the effect of air voids content on the thermal properties of asphalt roads.

For this reason, the main objective of this chapter is to quantify the extent to which the air voids content of an asphalt mixture influences its thermal conductivity, specific heat capacity or heat absorptivity and explain the influence of these factors on the temperature evolution of asphalt mixture slabs when their surface is exposed to a source of heat.

3.2 Material Selection

3.2.1 Bitumen

In this study, a conventional 40/60 penetration grade bitumen binder was selected to use for the production of asphalt concrete mixture samples since it is in common use in asphalt pavement construction. Based on BS EN 2000-49:2007 and BS EN 2000-58:2007, the softening point and penetration grade were found to be 53.80 C and 40 dmm, respectively.

3.2.2 Aggregate

Local limestone was selected to be used in this study due to its wide use in asphalt pavement construction. This limestone was provided by Tunstead Quarry, Staffordshire, UK. The particle size distribution (gradation) of all tested samples was based on four different coarse aggregate sizes of 20, 14, 10 and 6mm and a fine aggregate size of 4mm.

3.3 Material Preparation

To study the effect of air voids content on thermal properties of asphalt concrete mixtures, test samples with various air voids contents ranging from 4% to 26% have been studied.

3.3.1 Aggregate Gradation

The aggregate gradation was designed for six target air voids (TAV) contents of 4.5 %, 10.0 %, 13.0 %, 17.0 %, 21.0 % and 26.0 %. The aggregate gradation for the dense asphalt concrete mixture with 4.5% air void content was designed in accordance with the British standard for binder course layer 0/20mm **BS EN 12591 (2009)** (see **Table 3-1**), whereas the aggregate gradation for the porous asphalt concrete mixture with 21% air voids content was designed in accordance with a Dutch Standard (**Van Der Zwan et al., 1990**). The Dutch standard has been used in this study as it is considered to be a well-recognized standard for this type of asphalt pavement.

The aggregate gradation curves for asphalt mixtures with air voids contents of 10%, 13% and 17% were between those for 4.5% and 21%, whereas the aggregate gradation for the asphalt concrete mixture with 26% was outside those for 21%. Full details of the procedure are presented in Appendix A. **Figure 3-1** shows the particle size distribution and bitumen content for all target air voids contents.

Table 3-1 Specification for 0/20 mm size dense binder course (BS 4987 part 1, 2005)

Sieve size(mm)	% by mass Passing	% passing select
31.5	100	100
20	95-100	97
14	65-85	80
10	52-72	65
6.3	38-56	45
4	-	35
2	20-40	25
1	-	15
0.25	6-20	5
0.063	2-9	8

Target binder content 4.7% by mass of total mixture ($\pm 0.6\%$).
40/60 is the preferred grade for binder.

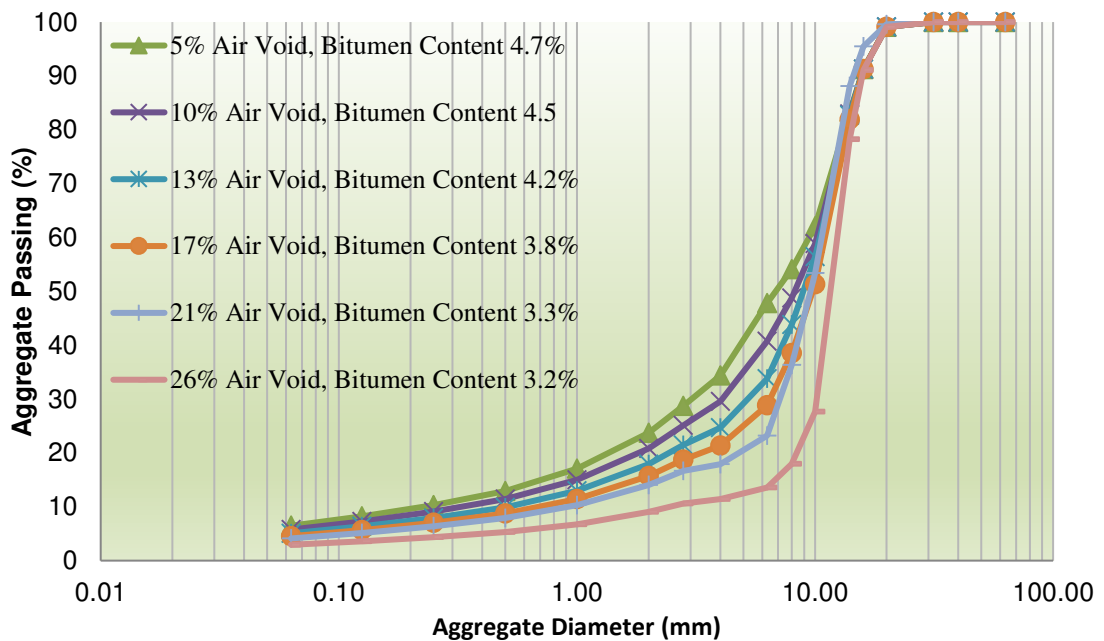


Figure 3-1 Composition of asphalt mixtures

3.3.2 Test Sample Preparation

The limestone aggregate was oven dried and then mixed with the binder at a temperature of 160 °C. Five slabs with a size of (306 x 306 x 50 mm³) were manufactured for each target air voids content and compacted to the target density using a laboratory roller compactor at a temperature of 140 °C.

3.4 Test Sample Density

3.4.1 Maximum Density

The maximum density is the ideal mass of asphalt concrete per unit volume, without air voids. There are three methods discussed in [BS EN 12697 part 5 \(2009\)](#) for determining the maximum density: the volumetric procedure, the hydrostatic procedure, and the mathematical procedure. In this study, the maximum density of asphalt mixture was determined through [BS EN 12697 PART 5 \(2009\)](#) by the mathematical method as the apparent densities of the aggregates and bitumen were measured in the laboratory.

$$\rho_m = \frac{100}{(p_{a1}/\rho_{a1})+(p_{a2}/\rho_{a2})+\dots+(p_b/\rho_b)} \quad \text{Eq. 3-1}$$

Where: ρ_m is the maximum density of the mixture, measured in Mg/m³, p_{a1} is the proportion of aggregate 1 in the mixture (by mass), measured in (%), ρ_{a1} is the apparent density of aggregate 1, measured in (Mg/m³); p_{a2} is the proportion of aggregate 2 in the mixture (by mass), measured in (%), ρ_{a2} is the apparent density of aggregate 2, measured in (Mg/m³); p_b is the proportion of binder in the mixture (by mass); ρ_b is the density of the binder, measured in (Mg/m³).

3.4.2 Bulk Density

The bulk density of the mixture is the mass per unit volume, including the air voids, of the sample. There are four methods discussed in [BS EN 12697 part 6 \(2003\)](#) for determining the bulk density. The dimension method was used to measure the bulk densities of all asphalt concrete test samples. In addition, the foil method was used to measure the bulk densities for selected samples for

Chapter 3. Effect of air voids content on thermal properties of asphalt mixtures

comparison purposes. The following procedure was carried for the dimension method.

Firstly, the dimensions of the test samples in millimetres were measured in accordance with **BS EN 12697-29**. Secondly, the mass of the dry test sample was measured in grams. Finally, **Eq. 3-2** was used to calculate the bulk density for each asphalt concrete test sample.

$$\rho_{b,dim} = \frac{m_1}{h \times l \times w} \times 10^6 \quad \text{Eq. 3-2}$$

Where: $\rho_{b,dim}$ is the bulk density of the specimen, measured in (kg/m³); m_1 is the mass of dry test sample number 1, measured in grams (g); h is the height of the specimen, measured in millimetres (mm); l is the length of the specimen, measured in millimetres (mm) and w is the width of the specimen, measured in millimetres (mm).

In order to check the results from the dimension method, the bulk densities of five selected test samples were measured by the foil method following this procedure:

Firstly, the mass of the dry test sample was measured. Secondly, the water density was measured. Thirdly, the dry test sample was sealed in a foil. Fourthly, the mass of the sealed sample was measured. Fifthly, the mass of the sealed sample immersed in water bath was measured. Finally, the bulk density of the sealed sample was calculated using the following equation:

$$\rho_{bsea} = \frac{m_1}{(m_2 - m_3)/\rho_w - (m_2 - m_1)/\rho_{sm}} \quad \text{Eq. 3-3}$$

Where: ρ_{bsea} is the bulk density sealed in kg/m³; m_1 is the mass of the test dry sample, measured in (g), m_2 is the mass of the sealed sample, measured in (g), m_3 is the mass of the sealed sample immersed in water, measured in (g), ρ_w is the density of the water at test temperature, measured in kg/m³; and ρ_{sm} is the density of the sealing material at test temperature in kg/m³. **Table 3-2** illustrates the bulk density and the maximum density for all test samples.

3.5 Test Sample Air Voids Content

The air voids content of each asphalt mixture was calculated based on the maximum and bulk density calculations. The percentage of air voids in the mixture can be calculated as:

$$V_m = \frac{\rho_m - \rho_b}{\rho_m} \times 100\% \quad \text{Eq.}$$

3-4

Where: ρ_m is the theoretical maximum density of the mixture without voids, measured in kg/m³, ρ_b is the bulk density in the mixture, measured in kg/m³, and V_m is the air voids content in the mixture, measured in %.

3.6 Experimental Program and Measurements

This section describes the design and construction of the experimental setup and also outlines the methods used to measure the model parameters such as temperature profiles, solar irradiation, thermo-physical properties (i.e. thermal conductivity, specific heat capacity, thermal diffusivity and thermal effusivity) and surface properties (i.e. Emissivity, Albedo, Absorptivity).

Table 3-2 Test sample maximum density, bulk density and air voids content

Target Air Voids Content (%)	Sample No.	Maximum Density (kg/m ³)	Bulk Density (kg/m ³)	Measured Air Voids Content (%)	Mean Air Voids Content (%)
4.5%	1	2496.0	2318.4	7.1	6.2
	2	2496.0	2371.7	5.0	
	3	2496.0	2331.9	6.6	
	4	2496.0	2356.2	5.6	
	5	2496.0	2330.7	6.6	
10.0%	6	2505.0	2264.9	9.6	10.2
	7	2505.0	2217.8	11.5	
	8	2505.0	2263.1	9.7	
	9	2505.0	2256.0	9.9	
	10	2505.0	2244.4	10.4	
13.0%	11	2519.0	2125.1	15.6	13.1
	12	2519.0	2232.1	11.4	
	13	2519.0	2186.8	13.2	
	14	2519.0	2172.6	13.8	
	15	2519.0	2231.4	11.4	
17.0%	16	2534.0	2143.6	15.4	17.2
	17	2534.0	2090.8	17.5	
	18	2534.0	2092.6	17.4	
	19	2534.0	2055.9	18.9	
	20	2534.0	2108.7	16.8	
21.0%	21	2555.0	1999.8	21.7	21.4
	22	2555.0	2021.1	20.9	
	23	2555.0	2004.7	21.5	
	24	2555.0	1996.7	21.9	
	25	2555.0	2020.6	20.9	
26.0%	26	2553.0	1925.8	24.6	25.0
	27	2553.0	1906.1	25.3	
	28	2553.0	1932.3	24.3	
	29	2553.0	1898.7	25.6	
	30	2553.0	1903.4	25.4	

3.6.1 Experimental Setup

Figure 3-2 and **Figure 3-3** illustrate the apparatus and experimental setup used to carry out the laboratory testing of asphalt concrete slabs. For this purpose, a rectangular box of 18 mm thick birch ply wood sheet, with an area of 392 × 392 mm² and a height of 75 mm was constructed to insulate the test samples during testing. The bottom and all four edges of the box were insulated

using 25 mm Polyisocyanurate boards in order to minimize heat losses or gains (see **Figure 3-4**). This mould contained asphalt mixture slabs of $306 \times 306 \times 50 \text{ mm}^3$ which had been prepared in a laboratory roller compactor.

Experimental tests were carried out at a constant air temperature (room temperature) of approximately $25 \text{ }^\circ\text{C} \pm 1$ and an average relative humidity of 50%. Infrared lamps were used as a source of heat. The heat source comprised four 250 W infrared lamps installed in two rows at approximately 730 mm (to simulate a real life temperature profile) above the asphalt concrete slab surface, covering the whole asphalt concrete test sample area (see **Figure 3-2** and **Figure 3-3**). The infrared lamps were fitted to a steel frame which was designed and constructed at the Nottingham Transportation Engineering Centre laboratory. Asphalt samples with air voids content closer to the target air voids content were selected and tested, see **Table 3-2**. The test was repeated three times for each asphalt sample.

In order to measure the emissivity of the asphalt concrete test samples, an infrared camera was setup at a constant distance from the test samples with a vertical angle of approximately 70° (see **Figure 3-3**).

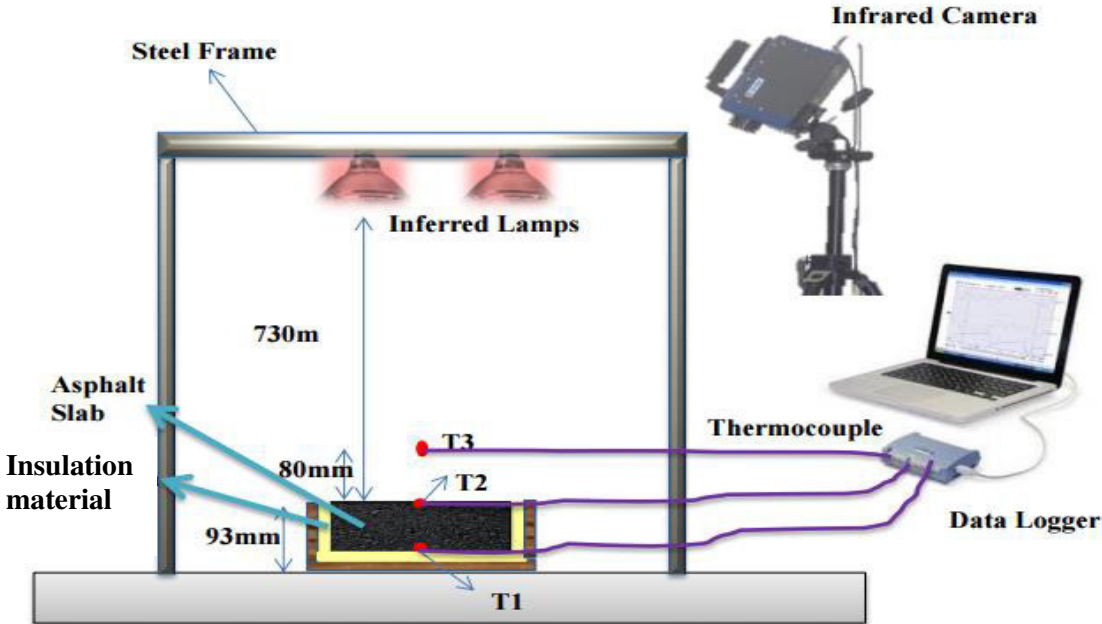


Figure 3-2 Experimental setup schematic diagram

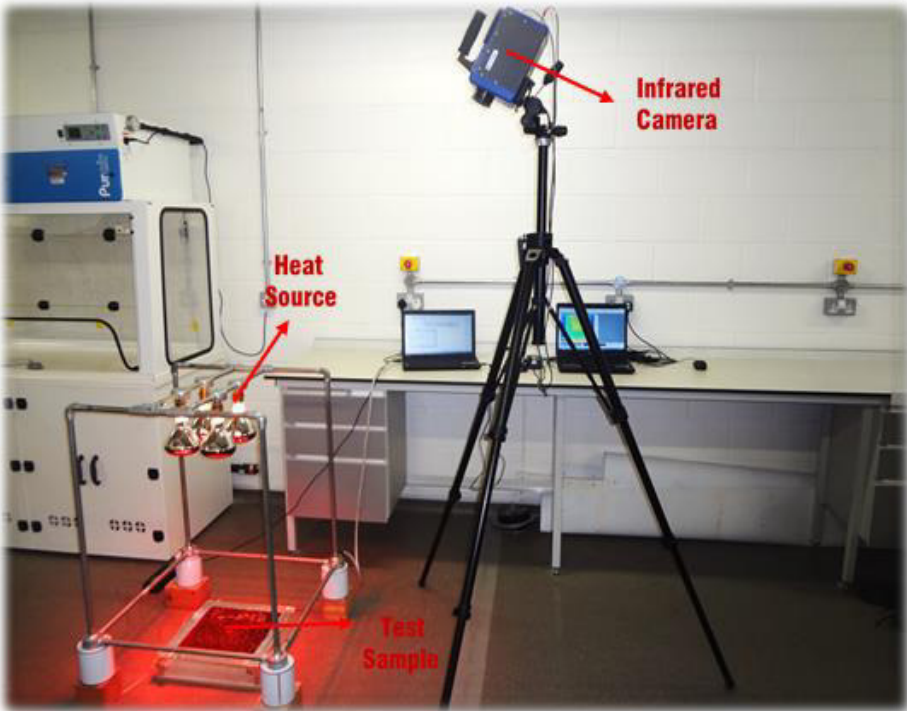


Figure 3-3 Laboratory Experimental Setup



Figure 3-4 Test sample preparation

3.6.2 Experimental Measurements

3.6.2.1 Irradiation Intensity Measurements

Solar intensity was measured using a pyranometer (Kipp & Zonen CMP 11) that measures the solar intensity up to 4000 W/m² with an accuracy of $\pm 3\%$ (see **Figure 3-5**). The pyranometer was levelled and positioned under the infrared lamps at the centre of the asphalt concrete slabs. To measure the heat intensity received by the asphalt concrete surface from the heat source at the position of the thermocouple, the height of the pyranometer sensor from the heat source was set at 730 mm. This height has been identified so the maximum steady state temperature of the asphalt slabs would not exceed 95 °C.

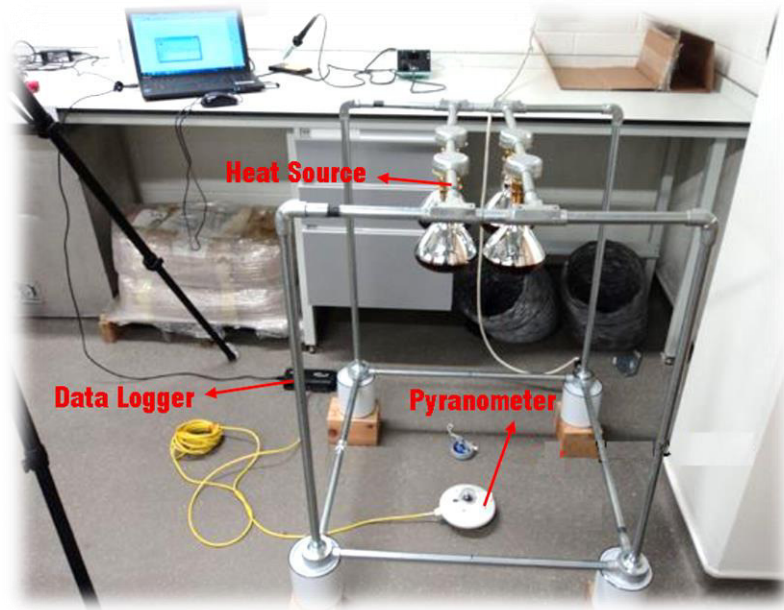


Figure 3-5 Irradiation intensity measurements

3.6.2.2 Temperature Profile

The temperatures of the air, the surface and the bottom of the asphalt concrete test samples were measured using J-type thermocouples. The test sample's cross-section and the position of thermocouples in the asphalt samples are shown in **Figure 3-2**. The temperature profile was recorded for 20 minutes under a constant environmental temperature of approximately 25°C before turning the infrared lighting on. The temperature evolution of test samples was measured during 12 hours heating and during 12 hours cooling down as shown in **Figure 3-6**, to simulate day and night time periods.

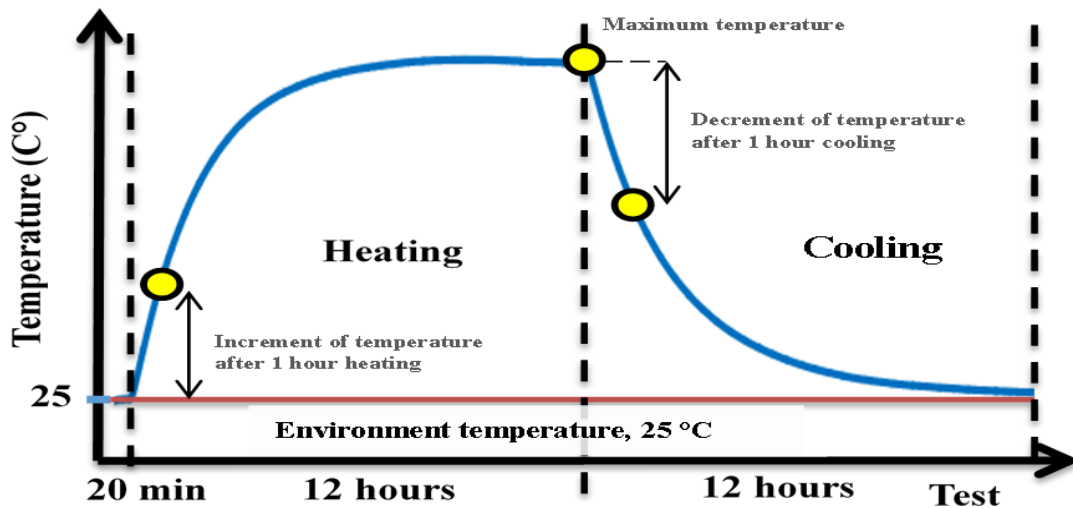


Figure 3-6 Schematic temperature evolution of the test samples

3.6.2.3 Data Acquisition System

The thermocouples and pyranometer were connected to a data logger (omega OMB-DAQ-54) where temperature profile and intensity rate were recorded at 2 second intervals.

3.6.2.4 Thermal Conductivity

The thermal conductivity of the asphalt concrete test samples was measured using a computer-controlled P.A. Hilton B480 uni-axial Heat Flow Meter (HFM) apparatus, due to its high accuracy and suitability for non-homogeneous mixtures. The HFM method measures steady state heat transfer through a material according to ASTM Standard C518, ISO 8301. **Section 2.3.1.1** described this method in more detail.

The thermal conductivity tests were performed on asphalt concrete slabs with dimensions $306 \times 306 \times 50 \text{ mm}^3$. The test samples were placed inside the apparatus between a temperature-controlled hot plate and a water-cooled cold

Chapter 3. Effect of air voids content on thermal properties of asphalt mixtures

plate connected to a thermoelectric chiller device. Two pieces of silicon rubber were used to ensure full contact between the asphalt concrete samples and the plates.

Once the test samples reached steady-state conditions, the thermal conductivity of the specimen was calculated using **Eq. 3-5 (BS EN 12697 PART 5, 2009)**:

$$k = \frac{l_s \cdot \left[(k_1 + (k_2 \cdot \bar{T})) + ((k_3 + (k_4 \cdot \bar{T})) \cdot HFM) + ((K_5 + (K_6 \cdot \bar{T})) \cdot HFM^2) \right]}{dT} \quad \text{Eq. 3-5}$$

Where: $k_1 - k_6$ are the calibration constants of the apparatus determined separately (from testing a sample of known thermal conductivity); $\bar{T} = \frac{T_{hot} + T_{cold}}{2}$ is the average temperature of the hot and cold plates, measured in (°C); $dT = T_{hot} - T_{cold}$, also measured in (°C); HFM is the heat flow meter output; and l_s is the thickness of the slab, measured in (mm).

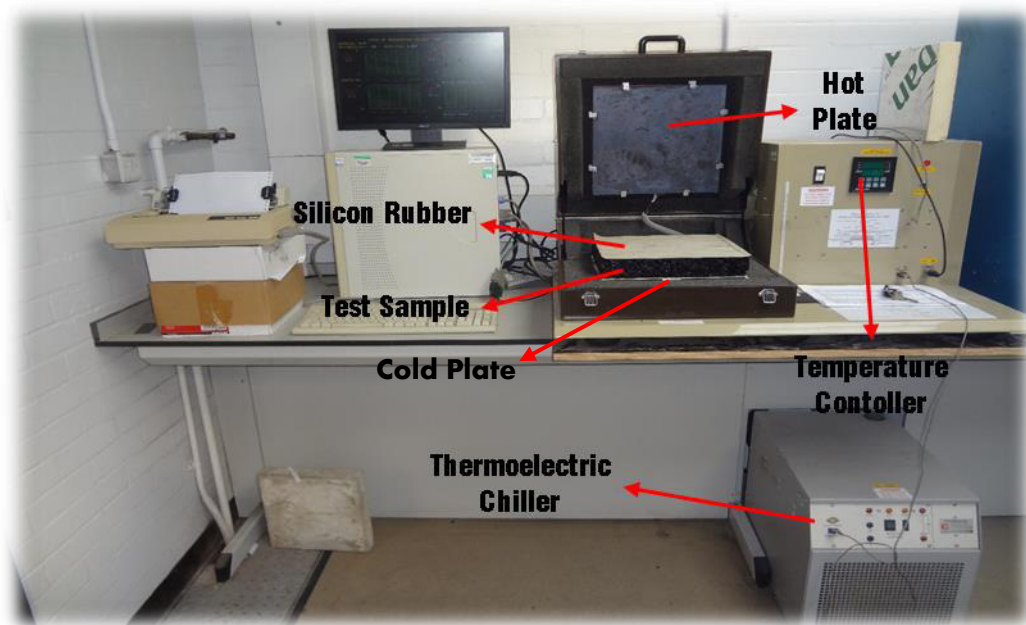


Figure 3-7 Thermal Conductivity Measurements by Heat Flow Meter

3.6.2.5 Emissivity Measurements

The surface emissivity of the pavement was measured using a high-resolution infrared camera (FLIR SC7000), with a spectral range of 3.5-5.0 μm and a sensitivity of 0.07 $^{\circ}\text{C}$, connected to the FLIR system software (ALTAIR) (see **Figure 3-8**). **Section 2.3.2.2** described this method in more detail.

The emissivity test was undertaken following this procedure:

- The slabs were heated using the infrared lamps until the surface and bottom temperatures reached a steady state condition (both temperatures were monitored using readings obtained from thermocouples).
- The infrared camera was turned on, and a point close to the surface thermocouple was selected, using the ALTAIR software to measure the temperature at the selected point (see **Figure 3-8**).
- The heat source was turned off.
- The emissivity value in the Altair software was varied until the readings from the infrared camera matched the surface temperature obtained from the thermocouples.
- The emissivity values were recorded at 5 $^{\circ}\text{C}$ temperature intervals, from 45 $^{\circ}\text{C}$ to 85 $^{\circ}\text{C}$.
- The final emissivity value was calculated by averaging the previously measured emissivity values.

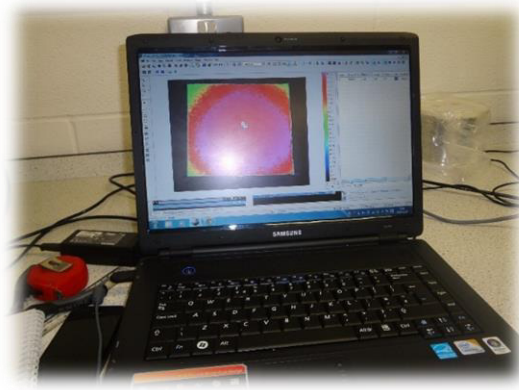


Figure 3-8 Emissivity Measurements by Infrared Camera and using ALTAIR Software

3.6.2.6 Heat Accumulation in Asphalt Mixture

The average temperature in the test samples during infrared heating and cooling can be considered as the area under the temperature-time curve (A_{tt}) in **Figure 3-6** divided by the total testing time. This method is similar to that used previously (García et al., 2013). For this purpose, the total area under the temperature-time curve was calculated using rectangles as the basic geometric units, dimensions being obtained from the temperature data at intervals of 2s:

$$A_{tt} = \frac{\sum_0^i (T_i - T_{env}) \cdot \Delta t}{t_t} \quad \text{Eq. 3-6}$$

Where: i is the number of measurements obtained during the heating-cooling tests; T_i is the average temperature between the surface and the bottom for each measurement, measured in °C or K; T_{env} is the environmental temperature, measured in °C or K; Δt is the time interval between each measurement, measured in seconds, and t_t is the total amount of seconds in 24 hours, 86,400 seconds.

In addition, the total amount of heat in the mixture can be calculated as:

$$Q = m \cdot c_p \cdot \Delta T \quad \text{Eq. 3-7}$$

Where: m is the total mass of each test specimen, measured in (kg), and c_p is the specific heat capacity of the test specimens, measured in (J/kg.K).

3.6.2.7 Computed Tomography Scans

Asphalt mixtures were observed in a XRadia Versa XRM-500 scanner operated at 80 kV and 120 μ A, before and after a rest period. The sample was mounted on a rotational table at a distance of 11.8 mm from the X-ray source and the distance between the X-ray source and the X-ray detector was 1155 mm. It was ensured that the focal spot size of the X-ray tube was about 2 μ m and therefore a spatial resolution of 4 μ m was achieved.

Reconstructions of the mixtures were prepared by segmenting the materials found in a specific volume, based on simple thresholding. With this simple method, aggregates and air voids could be readily separated. The softwares used for the reconstruction were ImageJ and MeshLab.

3.7 Test Results

3.7.1 Thermal Conductivity

Figure 3-9 shows the thermal conductivity values for all the asphalt concrete mixes studied. The thermal conductivity of asphalt mixtures decreased with the increase of air voids content, from 1.164 W/m·K, for mixtures with 5 % air voids content to 0.821 W/m·K for mixtures with 25.3 % air voids content. Similar results were reported in previous studies (Cote and Konrad, 2005, Canakci et al., 2007).

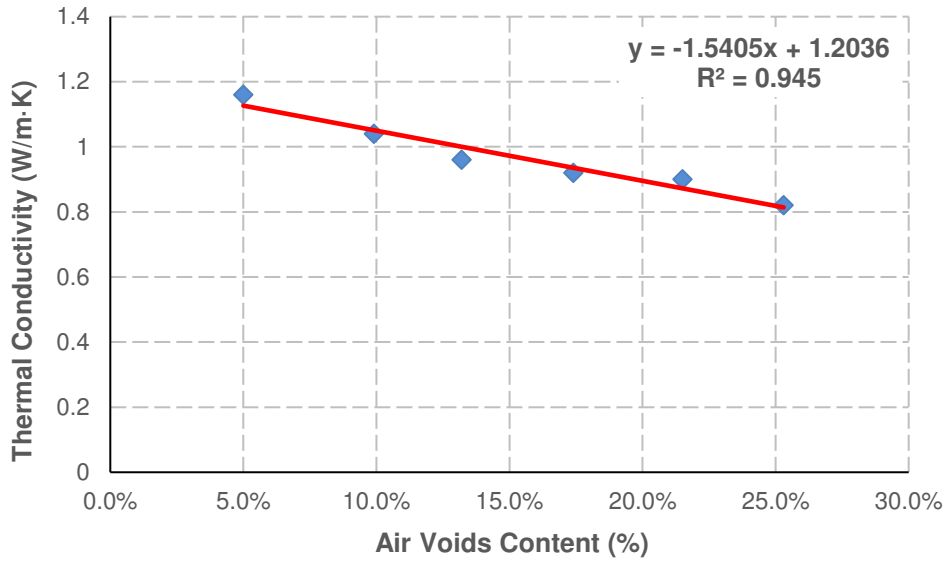


Figure 3-9 Thermal Conductivity Results

3.7.2 Specific Heat Capacity

The specific heat capacity of each mix design (c_p) was calculated as the sum of the heat capacities of the asphalt constituent parts multiplied by their proportion in the mixture (Sundberg, 1988, Hall, 2008, Somerton, 1992).

Section 2.3.1.2 described this method in more detail. The specific heat capacity for limestone aggregate and bitumen are 908 J/kg·K and 2093 J/kg·K, respectively. These values were obtained from an online reference (The Engineering ToolBox).

The final specific heat capacity of asphalt mixture was calculated as:

$$c_p = \frac{1}{m_{total}} [m_{Aggregate} * c_{Aggregate} + m_{Bitumen} * c_{Bitumen}] \quad \text{Eq. 3-8}$$

Where: m is the mass of each constituent, measured in kg, and c is the specific heat capacity of each constituent, measured in J/kg·K.

Figure 3-10 shows the calculated specific heat capacity for all the asphalt concrete mixtures studied. It can be observed that test samples with higher air voids content, 25.3 % have the lower specific heat capacity, 945.92 J/kg·K, while test samples with lower air voids content, 5.0 %, have the highest specific heat capacity, 963.70 J/kg·K. These values are similar to previous results reported by [Stempihar et al., \(2012\)](#). Basically, asphalt mixtures with lower air voids content has more constituents and more binder content in the mixture which is considered to be the main reason for having a higher specific heat capacity than the asphalt mixtures with lower air voids content.

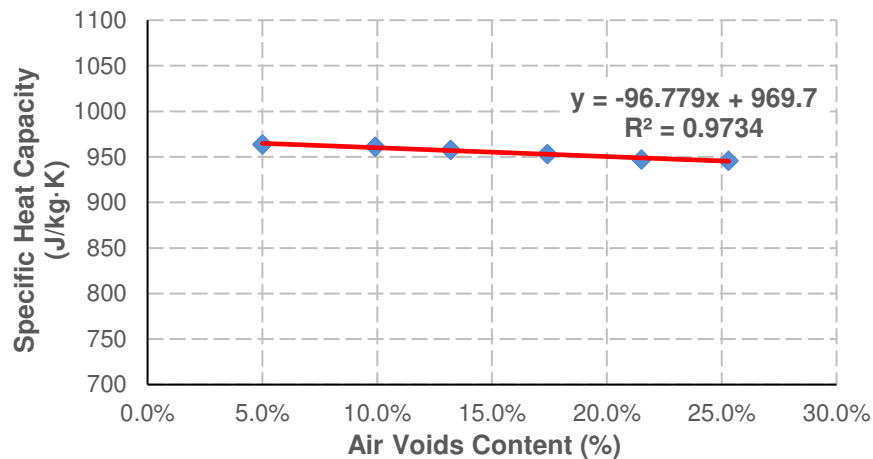


Figure 3-10 Specific Heat Capacity Results

3.7.3 Thermal Emissivity

Thermal emissivity is the ratio of energy radiated by the surface of an asphalt slab compared to the radiation emitted by a black body at the same temperature ([Incropera et al., 2013](#)). It is an indication of the amount of energy radiated to the atmosphere. In an asphalt mixture, the emissivity depends on the material, its surface microstructure and the temperature ([Stempihar et al., 2012](#)). **Figure 3-11** shows the emissivity values for all the test samples analysed over a

Chapter 3. Effect of air voids content on thermal properties of asphalt mixtures

temperature range from 45 °C to 85 °C. From this Figure, it can be observed that the emissivity value increased with temperature. This is a well-known effect already reported in the literature for different materials (Cengel, 2003). With the purpose of comparing the thermal emissivity of all studied material samples, the average of all emissivity values for each slab analysed has been presented in **Table 3-3**. It can be observed that the emissivity value decreased slightly with the increase in the air voids content, from 0.84 at 5.0% air voids content to 0.82 at 25.3% air voids content. In this study, the percentage of incident radiation absorbed by the test samples (absorptivity) has been considered to be equal to emissivity (Incropera et al., 2013). **Section 2.3.2.2** and **Section 2.3.2.3** described this assumption in more detail. In addition, the percentage of incident radiation reflected by the test samples (albedo) has been considered as (1-absorptivity) (Cengel, 2003, Incropera et al., 2013).

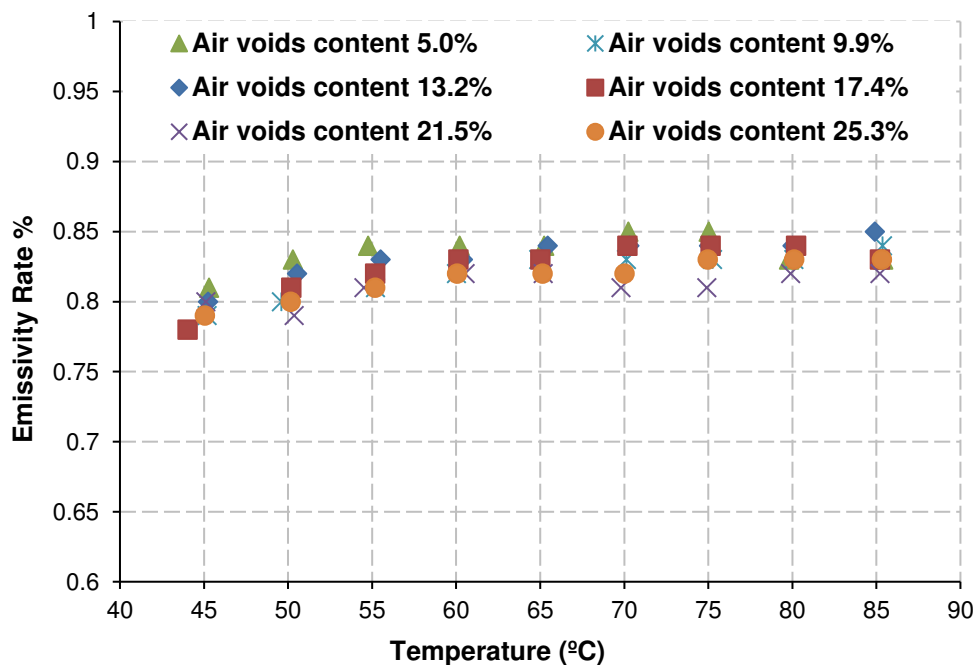


Figure 3-11 Emissivity results of the test samples

3.7.4 Thermal Diffusivity

Thermal diffusivity (α) is the measurement of how fast thermal energy moves through a material until it reaches a steady state equilibrium (Incropera et al., 2013). The method used to measure the thermal diffusivity was described in detail in Section 2.3.1.3. Its units are (m²/s) and it is calculated as:

$$\alpha = \frac{k}{c_p * \rho} \quad \text{Eq. 3-9}$$

Where: α is the Thermal diffusivity, measured in (m²/s), k is the Thermal conductivity, measured in (W/m.K), ρ is the Density, measured in (kg/m³) and c_p is the Specific heat capacity, measured in (J/kg.K).

Table 3-3 gives the thermal diffusivity of all the test specimens. It can be observed that the test samples with lowest air voids content, 5.0%, have the highest thermal diffusivity, 5.09 x 10⁻⁷ m²/s, while test samples with highest air voids content, 25.3%, have the lowest thermal diffusivity, 4.55 x 10⁻⁷ m²/s.

Table 3-3 Main parameters of the asphalt mixtures results

Air voids content (%)	5.0%	9.9%	13.2%	17.4%	21.5%	25.3%
Total weight (kg)	11.15	10.55	10.25	9.84	9.44	8.84
Percentage of bitumen by mass (kg)	0.52	0.47	0.43	0.37	0.31	0.28
Percentage of limestone by mass	10.63	10.08	9.82	9.46	9.13	8.55
Density (kg/m ³)	2371.67	2256.0	2186.75	2092.6	2004.7	1906.10
Thermal conductivity (W/m.K)	1.16	1.04	0.96	0.92	0.90	0.82
Specific Heat capacity (J/kg.K)	963.70	961.33	957.77	953.03	947.11	945.92

Thermal diffusivity (x10 ⁻⁷) (m ² /s)	5.09	4.79	4.6	4.61	4.72	4.55
Average thermal emissivity	0.84	0.82	0.83	0.82	0.81	0.82

3.7.5 Evolution of temperature under infrared heating and cooling

Figure 3-12 shows the maximum steady state temperatures at the surface and at the bottom of the asphalt slabs for all the test samples analysed. This figure shows that the steady state surface temperature of asphalt slabs was higher for materials with higher air voids content: temperatures in asphalt slabs with 25.3 % air voids content were 2.5 °C higher than in asphalt slabs with 5.0 % air voids content. In addition, it can be observed that the bottom temperature at the steady state was higher in asphalt slabs with higher air void content by 1.26 °C: 88.57 °C for asphalt slabs with 25.3 % air voids content and 87.41 °C for asphalt slabs with 5.0 % air voids content. Finally, it can be observed that the maximum steady state temperatures increased gradually with the air voids content. In addition, the difference between the bottom and surface temperatures at the steady state condition increased with air voids content, from 3.06 °C for asphalt slabs with 5.0 % air voids content to 4.45 °C for asphalt slabs with 25.3 % air voids content.

In addition, **Figure 3-13** shows the temperature differentials in the asphalt slab surfaces after 1 hour heating and cooling. The temperature profile results after 1 hour of heating and cooling are clearly differ for asphalt slabs with different air voids content. Therefore, this period has been studied in detail as it is believed that this is due to the effect of heat transfer properties of the

asphalt mixtures. During the first hour of heating, the surface temperature of asphalt mixture slabs with 25.3% air voids content increased to 40.12 °C, while the surface temperature of asphalt mixture slabs with 5.0% air voids content only increased to 32.09 °C. Moreover, the temperature reduction at the surface of porous asphalt mixture slabs was higher than the temperature reduction at the surface of dense asphalt mixture slabs during cooling. For example, during the first hour of cooling, the surface temperature of asphalt mixture slabs with 25.3% air voids content decreased to 34.23 °C, while the surface temperature of asphalt mixture slabs with 5.0% air voids content decreased to 31.02 °C.

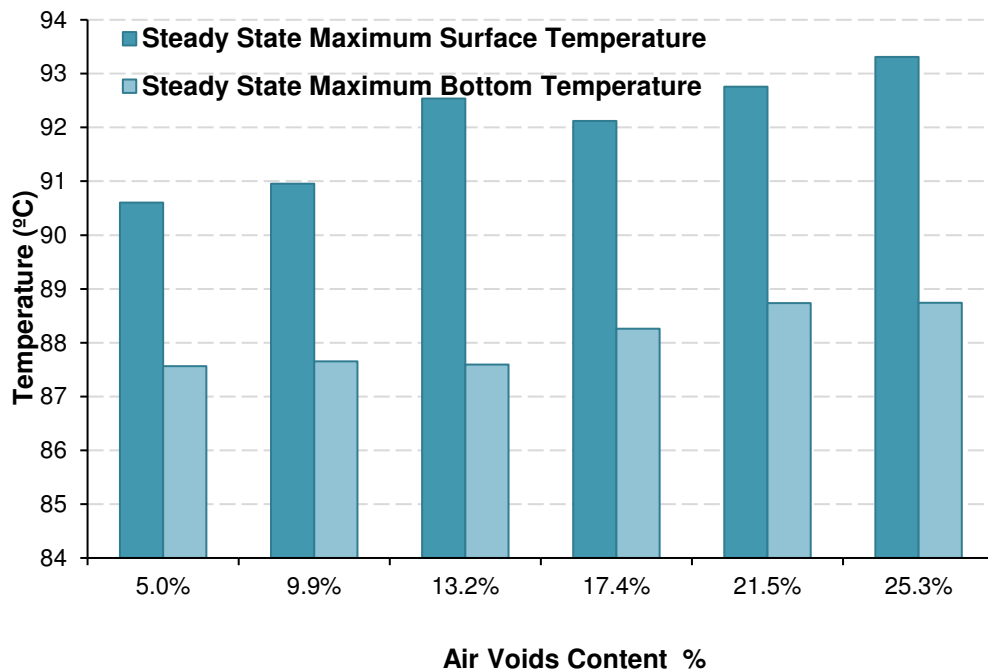


Figure 3-12 Maximum surface and bottom temperature at the steady state condition for all the test samples

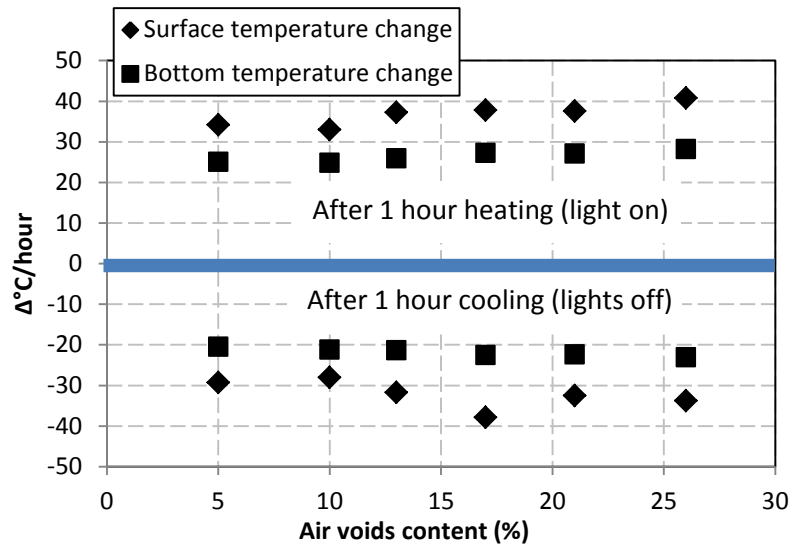


Figure 3-13 Increments and decrements of temperature after 1 hour heating and cooling

Furthermore, **Figure 3-13** also shows the temperature differentials of the asphalt slab bottoms after 1 hour heating and cooling. Similar temperature characteristics to those on the surface were found at the bottom of the test samples. During the first hour of heating, the bottom temperature of asphalt mixture slabs with 25.3% air voids content increased to 29.05 °C, while the bottom temperature of asphalt mixture slabs with 5.0% air voids content increased to 26.11 °C. In addition, the temperature reduction at the bottom of porous asphalt mixture slabs was higher than the temperature reduction at the bottom of dense asphalt mixture slabs during cooling. During the first hour of cooling, the bottom temperature of asphalt mixture slabs with 25.3% air voids content decreased to 24.10 °C, while the bottom temperature of asphalt mixture slabs with 5.0% air voids content decreased to 22.01 °C.

3.8 Discussion

When the infrared lights are on, incident radiation hits the test samples. A percentage of this radiation is absorbed; this amount is a function of the absorptivity of the test samples. It depends on the colour of the asphalt mixture, as lighter coloured pavements reflect higher amounts of radiation than darker pavements (Mallick et al., 2009). It depends also on the surface texture; for example, in **Table 3-3** it can be observed that asphalt slabs with higher air voids content have slightly lower absorptivity than asphalt slabs with lower air voids content. This could be due to the deeper texture at the surface of the porous slabs, which creates surfaces with multiple reflection angles and shadow areas, when compared to smoother materials (Stephens, 1977).

The surface temperature of the test samples increases by the effect of the absorbed radiation, as a function of the specific heat capacity of the mixture. Materials with higher specific heat capacity need more energy to increase their temperature. For example, in **Table 3-3**, it can be observed that slabs with lower air voids content have higher specific heat capacity than slabs with higher air voids content. In addition, in **Figure 3-13**, it can be observed that the heating rate of denser slabs is lower than the heating rate of slabs with higher air voids content. This happens because asphalt mixtures with higher specific heat capacity need more time at the same level of incident radiation to reach the same temperature.

Energy is transported through the test samples from hot areas to colder areas as a function of the thermal conductivity of the asphalt mixture. Asphalt mixtures with higher thermal conductivity conduct more energy through the

Chapter 3. Effect of air voids content on thermal properties of asphalt mixtures

slabs than asphalt mixtures with lower thermal conductivity. In the case of two asphalt mixture slabs with similar specific heat capacities but different thermal conductivities, the material with higher thermal conductivity would have lower surface temperature heating rate and a lower steady state surface temperature. In the case of two asphalt mixture slabs with similar thermal conductivities but different specific heat capacities, the material with higher specific heat capacity would have a lower surface temperature heating rate. This is confirmed in **Figure 3-13**, where test slabs with lower air voids content have lower surface temperature heating rate. In addition, the relationship between the thermal conductivity and specific heat capacity is confirmed through the thermal diffusivity values in **Table 3-3**, which are higher in asphalt mixtures with low air voids content. Finally, asphalt mixtures with low diffusivity, those with higher air voids content, cannot transport heat out of the hot areas in the test specimens as efficiently as asphalt mixtures with high diffusivity, those with lower air voids content. This happens because air is a very poor thermal conductor. This causes mixtures with higher air voids content to reach higher temperatures at the steady state condition, as can be confirmed in **Figure 3-12**.

Moreover, when the infrared lights are off, asphalt mixtures with low specific heat capacities and low thermal conductivities, i.e. those with high air voids contents, will cool down faster than asphalt mixtures with high specific heat capacities and high thermal conductivities, those with low air voids contents. The reason for this is the higher volume of air voids in the asphalt mixture and lower specific heat capacity of porous materials.

Furthermore, the surface area of air voids connected to the upper face of the test specimens has been measured using results obtained from X-ray tomography samples (see **Figure 3-14**). As it was not possible to obtain quantitatively definitive results from the 3-dimensional reconstructions, the area of air voids has been represented in relation to the mixture with 5.0% air voids content. **Figure 3-15** shows that the area of air voids in mixtures with 21.5% air voids was 7 times higher than in the mixture with 5.0% air voids. On the other hand, **Figure 3-13** shows that the cooling rate is practically constant for all the test specimens analysed. This shows that the total area exposed to the air did not contribute to the temperature changes of the test specimens. The reason for this is probably because the tests were carried out in a closed box, which did not allow any convective air currents through the air voids for test samples with percolated air voids. Moreover, in the case of test samples with lower air voids content air voids were not connected (see **Figure 3-14a**), and air could not flow through the material.

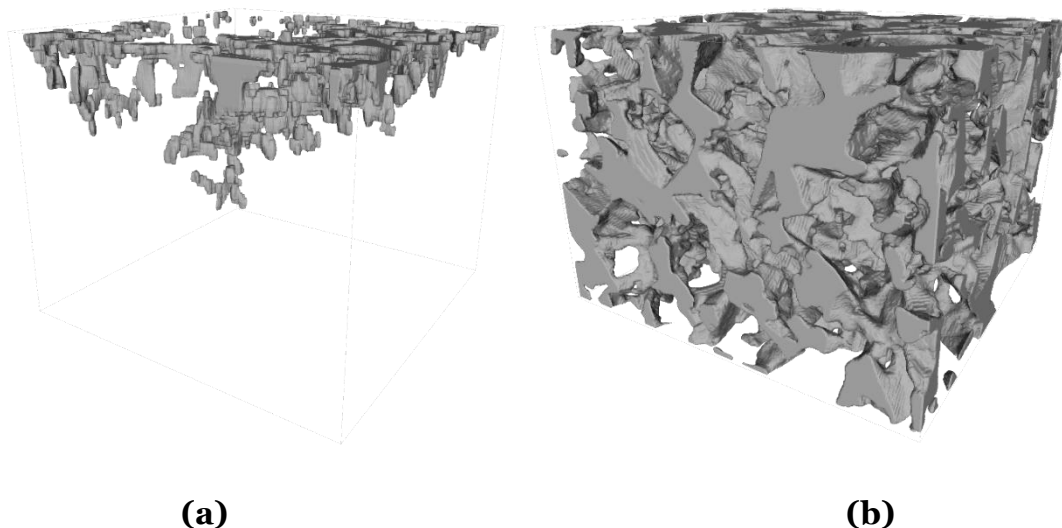


Figure 3-14 Air voids connected to the surface of tests specimens with (a) 5.0% air voids content and (b) 25.3% air voids content.

Chapter 3. Effect of air voids content on thermal properties of asphalt mixtures

In addition, in **Figure 3-16** it can be observed that the maximum temperature difference between the surface and bottom during heating is higher in mixtures with 25.3 % air voids content than in mixtures with 5.0% air voids content: 15.16 °C and 9.34 °C, respectively. This difference happened during the first 0.5 hours of heating. This confirms that the thermal energy transfer from the surface to the bottom layer in the slabs was higher in mixtures with lower air voids content, and this is because air has lower thermal conductivity than solids: high thermal conductivity transfers the heat through the asphalt slabs very fast.

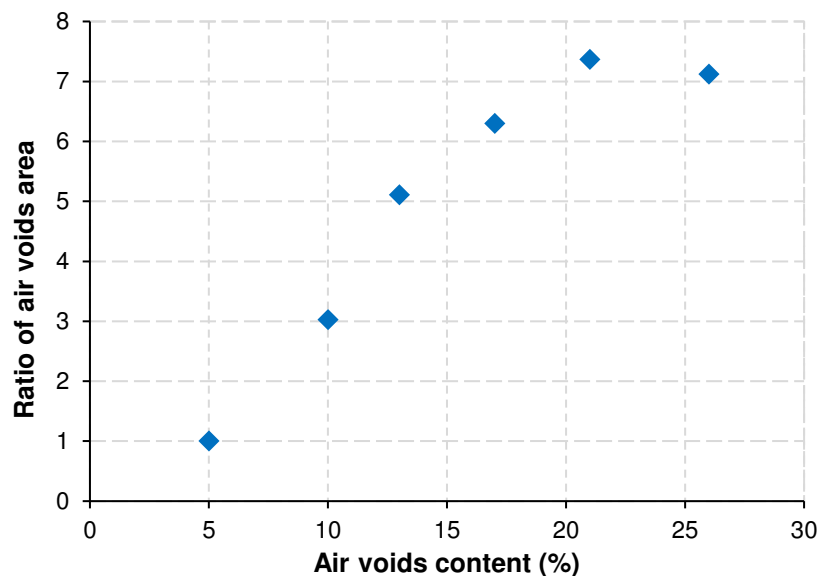


Figure 3-15 Ratio of air voids area versus air voids content

Figure 3-17 (a) illustrates the average temperature of the test samples, obtained from **Eq. 3-6**. It can be observed that although the porous asphalt mixture reaches a higher temperature under infrared heating, the difference with denser asphalt mixtures is only 1.1 °C. Changes in thermal conductivity in the mixture will not have a very strong effect on the average temperature of the material. Furthermore, adding thermal conductive materials to the mixture, such as graphite (Mingyu et al., 2010) or metallic fibres (Garcia, 2013) will not

affect substantially the final average temperature of the pavement, only the rate at which that temperature develops upon a change in the boundary temperature.

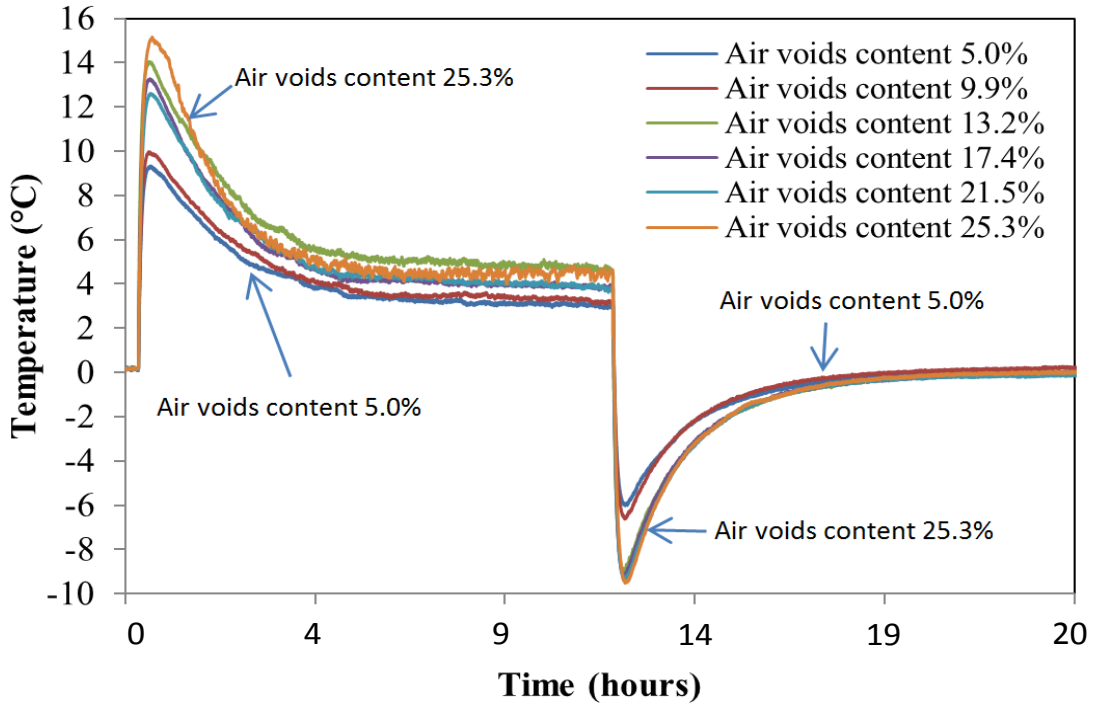


Figure 3-16 Difference between surface and bottom temperature for all test slabs

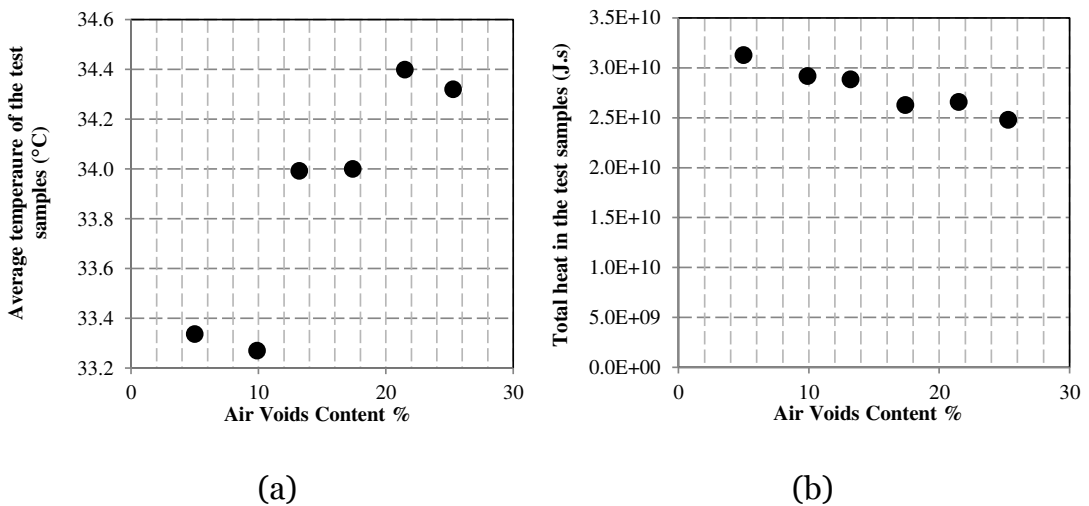


Figure 3-17 (a) Average temperature of the test samples. (b) Total accumulated heat in the test samples.

Chapter 3. Effect of air voids content on thermal properties of asphalt mixtures

In **Figure 3-17 (b)**, the total accumulated heat in the test samples obtained from **Eq. 3-7** has also been presented. From this figure, it can be observed that asphalt mixtures with 25.3 % air voids content have approximately 20 % less accumulated heat than asphalt mixtures with 5.0 % air voids content. This probably happened because mixtures with lower air voids content have higher specific heat capacity and mass than porous mixtures. To demonstrate this point, the total heat in the test samples (T_h) obtained from **Eq. 3-10**, and the density of asphalt slabs (ρ_a) have been made dimensionless by dividing their values by the maximum value of total heat and density obtained from the test samples analysed, which correspond to those with 5.0% air voids content:

$$\text{Dimensionless total heat: } T_h = \frac{T_h(\% \text{ air voids})}{T_h(5.0\%)} \quad \text{Eq. 3-10}$$

$$\text{Dimensionless density: } \rho_a = \frac{\rho_a(\% \text{ air voids})}{\rho_a(5.0\%)} \quad \text{Eq. 3-11}$$

Where: $T_h(\% \text{ air voids})$ is the total heat in test samples with different air voids content, measured in (K·s), $\rho_a(\% \text{ air voids})$ is the density of test samples with different air voids content, measured in (kg/m³), $T_h(5.0\%)$ is the total heat in test samples with 5.0 % air voids content, measured in (K·s) and $\rho_a(5.0\%)$ is the density of test samples with 5.0 % air voids content, measured in (kg/m³).

In **Figure 3-18** the dimensionless total heat has been represented versus the dimensionless density. It can be observed that the relationship is linear and that the slope is almost 1. The deviation in the slope can be attributed to experimental errors. This means that the total heat accumulated by asphalt mixtures with the same surface colour and constant materials depends only on

its density or its air voids content. Radiation losses and convective losses do not independently play a role on the total heat accumulated in an asphalt mixture. In addition, looking at **Eq. 3-7** one can deduce that the only difference between test samples with various air voids contents was the mass, while the specific heat capacity of the constituent materials used for building the mixture remained constant. Changing the air voids content in an asphalt mixture will have an effect on its total specific heat capacity when the slabs are considered as a whole.

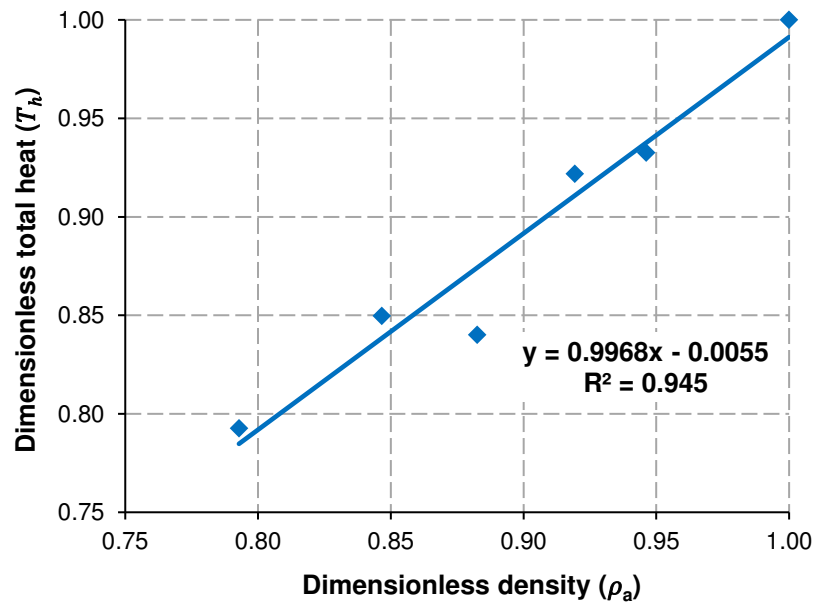


Figure 3-18 Dimensionless total heat versus dimensionless density in the test samples studied

In **Figure 3-19**, the effect of various thermal properties on the temperature evolution of asphalt mixtures with different air voids contents under infrared heating has been represented. If the specific heat capacity of asphalt slabs could be changed and the thermal conductivity of the materials could be maintained constant, the steady state temperature of the mixture would also remain constant, although the heating and cooling rates would change. Moreover, if

Chapter 3. Effect of air voids content on thermal properties of asphalt mixtures

the thermal conductivity could be increased and the specific heat capacity of an asphalt mixture could be maintained constant, the average temperature of the mixture would be reduced, because the exchange of energy between the test samples and the environment would be very high. In reality, it is impossible to increase the thermal conductivity by changing the air voids content, without affecting the density and specific heat capacity of the asphalt mixture. Following this explanation, the temperature evolution versus time of a porous asphalt mixture can be considered as the combination of its low thermal conductivity and low specific heat capacity, while the temperature evolution versus time of dense asphalt mixture can be considered as the combination of its high thermal conductivity and high specific heat capacity.

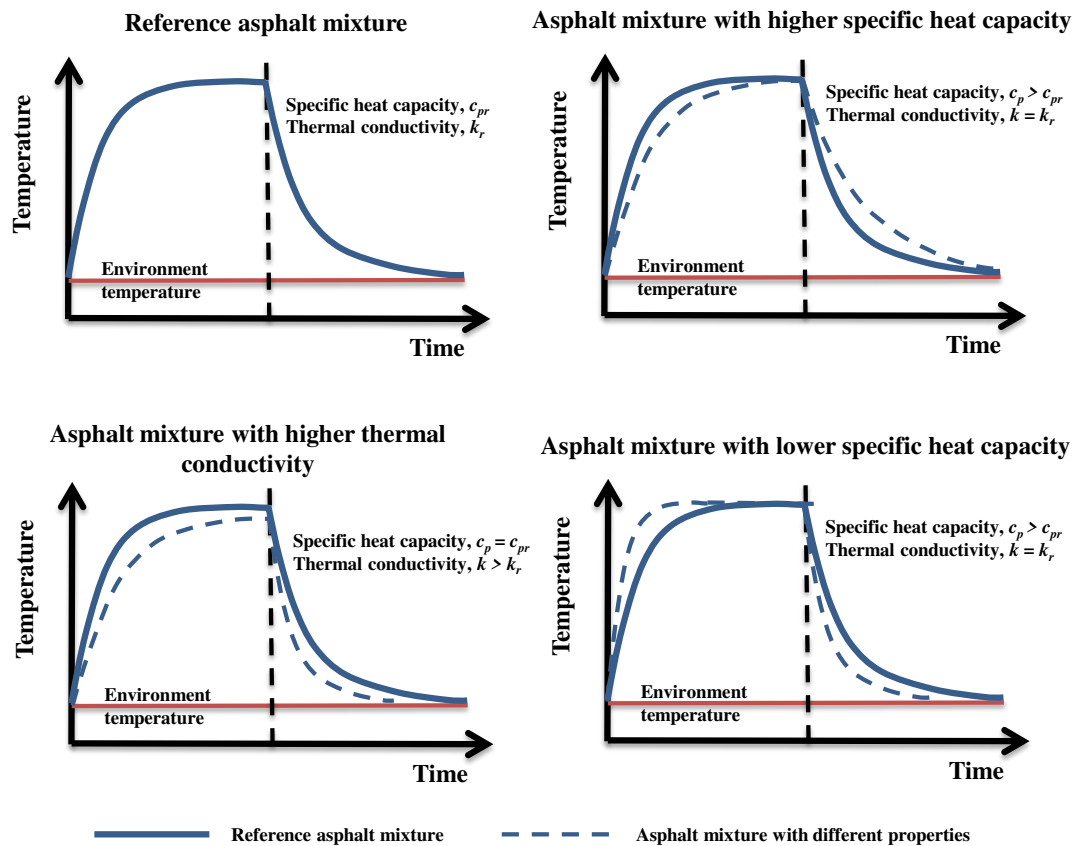


Figure 3-19 Effect of various thermal properties on the temperature evolution of asphalt mixture under infrared heating

For these reasons, it is recommended that dense asphalt mixtures are used to harvest energy from asphalt pavements, because they can accumulate more heat and can transfer energy faster than porous asphalt mixtures; while mixtures with high air voids content should be used to fight the urban heat island effect, although they may reach slightly higher temperatures than denser asphalt mixtures.

3.9 Summary

This chapter has explained how air voids content influences the thermal conductivity, specific heat capacity, infrared absorptivity, maximum temperature and heating and cooling rates of asphalt mixture. The main conclusions in this study are summarised as follows:

- An asphalt mixture with high air voids content has lower thermal conductivity and specific heat capacity than an asphalt mixture with lower air voids content. This is because air has lower thermal conductivity compared to asphalt mixture; thereby the heat transfer rate through the mixture is reduced.
- The emissivity of dense asphalt mixture is higher than the emissivity of porous asphalt mixture by a value of 0.02. This value is very small when compared to the emissivity of asphalt concrete; thus, the air voids content can be considered to have an insignificant effect on the emissivity of asphalt mixtures.
- Asphalt mixtures with high thermal conductivity and specific heat capacity, i.e. dense asphalt mixtures, have lower heating and cooling

Chapter 3. Effect of air voids content on thermal properties of asphalt mixtures

rates than asphalt mixtures with lower thermal conductivity and specific heat capacity, i.e. porous asphalt mixtures.

- The surface of asphalt slabs with high air voids content reaches a higher steady state temperature than the surface of asphalt slabs with lower air voids content. This is probably due to the rougher surface, caused by the voids, intercepting radiative energy from the surface more effectively and reflecting it less. The average temperature of asphalt mixture during heating and cooling is almost independent of the air voids content in the mixture.
- In conclusions, these findings are based on tests in sealed boxes and probably would not apply where air flow from the boundaries was allowed.

4. Multivariable analysis of water evaporation from moist asphalt mixture

4.1 Introduction

Water evaporation from porous media is a fundamental engineering problem that has an influence in fields such as food processing (Fernando, 2008) agriculture and environment (Liu, 2012, Chatzithomas, 2015), and construction technology (Goncalves, 2009). Moreover, water evaporation can be used to control the urban heat island (UHI) effect by reducing the temperature of pavements (Takebayasi, 2012) and building facades (Perini, 2011). Much research has described the drying behavior of porous media (Lohman, 1972, Vorhauer, 2010), which is normally characterized as a two stage process. In Stage 1, evaporation is limited by the atmospheric conditions and water is supplied by a capillary flow that connects the receding drying front to the evaporating surface. Between the evaporation surface and the drying front lies a capillary fringe with continuous saturated capillary channels connecting the two (Lohman, 1972), even though the overall saturation of this fringe is less than 100%. For a porous material experiencing evaporation from its top surface (such as a soil or pavement), when the drying front reaches a given depth, the downward gravity and viscous forces overcome the capillary force, and the water supply for evaporation by absorption of latent heat is stopped (Lehmann, 2008). The disruption of the capillary flow marks the beginning of Stage 2, which is characterized by a lower evaporation rate and is limited by diffusion through the porous media (Shokri et al., 2009). During this stage, the location of evaporation shifts from surface to sub-surface, resulting in the formation of

a dry layer where only vapor flow occurs (Yamanaka, 1998). This affects the total flux of energy through the material, as the energy that before was directly used for evaporation, will have to be transported from the surface, through the material to reach the drying front (Jiangbo, 2013). Transition from evaporation Stages 1 to 2 in porous media is controlled by the pore size distribution (Haghighi, 2013), capillary length (Lehmann, 2008), material wettability (Shokri et al., 2009) and capillary pressure (Shokri et al., 2010). Moreover, it is known that capillary pressure at constant degrees of saturation decreases as temperature increases (She, 1998).

Most of the previous studies on the dynamics of water evaporation have considered evaporation only at an environmentally constant temperature, which is not representative of the real world evaporation in soils or construction materials, as these may reach higher temperatures than in the surrounding environment due to their dark color (Salvucci, 1997). The goal of this study is to obtain complete dynamic information on the water evaporation process from an asphalt surface during a continuous drying event that includes both Stages 1 and 2. The main aim is to understand the effect of voids content on the thermal properties of asphalt mixtures, on transport and storage of heat under wet condition, and how that could affect the energy harvesting application and urban heat island effect. For this purpose, asphalt mixtures with air contents ranging from 4 % to 26 % were manufactured, and observations relating the time-dependent evaporation rates of saturated asphalt mixtures were compared to the development of a number of parameters, such as asphalt surface temperatures during heating, heat flux, porosity, and thermal conductivity. In addition, the voids configuration was characterized and their

properties, e.g., Euler number, tortuosity, diameter of voids, and macroporosity, were compared to the parameters mentioned above. The results are expected to have a strong impact on the design of asphalt mixtures to minimize the pavement contribution to the urban heat island effect and on the design of new types of asphalt solar energy collectors such as those described in [Garcia and Partl, \(2014\)](#) and [Chiarelli et al., \(2015\)](#).

4.2 Description of Materials

Six asphalt concrete slabs were used to measure the evaporation rate (each 306 x 306 x 50 mm). The samples were produced using a 60/40 penetration grade bitumen binder and 20 mm maximum limestone aggregate size, mixed at 160 °C, and compacted at 140 °C to the target air voids of 4.5 %, 10.0 %, 13.0 %, 17.0 %, 21.0 %, and 26.0 % using a roller compactor (see [Table 4-1](#) to know the aggregate gradation for every asphalt mixture analysed). In addition, the gradation curves for each type of aggregate used are shown in [Figure 3-1](#). [Section 3.2](#) described the material selection for the asphalt concrete mixtures in more detail.

Table 4-1 Composition of asphalt mixture

Target air voids	4.5%	10.0%	13.0%	17.0%	21.0%	26.0%
Sieve size (mm)	Cumulative aggregate Weight % retained					
28.0-20.0	20	20	20	20	10	20
20.0-14.0	40	43	45	51	48	80
14.0-10.0	55	63	71	76	83	90
10.0-6.3	70	74	78	81	83	90
Dust (<6.3 mm)	100	100	100	100	100	100
Bitumen (% of Weight of mixture)	4.7	4.5	4.2	3.8	3.5	3.2

4.3 Density of Test Samples

Asphalt mixture density was determined according to [BS EN 12697 PART 5 \(2009\)](#) by the mathematical method. In addition, the bulk density of the test specimens was determined according to [BS EN 12697 PART 6 \(2003\)](#) by the dimensions method from the average of three test specimens for every asphalt mixture type analyzed. [Section 3.4](#) described this procedure in more detail.

4.4 Air Voids Content

The air voids content of the asphalt mixtures was calculated based on the maximum and bulk densities. [Eq. 3-4](#) was used to calculate the test sample air voids content. More detail about this procedure can be found in [Section 3.5](#).

4.5 Experimental Setup

The experimental setup is illustrated in [Figure 4-1](#). First, the mass of every slab was recorded using a digital balance (Ohaus Ranger 3000), which has a capacity of 15 kg and a resolution of 0.005 kg. Then, asphalt slabs were

saturated by placing them under water for 12 hours. Later, the saturated asphalt concrete slabs were placed into a 310 × 310 × 50 mm rectangular acrylic transparent box (i.e. with a 2mm gap on the four vertical edges). The acrylic box was then placed on the digital balance. Finally, more water was added to the slabs until the box was completely filled just covering the top of the asphalt.

Asphalt samples with air voids content closer to the target air voids content were selected and tested, see **Table 3-2**. The test was repeated three times for each asphalt sample. Each asphalt concrete slab was placed under a heat source for 16 hours. Experimental tests were carried out at a constant air temperature (room temperature) of approximately 25 °C ± 1 and an average relative humidity of 50%. Four 250 W infrared lamps were used as the heat source. The infrared bulbs were placed at 730 mm from the samples. The digital balance was then continuously monitored to determine the mass reduction rate during the experiments.

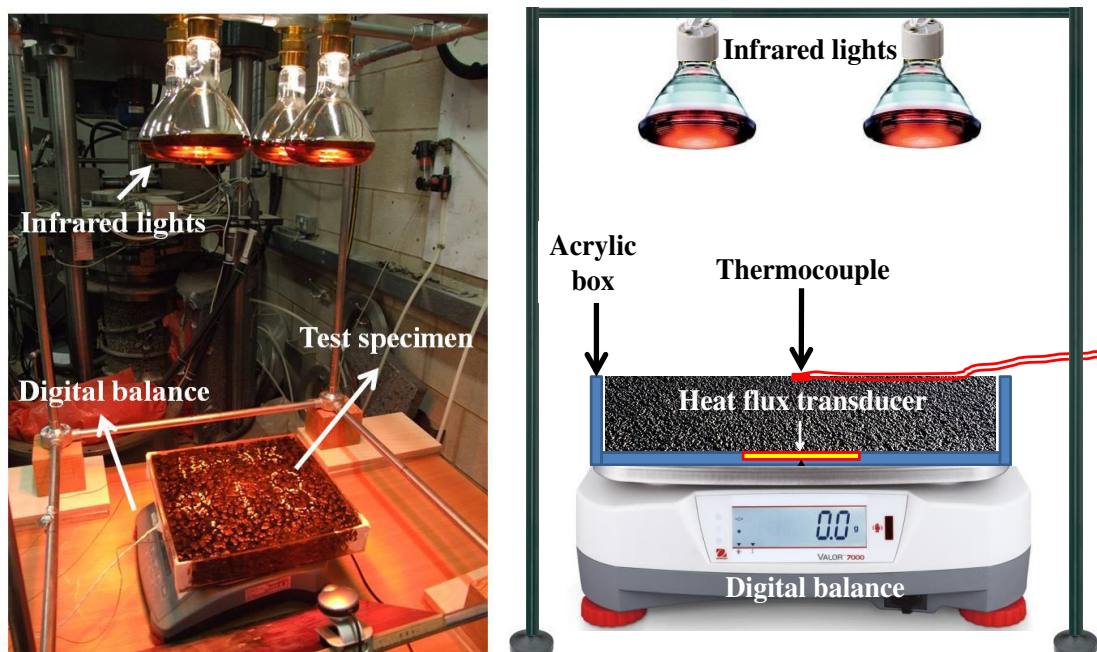


Figure 4-1 Experimental setup

4.6 Heat Flux and Temperature Measurements

An ITI model GHT-2C Geothermal Heat Flux Transducer with a size of $50.8 \times 50.8 \text{ mm}^2$ and a height of approximately 4.8 mm was used to measure the heat conducted through the asphalt concrete slabs (see **Figure 4-2**). The sensor is a water-proof meter, with a nominal sensitivity of $5\text{W}/\text{m}^2.\text{mVolt}$, an accuracy of 1% and a temperature range of $-38 \text{ }^\circ\text{C}$ to $+121 \text{ }^\circ\text{C}$.

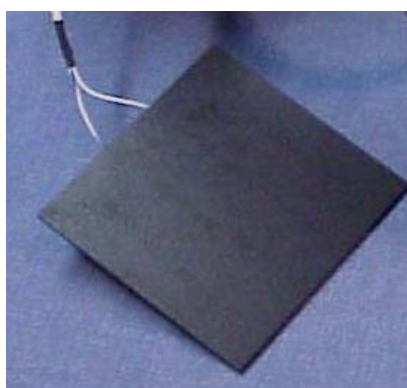


Figure 4-2 ITI model GHT-2c Geothermal Heat Flux Transducer

The transducer was embedded into the bottom of the acrylic box in order to have good contact with the asphalt concrete slabs (see **Figure 4-3**). The sensor measures the heat flux as a DC voltage generated by the temperature difference between its top and bottom surfaces. This voltage is proportional to the local heat flux and it was digitally recorded for all the experiments performed.

The surface temperature of the asphalt concrete slabs was measured by using a J-type thermocouple placed in the geometrical center of the slab. The temperature profile was recorded for 16h with a constant environmental (air) temperature of $25^\circ\text{C} \pm 2$.

The heat flux meter and the thermocouple were connected to a data logger (Omega OMB-DAQ-54) that allowed measurements at 1-minute intervals.

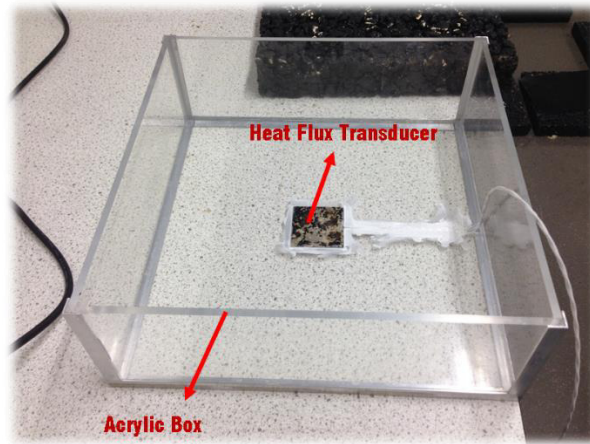


Figure 4-3 Position of Heat Flux Transducer

4.7 X-ray Computed Tomography (CT scans)

In order to have an indication of the internal structure of the asphalt mixtures evaluated, X-ray tomography on different samples has been employed.

The X-ray micro tomography scans were carried out on the micro computed tomography facility at the University of Nottingham. The X-ray source was operated with an acceleration voltage of 290 kV and a current of 1.55 mA. The sample was mounted on a rotational table at a distance of 50 cm from the X-ray source. The pixel size obtained was 65.2 μm .

The images were processed with the commercially available Materialise Mimics and the open source software ImageJ Version 1.49 (Abramoff, 2004). The images were converted to 8-bit grayscale resolution and cropped to a region of interest (ROI) of 8cm x 8cm x 6cm. Reconstructions of the microstructure were prepared by segmenting the materials found in a specific volume, based on

grayscale thresholding. With this simple method, aggregates, bitumen and air voids could be readily separated. The thresholded images of the voids were stacked with the software Materialise Mimics. Each pixel in the porous space can then be connected to 26 other pixels around it (alongside, above, and below), which are called neighbouring pixels. Therefore, it is possible to generate surfaces that encase each group of neighbouring pixels belonging to a common void space.

As it is known that small isolated clusters of void or grain voxels may correspond to small isolated pores or to noise effects (Peth, 2008), these were removed from the image prior to further analyses. All features smaller than 2 voxels in width (minimum Feret's diameter <0.13 mm) were removed from the segmented binary data to prevent their classification as pores.

4.8 Topology of Air Voids

The macropore characteristics that were quantified based on CT Scans included air voids content, mean macropore thickness, connectivity and tortuosity (T). These are commonly used properties to analyse the topology of soils and porous media (Katuwal et al., 2015).

The total air voids content was calculated as the volume of macropores per unit of volume in the ROI. The diameter of air voids was calculated using a thickness algorithm within the Particle Analyser plugin in Image J (Dougherty, 2007).

The mean d_m was calculated as:

$$d_m = \frac{\sum_{i=1}^n d_i V_i}{\sum_{i=1}^n V_i} \quad \text{Eq. 4-1}$$

Where: d_m and V_i are the diameter and volume of each macropore in the asphalt mixture.

Moreover, the interconnectivity of pore networks is commonly expressed based on the Euler number (χ), the total number of pores in the mixture (N), the number of redundant connections in the air paths, or genus (Katuwal et al., 2015) (C), and the total number of enclosed cavities within the air voids structure (H) (Vogel, 1997, Vogel, 2001). When the Euler number is negative, it is an indication that the air voids are percolated (Katuwal et al., 2015). These values were determined with the Bone J particle analyser plugin (Version 1.4.0) in ImageJ (Doube, 2010).

Note that the Euler number is calculated as

$$\chi = N - C + H \quad \text{Eq. 4-2}$$

In addition, the air voids tortuosity was calculated following the explanations in Katuwal et al. (2015), as the ratio of the total branch length to the total shortest branch length between the ends of the macropores in the specimen analysed. Macropore length was calculated using the Skeletonize 2D/3D and analyses skeleton modules in ImageJ (Doube, 2010), with no pruning of the dead ends.

Finally, the percolation of air voids was defined as the relationship between the volume of the biggest air void (V_b) and the total volume of air voids in the ROI. This parameter was called Percolation Number (PN). When this value approaches 1, it means that all the air voids are connected.

4.9 Statistics

The correlations between the various parameters studied were analysed with linear regression and described by means of Pearson's correlation coefficients. This correlation coefficient has values between 0 and 1; 0 being no correlation at all, and 1 a perfect correlation. As an indication, it can be said that when the Pearson's correlation coefficient ranges from 0 to 0.4, there is a low or very low correlation; from 0.4 to 0.7, there is a moderate correlation and from 0.7 to 1 there is a high or very high correlation (Hogg and Craig, 1995). This is a very helpful statistical formula that measures the strength between variables and relationships. The calculation of Pearson's correlation coefficient and subsequent significance testing of it requires to hold the data assumptions. The data assumptions of the Pearson's correlation have been examined which includes: level of measurement, related pairs, absence of outliers, normality of variables, linearity, and homoscedasticity.

4.10 Experimental Results

4.10.1 Thermo-physical properties of asphalt slabs

The air voids content, density, specific heat capacity, and thermal conductivity of the asphalt slabs studied are reported in **Table 3-3**. It can be observed that the measured air void content of the slabs was 5.0%, 9.9%, 13.2%, 17.4%, 21.5%, and 25.3%. The density of asphalt mixture decreased linearly with the increase in air voids content, from 2371.67 kg/m³ for the asphalt mixture with 5.0% air voids content, to 1906.10 kg/m³ for the asphalt mixture with 25.3% air voids content. In addition, the specific heat capacity decreased approximately linearly

with the density, from 963.7 J/kg·K to 945.92 J/kg·K, in slabs with 5.0% and 25.3% air voids content, respectively. Finally, the thermal conductivity also decreased with the air voids content, from 1.16 W/m·K to 0.82 W/m·K in slabs with 5.0% and 25.3% air voids content, respectively.

4.10.2 Air voids characteristics

The vertical distribution of macroporosity (M) as a function of the region of interest (ROI) height is depicted in **Figure 4-4**, while the average percentage of air voids for the whole region of interest has been represented in **Table 4-2**. It can be observed that its value is always smaller than the air voids content calculated through the densities method (see **Section 3.5**). This effect is particularly evident in the case of samples with low air voids content, and the reason for this is almost certainly because air voids smaller than 0.5 mm were removed from the thresholded images.

In addition, in **Figure 4-5** the average diameter of air voids (A_{vd}) in every stacked image has been represented versus the vertical coordinate in the region of interest. From the data in **Table 4-2**, it can be observed that the dimensions of macroporosity are proportional to the air voids content. In addition, the bathtub shape of the air voids distribution is consistent with previous studies on asphalt mixture (Walubita, 2012) and is due to differences in density caused by the compaction procedure.

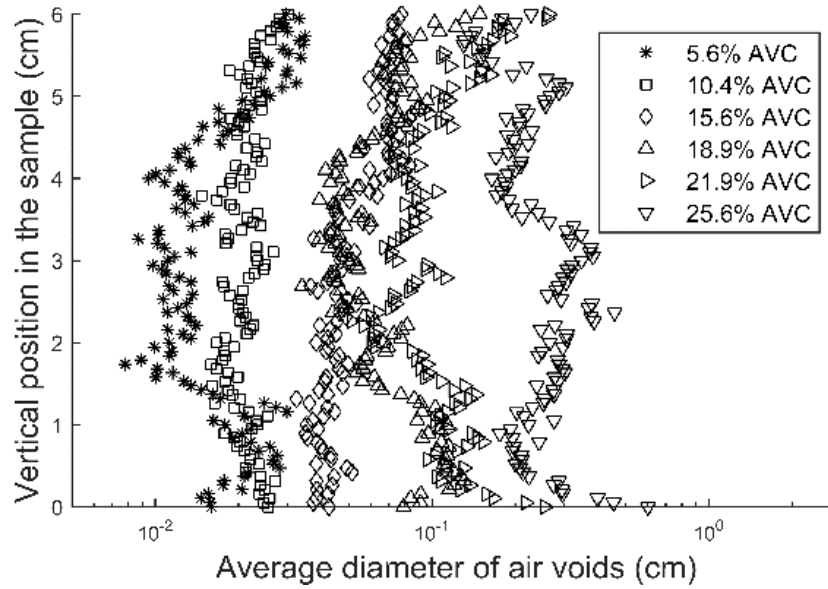


Figure 4-4 Vertical distribution of macroporosity in the ROI against average diameter of air voids

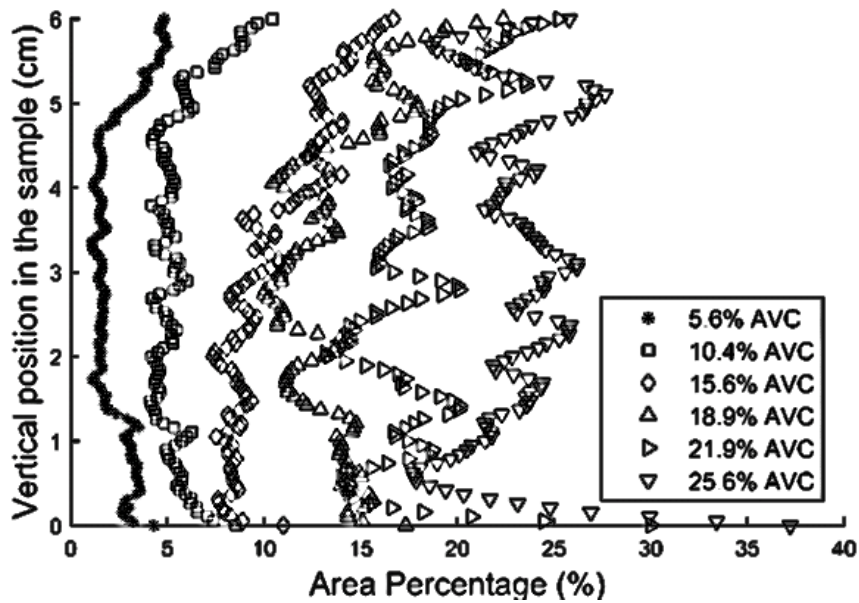


Figure 4-5 Vertical distribution of macroporosity in the ROI against Area Percentage

N , C , and H have been used to calculate χ . It can be observed that for low air voids content, the Euler number remains positive, while above 15.6% air voids

content, χ becomes negative. Note that if only one single connected path existed, the value of χ would be 1 and no redundant paths would exist, while for higher air voids in the region of interest (ROI), the value of C would increase and χ would reduce. This is an indication that the percolation threshold happens between 10.4% and 15.6% air voids content, as can be clearly observed in **Figure 4-6**. Besides, the Euler number increases above the percolation threshold, which is consistent with the reduction in the void channels in **Figure 4-6**. Note that if the air voids content were to increase up to 100%, there would be only one channel to conduct the water and the Euler number would be 1. This is confirmed by the tortuosity of the air voids skeleton in the ROI's (see **Table 4-2**), which increases with the air voids content.

Table 4-2 Topological constants

Air voids content (%)	5.6	9.9	13.2	17.4	21.5	25.3
Macroporosity (%)	2.6	6.2	11.0	13.9	19.1	23.2
Average voids diamtere (Avd), (cm²)	2.0E-02	2.0E-02	5.0E-02	7.0E-02	1.2E-01	2.5E-01
Euler number (χ)	1658	711	-236	-2360	-2094	-1249
Genus (C)	411	1665	1551	3677	3061	1826
Number of enclosed cavities (H)	157	286	382	719	317	553
Number of objects (N)	1912	2100	931	598	650	24
Volume of the biggest object (V_b), (cm³)	0.33	3.97	17.09	21.40	32.43	120.58
Percolation number (PN)	0.09	0.39	0.93	0.98	1.00	1.00
Macropore tortuosity	NA*	NA*	0.77	0.78	0.79	0.81

* NA: Not applicable

Furthermore, the percolation number shows that the size of the biggest connected macroporosity network increases from 39% to 93% of the total volume of air voids in the region of interest, when the air voids content moves from 10.40% to 15.60%. This sudden increase is another indication that the air voids then connect both sides of the ROI. See also **Figure 4-6** for a visual indication of the percolation.

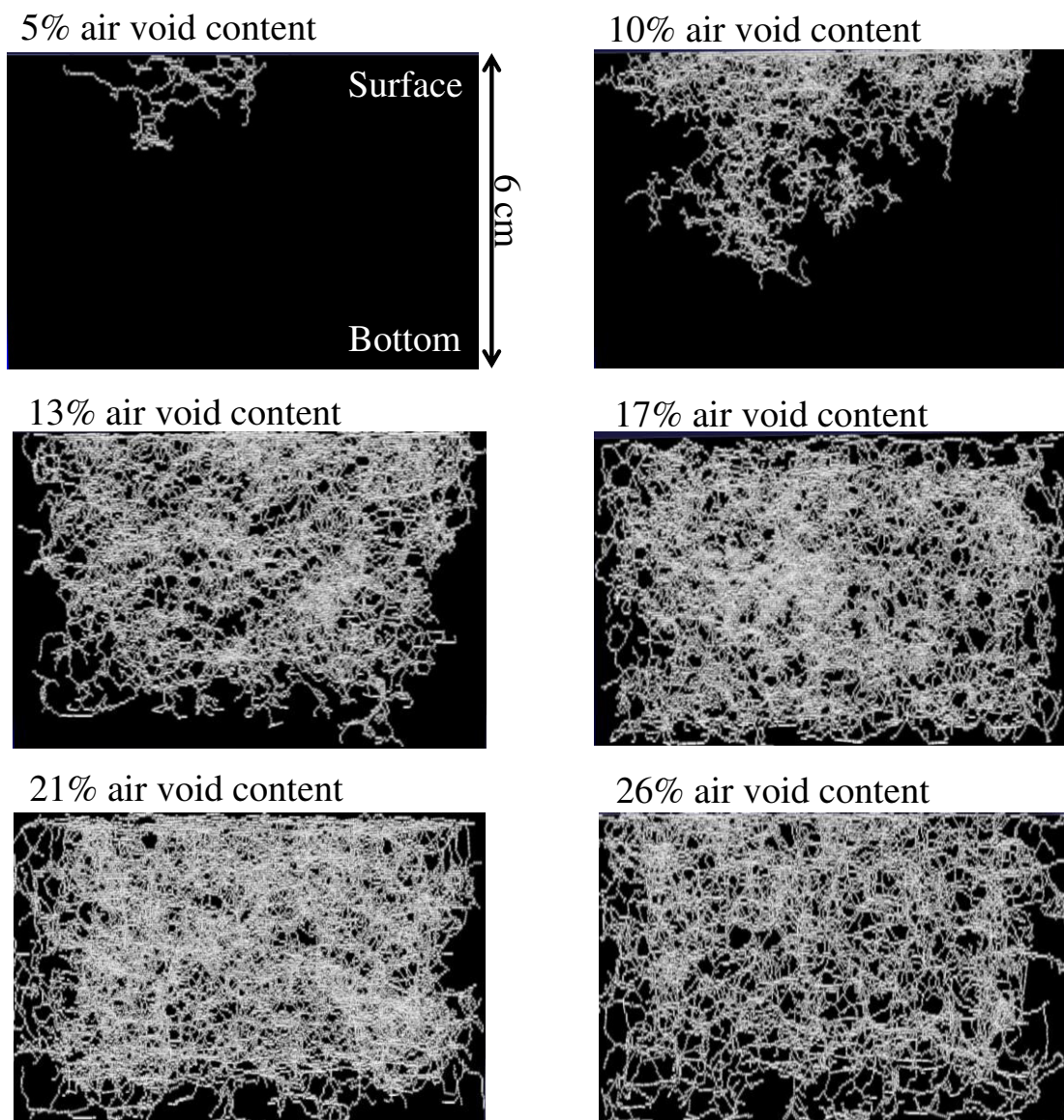


Figure 4-6 Largest connected air voids network for the test samples studied

Table 4-3 Pearson’s correlation between all the parameters studied

Variable used	Name	Abbrevi	Unit
Classification			
Characteristics of air voids	Air voids content (%)	<i>AVC</i>	%
	Macroporosity (%)	<i>M</i>	%
	Average voids diameter	<i>Avd</i>	cm ²
	Euler number	χ	--
	Genus	<i>C</i>	--
	Number of enclosed cavities	<i>H</i>	--
	Number of objects	<i>N</i>	--
	Volume of the biggest object	<i>Vb</i>	cm ³
	Percolation number	<i>PN</i>	--
	Tortuosity	ω	--
	Time and temperature	Temperature at point A	<i>Ta</i>
Temperature at point B		<i>Tb</i>	°C
Temperature at point C		<i>Tc</i>	°C
Time for point A		<i>ta</i>	min
Time for point B		<i>tb</i>	min
Time for point C		<i>tc</i>	min

	Characteristics of air voids										Time and temperature					
	<i>AVC</i>	<i>M</i>	<i>Avd</i>	χ	<i>C</i>	<i>H</i>	<i>N</i>	<i>Vb</i>	<i>PN</i>	ω	<i>Ta</i>	<i>Tb</i>	<i>Tc</i>	<i>ta</i>	<i>tb</i>	<i>tc</i>
Characteristics of air voids	1															
<i>AVC</i>	1															
<i>M</i>	0.99	1														
<i>Avd</i>	0.95	0.96	1													
χ	0.84	0.82	0.54	1												
<i>C</i>	0.62	0.58	0.24	0.93	1											
<i>H</i>	0.63	0.6	0.47	0.77	0.72	1										
<i>N</i>	0.92	0.93	0.84	0.83	0.56	0.73	1									
<i>Vb</i>	0.84	0.85	0.98	0.27	0.16	0.35	0.75	1								
<i>PN</i>	0.87	0.87	0.62	0.91	0.74	0.73	0.9	0.47	1							
ω	0.98	0.99	0.91	0.23	0.12	0.12	0.95	0.93	0.81	1						
Time and temperature																
<i>Ta</i>	0.52	0.52	0.79	0.07	0.12	0.14	0.35	0.82	0.06	0.99	1					
<i>Tb</i>	0.10	0.13	0.16	0.21	0.2	0.04	0.12	0.2	0.47	0.72	0.57	1				
<i>Tc</i>	0.22	0.23	0.11	0.44	0.46	0.25	0.27	0.16	0.64	0.91	0.6	0.95	1			
<i>ta</i>	0.25	0.29	0.1	0.17	0.07	0.41	0.16	0.07	0.32	0.02	0.06	0.63	0.46	1		
<i>tb</i>	0.95	0.94	0.93	0.76	0.56	0.69	0.87	0.88	0.72	0.95	0.69	0.19	0.04	0	1	
<i>tc</i>	0.98	0.97	0.89	0.84	0.62	0.77	0.96	0.84	0.88	0.95	0.5	0.05	0.21	0.02	0.92	1

Note : High Correlation

4.10.3 Evolution of surface temperature with time

The surface temperature of asphalt mixtures is presented as a function of time in **Figure 4-7**. It can be observed that the temperature increase rate was lower

in test samples with higher air voids content. In addition, all the curves developed through two steps, the first one, being a transient evolution from room temperature to approximately 50 °C, and the second one being from approximately 50 °C to 100 °C when steady state behavior is reached. The curves with air voids content from 5.0 % to 13.2 % show a very sudden transition between the steps, while the curves with air voids content from 17.4 % to 25.3 % show a smoother development through two changes of temperature concavity.

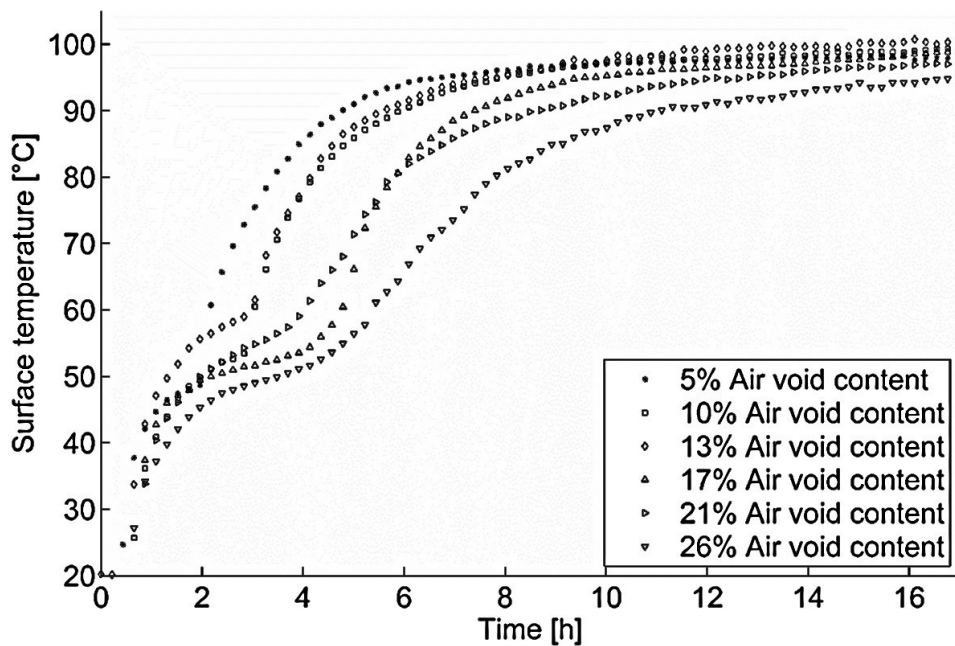


Figure 4-7 Surface temperature versus time

4.10.4 Mass loss and evaporation rate with time

The mass loss versus time for all the asphalt mixtures studied is presented in Figure 4-8. It can be observed that the mass loss increased with time and with the air voids content. Although the test did not run for enough time, it can be

assumed that the curves tend to an asymptotic value that corresponds to a volume equal to the initial amount of water in the asphalt mixture.

The evaporation rate versus time for all the asphalt mixtures studied is presented in **Figure 4-9**. It can be observed that the evaporation rate increases up to a maximum point when it starts decreasing and then tends to approximately 0 g/s. The time at which evaporation peaks increases with the voids content. Also, the maximum value of the evaporation rate increases with the voids content of the analyzed specimens. Both increases are due to the increasing amount of water in the test samples which leads to a larger time being needed for evaporation and, as the specimen has more time to warm, a faster final stage 1 evaporation rate. The reason behind the rate of the mass loss decreasing so sharply for the low voids content mixes but not for the higher voids content mixes is that the mixes with lower voids content have a lower volume of water available for the absorption of latent heat.

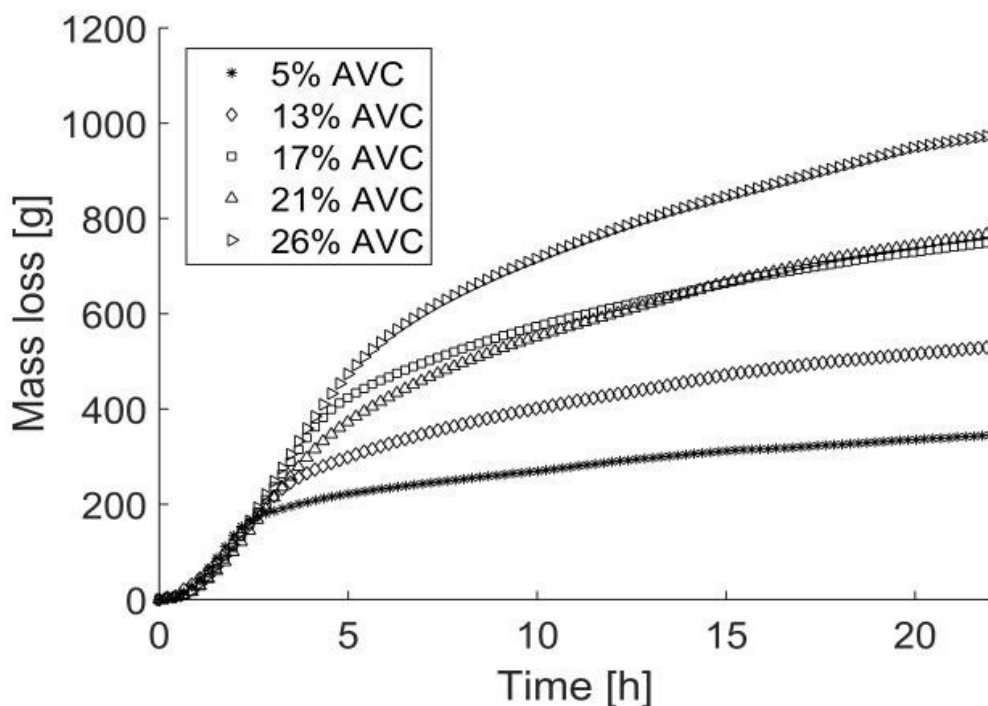


Figure 4-8 Mass Loss of saturated samples versus time

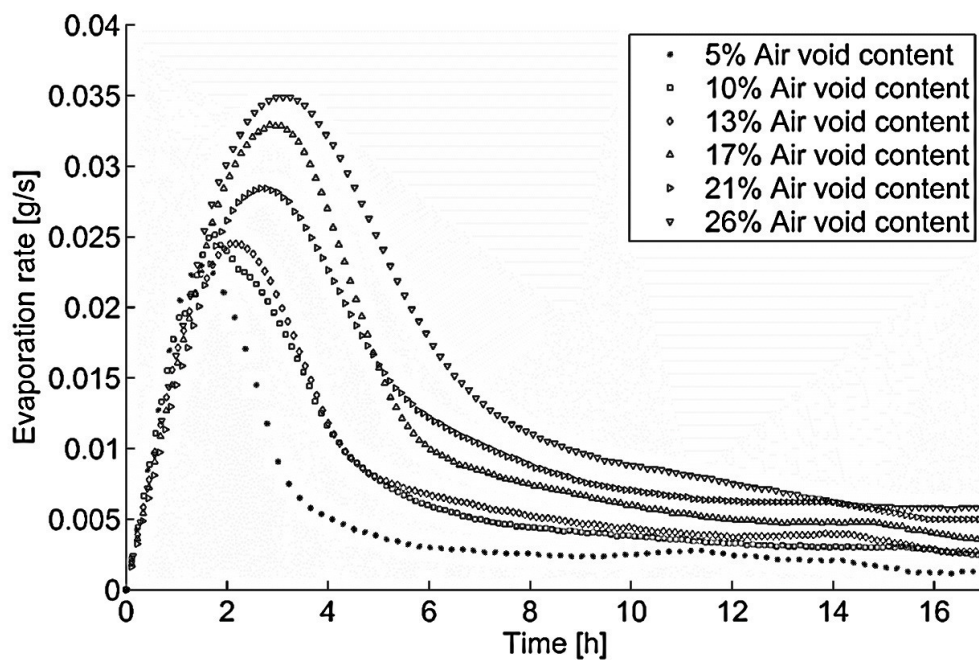


Figure 4-9 Evaporation rate versus time

4.10.5 Heat flux evolution with time

The heat flux evolution with time of every test sample studied is shown in **Figure 4-10**. It can be observed that the measured heat flux decreased with increases in the air voids content. The heat flux first increases, then decreases, and finally increases again up to a maximum value, which depends on the air voids content. As a result, both local maxima and minima can be observed in the heat flux curves before they reach steady state conditions. The times at which local maxima and minima occur show a generally increasing trend.

In addition, it can be observed that the local heat flux is contemporaneous with the evaporation rate maximum point.

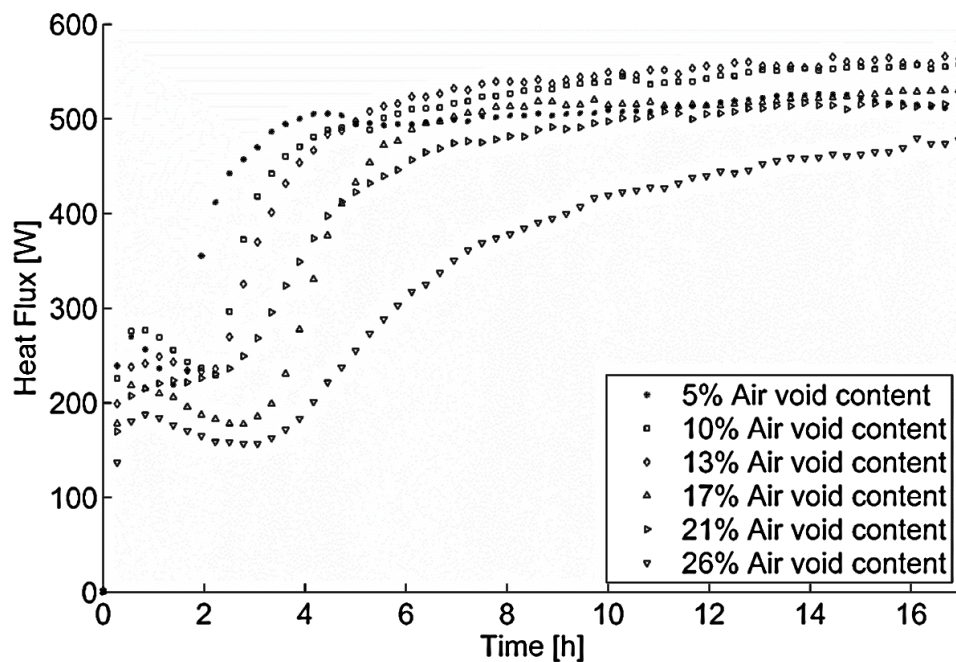


Figure 4-10 Heat flux versus time

A visual observation of the experimental process suggested that as soon as the heating experiment started, the evaporative front started receding inside the

asphalt mixture, and a semi-saturated area appeared (see **Figure 4-11**, Image 2). This corresponded to the first stage of evaporation through a porous medium (Stage 1), where the evaporative flow was ruled by surface tension and hydrostatic pressure (Lehmann, 2008). As happens in porous materials such as soils under evaporative processes, water flowed to the evaporative front thanks to capillarity until gravity and surface tension overcame the evaporative forces (Shokri and Or, 2011) (see **Figure 4-11**, Image 3). At this point in time, the surface of the slabs became dry and water evaporation was dominated by the diffusion of vapour through the pores in the asphalt mixture (Shokri et al., 2009) (see **Figure 4-11**, Image 4) from a free water surface now at the same depth within the pore system of the asphalt.

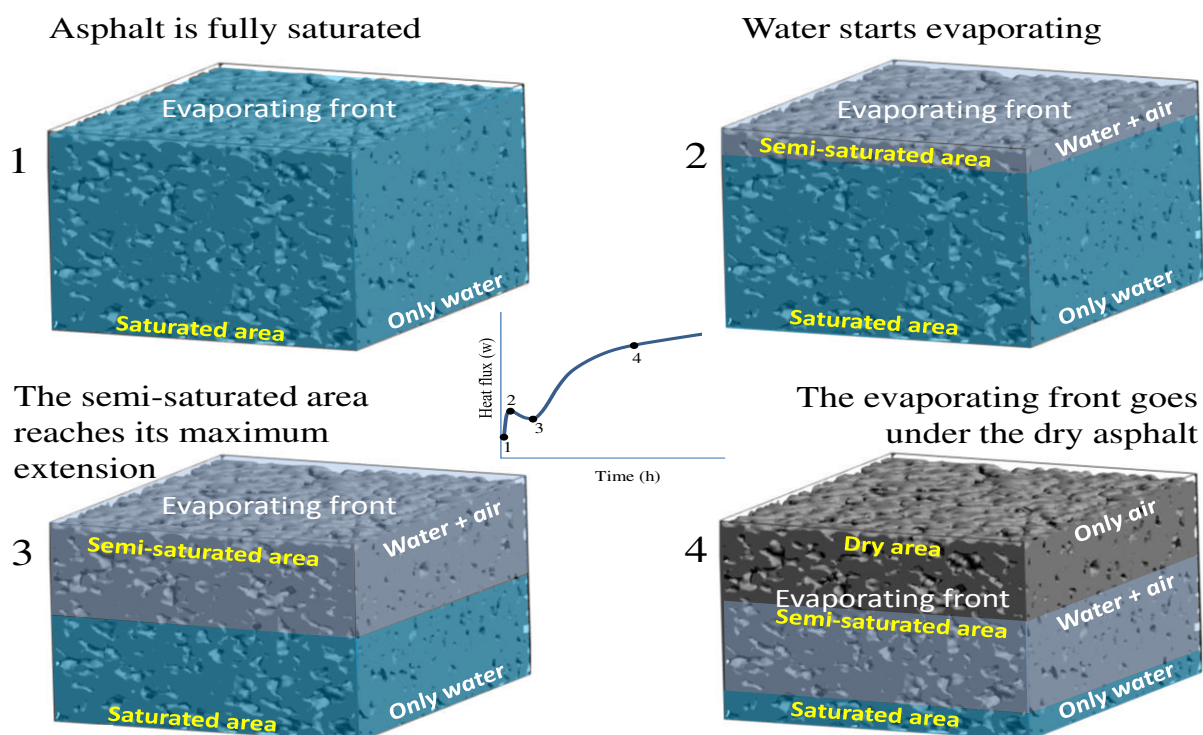


Figure 4-11: Scheme of water evaporation in asphalt mixture.

4.11 Discussion

4.11.1 Stages of water evaporation

In **Figure 4-12** the surface temperature, evaporation rate, and heat flux have been represented versus time with the objective of identifying the main stages of water evaporation. The curves have been divided in three parts, corresponding to the first peak of heat flux (point A), the maximum evaporation rate (point B), and the final concavity change of the curves (C).

As can be observed in **Table 4-3**, the temperature at Point A is strongly related to the diameter and volume of voids and to the tortuosity of connected air paths. In addition, it is moderately related to the amount of air voids in the mixture, while it is not related to the Euler number. This is an indication that the amount of energy needed to evaporate water up to Point A is just a function of the total surface of water exposed to the atmosphere and the amount of water in the mixture.

When the infrared lamps over the saturated test samples are powered, the surface temperature of the slabs starts increasing, so does the evaporation rate of water in the superficial voids of the mixture and the heat flux through the pavement (see **Figure 4-12**). Imagine a saturated capillary channel in an increasingly hot asphalt mixture. If the water on the surface of the channel starts evaporating, water will be drawn upwards, through the asphalt by surface tension and the induced suction (Yiotis, 2006). This process depends only on the diameter of the voids and the total amount of water available (see **Table 4-3**). As a result of the evaporative process, the water level reduces and, hence,

the level of the evaporation front increases. As the temperature of the water continues rising, the evaporative rate increases up to a point when an increasing proportion of the incoming heat flux is absorbed in evaporating water, i.e. as latent heat. For this reason, the temperature increase rate reduces, the heat flux having reached a local maximum (see Point A in **Figure 4-12**).

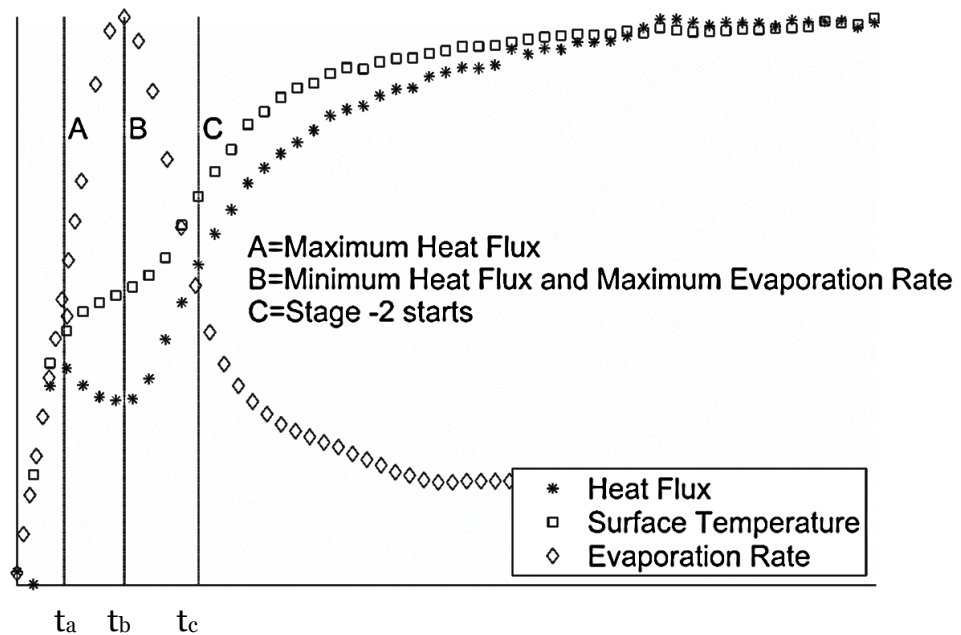


Figure 4-12 Reference points in the evolution of the physical parameters

On the other hand, the time to reach point A does not seem to be related to any specific air void characteristics, and when examining **Figure 4-10**, it appears to be consistently distributed around 46 minutes after the beginning of the test. The reasons for this are unclear and need further investigation.

Moreover, in **Table 4-3** it can be observed that the factors affecting the temperature at the maximum evaporation rate (Point B) are, first, the connectivity of voids and, second, the tortuosity of the connected paths:

although the Pearson's correlation coefficient is higher for T , the tortuosity can be calculated only for the percolated voids. The diameter and volume of voids in the mixture are not related to the time when the maximum evaporation rate happens and this is an indication that water is not evaporating directly into the atmosphere any more. In addition, the time to reach point B is clearly related to the voids structure, being linearly related to the air voids content.

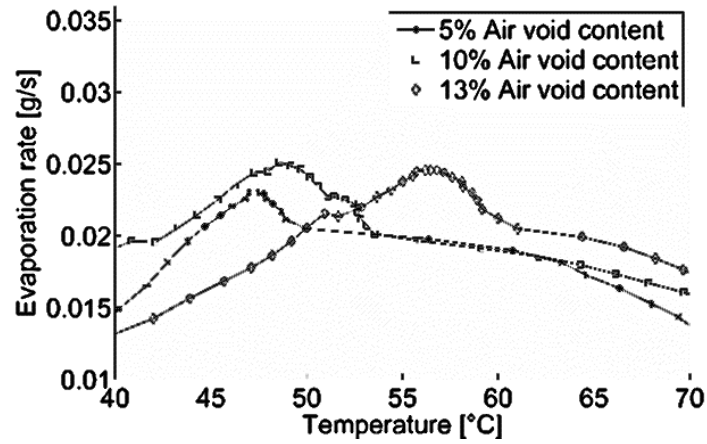
As explained by [García \(2008\)](#), during evaporation in porous media, the internal suction increases, as there is less water contained in the pores, which makes water evaporation increasingly difficult. If an asphalt mixture keeps receiving energy, evaporation continues up to a point when the pore suction starts to overcome the forces powering the upward flow of water ([Shokri and Or, 2011](#)). At that moment, evaporation drops and as a result, the energy that was previously used to evaporate water starts accumulating in the asphalt mixture (see Point B in [Figure 4-12](#) and the track of surface temperature and of evaporation rate to the right of Point B). As a consequence, the heat flux reaches a local minimum and starts increasing again. Note that this is not the end of Stage 1. The temperature for this process increases with the connectivity of voids (see the relationship between Ta and ω in [Table 4-3](#)) because there are more channels available for water flow allowing more water to be evaporated from the mixture, and with the tortuosity (with the straightness of the channels), because water needs less energy to evaporate out of the mixture.

The process described so far can be seen in [Figure 4-13](#). In mixtures with 5% and 10% voids where the voids are not percolated, the evaporation rate rises, initially, approximately constantly for a certain temperature range and drops

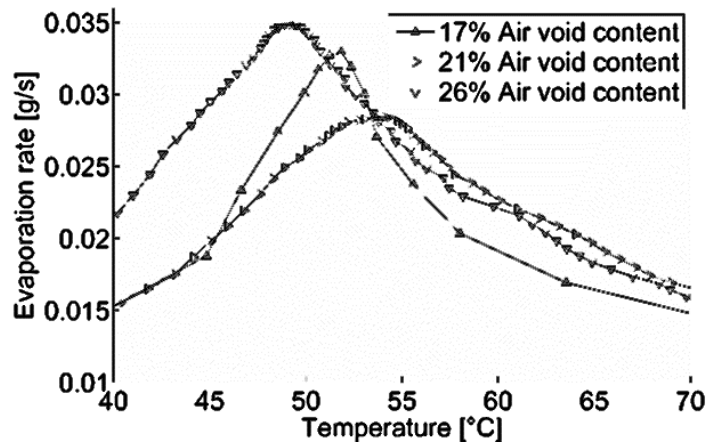
suddenly over a small temperature range, up to a point when the evaporation regime is clearly disrupted. From that point on, the evaporation rate decreases while the surface temperature keeps growing. This disruptive change in the evaporation rate can be defined as the onset of Stage 2, which happens when the drying front reaches a depth greater than the capillary head that would ensure the continuity of liquid inside the porous material (Salvucci, 1997, Shokri et al., 2008). The consequence of this is that the water front in the asphalt mixture recedes in the material, as the surface-anchored menisci are not sustained by capillarity any more (Shokri et al., 2008). The water at the surface and near the surface now exist in unconnected beads. These get smaller as evaporation continues and consequently develop increasing suction as the surface tension around them increases due to their reducing diameter. This results in progressively reducing evaporability. The curves with higher porosity, where a simple visual inspection does not provide the stage 1-2 transition points, here a more strict evaluation method has to be defined because the transition between stages is smoother (see **Section 4.11.2**).

In **Table 4-3**, it can be seen that the factor affecting the temperature at the onset of Stage 2 and the time to reach it are the tortuosity, percolation number, Euler number, and the number of redundant connections in the air paths. Comparing **Table 4-2** and **Table 4-3** it can be concluded that the energy needed to reach the onset of Stage 2 increases (1) with the number of redundant paths in the mixture; (2) when the Euler number decreases; (3) with the percolation number; and (4) with the length of the connected paths or tortuosity. It is known that below the air void percolation threshold the diffusion coefficient is proportional to temperature (Shokri and Or, 2011) and

increases with the voids content (Shokri et al., 2008). When the voids content increases and the pores get connected, the movement of water will increase up to a point when the voids become percolated. Initially the channels will be small enough to allow the capillary movement of water, the movement of water being mainly ruled by surface tension. However, as the pore size increases, the surface tension effect will reduce and the ability of water to move by capillary action to a surface or near surface evaporation front will, thus, reduce. For these reasons, more energy is needed to evaporate water when there is more water available for evaporation.



(a)



(b)

Figure 4-13 Evaporation rate versus temperature.

(a) Samples with air voids content below the air voids content percolations threshold. (b) Samples with air voids content above the air voids content percolations threshold.

Moreover, the time to reach Stage 2 is linearly related to the time for reaching Point B. This is an indication that the physical processes affecting water evaporation until Point A are different from the processes around Point B and Point C.

In the research cited in the present study, previous authors (Shokri et al., 2009b, Shokri et al., 2009a, Shokri and Or, 2011, Salvucci, 1997), always describe a constant and relatively high value of evaporation rate during Stage 1. This was not observed in this study due to the substantially different porous medium. In fact, in previous researches, sand was used, which has an approximately constant pore size due to the similarity between the grains, while here asphalt mixtures were considered.

Asphalt mixtures have widely variable pore sizes, thus, they show a completely different behavior during the evaporation process, see for example that there is no correlation between T_c and the average diameter of air voids. This can be explained if the soil-water characteristic curves for these materials are considered (Choo, 2000): if sand is used, the suction increases significantly and suddenly, while in materials with a range of grain sizes the increase is gradual (Martin, 2004). As a result, sand shows a nearly constant evaporation rate in Stage 1, while in asphalt mixtures the phenomenon has a gradual evolution.

4.11.2 Determination of the onset of Stage 2

The current method to estimate the transition point from Stage 1 to Stage 2 response is explained in references (Shokri and Or, 2011, Brutsaert, 1995), where the inverse of the square of evaporation rate is plotted as a function of time. With this method, Stage 1 response appears as a horizontal line, while Stage 2 behavior can be observed as a straight line of a given slope. The onset of Stage 2 is defined as the geometric intersection of both lines. This is an arbitrary point that does not reflect a physical phenomenon.

As an alternative to the methods of [Shokri and Or \(2011\)](#) and [Brutsaert \(1995\)](#), the first derivative of the evaporation rate versus time was represented in **Figure 4-14**.

The onset of Stage 2 can be observed as a minimum for all the air voids contents analyzed and corresponds to the point with the steepest slopes in **Figure 4-12**. This point also corresponds to the de-percolation point of water in the test samples. Before it, the material is saturated and after this point, water in the voids is not connected any more.

The same point can be observed if the first derivative of evaporation rate versus surface temperature is plotted.

This method can be applied even if the tests are done at a constant temperature, as in several previous studies on this topic ([Shokri et al., 2009](#), [Shokri et al., 2010](#), [Shokri et al., 2008](#)).

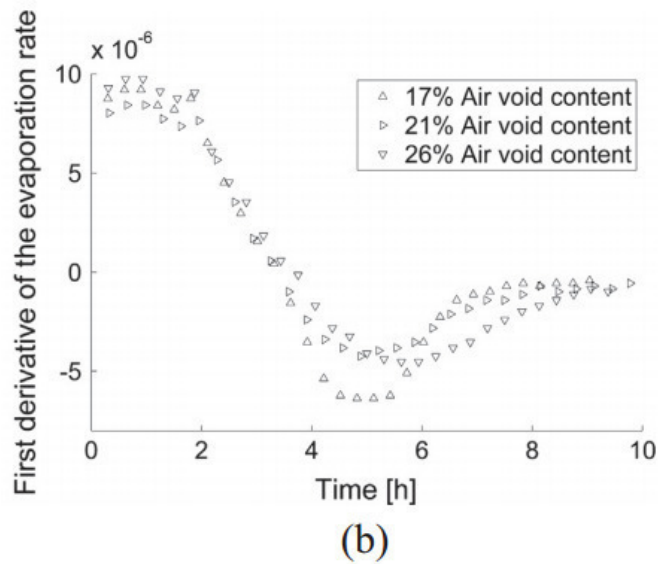
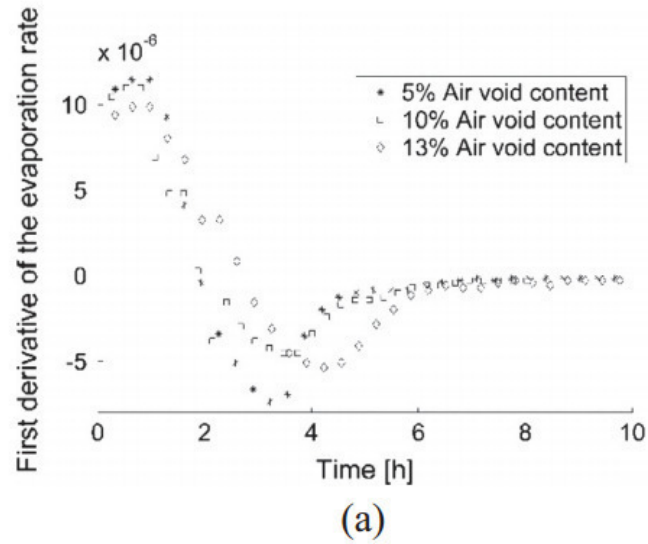


Figure 4-14 First derivative of evaporation rate versus time

(a) Samples with air voids content below the air voids content percolation threshold. (b) Samples with air voids content above the air voids content percolation threshold.

4.12 Summary

This research has shown for the first time the evaporative processes in asphalt mixture with various void contents. It was found that the evaporative process of water in asphalt mixture under a constant energy source follows a three-stage process:

- At first, water evaporates from the pores directly into the atmosphere. The time that this stage lasts is independent of the characteristics of voids in the mixture, and the reasons for this are still unclear. This is reflected by an increase in the temperature and heat flux through the asphalt mixture.
- Then, the evaporation rate increases up to a maximum, which causes the heat flux to reduce through the absorption of latent heat, and a reduction of the temperature of asphalt mixture. The temperature reached at the maximum evaporation rate depends on the connectivity of voids and the tortuosity of the connected paths. In addition, the time for the maximum evaporation rate is proportional to the voids content due to the higher volume of water available for the absorption of latent heat. In this stage the surface of the mixture appears dry, and water does not evaporate directly to the atmosphere: previous researches have concluded that at this stage, a semi-saturated area appears above the water table, and water evaporation is powered by diffusion.
- Finally, the evaporation rate decreases until there is no more water available in the material. At this stage, the surface temperature of the

Chapter 4. Multivariable analysis of water evaporation from moist asphalt mixture

material increases and tends to a horizontal asymptote related to the thermal properties of the asphalt mixture and the incoming heat flux.

- Moreover, stage transition can be calculated by obtaining the first derivative of the evaporation rate versus time or versus temperature. This method is based on the observation of physical phenomena rather than on geometrical assumptions, as previous researchers propose.

5. Thermal properties of asphalt mixture under dry and wet conditions

5.1 Introduction

Asphalt mixture is a composite material consisting of aggregates, bitumen, and air voids. Depending on the asphalt mixture design, the amount of air voids may vary between 2% to almost 30% of the total volume, thus affecting a number of physical properties, such as the thermal conductivity and the specific heat capacity (Mallick et al., 2009, Garcia, 2015). For this reason, understanding the influence of air voids on the thermal behaviour of pavements is a significant consideration in the design of the most appropriate pavement types in any particular climate.

Generally, if asphalt is saturated, part of the energy is absorbed by water to evaporate to the atmosphere, which causes a reduction in the surface temperature (Hendel et al., 2015).

There are previous studies (Mallick et al., 2009), that explain the interaction between factors such as the thermal conductivity and specific heat capacity with water evaporation, and manipulate the factors influencing the thermal properties of asphalt pavements, (Wu et al., 2001, Mallick et al., 2008, Dawson et al., 2011). However, most of the previous information on the thermal properties of asphalt pavements is based on field observations under diverse climatic conditions, (Novo et al., 2010, Gui et al., 2007), or simple modelling (Cenk and Khaled, 2002). The scientific literature on the thermal behaviour of

asphalt mixtures subject to an incident heat flux is not extensive; thus, further studies are needed to better understand the phenomena that characterise the temperature evolution of asphalt mixtures.

The objective of this work is to obtain more complete information concerning the asphalt temperature evolution and the relevant hydro-thermal mechanisms at work under dry and saturated conditions. For this purpose, asphalt mixtures with air voids contents ranging from 4% to 26% were manufactured and the temperatures of dry and saturated asphalt mixtures were compared to one another and related to a number of parameters, such as thermal conductivity and emissivity. These results are expected to have a strong impact on (i) the design of pavements for different climatic conditions, (ii) treatments to reduce the heat urban island effect (Stempihar et al., 2012), such as watering (Lehmann, 2008), and (iii) techniques to harvest solar energy from the pavement layers (Garcia and Partl, 2014, Chiarelli et al., 2015).

5.2 Experimental Method

5.2.1 Material Description

In order to study the effect of air voids content on the thermal properties of asphalt concrete mixtures under different wwater conditions, test samples with various air voids contents ranging from 4.5% to 26% were studied. The same procedure as described in **Section 3.3** of preparing the asphalt mixture slabs was followed. Five slabs with a size of (306 x 306 x 50 mm³) were manufactured for each target air voids content using a 60/40 penetration grade bitumen binder and 20mm maximum limestone aggregate size, mixed at 160 °C and

compacted to the target air voids contents of 4.5%, 13.0%, 17.0%, 21.0%, and 26.0%, using a roller compactor. **Figure 3-1** shows the grading of the aggregate used to make the asphalt mixture samples.

5.2.2 Density and Air Voids Content

Asphalt mixture maximum density was determined according to (BS EN 12697 PART 5, 2009) by the mathematical method. In addition, the bulk density of the test specimens was determined according to (BS EN 12697 PART 6, 2003) by the dimensions method from the average of three test specimens for every asphalt mixture type analysed. The density of each slab and the air voids content obtained for each slab are shown in **Table 3-3**.

5.2.3 Experimental Setup and Measurements

The experimental setup is as previously described and illustrated in **Section 4.5**.

5.2.4 X-ray Computed Tomography

Using the results obtained by the method described in **Section 4.7**, the following images of air voids are created, see **Figure 5-1**. These are 2-dimensional representations, but 3D reconstructions were also produced.

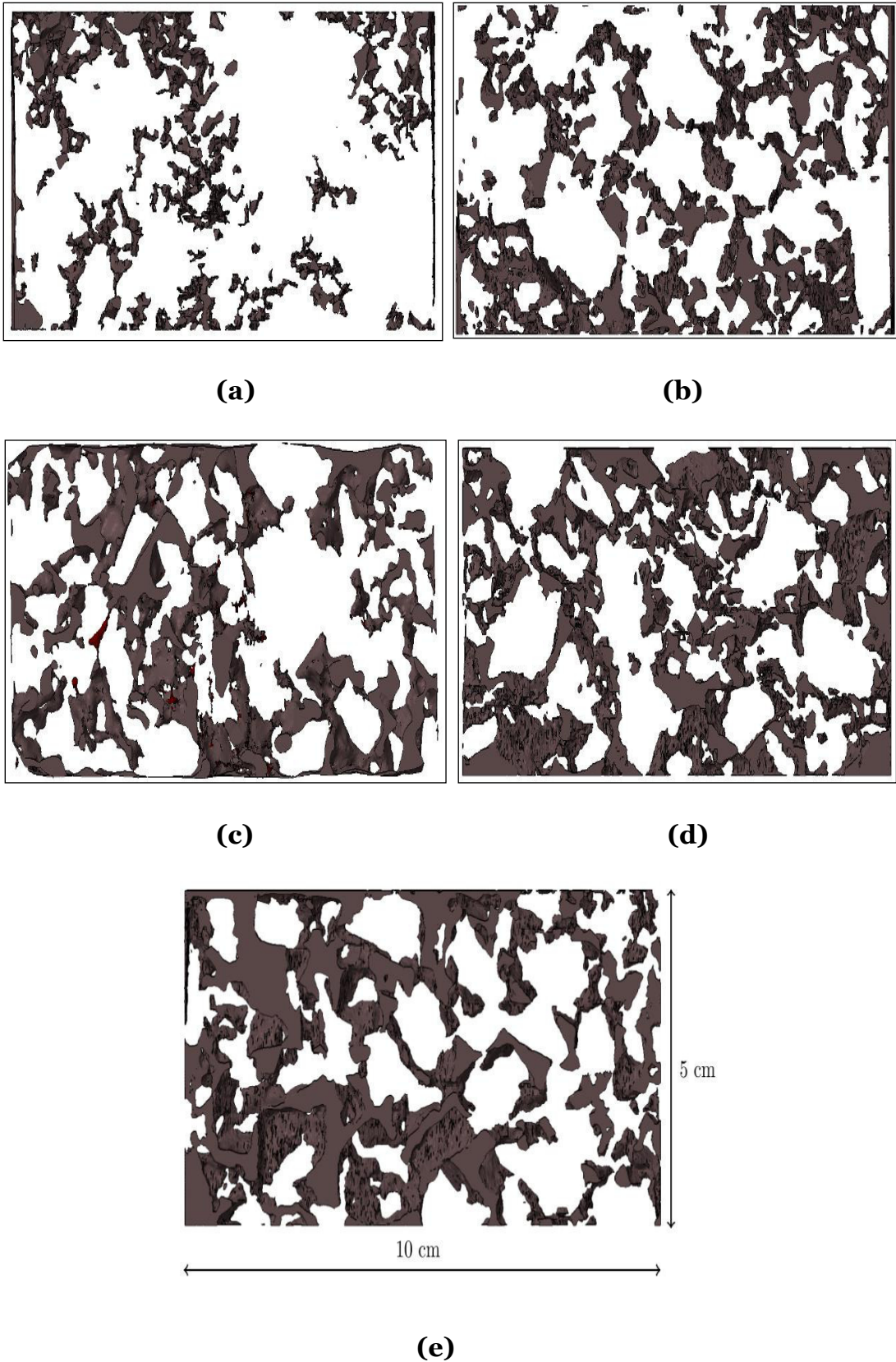


Figure 5-1: Reconstructed air voids in the test samples studied (a) 5%, (b) 13.2%, (c) 17.4%, (d) 21.5%, (e) 25.3%.

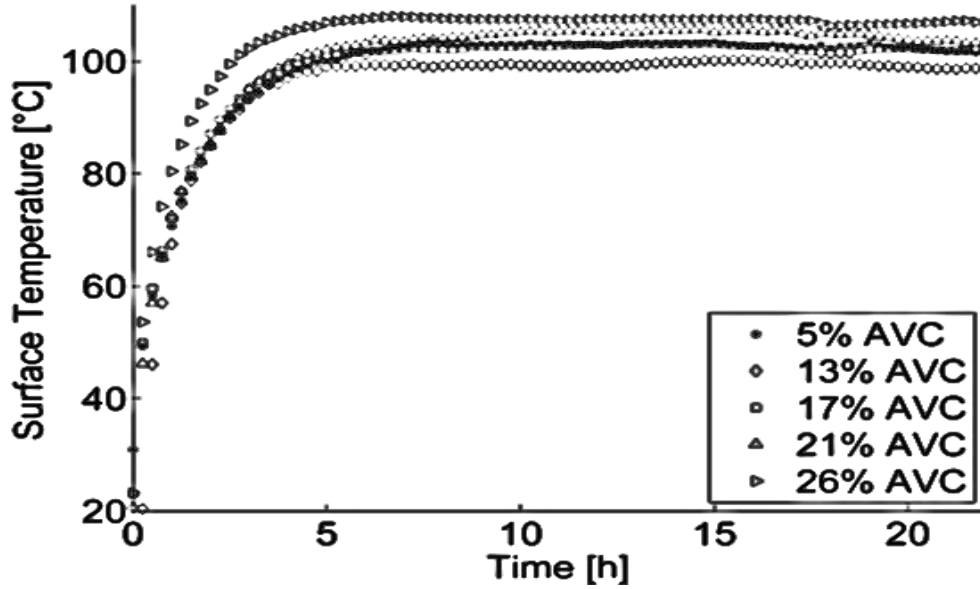
5.3 Experimental Results

5.3.1 Evolution of Surface Temperature with Time

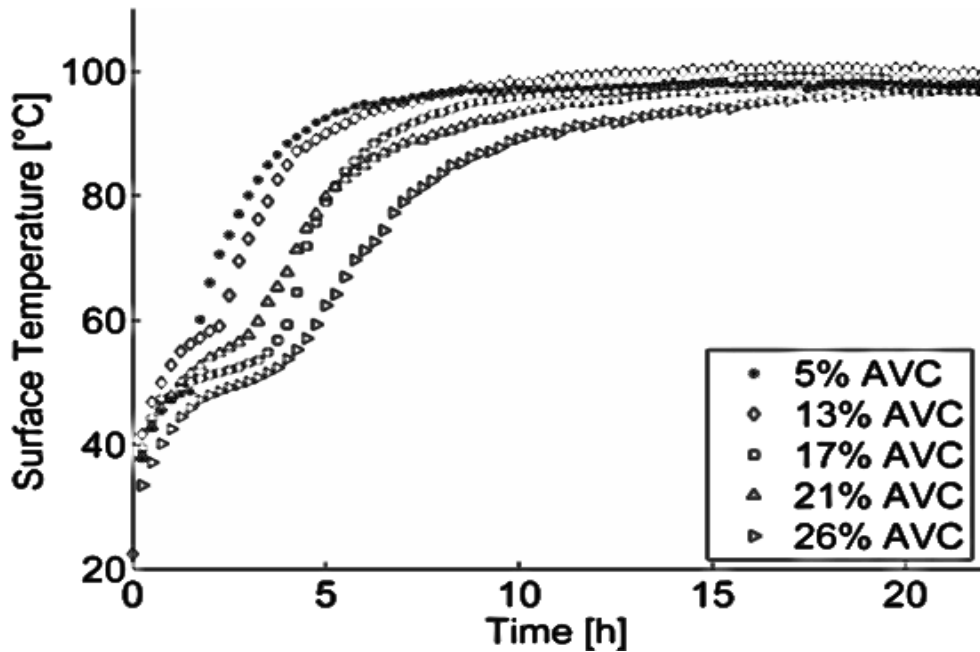
The surface temperature of dry asphalt mixtures is presented in **Figure 5-2** (a). It can be observed that the temperature increase rate was higher in test samples with higher air voids content. The temperature after 24 h testing, which can be considered steady state, was 101.4°C, 98.4°C, 102.1°C, 104.5°C and 107.5°C, for test specimens with air voids contents of 5.0 %, 13.2 %, 17.4 %, 21.5 %, and 25.3 %, respectively.

The surface temperature of wet asphalt mixtures is presented as a function of time in **Figure 5-2** (b), **Chapter 4** provides a detailed discussion. It can be observed that the temperature increase rate was lower in test samples with higher air voids content. In addition, all the curves developed through two steps, the first one, being a transient evolution from 25 °C to 50 °C, and the second one being approximately from 50 °C to 100 °C when steady state behaviour is reached. The curve with air voids content 5.0 % showed a very sudden transition between the steps, while the curves with air voids content from 17.4 % to 25.3 % showed a smoother time-temperature curve at their points of concavity. The temperature after 24 h of testing was 99.5°C, 100.4°C, 98.4°C, 97.8°C and 97.1°C for test specimens with air voids content, 5.0 %, 13.2 %, 17.4 %, 21.5 %, and 25.3 %, respectively. It is obvious that in this chapter, asphalt samples reached higher temperature profile than those in chapter 3. The reason behind this is that the steel frame with fitted infrared lamps are differ from the one used previously in chapter 3 where the infrared lamps were

set closer to each other in this chapter. This would increase the light intensity rate.



(a)



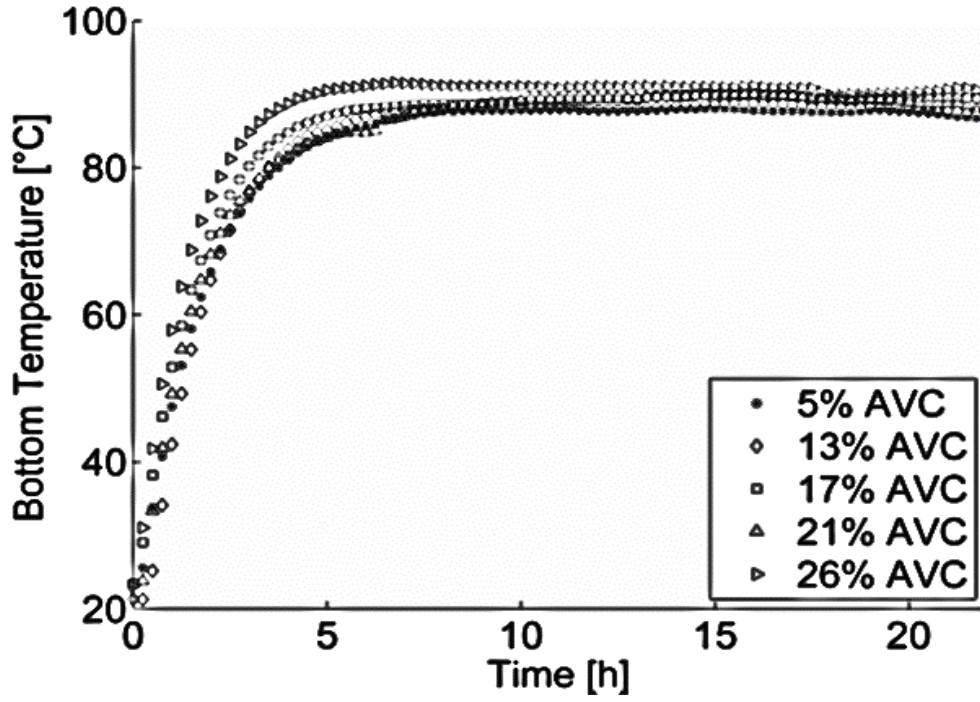
(b)

Figure 5-2: Evolution of the surface temperature (a) in dry conditions. (b) in wet conditions.

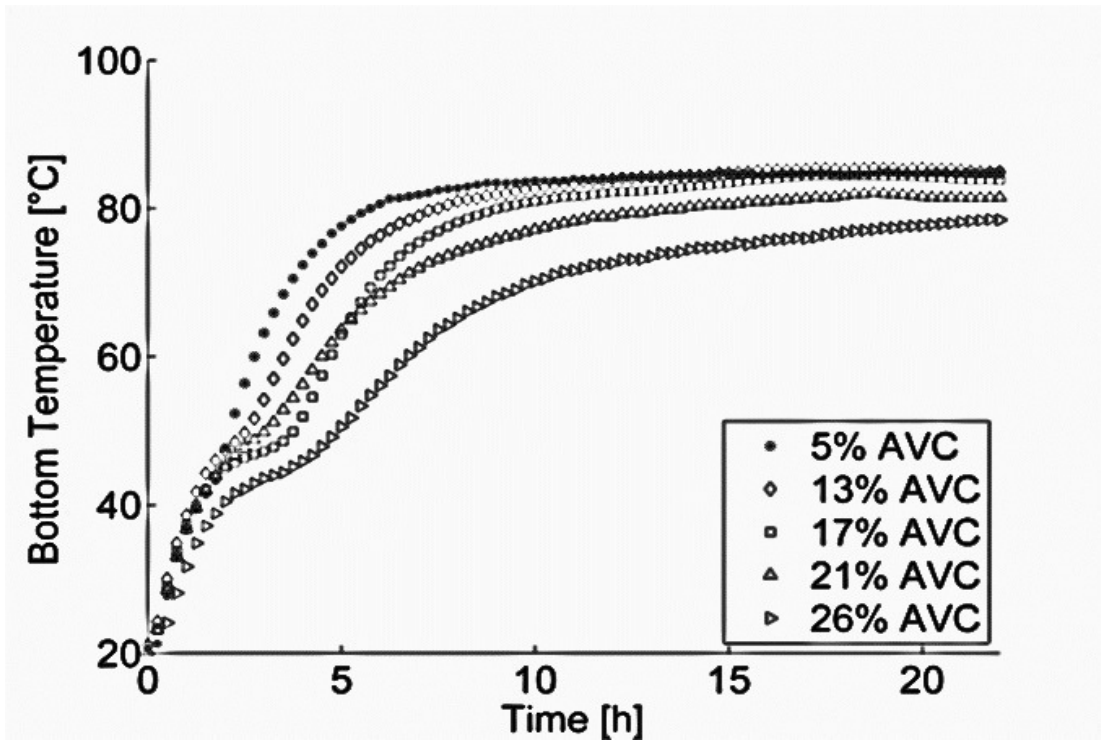
5.3.2 Evolution of Bottom Temperature with Time

The bottom temperature of the dry asphalt mixtures is presented in **Figure 5-3 (a)**. It can be observed that the temperature increase rate was higher in test samples with higher air voids content. The bottom temperature after 24 h testing was 86.9°C, 87.7°C, 89.6°C, 89.1°C, and 91.4°C for test specimens with 5.0 %, 13.2 %, 17.4 %, 21.5 %, and 25.3 %, respectively (i.e. final bottom temperature generally increases with void content).

The bottom temperature of moist asphalt mixtures is presented in **Figure 5-3 (b)**. The temperature increase rate was lower in test samples with higher air voids content. As for the bottom surface temperature, the curves also developed through two steps, the first one, being a transient evolution from 20°C to approximately 45°C, and the second one being approximately from 45°C to approximately 85°C, which was the maximum temperature reached by the slabs. The temperature transition between both steps was very smooth. The temperature after 24 h testing was 86.1°C, 84.6°C, 83.9°C, 81.6°C and 80.9°C for test specimens with air voids content, 5.0 %, 13.2 %, 17.4 %, 21.5 %, and 25.3 %, respectively (i.e. final bottom temperature generally decreases with voids content).



(a)



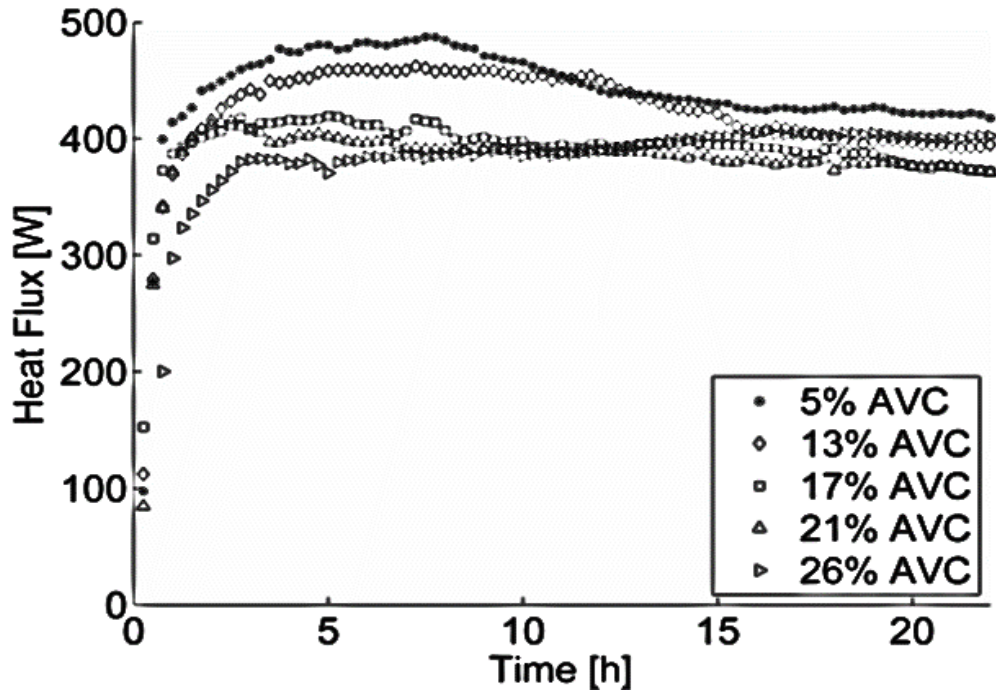
(b)

Figure 5-3: Evolution of the bottom temperature (a) in dry conditions. (b) in wet conditions.

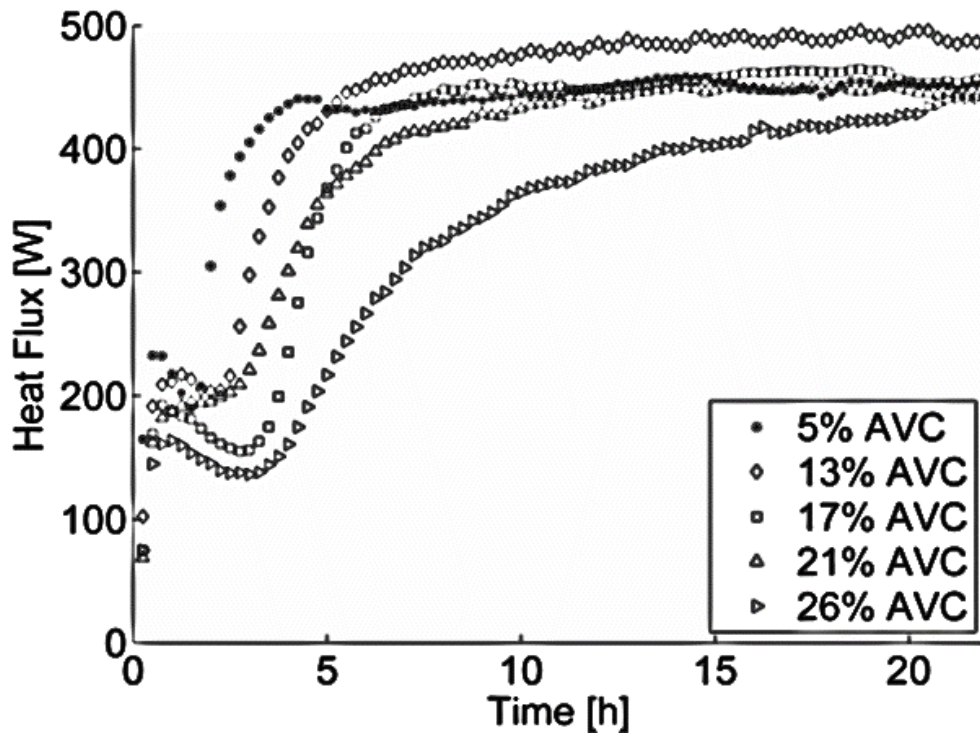
5.3.3 Heat Flux Evolution with Time

The evolution of the vertical, downward, heat flux in dry conditions is shown in **Figure 5-4** (a). It can be observed that the heat flux increased with the heating time until it reached a horizontal asymptote value of around 400W (in some cases having first reached a maximum before decreasing slowly). The initial heat flux was generally higher in mixtures with lower air voids content but the final asymptotic, heat flux achieved does not appear to be related to void content. Note that the asymptotic value corresponds to the condition of steady state heat losses from the bottom of the slabs, which were not insulated.

The evolution of the vertical, downward, heat flux in dry conditions is shown in **Figure 5-4** (b). The heat flux first increased, then decreased, and finally increased again up to a maximum value, which generally depended on the air voids content. As a result, both local maxima and minima could be observed in the heat flux evolution curves before they reached steady state conditions. The times at which local maxima and minima occurred show a generally increasing trend with void content. Moreover, the heat flux was lower in slabs with higher air voids content.



(a)



(b)

Figure 5-4: Heat flux versus time (a) in dry conditions. (b) in wet conditions.

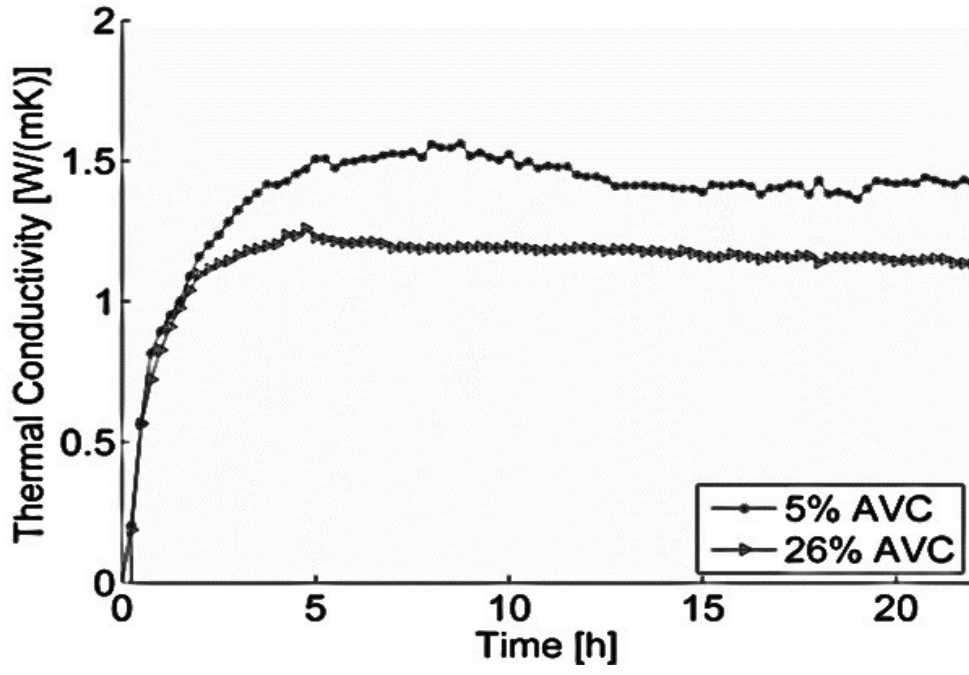
5.3.4 Thermal Conductivity Evolution with Time

The thermal conductivity of asphalt slabs in W/(mK), k , has been calculated using data in **Figure 5-2 (a)**, **Figure 5-3**, and **Figure 5-4** as:

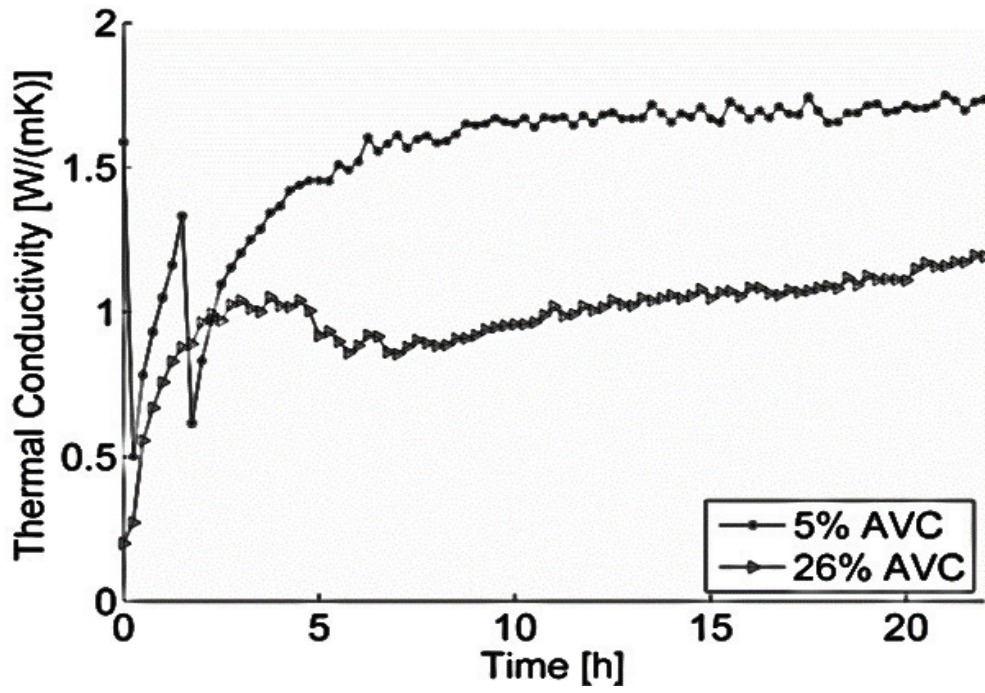
$$k = \frac{Hf(t) \cdot H_s}{T_s(t) - T_b(t)} \quad \text{Eq. 5-1}$$

Where: $Hf(t)$ is the heat flux through the test slab at time, t , measured in W/m²; H_s is the height of the test slab in m; $T_s(t)$ is the surface temperature, measured in °C; $T_b(t)$ is the bottom temperature, measured in °C.

The calculated thermal conductivity of asphalt slabs with 5% and 25% air voids content, in dry conditions has been represented versus time in **Figure 5-5 (a)**. The thermal conductivity increased with time until it reached a maximum, and then decreased, following a similar trend as the heat flux represented in **Figure 5-4 (a)**. Only the two extreme data sets have been represented, to improve the clarity of the figure. The thermal conductivity of the same slabs, but in wet conditions, has been represented versus time in **Figure 5-5 (b)**. It can be observed that the thermal conductivity of the test samples increased until a time when it dropped and then, it continued increasing again. For the 5% air voids slab, the drop is at an earlier time, is larger and is much more immediate than for the more porous slab.



(a)



(b)

Figure 5-5: Thermal conductivity versus time for samples containing 5% and 26% air voids (a) in dry conditions. (b) in wet conditions.

5.4 Discussion

All the experiments run for this work consisted in heating up asphalt slabs with infrared lamps. In the case of dry samples, when the lamps are powered on, the surface temperature increases rapidly and all samples reach steady state conditions after about 24 hours. In **Figure 5-2 (a)**, the curve with the highest temperature is the one corresponding to the sample with 26% air voids content, which has the lowest thermal conductivity. This can be also seen in **Figure 5-5 (a)**, where the thermal conductivity is represented versus time. It is apparent that heat cannot be efficiently conducted downwards by the sample with highest air voids content and it accumulates on the surface. In addition, the sample with 26% air voids content also has the lowest specific heat capacity of all samples (see **Table 3-3**) thus, a lower amount of heat could be accumulated in the material at a given temperature. A possible explanation for this trend is that the low thermal conductivity is what most affects the surface temperature in dry asphalt mixtures, as this parameter regulates how easily heat can be conducted downwards to lower layers. Air convection in the pores is not considered as a heat transfer mechanism, because its influence was proven to be negligible; see **Chapter 4** for more detail.

In **Figure 5-3 (a)**, the evolution of the bottom temperature of dry asphalt samples is shown. The bottom temperature is proportional to the surface temperature, as mandated by Fourier's law of thermal conduction. This can be seen by comparing **Figure 5-2 (a)** and **Figure 5-3 (a)**, where the curves show the same behaviour but lower values in the case of the bottom temperature. Steady-state conditions were reached at a later time than for the surface

temperature, due to the effect of specific heat capacity in the transient phase of the heating process. It can be observed that the steady-state values of the bottom temperature are more uniform between the samples than those seen for the surface temperature.

The evolution of the heat flux in dry specimens shown in **Figure 5-4 (a)** had a similar trend to that of the surface and bottom temperatures, see **Figure 5-2 (a)** and **Figure 5-3 (a)**. In fact, the heat flux increased to its maximum level in about 22 hours, and then stabilised to a steady-state value. The time needed depends a lot on voids: the peak for 5% voids is at about 8 hours. Furthermore, the values of the heat flux reported in **Figure 5-4 (a)** appear in a clear order during the transient period, i.e. the curve with the highest average heat flux is the one with the lowest air voids content, while the curve with the lowest average heat flux is the one with the highest air voids content. This is because the sample with 5% air voids content had the highest thermal conductivity (see **Figure 5-5 (a)**), thus, the thermal flux reaching the bottom of the specimen was the highest. In contrast, the sample with 26% air voids content had the lowest thermal conductivity and its average heat flux was the lowest. As a result, most of the heat was accumulated in the surface of the slab.

In the case of wet samples, the curves shown for all parameters were completely different due to the presence of a two-phase flow in the material's pores as described in **Chapter 4 (Garcia, 2015)**. The evaporative process had a clear effect on the curves shown in **Figure 5-2 (b)**, and **Figure 5-4 (b)**, as they all show oscillations as a consequence of the hydro-thermal effects incurred due to the presence of water in the material.

In **Figure 5-2 (b)**, the curves show that the final temperatures at the end of the tests were generally lower than those seen in **Figure 5-2 (a)**. The reason for this is that in the case of moist samples an amount of water proportional to the air voids content was still trapped in the pores of the materials (see **Figure 5-3 (a)**). As a result, part of the incident energy was absorbed by water, which kept evaporating at an increasingly slow rate. The presence of water in the pores must also be responsible for an increase in the thermal conductivity of the whole material as compared to the situation when the pores were filled with air, see **Figure 5-4 (b)**.

The temperature evolution of moist samples in **Figure 5-2 (b)** and **Figure 5-3 (b)** was also much slower than that seen in their dry counterparts. When the infrared lights were on, water started evaporating directly to the atmosphere, which absorbed (latent) heat and reduced the surface temperature of the asphalt mixture. From this moment, the temperature evolution in **Figure 5-2 (b)** and **Figure 5-3 (b)** showed a reversal in the temperature increase rate.

As can be observed in **Figure 5-3 (b)**, the time for the intermediate minimum coincided with the peak in the evaporation rates in the test samples. From this moment, the temperature increase rate accelerated, which was coincident with the reduction in the water evaporation rate. Therefore, a reduction in the amount of energy used for water evaporation was recorded. This process is also reflected in the heat flux curve in **Figure 5-4 (b)**, which shows a drop in the energy flux at a time coincident with the temperature increase reversal and maximum evaporation rate. In addition, the absence of water in the pores at the end of stage 1, caused a reduction in the thermal conductivity of the asphalt

slabs, because air and water vapour have a much lower thermal conductivity than liquid water (Powell et al., 1966) (see **Figure 5-5 (b)**).

Furthermore, only the samples with 5% and 13% air voids content reached a steady state temperature (see **Figure 5-2 (b)** and **Figure 5-3 (b)**). The reason for this is that only the pores that are connected with the irradiated surface experienced water evaporation, as they were the only ones connected to the atmosphere but, in the densest samples, these pores are not connected to pores lower in the specimen. The connectivity of the pore space can be assessed based on the procedure introduced by Garcia (2015) using 3D CT

As an example, **Figure 5-6** shows the biggest connected air voids skeleton for the reconstructed test samples shown in **Figure 5-1**. In this Figure, it can be visually appreciated how the percolation threshold occurs for test samples with an air voids content somewhere between 13.2% and 17.4%. At voids content $\leq 13.2\%$, due to the lack of connected air voids, the water in the surface pores evaporated very fast and the materials rapidly reached a steady-state temperature. On the other hand, in samples with air voids content $\geq 17.4\%$, there were connected air channels in the materials, thus, water evaporation and diffusion could happen for a longer time. The actual threshold must therefore be somewhere between these two values.

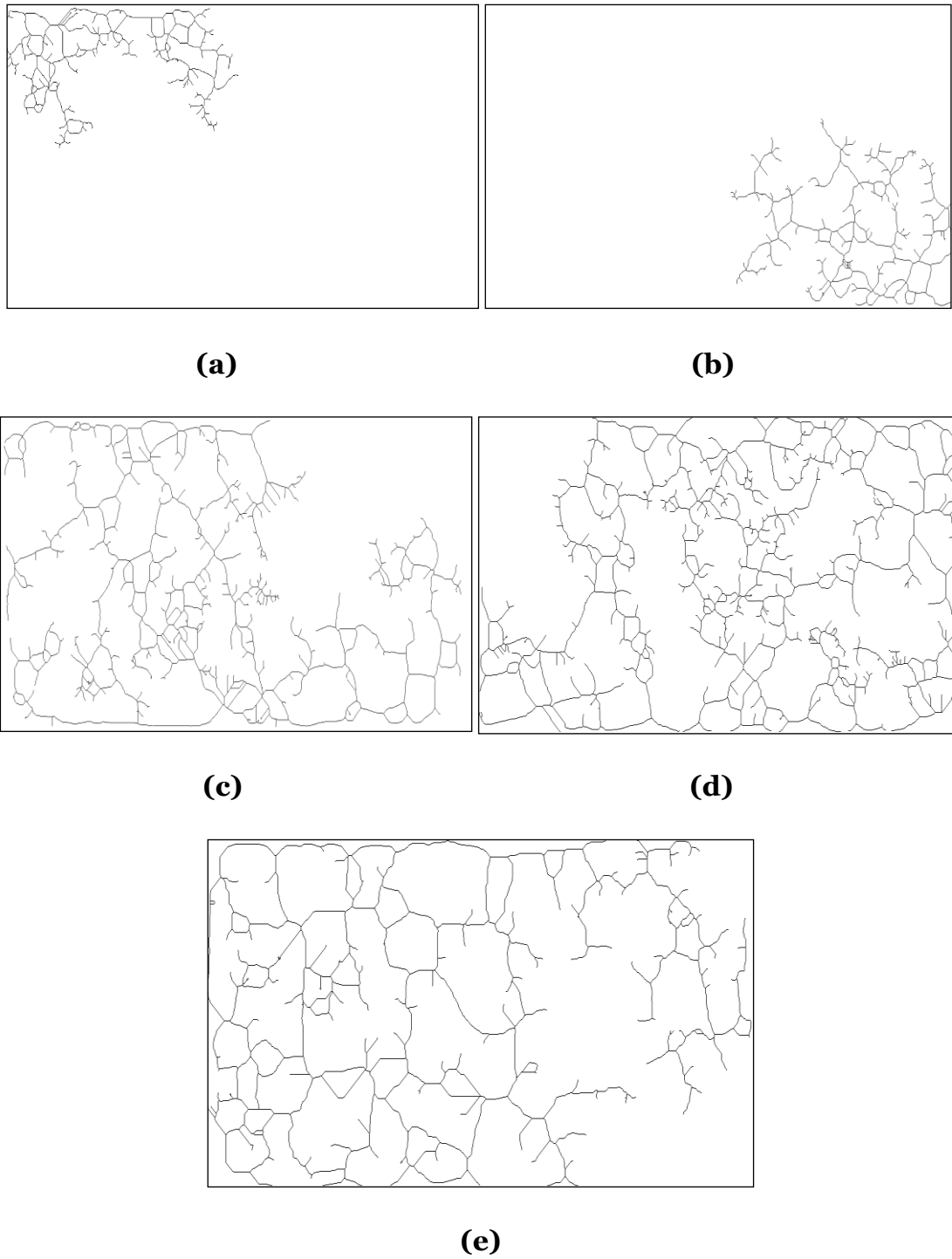


Figure 5-6: Biggest connected air voids skeleton for reconstructed test samples in Figure 2. (a) 5%, (b) 13.2%, (c) 17.4%, (d) 21.5%, (e) 25.3%.

5.5 Summary

In this work, the thermal properties of asphalt slabs with various air voids contents have been analysed under dry and wet conditions. It was found that:

- The steady-state surface temperature reached by asphalt mixtures under a constant energy source increased with the air voids content of the material.
- The temperature increase rate of asphalt mixture under dry conditions was higher than under wet conditions. This happened because the water in the air voids used energy for evaporation, that otherwise, would have raised the temperature.
- When wet asphalt materials were heated, the water evaporation rate increased until it reached a peak, and then decreased until all the water in the connected pores was consumed. The reason for the rapid, post-peak, decrease in evaporation rate is due to the evaporative forces that power the movement of water to the surface of the asphalt mixture becoming smaller than the gravity and surface tension forces that act to keep water in the material.
- The temperature increase rate under wet conditions decreased with the increase in the air voids content of asphalt mixture. This happened because there was more water available for evaporation and, hence, a greater latent heat demand. While the temperature increase rate in dry conditions showed a continuous decrease until steady state, the temperature increase rate of asphalt mixture in wet conditions initially

increased, then reduced as evaporation became easier due to the raised temperature. Temperature increased again when all the easily evaporated water had been consumed, and, finally, decreased towards an asymptotic value representing dry steady-state conditions.

- The heat flux through dry asphalt mixture increased until it reached a peak, and then decreased towards an asymptotic value. On the other hand, the heat flux through asphalt mixture in wet conditions decreased initially due to the effect of water evaporation, and then increased again towards the same asymptotic value as the materials in dry condition. At the end of heating both initially-wet and initially-dry specimens had reached the same condition and, hence, the same response.
- Under dry conditions, the heat flux was higher in asphalt mixtures with low air voids content. This happened due to the solid fraction's higher thermal conductivity. In contrast, under wet conditions, the heat flux and temperature reduction due to water evaporation was higher in more porous materials, because these contained a higher amount of water.
- In wet conditions, the thermal conductivity of an asphalt mixture dropped suddenly when the water available for evaporation was consumed.

6. Harvesting heat from pavement by thermoelectric power generators

6.1 Introduction

Over recent years, although there have been some previous attempts to recover heat energy from pavements, the work has been extremely limited in terms of installation. Incorporating tubes in the asphalt pavement is considered the most practical solution applying a heat exchanger design, with water or air circulating inside. There are major drawback to these systems such as the effect of traffic and pavement load on the installed pipes, effect of pipes on pavement performance and pavement maintenance technology that can be applied.

Another promising technique for beneficially recovering heat is the use of Thermoelectric Power Generators (TEG) (Snyder, 2006).

Thermoelectric power generators have been applied in a variety of waste heat energy applications over the past decades. These include industrial instruments, medical, aerospace, military, and portable or remote power generation applications (Eibl, 2015). Although the low conversion efficiency of the thermoelectric power generator is the major drawback of this instrument, a thermoelectric power generator using waste heat energy can be considered as an almost ideal application, as the cost of thermal energy input is zero. Therefore, the most important objective in thermoelectric power generation in a pavement application is to improve its performance and to reduce the device cost. Researchers have conducted a large amount of work in order to improve

the heat to electricity transformation efficiency of the TEG through improving the three main physical properties that affect the output: Seebeck effect, thermal conductivity and electrical resistivity (Zheng, 2014). Such studies have included the use of nanotechnology (Alam, 2013), novel technology in solid state physics and semiconductor physics (Shakouri, 2011).

The main aim of the study reported in this thesis was to investigate the feasibility of recovering solar heat energy from asphalt concrete pavement materials by converting heat into electricity through TEGs. The second aim was to study the effect of the asphalt concrete air voids content on that heat energy recovery. The third objective was to investigate the effect of a cold junction on the total heat recovery through using different cold junction configurations. For this purpose, three asphalt mixtures with different air voids contents, 5%, 13% and 21%, were manufactured and three configurations of cold junction were set up. A number of parameters were observed for comparison purposes, this including the asphalt surface and bottom temperature profile, soil temperature profile at different depths, temperature difference between hot and cold junction, and output voltage. This study is an initial investigation into the feasibility of using TEGs to recover heat from pavements.

6.2 Background

The thermoelectric phenomenon associated with the Seebeck effect is due to the simultaneous presence of an electric field in a material. The discovery of this phenomenon was back in 1821 by Thomas Johann Seebeck, where he observed that the magnitude of the voltage generated was proportional to the temperature difference and dependent on the type of conducting material

(Rowe, 1995). A TEG consists of thermocouples of n-type (materials with excess electrons) and p-type (materials deficient in electrons) elements connected electrically in series and thermally in parallel. Heat is input on one side and rejected from the other side, generating a voltage across the TE couple **Figure 6-1**. The magnitude of the voltage produced is proportional to the temperature difference.

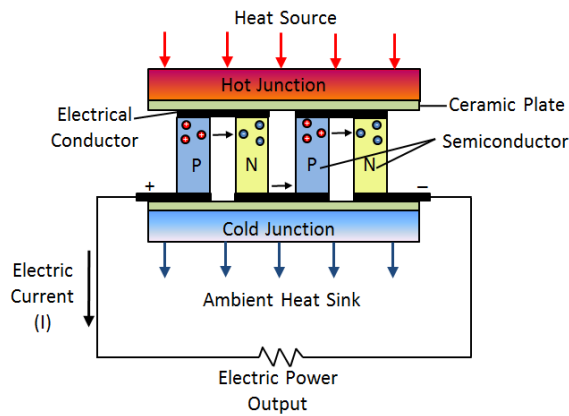


Figure 6-1 Schematic Diagram of Thermoelectric Power Generator

Thermoelectric technology is used to convert the heat energy into electricity. The efficiency of the TEG is evaluated based on what is known as the thermoelectric figure of merit, ZT (Eibl, 2015). The larger the value of ZT , the better is the thermoelectric material. The figure of merit is defined as:

$$ZT = \left(\frac{S^2 \cdot \partial}{K} \right) * T \quad \text{Eq. 6-1}$$

Where, S is the Seebeck coefficient, measured in V/K, ∂ is the electrical conductivity, measured in s/m, T is the absolute temperature, measured in K and k is the thermal conductivity, measured in W/mK, and is defined as:

$$k_n = (0.0000334545 * T^2 - 0.023350303 * T + 5.606333) \quad \text{Eq. 6-2}$$

$$k_p = (0.0000361558 * T^2 - 0.026351342 * T + 6.22162) \quad \text{Eq. 6-3}$$

Where: the subscript n refers to the n-type thermo-element and the subscript p refers to the p-type thermo-element.

The Seebeck coefficient is defined as:

$$S_n = (0.001530736 * T^2 - 1.08058874 * T - 28.338095) * 10^{-6} \quad \text{Eq. 6-4}$$

$$S_p = (-0.003638095 * T^2 + 2.74380952 * T - 296.214286) * 10^{-6} \quad \text{Eq. 6-5}$$

Electrical conductivity is defined as:

$$\sigma_p = (0.015601732 * T^2 - 15.708052 * T + 4466.38095) * 10^2 \quad \text{Eq. 6-6}$$

$$\sigma_n = (0.01057143 * T^2 - 10.16048 * T + 3113.71429) * 10^2 \quad \text{Eq. 6-7}$$

The absolute temperature T is known as:

$$T = \frac{T_H - T_C}{T_H} = \frac{\Delta T}{T_H} \quad \text{Eq. 6-8}$$

Where: T_H and T_C are the temperature of the hot junction and the cold junction respectively, measured in K.

The above equations are used for calculating thermoelectric properties (best fit derived from measured material characteristics).

The efficiency of a thermoelectric converter is highly dependent on the temperature difference ($T_H - T_C$) across the device. This is because the thermoelectric generator, like all engines, cannot have an efficiency greater

than that of a Carnot cycle ($\frac{\Delta T}{T_H}$) (Snyder, 2008). The efficiency of the TEG is defined as:

$$\eta = \frac{T_H - T_C}{T_H} * \left[\frac{(1 + ZT)^{\frac{1}{2}} - 1}{(1 + ZT)^{\frac{1}{2}} + \frac{T_C}{T_H}} \right] \quad \text{Eq. 6-9}$$

Where the first part is the Carnot cycle, ZT is the figure of merit as defined in **Eq. 6-1**.

The efficiency η is proportional to the ZT and also to the increase of ΔT , therefore a large ΔT is preferred for better efficiency. Due to the enhancement in the currently available thermoelectric materials the range of ZT is broadening and so that ZT values > 2 are now available.

6.3 Experimental Method

6.3.1 Material Description

Three asphalt concrete slabs (each 306 x 306 x 50 mm) were used to measure the output voltage. The samples were produced using a 60/40 penetration grade bitumen binder and 20 mm maximum limestone aggregate size, mixed at 160 °C, and compacted at 140 °C to the target air voids content of 4.5 %, 13.0 % and 21.0 % using a roller compactor (see **Section 3.3**). In this chapter only three different air voids content were studied as the main objective from this chapter is to study the feasibility of harvesting heat from asphalt pavement by thermoelectric power. In addition, the gradation curves for each type of aggregate used are presented in **Figure 6-2**. Detailed information about the aggregate gradation was described in **Section 3.3.1**.

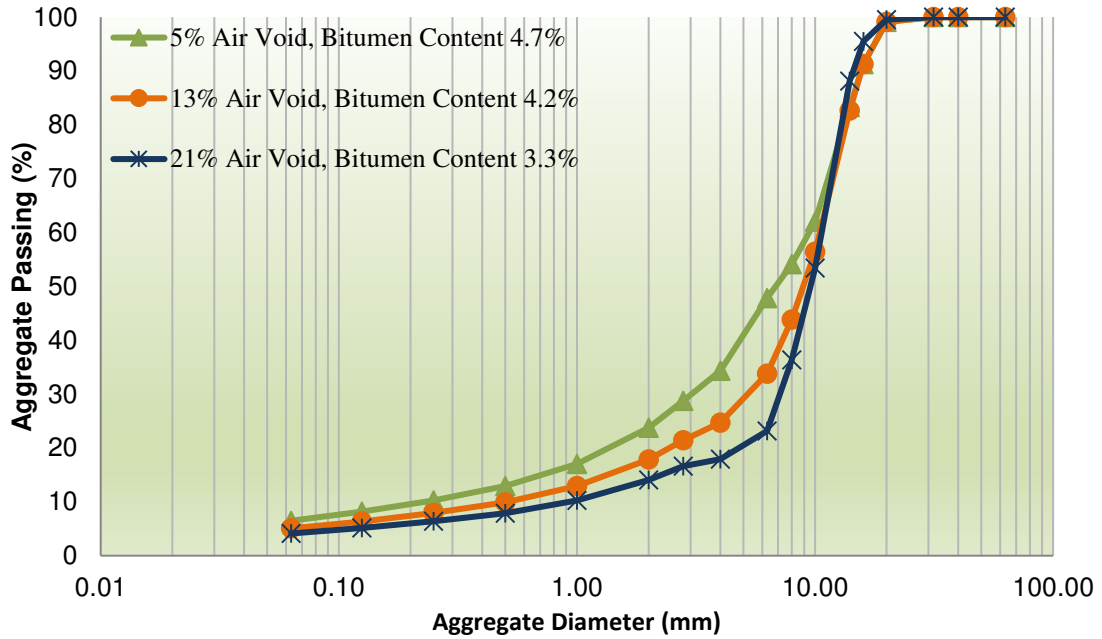


Figure 6-2 Composition of asphalt mixtures

6.3.2 Density and Air Voids Content

Asphalt mixture density was determined according to [BS EN 12697 PART 5 \(2009\)](#) by the mathematical method. In addition, the bulk density of the test specimens was determined according to [BS EN 12697 PART 6 \(2003\)](#) by the dimensions method from the average of three test specimens for every asphalt mixture type analyzed. [Section 3.4](#) described this procedure in more detail.

In addition, the air voids content of the asphalt mixtures was calculated based on the maximum and bulk densities. [Eq. 3-4](#) was used to calculate the test sample air voids content. More detail about this procedure can be found in [Section 3.5](#).

6.3.3 Experimental Setup

Figure 6-3 and **Figure 6-4** present a schematic and laboratory diagram of the experimental setup, respectively. A rectangular box with dimensions of 350 x 650 x 600 mm was filled with a sandy dry soil, comprised of particles larger than 0.05 millimetres and smaller than 2 milliammeters. Three different configurations were used for measuring the output voltage produced as shown in **Figure 6-5**. The main reason behind the three-configuration set up was to study the effect of cold junction type on the heat energy recovery. In configuration 1, insulation material was placed over the soil surface and then three holes were made in the insulation material having the size of the Thermoelectric Power Generator (TEG) devices ($40 \times 40 \times 3.4 \text{ mm}^3$). Then, the three TEG devices, were installed on the bottom of the asphalt mixtures using thermally conductive epoxies which serve as a glue layer (see **Figure 6-6**). A thermal interface self-adhesive graphite pad with a dimension of 65 x 50mm x 0.25mm was used to provide an essential interface between the hot side of the TEG module and the asphalt mixture. This layer will serve as a glue layer as well as transferring the heat from the asphalt mixture to the TEG device. Later, the asphalt slab with installed TEG devices was placed on top of the insulation material above the soil with the TEG devices placed in the three holes to ensure a good contact with the soil.

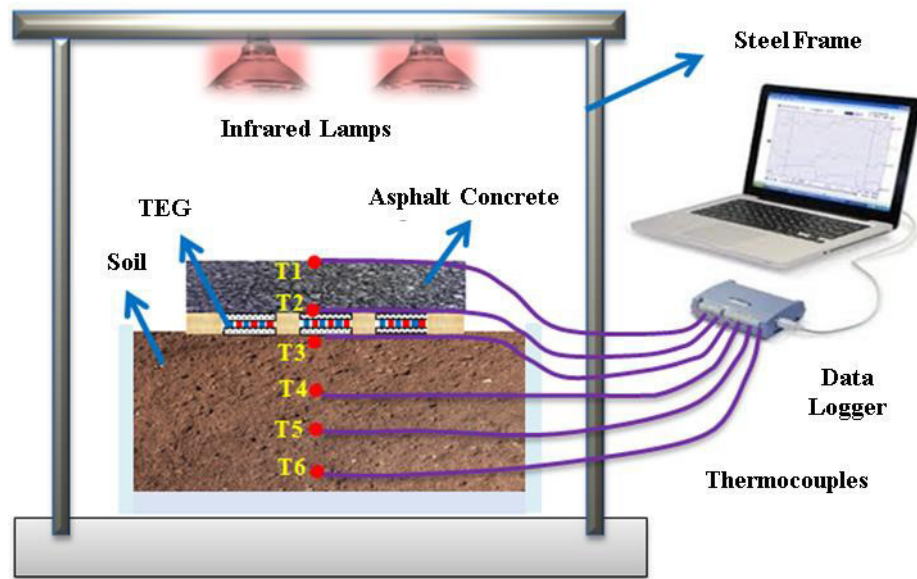


Figure 6-3 Experimental setup schematic diagram

In configuration 2, the same process as configuration 1 was used except that the asphalt slab with installed TEG devices was placed on the top of an aluminium plate positioned on top of soil surface as shown in **Figure 6-5**. In configuration 3, the insulation material was placed over the soil surface which acts as a medium layer between the asphalt slab and soil surface. Then, the lights are switched on until the asphalt slab reaches the maximum steady state temperature. Later, the aluminium plate was installed inside the soil at 40mm depth and covered by a thermal insulator material from all sides except the last 10mm inside the soil. Thereafter, the TEG device was installed between the asphalt slab and aluminium plate using thermally conductive epoxies spread on the aluminium plate and asphalt slab as shown in **Figure 6-5**. The test for this configuration ran over a short period of time (two hours). Though the setup of Configuration 3 is not comparable to the other two configurations, this configuration is only used to illustrate how much energy can be recovered by

maintaining the temperature difference between the asphalt pavement and the deep soil (subgrade layer).

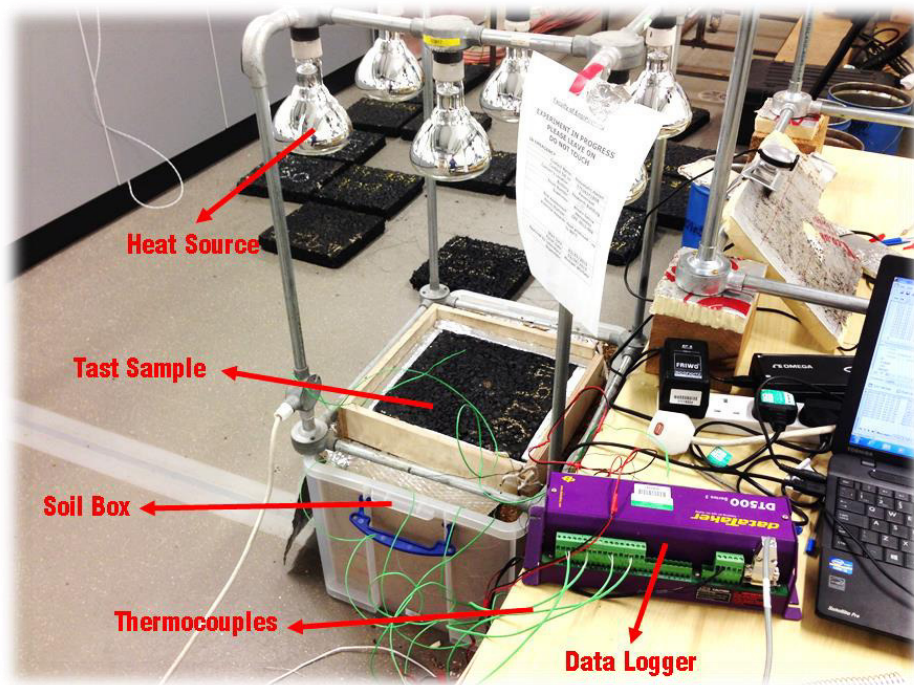


Figure 6-4 Laboratory experimental setup

Infrared lamps were used as a source of heat. The heat source comprised six 250 W infrared lamps installed in two rows at approximately 730 mm above the asphalt slab surface, arranged so that their warming effect was almost uniform over the whole asphalt area (see **Figure 6-3**). The output voltage for each asphalt concrete slab was measured over two days at 10 second intervals. In addition, the temperature profiles for the: surface of the test sample, the bottom of the test sample and the soil at four different depths were recorded over the test period as shown in **Figure 6-3**.

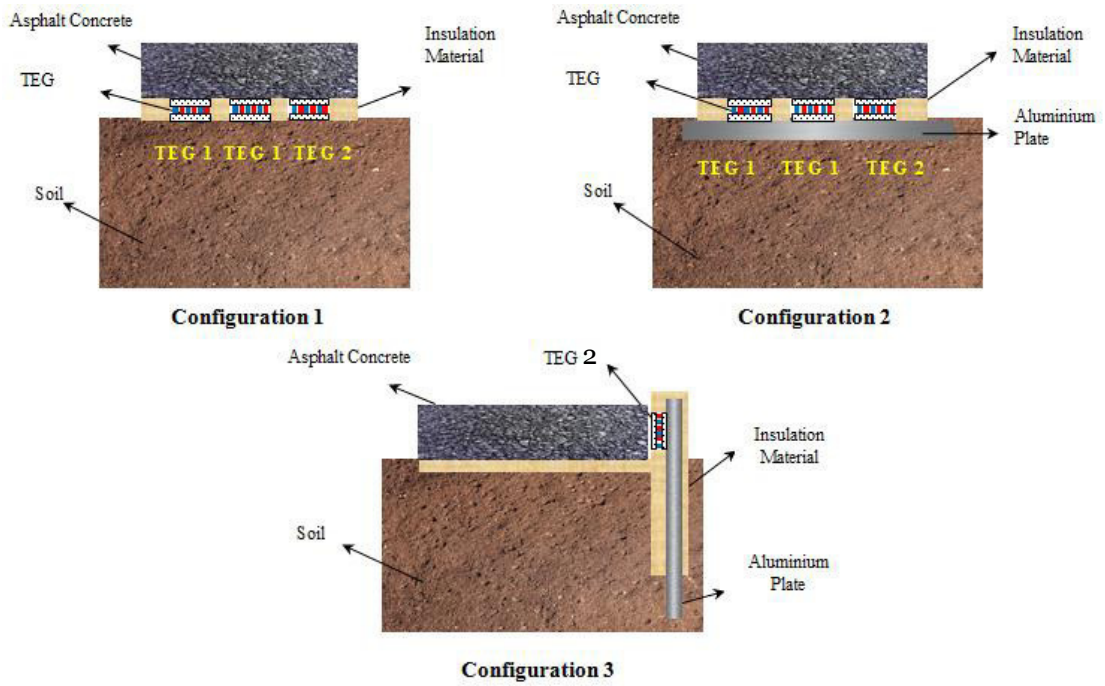


Figure 6-5 Experimental setup configuration

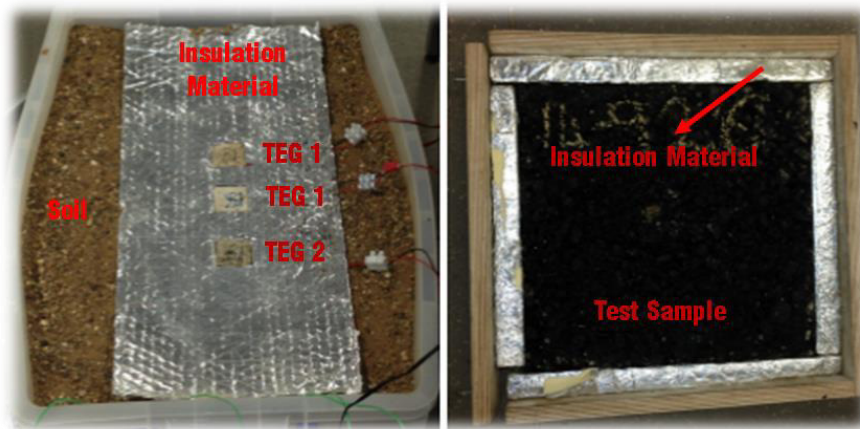


Figure 6-6 Experimental test preparation

6.3.4 Thermoelectric Power Generator Measurements

There are various existing types of TEG device with different property parameters on the market. For the purpose of this study, two different thermoelectric generation modules GM 250-127-14-10 (TEG1) and GM 250-241-10-16

(TEG2) were used with dimensions of $40 \pm 0.5 \times 40 \pm 0.5 \text{ mm}^2$ and a thickness of $3.40 \pm 0.1 \text{ mm}$. The selection of these two types was based on the maximum operating temperature for the hot side and cold side of the TEG to ensure that it can work with the pavement temperature. The maximum operating temperatures for the hot side and the cold side are 250°C and 175°C , respectively for both TEG module types. In addition, the other factor that has been considered in the selection of these two devices was the output voltage value. The maximum open circuit voltage for the EG 1 module and TEG2 module are 8.0V and 18.6V , respectively. **Table 6-1** illustrates the main performance parameters of the two selected TEG devices with the full technical specifications attached in **Appendix B**.

Table 6-1 Performance Parameters

	TEG1	TEG2
Matched Load Output Power	11.6W	9.1W
Matched Load Resistance	$1.38\Omega \pm 15$	$9.5\Omega \pm 15$
Open Circuit Voltage	8.0V	18.6V
Matched Load Output Current	2.9A	1.0A
Matched Load Output Voltage	4.0V	9.3V
Heat Flow Through Module	~232W	~182W
Maximum Compress (non-destructive)	1MPa	1MPa
Max Operation Temperature Hot Side	250°C	250°C
Max Operation Temperature Cold Side	175°C	175°C

6.3.5 Light Intensity Measurements

Solar intensity was measured using a pyranometer (Kipp & Zonen CMP 11) that measures the solar intensity up to 4000 W/m^2 with an accuracy of $\pm 3 \%$. The

pyranometer was levelled and positioned under the infrared lamps at the centre of the asphalt concrete slabs. To measure the light intensity received from the heat source by the asphalt concrete surface at the position of the thermocouple, the height of the pyranometer sensor was set at 730 mm from the lamps before the asphalt specimen was positioned. This height has been identified so the maximum steady state temperature of the asphalt slabs would not exceed 85 °C.

6.3.6 Temperature Measurements

The temperatures at six different positions were measured using J-type thermocouples. These include the surface and bottom temperature of asphalt concrete slabs, surface soil temperature, soil temperature at 10cm depth, 20cm depth and 30cmdepth. The reason behind measuring the temperature at different soil depths was to study the temperature profile of the soil during the heating and cooling process. The test specimen's cross-section and the position of the thermocouples in the pavement are shown in **Figure 6-3**. The temperature profile for each asphalt slab was recorded for 2 days under a constant environmental temperature of $25\text{ }^{\circ}\text{C} \pm 2$. The thermoelectric power generator and the thermocouples were connected to a data logger (dataTaker DT 500) that allowed measurements at 10 second intervals. T2 represents the temperature of the hot side and T3 represents the temperature of the cold side.

6.4 Results and Discussion

6.4.1 Asphalt Temperature Profile

Figure 6-7 illustrates the surface and bottom temperature profiles for asphalt mixtures as a function of time. It can be observed that when the infrared lights were switched on, the surface and bottom temperature profile's trends increased until reaching a steady state condition after approximately 8 hours. Then when the lights were switched off, the surface and bottom temperature profile's trends decreased until room temperature was reached after approximately 13 hours.

In addition, **Table 6-2** shows the maximum steady state surface and bottom temperature of asphalt slabs. It can be observed that the steady state surface temperature of asphalt slabs with higher air voids content was higher than the temperature of asphalt slabs with lower air voids content. In detail, the steady state surface temperature of asphalt slabs with 21.5% air voids content was 3.69 °C higher than asphalt slabs with 5.0% air voids content. The reason for this is that the asphalt mixtures with high air voids content have lower diffusivity and thermal conductivity. Therefore, it cannot transport heat out of the hot areas in the test specimens as efficiently as asphalt mixtures with high diffusivity and high thermal conductivity, those with lower air voids content.

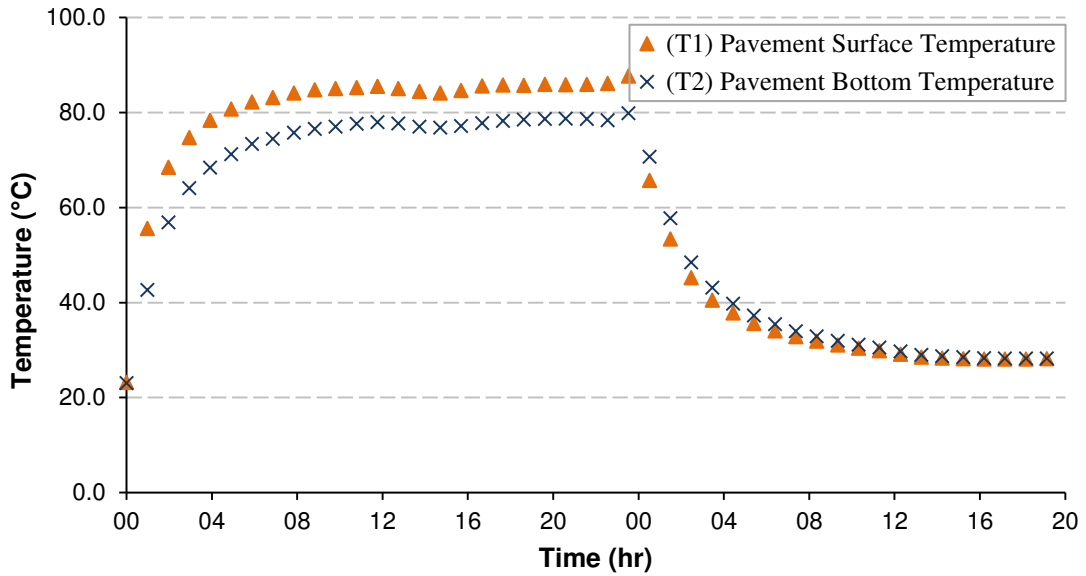


Figure 6-7 Asphalt surface and bottom temperature profile

Furthermore, it can be observed that the bottom temperature in the steady state was higher in asphalt slabs with higher air voids content by 3.49 °C: 86.64 °C for asphalt slabs with 21.5 % air voids content and 83.15 °C for asphalt slab with 5.0 % air voids content. Finally, it can be observed that the maximum steady state temperatures increased gradually with the air voids content. These values are similar to previous results reported by [Hassn \(2016\)](#).

Table 6-2 Experimental results

	Air Voids Content %	5%	13%	21%
Configuration 1	Asphalt Surface T (°C)	88.16	90.19	91.85
	Asphalt Bottom T (°C)	83.15	85.08	86.64
	Max ΔT (°C)	18.32	18.82	19.16
	Max Voltage TEG 1 (mV)	73.96	75.52	76.92
	Max Voltage TEG 1 (mV)	75.15	76.74	78.16
	Max Voltage TEG 2 (mV)	198.14	202.32	206.07
Configuration 2	Asphalt Surface T (°C)	88.16	89.38	92.36
	Asphalt Bottom T (°C)	83.15	84.67	86.27
	Max ΔT (°C)	22.37	23.48	24.64
	Max Voltage TEG 1 (mV)	83.93	85.14	86.83
	Max Voltage TEG 1 (mV)	80.14	81.40	83.01
	Max Voltage TEG 2 (mV)	249.37	251.86	256.85
Configuration 3	Max ΔT (°C)	55.34	56.65	57.67
	Max Voltage TEG 2 (mV)	997.19	1018.13	1036.84

6.4.2 Soil Temperature Profile

The soil temperature profile at various depths is presented in **Figure 6-8**. It can be observed that when the infrared lights are switched on, the soil temperature profiles increased until they reached a reasonably steady state condition. In addition, the soil temperature profile at greatest depth increased slightly compared to the soil temperature profiles closer to the asphalt concrete slabs. The maximum soil surface temperature was almost 78.3 °C, whereas the maximum soil temperature at 30cm depth was 33.7 °C. This trend is similar to the previous findings reported by **Ongel and Harvey, (2004)**, see **Figure 6-9**. This figure illustrates a real life daily temperature profile across a pavement structure in Los Angeles. It can be seen that the underground soil temperature remains constant at a certain depth. Therefore, a thermal gradient between the asphalt temperature and the soil temperature exists which could be considered as a potential source for energy using the thermoelectric power generators.

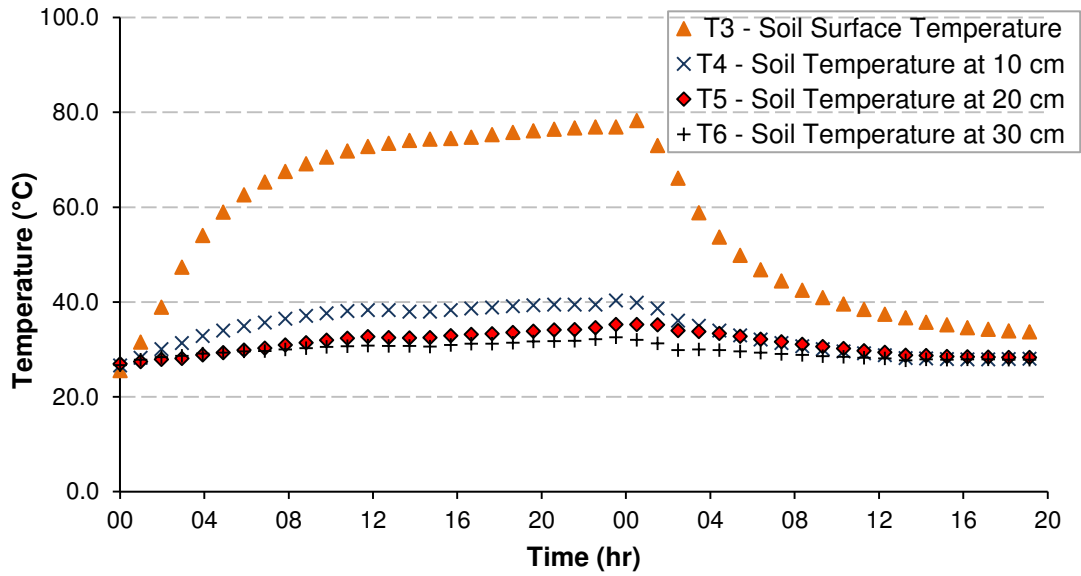


Figure 6-8 Soil temperature profile versus time

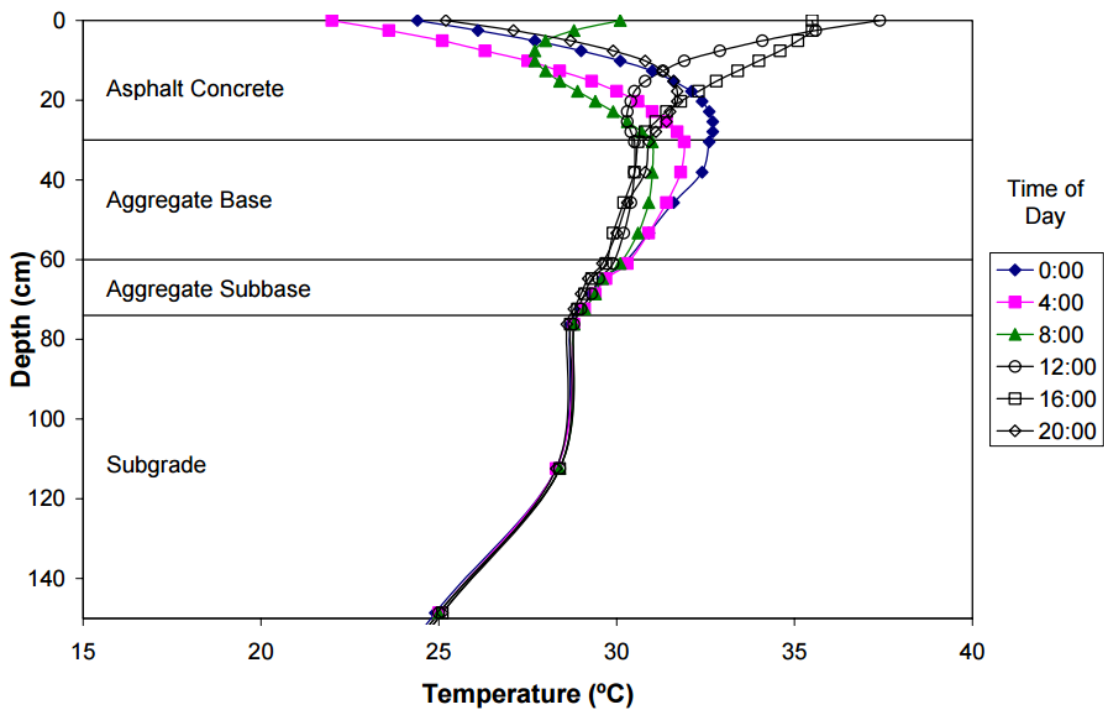


Figure 6-9 Pavement temperature profile (Ongel and Harvey, 2004)

6.4.3 Temperature Difference between Hot and Cold Junction

- *Configuration 1*

The temperature difference (ΔT) between the hot (bottom surface of asphalt concrete slab) and cold junction (soil surface) for Configuration 1 is depicted in **Figure 6-10**. It can be observed that ΔT increases up to a maximum point after an approximate time of 2 hours and then decreases until nearly reaching 5 °C approximately after 12 hours.

When the infrared lights are switched on, the heat absorbed by the asphalt sample starts to move through the test sample from hot areas to colder areas as a function of the thermal conductivity of the asphalt mixture. As a result, the hot side of the TEG devices in contact with the asphalt bottom surface starts to absorb heat and then this heat is transferred to the cold side of the TEG through the thermoelectric elements. At this point, the cold side of the TEG starts to transfer the heat to the surface soil. The surface soil in this Configuration does not reject the heat for a long time. The reason behind this is that the soil type used in this study is a sandy soil. In more detail, the particles of the sandy soil are not well connected and the heat is transferred to the sand particles which are in direct contact with the cold side of the TEG device. Therefore, the observed time of two hours is the time when the heating rate of the soil particles (those in contact with the hot side of the TEG) started to increase.

In addition, it can be observed from **Table 6-2**, that the maximum ΔT of asphalt slabs increases slightly with air voids content. In detail, the maximum ΔT observed were 18.32 °C, 18.82 °C, and 19.16 °C for asphalt slabs with air

voids content of 5%, 13.2% and 21.5 %, respectively. This trend is similar to the previous findings in **Chapter 3** and **4**.

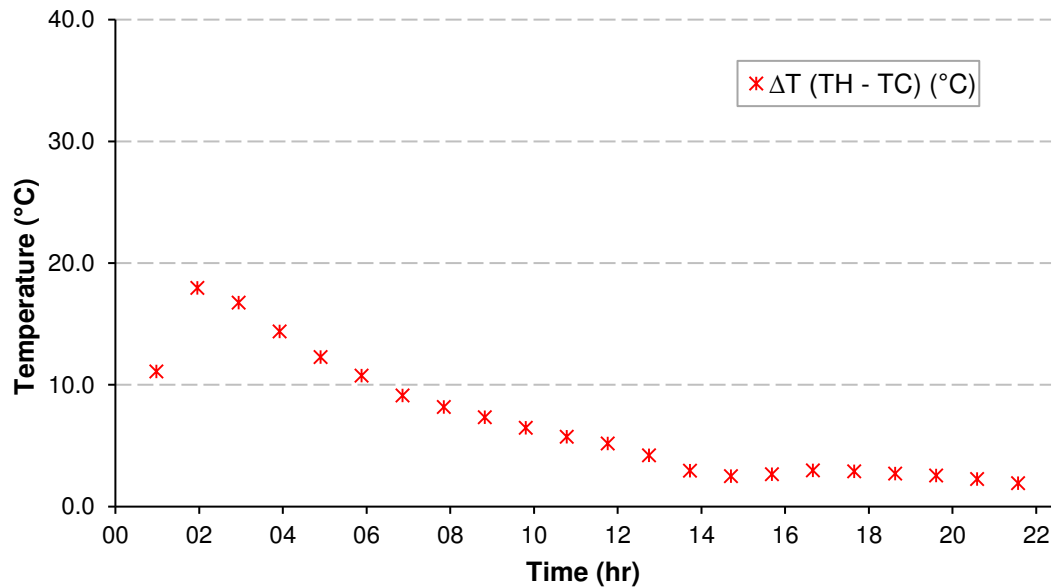


Figure 6-10 Temperature difference between hot and cold junction (Configuration 1)

- *Configuration 2*

The temperature difference (ΔT) between the hot (asphalt concrete slab) and cold junction (soil) for Configuration 2 is presented in **Figure 6-11**. It can be observed that ΔT increases up to a maximum point after an approximate time of 3 hours and then decreases until nearly reaching 8 °C approximately after 12 hours.

When the infrared lights are switched on, a similar pattern to Configuration 1 was obtained except that the temperature difference was higher by approximately 4 °C. Introducing an aluminium plate working as a heat sink has rejected the heat slightly longer which in turn reduced the heating rate in comparison with the case of using soil as a heat sink. The reason behind this is that the aluminium plate particles are very well connected and working as one

object which means higher density and higher specific heat capacity. Therefore, extra time would be required for the temperature of the aluminium plate to reach the steady state temperature. This is similar to the previously observed results provided in **Chapter 3** where materials with higher specific heat capacity need more energy to increase their temperature. In addition, another reason behind this is that the aluminium plate has a larger area than the TEG, so it transfers more energy from the TEG to the soil for the same soil temperature change.

In addition, it can be observed from **Table 6-2**, that the maximum ΔT of asphalt slabs increases slightly with air voids content. In detail, the maximum ΔT observed were 22.37 °C, 23.48 °C, and 24.64 °C for asphalt slabs with air voids content of 5%, 13.2% and 21.5 %, respectively. This trend is similar to the previous findings in **Chapter 3, 4** and for Configuration 1 above.

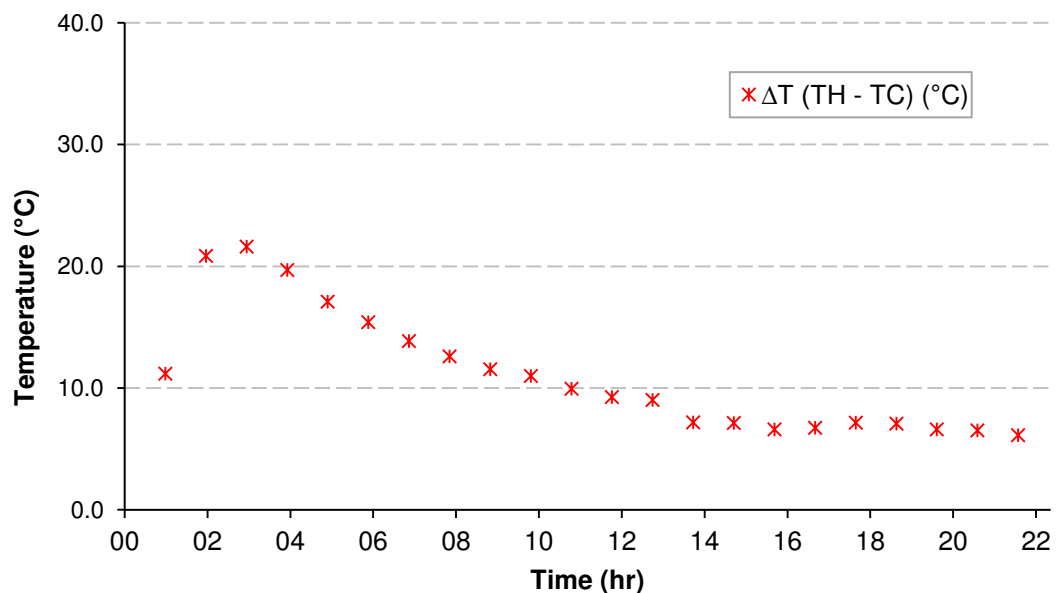


Figure 6-11 Temperature difference between hot and cold Junction (Configuration 2)

- *Configuration 3*

The temperature difference (ΔT) between the hot (asphalt concrete slab) and cold junction (soil) for Configuration 3 is illustrated in **Figure 6-12**. It can be observed that ΔT decreases from an initial maximum point until reaching a steady state condition after an approximate time of 40 minutes. This configuration is not similar to the previous configurations in the way that the test started with heating the asphalt slab until it reached the steady state condition, then the aluminium plate with the attached TEG device was installed as described in **Section 6.3.3**. At this point, the measurement of the temperature difference (ΔT) between hot side and cold side was started. The temperature difference at the start of the test was at the highest value as the asphalt sample had already reached the maximum steady state temperature and the aluminium plate was at room temperature. The temperature difference suddenly dropped by approximately 10 °C in a short period of time. This could be a measurement error due to the installation of the aluminium plate. The observed average temperature difference between the hot side and cold side of the TEG reduced to a steady-state value of approximately 44°C.

In addition, from **Table 6-2** it can be observed that, the maximum ΔT of asphalt slabs increases slightly with air voids content. In detail, the maximum ΔT observed were 55.34 °C, 56.65 °C, and 57.67 °C for asphalt slabs with air voids content of 5%, 13.2% and 21.5 %, respectively. This trend is similar to the previous findings in **Chapter 3** and **4** and for Configuration 1 and 2 above.

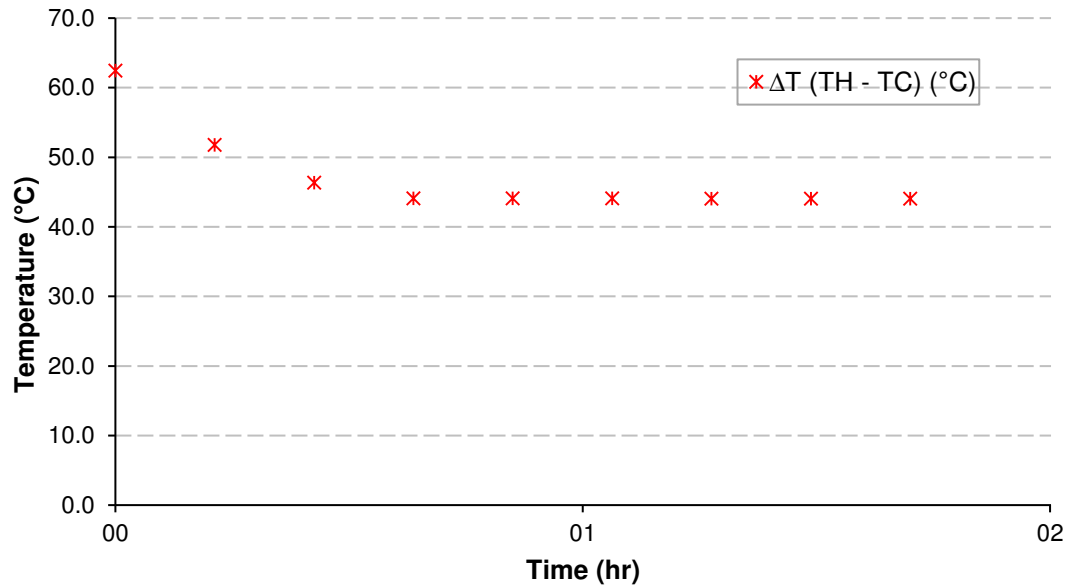


Figure 6-12 Temperature Difference between Hot and Cold Junction (Configuration 3)

6.4.4 Output Voltage

- Configuration 1

Configuration 1 output voltage profiles versus time for the two used types of Thermoelectric Power Generator TEG 1 and TEG 2 for all asphalt mixtures studied are presented in **Figure 6-13**. It can be observed that the output voltage profiles for TEG 1 and TEG 2 increase up to a maximum point after approximately 2 hours and then decrease until nearly reaching zero after an approximate period of 22 hours. The maximum output voltage was observed at the maximum temperature difference between the hot side and cold side of the TEG devices.

In addition, the observed output voltage from TEG 2 type for all the asphalt mixture studied was higher than the observed output voltage from TEG 1 type by a factor of approximately 2.7. The reason behind this is that TEG2 has higher performance parameters than TEG1 in terms of output voltage, see **Table 6-1**.

Furthermore, it can be observed from **Table 6-2**, that the maximum output voltage for the same TEG type was higher for asphalt slabs with higher air voids content. In detail, the maximum output voltages for TEG 2 type observed were 198.14 mV, 202.32 mV and 206.07 mV for asphalt slabs with air voids content of 5%, 13.2% and 21.5 %, respectively.

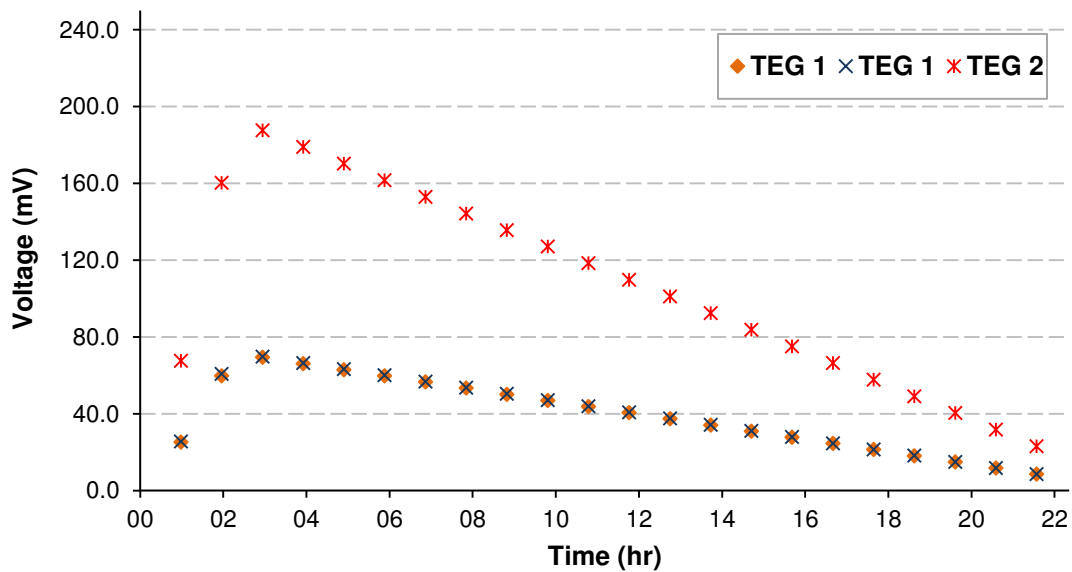


Figure 6-13 Output Voltage (Configuration 1)

- *Configuration 2*

Configuration 2 output voltage profiles versus time for the two types of Thermoelectric Power Generator, TEG 1 and TEG 2, for all asphalt mixtures studied are presented in **Figure 6-14**. Similar results to Configuration 1 were obtained except that the magnitude of voltage generated was about 20% higher and the ratio of TEG 2 to TEG 1 output about 3 rather than 2.7.

In detail, the maximum output voltages for TEG 2 type observed were 249.37 mV, 251.86 mV and 256.85 mV for asphalt slabs with air voids content of 5%, 13.2% and 21.5 %, respectively.

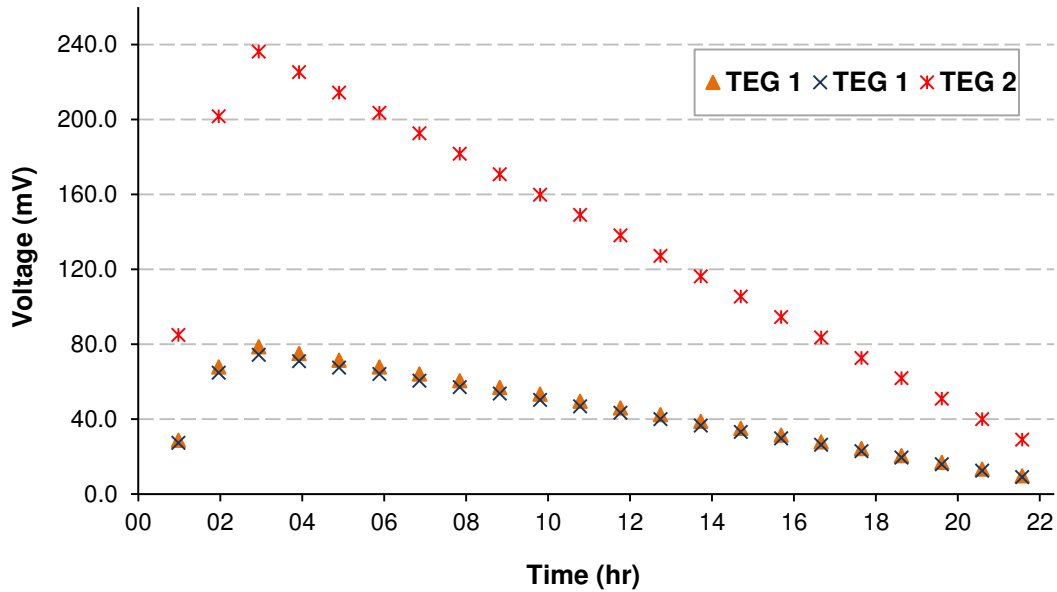


Figure 6-14 Output Voltage (Configuration 2)

- *Configuration 3*

Configuration 3 output voltage profiles versus time for the TEG 2 type for all asphalt mixtures studied are presented in **Figure 6-15**. It can be observed that the output voltage reaches the maximum point at the start of the test and then decreases until reaching a steady state condition after a short period of time of less than one minute, i.e. it follows the same trend as temperature difference (see **Figure 6-12**).

In addition, it can be observed from **Table 6-2**, that the maximum output voltage for the same TEG type was higher for asphalt slabs with higher air voids content. In detail, the maximum output voltages for TEG 2 type observed were 997.19 mV, 1018.13 mV and 1036.84 mV for asphalt slabs with air voids content of 5%, 13.2% and 21.5 %, respectively.

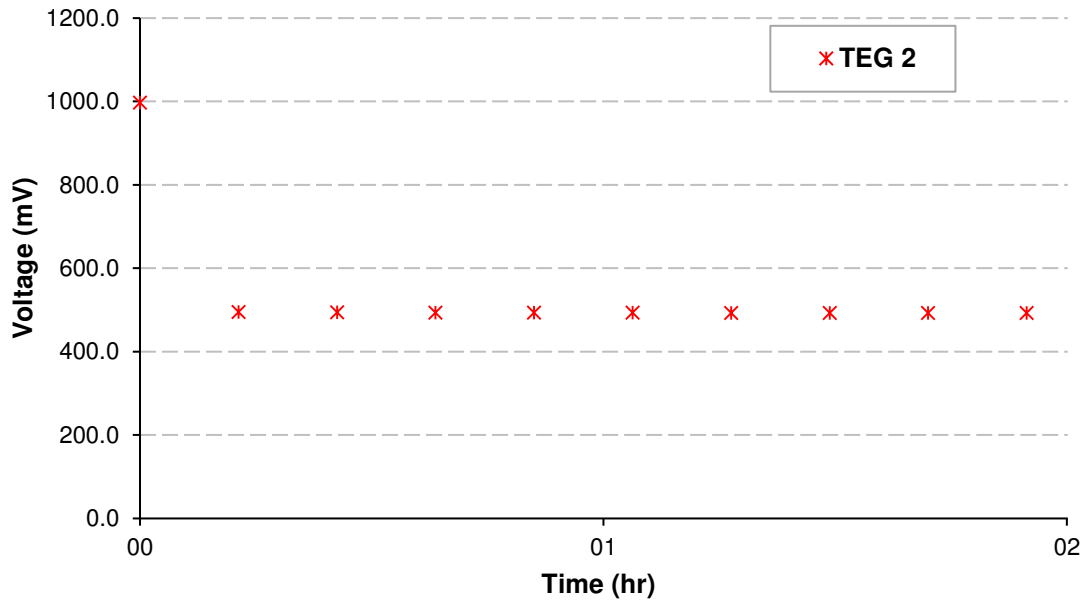


Figure 6-15 Output Voltage (Configuration 3)

6.4.5 Output Voltage against ΔT

- *Configuration 1*

Figure 6-16 illustrates the Configuration 1 output voltage versus temperature difference (ΔT) profile for all asphalt mixtures studied for TEG 1 and TEG2 type. It can be observed that the output voltage from TEG 2 was higher than the output voltage from TEG 1 at the same temperature difference by a factor of about 2.5. In detail, the output voltages observed at a temperature difference of approximately 18 °C were 200 mV and 80 mV for TEG 2 and TEG 1, respectively. The output voltage increases gradually with the increase of ΔT . Therefore, in this configuration to obtain a maximum benefit it is desirable to maintain a temperature difference at least as large as 18 °C.

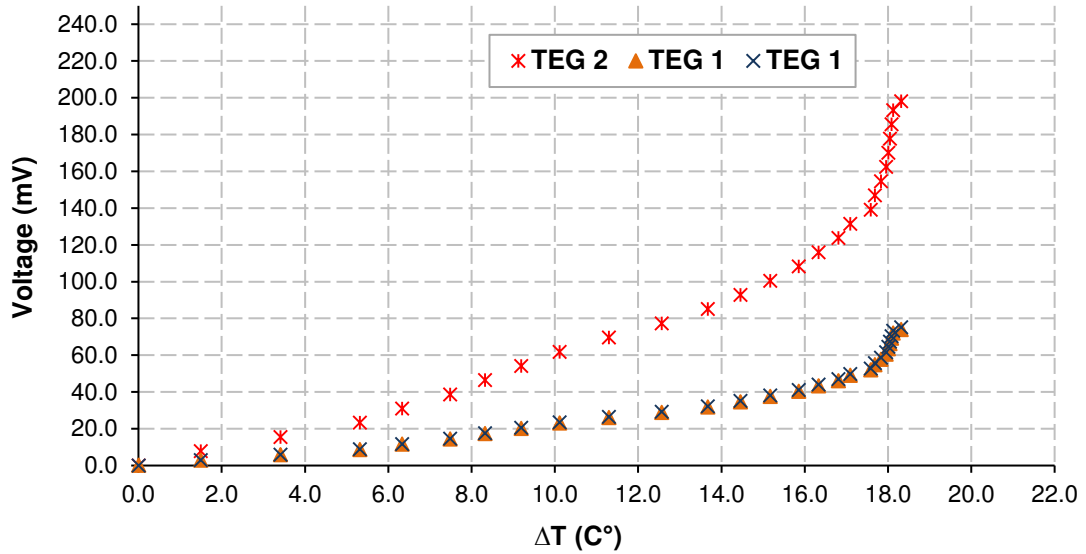


Figure 6-16 Output Voltage against ΔT (Configuration 1)

- *Configuration 2*

Figure 6-17 shows the Configuration 2 output voltage versus temperature difference (ΔT) profiles for all asphalt mixtures studied for TEG 1 and TEG 2 type. Similar results to those obtained for Configuration 1 are observed except that the ratio between the TEG 2 and TEG 1 results was approximately 3 and the temperature difference at which the output voltage rapidly increases is about 22 °C.

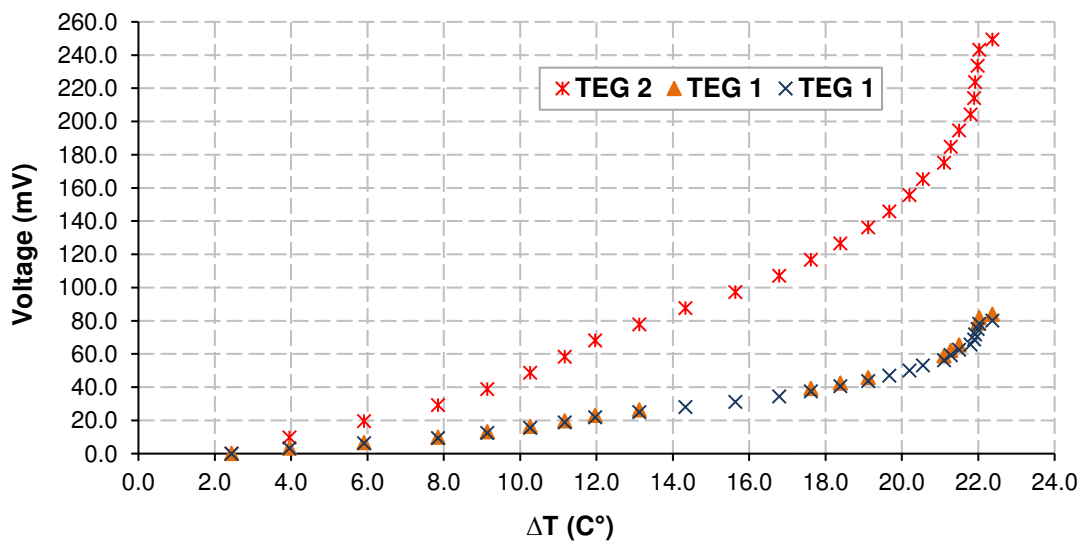


Figure 6-17 Output Voltage against ΔT (Configuration 2)

- Configuration 3

Figure 6-18 shows the Configuration 3 output voltage versus temperature difference (ΔT) profile for all asphalt mixtures studied for TEG 2 type. It can be observed that the output voltage increases sharply with the increase of ΔT .

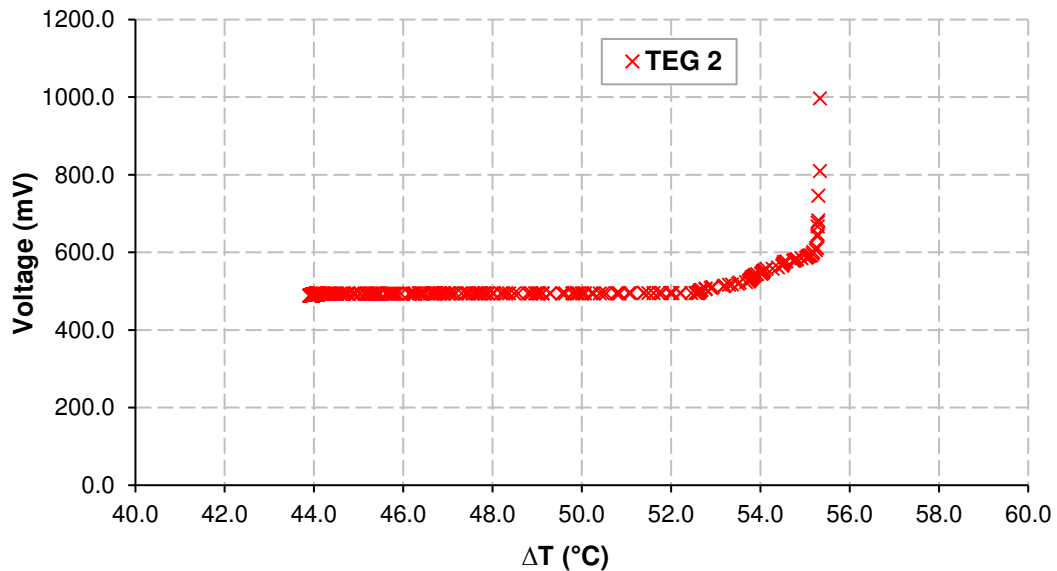


Figure 6-18 Output Voltage against ΔT (Configuration 3)

6.4.6 Output power

The output power (Watts) for all test configurations has been calculated for both Thermoelectric Power Generators TEG 1 and TEG 2. It is calculated based on the observed maximum output voltage for Configuration 1 and 2 and based on the maximum and average output voltage for Configuration 3. The output current values for TEG 1 and TEG 2 presented in Table 6-1 were used in the calculation of the output power. The calculated output power calculated is the maximum power that can be obtained as the calculation was based on open circuit i.e. load resistance and electricity losses not considered in the calculation.

Figure 6-19 illustrates the calculated maximum and average output power in Watts for all three test configurations. It can be observed that the maximum output powers were 0.22 Watt, 0.25 Watt and 1.02 Watt in Configurations 1, 2 and 3 respectively. In addition, it has been noted that the output power from TEG 1 and TEG 2 in the same configuration had similar values. The reason behind this is that although TEG 2 had the higher observed output voltage in Configuration 1 and 2, TEG 1 has the higher output current value, see **Table 6-1**. In Configuration 3, the average observed output power was 0.49 Watt. This value is considered to be more realistic than the maximum value as the maximum value dropped suddenly in a short period of time.

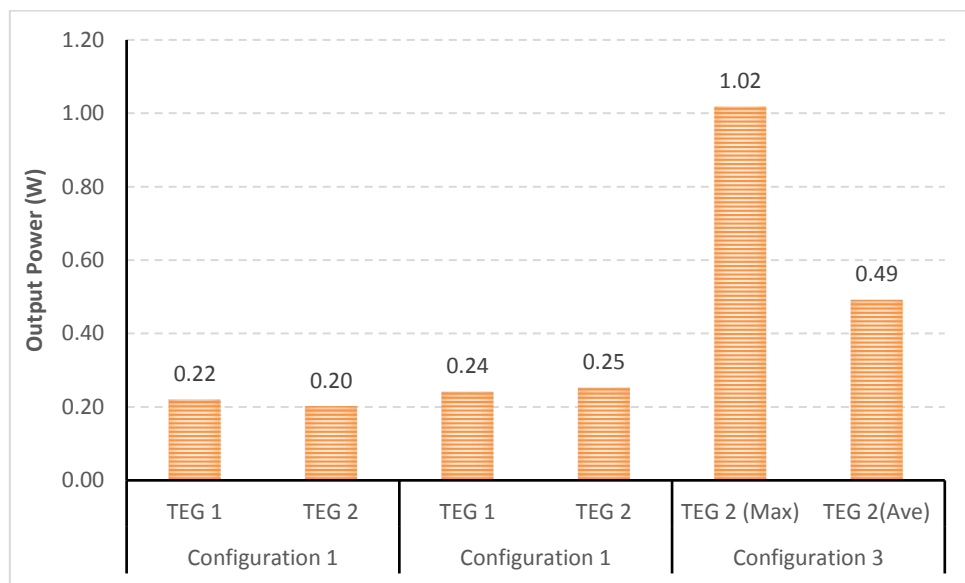


Figure 6-19 Maximum Output Power

Increasing the temperature difference between the hot side and cold side of the Thermoelectric Power Generators would increase the output power. This is confirmed in **Figure 6-19**, where; in Configuration 1 the observed output power was 0.22 Watt at a temperature difference of 18°C, in Configuration 2 the observed output power was 0.25 Watt at a temperature difference of

approximately 22°C and in Configuration 3 the average observed output power was 0.49 Watt at a temperature difference of approximately 44°C. This demonstrates that the temperature gradient between the asphalt pavement and the subgrade could be a potential location for energy recovery through using the Thermoelectric Power Generators.

The observed output power for the three test configurations was only for an area of 0.0016m² (the area of the thermoelectric power generators); therefore, for an area of 1 m² the output power could be 130 Watt, 150 Watt and 300 Watt in Configuration 1, 2 and 3 respectively. This is a simple calculation based on open circuit assumption which does not consider all factors (i.e. load resistance, electricity losses, connection of TEG and maintaining the maximum temperature difference). In addition, the test assumes one dimensional for heat movement which does not reflect the real-life case. However, the test results show that there is an existing potential to use the temperature gradient between the asphalt pavement and the subgrade for energy recovery by using Thermoelectric Power Generators.

6.5 Summary

In this work, heat recovery from an asphalt pavement using Thermoelectric Power Generators has been analysed and it was found that:

- The efficiency of thermoelectric generators for converting heat into electricity depends upon the temperature difference between the hot and cold side, on its average temperature of operation and on the performance of the thermoelectric material through its figure-of-merit.

Chapter 6. Harvesting heat from a pavement by thermoelectric power generators

- Increasing and/or maintaining the temperature difference between the hot side and cold side of the Thermoelectric Power Generators is considered to be the most important factor in energy recovery application.
- It is proved that using a sandy soil as a cold junction would not reject the transfer of heat from the hot side to the cold side for a long period of time. Therefore, a maximum temperature difference of approximately 18 °C can be achieved when using sandy soil as a heat sink. However, by using higher specific heat capacity material (i.e. aluminum) with dense particles as a heat sink, the heat would be rejected for a slightly longer period of time which in turn increases the temperature difference between hot and cold sides. The temperature difference increased by 4 °C when the aluminum plate was used as a heat sink instead of sandy soil.
- Increasing the temperature difference between the hot and cold sides of Thermoelectric Power Generators will increase output voltage and output power which in turn improves the energy recovery performance.
- It is proved that there is an existing potential to use the temperature gradient between an asphalt pavement and the subgrade for energy recovery by using Thermoelectric Power Generators.
- Although the test results show that there is a potential to use the temperature difference between the asphalt pavement and the subgrade to recover heat through the use of TEG devices there are still some limitations to the preliminary test investigation. These limitations

include; the output power was calculated based on open circuit assumption, one dimension was assumed for the heat movement, practical and routinely implementable arrangements for heat sink were not studied, and finally the test was performed with high asphalt pavement temperature (hot area climate).

7. Conclusions and Recommendations

In this thesis the effect of air voids content in asphalt concrete pavements under different weather conditions (dry and hot) on its thermo-physical properties and thermal surface properties, and how that could affect the application of harvesting thermal heat from pavement materials and also the urban heat island effect have been studied. For this purpose, the effect of air voids content on thermal properties (i.e. density, specific heat capacity, thermal conductivity, thermal diffusivity, thermal effusivity, Albedo, absorptivity, emissivity) of asphalt concrete mixtures under dry conditions was studied and presented in **Chapter 3**. An experimental investigation on the water evaporation dynamics of moist porous asphalt concrete mixtures was carried out, as presented in **Chapter 4**. A comparison between the effect of air voids content under dry and wet conditions on the thermal properties of asphalt mixture and on transport and storage of heat were studied and presented in **Chapter 5**. In addition, in this thesis an initial experimental feasibility study of recovering solar heat from asphalt concrete pavement materials by converting heat into electricity through the use of Thermoelectric Power Generators was performed and presented in **Chapter 6**.

This chapter summarises the main findings in each of the previous chapters with the main conclusions presented in **Section 7.1** and the recommendations for future research presented in **Section 7.1.1**.

7.1 Overall Discussion

7.1.1 Effect of air voids content on thermal properties of asphalt mixtures under dry conditions

The effect of air voids content on thermal properties of asphalt concrete mixtures and how that could affect the energy harvesting application and the urban heat island effect under dry condition was investigated in **Chapter 3**. The thermo-physical properties (i.e. density, specific heat capacity, thermal conductivity, thermal diffusivity and thermal effusivity) and the surface thermal properties (i.e. absorptivity, emissivity and albedo) were measured with various techniques and the effect of air voids content was analysed. The main conclusions in this study can be drawn:

- Asphalt mixtures with high air voids content have lower thermal conductivity and specific heat capacity than those with lower air voids content.
- Asphalt mixtures with high air voids content reach higher steady-state surface temperatures under a constant energy source.
- Voids content has an insignificant effect on the emissivity of asphalt mixtures (the emissivity of dense asphalt mixture was higher than the emissivity of porous asphalt mixture by a value of only 0.02).
- Asphalt mixtures with high thermal conductivity and specific heat capacity, i.e. dense asphalt mixtures, have lower heating and cooling

rates than asphalt mixtures with lower thermal conductivity and specific heat capacity, i.e. porous asphalt mixtures.

- The total amount of energy accumulated in asphalt mixtures with different air voids contents, but with the same constituent materials, during heating and cooling depends only on the density of the mixtures. Convective and radiative heat losses can be considered constant for mixtures with different air voids contents.
- In general, asphalt mixtures with high air voids content accumulate less energy than asphalt mixture with lower air voids content. For this reason, mixtures with high air voids content are recommended to alleviate the urban heat island effect while mixtures with low air voids content are recommended for harvesting solar energy from the pavement.

7.1.2 Water evaporation dynamics of moist porous asphalt concrete mixtures

A detailed experimental study of the evaporation process of asphalt mixtures was carried out and presented in **Chapter 4**. The time dependent evaporation rates of saturated asphalt mixtures with air voids content ranging from 4 % to 26 % were investigated and compared to the values of a number of parameters, such as asphalt surface temperature during heating, heat flux, porosity, and thermal conductivity. In addition, the air voids configuration was characterized and its properties, i.e., Euler number, tortuosity, diameter of air voids and macroporosity, were compared to the parameters mentioned above. The following conclusions are derived:

- At first, water evaporates from the pores directly into the atmosphere. The time that this stage lasts is independent of the characteristics of air voids in the mixture, and the reasons for this are still unclear. This is reflected by an increase in the temperature and heat flux through asphalt mixture.
- Then, the evaporation rate increases up to a maximum, which causes the heat flux to reduce through the absorption of latent heat, and a reduction of the temperature of the asphalt mixture. The temperature reached at the maximum evaporation rate depends on the connectivity of air voids and the tortuosity of the connected paths. In addition, the time to reach maximum evaporation rate is proportional to the air voids content due to the higher volume of water available for the absorption of latent heat. In this stage, the surface of the mixture appears dry, and water does not evaporate directly to the atmosphere: previous researches have concluded that at this stage, a semi-saturated area appears above the water table, and water evaporation is powered by diffusion through air void channels.
- Finally, the evaporation rate decreases until there is no more water available in the material. At this stage, the surface temperature of the material increases and tends to a horizontal asymptote related to the thermal properties of the asphalt mixture and the incoming heat flux.
- Stage transition can be calculated by doing the first derivative of the evaporation rate versus time or versus temperature. This method is

based on the observation of physical phenomena rather than on geometrical assumptions, as previous researchers propose.

- Understanding the air voids properties is fundamental to identifying the evolution of water evaporation. It has been proven that the evaporation of water is the result of the complex interplay of various geometrical properties such as the percentage and diameter of air voids, the tortuosity, or the Euler number. This may play an important role in addressing phenomena such as the urban heat island, or damage of asphalt mixture due to the presence of water.

7.1.3 Thermal properties of asphalt mixtures under dry and wet conditions

An experimental study was carried out, to compare the effect of air voids content in asphalt concrete mixtures on its thermal properties under dry and wet conditions. The conclusions of this study can be summarised as follows:

- The temperature increase rate of asphalt mixture under dry conditions was higher than under wet conditions. In the case of the wet condition, energy was required for the evaporation process.
- When wet asphalt materials were heated, the water evaporation rate increased until it reached a peak, and then decreased until all the water in the pores was consumed. The reason for the rapid, post-peak, decrease in evaporation rate is due to the evaporative forces that power the movement of water to the surface of the asphalt mixture becoming

smaller than the gravity and surface tension forces that act to keep water in the material.

- The temperature increase rate under wet conditions decreased with the increase in the air voids content of the asphalt mixture. This happened because there was more water available for evaporation and, hence, a greater latent heat demand. While the temperature increase rate in dry conditions showed a continuous decrease until the steady state, the temperature increase rate of asphalt mixtures in wet conditions initially increased, then reduced as evaporation became easier due to the raised temperature. Temperature increased again when all the water for evaporation had been consumed, and, finally, decreased towards an asymptotic value representing steady-state conditions.
- The heat flux through dry asphalt mixtures increased until it reached a peak, and then decreased towards an asymptotic value. On the other hand, the heat flux through asphalt mixtures in a wet condition decreased initially due to the effect of water evaporation, and then increased again towards the same asymptotic value as the materials in a dry conditions. At the end of heating both initially-wet and initially-dry specimens had reached the same condition and, hence, the same response.
- When dry, the heat flux was higher in asphalt mixtures with low air voids content. In contrast, under wet conditions, the heat flux and temperature reduction due to water evaporation was higher in more porous materials, because this contained energy consuming water.

- In wet conditions, the thermal conductivity of an asphalt mixture dropped suddenly when the water available for evaporation was consumed.

7.1.4 Harvesting heat from pavement material by using Thermoelectric Power Generators

An experimental investigation into the feasibility of recovering solar heat from asphalt concrete pavement materials by converting heat into electricity through the use of Thermoelectric Power Generators was performed and presented in Chapter 6. In addition, the effect of the air voids content in asphalt concrete mixtures on the heat energy recovery was studied. Furthermore, the effect of the cold junction on the heat recovery was investigated. The results from this study can be summarised as follows:

- The efficiency of thermoelectric generators of converting heat into electricity depends upon the temperature difference between the hot and cold side, on its average temperature of operation and on the performance of the thermoelectric material through its figure-of-merit.
- Increasing the temperature difference between the hot side and cold of the Thermoelectric Power Generators will increase output voltage and output power which in turn improves the performance of the energy recovery. In principle, this can be achieved through a well-designed heat sink although practical and routinely implementable arrangements were not studied. The heat sink should be designed to reject the transfer of heat from the hot side to the cold side of the Thermoelectric Power

Generator which in turn increases or maintains the temperature difference between the hot side and cold side of the TEG devices.

- Using a sandy soil as a cold junction would not reject the transfer of heat from hot side to the cold side for a long period of time. Therefore, a maximum temperature difference of approximately 18 °C can be achieved when using the sandy soil as a heat sink. However, by using higher specific heat capacity material (i.e. aluminum) with a dense particle as a heat sink, the heat would be rejected for slightly longer period of time or may be spread to more soil, so stay up cooler longer which in turn increases the temperature difference between hot and cold sides. The temperature difference increased by 4 °C when the aluminum plate used as a heat sink instead of sandy soil.
- The initial investigation on the use of TEG devices shows that though there is existing potential to use the temperature gradient between the asphalt pavement and the subgrade, however, the efficiency is likely to be low. In addition, the tests were performed on high temperature pavement, in real life this can only be applicable in some parts of the world (very hot area).

7.2 Recommendations

This section summarises the main recommendations for any further study.

- Although the effect of air voids content in asphalt concrete mixtures on the thermal properties was studied under dry and wet condition, it is recommended to carry out further investigation on the effect of wind.

Chapter 7. Conclusions and Recommendations

- In this study, it has been proven that the evaporation of water is the result of the complex interplay of various geometric properties such as the percentage and diameter of air voids, the tortuosity, or the Euler number. This could play an important role to approach phenomena such as the urban heat island, or damage of asphalt mixture due to the presence of water. Therefore, it is recommended that further research should tackle the complex modelling of water evaporation, including experimental measurements of matric suctions on unsaturated slabs with different air voids properties.
- In the present study, it has been proven that there is an existing potential to harvest energy from the pavement by using Thermoelectric Power Generators if the temperature gradient between the asphalt pavement and subgrade can be maintained. Therefore, it is highly recommended to investigate how to maintain the temperature difference between the asphalt pavement and the subgrade.
- A cost-efficiency analysis should be performed to determine the applicability of harvesting heat from the pavement through the use of Thermoelectric Power Generators.

8. References

- ABRAMOFF, M. D., MAGALHAES, P.J., RAM, S.J., 2004. Image Processing with ImageJ. *Biophotonics International*, 11, 36-42.
- ALAM, H. A. R., S., 2013. A review on the enhancement of figure of merit from bulk to nano-thermoelectric materials. *Nano Energy*, 2, 190-212.
- ASAEDA, T., CA, V. T. & WAKE, A. 1996. Heat storage of pavement and its effect on the lower atmosphere. *Atmospheric Environment*, 30, 413-427.
- BANKS, D. 2012. An introduction to thermogeology: ground source heating and cooling, John Wiley & Sons.
- BECKER, R. & KATZ, A. 1990. Effect of moisture movement on tested thermal conductivity of moist materials. *Materials in Civil Engineering*, 2, 72-83.
- BENAZZOUK, A., O. DOUZANE, K. MEZREB, LAIDOUDI, B. & QUÉNEUDEC, M. 2008. Thermal conductivity of cement composites containing rubber waste particles: Experimental study and modelling. *Construction and Building Materials* 22(4), 573-579.
- BERGMAN, T. L., INCROPERA, F. P., DEWITT, D. P. & LAVINE, A. S. 2011. Fundamentals of heat and mass transfer, John Wiley & Sons.
- BIJSTERVELD, V., T., W. & BONDT, A. H. D. 2002. Structural aspects of asphalt pavement heating and cooling systems. Third International Symposium on 3D Finite Element Modeling, Design and Research. Amsterdam, Netherland.
- BROWN, E. R. & CROSS, S. A. 1992. A National study of rutting in hot mix asphalt (HMA) pavements. National Center for Asphalt Technology, NCAT Report 92-5, Auburn, Alabama.
- BRUTSAERT, W. A. C., D., 1995. Desorption and the two stages of drying of natural tallgrass prairie. *Water Resources Research*, 31, 1305-1313.

Chapter 8. References

- BS EN 12591 2009. Bitumen and bituminous binders - specifications for paving grade bitumens
- BS EN 12697 PART 5 2009. British Standard Institute (BSI). Bituminous mixtures, test methods for hot mix asphalt: Determination of the maximum density.
- BS EN 12697 PART 6 2003. British Standard Institute (BSI). Bituminous mixtures, test methods for hot mix asphalt: Determination of bulk density of bituminous specimens.
- BUDIKOVA, D., HOGAN, C., HALL-BEYER, M., HASSAN, G. & PIDWIRNY, M. 2010. Albedo. The Encyclopedia of Earth. Washington, DC: Environmental Information Coalition, National Council for Science and the Environment.
- BUSBY, J., LEWIS, M., REEVES, H. & LAWLEY, R. 2009. Initial geological considerations before installing ground source heat pump systems. Quarterly Journal of Engineering Geology and Hydrogeology, 42, 295-306.
- CANAKCI, H., DEMIRBOGA, R., KARAKOC, M. B. & SIRIN, O. 2007. Thermal conductivity of limestone from Gaziantep (Turkey). Building and Environment, 42, 1777-1782.
- CARDER, D., BARKER, K., HEWITT, M., RITTER, D. & KIFF, A. 2008. Performance of an interseasonal heat transfer facility for collection, storage, and re-use of solar heat from the road surface. TRL Published Project Report.
- CENGEL, Y. A. 1998. Heat Transfer A practical Approach, WBC McGraw Hill.
- CENGEL, Y. A. 2003. Heat Transfer: A Practical Approach, "McGraw-Hill, New York.
- CHATZITHOMAS, C. D., ALEXANDRIS, S.G., 2015. Solar radiation and relative humidity based, empirical method, to estimate hourly reference evapotranspiration. Agricultural Water Management, 152, 188-197.

Chapter 8. References

- CHEN, T. G., YU, P., CHOU, R.H. AND PAN, C.L., 2010. Phonon thermal conductivity suppression of bulk silicon nanowire composites for efficient thermoelectric conversion. *Optics express*, 18, A467-A476.
- CHIARELLI, A., DAWSON, A. & GARCIA, A. 2015. Analysis of the performance of an air-powered energy-harvesting pavement. *Transportation Research Record: Journal of the Transportation Research Board*, 156-163.
- CHOO, L. P. A. Y., E.K., 2000. Water flow through cover soils using modeling and experimental methods. *Journal of Geotechnical and Geoenvironmental Engineering*, 126, 324-334.
- CIBSE 2006. *Guide A: Environmental design*. London: Chartered Institution of Building Services Engineers.
- COTE, J. & KONRAD, J. M. 2005. Thermal conductivity of base-course materials. *Canadian Geotechnical Journal*, 42, 61-78.
- CROMPTON, T. R. 2010. *Determination of Thermal Conductivity*.
- DAS, S. K. 2010. *Fundamentals of heat and mass transfer*, Alpha Science International.
- DAWSON, A.R., DEHDEZI, P.K., HALL, M.R., WANG, J. and ISOLA, R., 2011. Enhancing thermo-physical properties of asphalt materials for pavement energy system (PES) applications. *Road Materials and Pavement Design*.
- DE BONDT, A. 2003. *Generation of energy via asphalt pavement surfaces* [Online]. Netherland. [available online at: <http://www.roadenergysystems.nl/pdf/Fachbeitrag%20in%20OIB%20-%20de%20Bondt%20-%20English%20version%2013-11-2006.pdf>].
- DEHDEZI, P. K. 2012. *Enhancing pavements for thermal applications*. PhD., University of Nottingham.
- DEMIRBOĞA, R. 2007. Thermal conductivity and compressive strength of concrete incorporation with mineral admixtures. *Building and Environment*, 42, 2467-2471.

Chapter 8. References

- DEMIRBOĞA, R. & GÜL, R. 2003. The effects of expanded perlite aggregate, silica fume and fly ash on the thermal conductivity of lightweight concrete. *Cement and Concrete Research*, 33, 723-727.
- DIEFENDERFER, B. K. 2002. Moisture content determination and temperature profile modeling of flexible pavement structures, Doctor of Philosophy., Virginia Polytechnic Institute and State University.
- DOS SANTOS, W. N. 2003. Effect of moisture and porosity on the thermal properties of a conventional refractory concrete. *Journal of the European Ceramic Society*, 23(5), 745-755.
- DOUBE, M., KŁOSOWSKI, M. M., ARGANDA-CARRERAS, I., CORDELIERES, F. P., DOUGHERTY, R. P., JACKSON, J. S., SCHMID, B., HUTCHINSON, J. R., AND SHEFELBINE, S. J., 2010. BoneJ: Free and extensible bone image analysis in ImageJ. *Bone*, 47, 1076-1079.
- DOUGHERTY, R. K., K.-H., 2007. Computing local thickness of 3D structures with ImageJ. *Microscopy and Microanalysis*, 13, 1678-1679.
- DUFFIE, J. A. & BECKMAN, W. A. 2013. *Solar engineering of thermal processes*, John Wiley & Sons.
- DUTTA, S. K., NEMA, V. K. & BHARDWAJ, R. K. 1988. Thermal-Properties of Gram. *Journal of Agricultural Engineering Research*, 39, 269-275.
- EDERY-AZULAY, L. 2010. Innowattech energy harvesting system. Harvesting energy and data, a stand alone technology. First International Symposium, The Highway to Innovation.
- EIBL, O., NIELSCH, K., PERANIO, N. AND VÖLCKLEIN, F. EDS., 2015. *Thermoelectric Bi₂Te₃ Nanomaterials*. John Wiley & Sons.
- EUGSTER, W. J. 2007. Road and bridges heating using geothermal energy. Overview and examples. *Proceedings European Geothermal Congress Unterhaching, Germany*.
- FERNANDO, W. J. N., A. L. AHMAD, S. R. ABD. SHUKOR, AND Y. H. LUK., 2008. A model for constant temperature drying rates of case hardened slices of papaya and garlic. *Journal of Food Engineering*, 88, 229–238.

Chapter 8. References

- FIP 1978. State of Art Report: Principles of thermal insulation with respect to lightweight concrete. Slough, England: Cement and Concrete Association for F.I.P.
- GARCÍA, A., BUENO, M., NORAMBUENA-CONTRERAS, J. & PARTL, M. N. 2013. Induction healing of dense asphalt concrete. *Construction and Building Materials*, 49, 1-7.
- GARCÍA, A., CASTRO-FRESNO, D., POLANCO, J. A., 2008. Evolution of penetration resistance in fresh concrete. *Cement and Concrete Research*, 38, 649-659.
- GARCIA, A., HASSN, A., CHIARELLI, A., DAWSON, A. 2015. Multivariable analysis of potential evaporation from moist asphalt mixture. *Construction and Building Materials*, 98, 80-88.
- GARCIA, A., NORAMBUENA-CONTRERAS, J., PARTL, N. 2013. Experimental evaluation of dense asphalt concrete properties for induction heating purposes. *Construction and Building Materials*, 46, 48-54.
- GARCIA, A. & PARTL, M. N. 2014. How to transform an asphalt concrete pavement into a solar turbine. *Applied Energy*, 119, 431-437.
- GONCALVES, T. D., L. PEL, AND J. D. RODRIGUES., 2009. Influence of paints on drying and salt distribution processes in porous building materials. *Construction and Building Materials*, 23, 1751-1759.
- GOSWAMI, D.Y., KREITH, F. and KREIDER, J.F., 2000. *Principles of Solar Engineering*. CRC Press
- GUI, J., GAVIN, PHELAN, P. E., KALOUSH, K. E. & GOLDEN, J. S. 2007. Impact of pavement thermophysical properties on surface temperatures. *Materials in Civil Engineering*, 19(8), 683-690.
- HAGHIGHI, E., E. SHAHRAEENI, P. LEHMANN, AND D. OR, 2013. Evaporation rates across a con-vec-tive air boundary layer are dominated by diffusion. *Water Resources Research*, 49, 1602-1610.

Chapter 8. References

- HALL, M. & ALLINSON, D. 2009. Assessing the effects of soil grading on the moisture content-dependent thermal conductivity of stabilised rammed earth materials. *Applied Thermal Engineering*, 29, 740-747.
- HALL, M. A., D. 2008. Assessing the moisture-content-dependent parameters of stabilised Earth materials using the cyclic-response admittance method. *Energy and Buildings*, 40, 2044-2051.
- HALL, M. R., DEHDEZI, P. K., DAWSON, A. R., GRENFELL, J. & ISOLA, R. 2012. Influence of the thermophysical properties of pavement materials on the evolution of temperature depth profiles in different climatic regions. *Journal of Materials in Civil Engineering*, 24, 32-47.
- HASSN, A., CHIARELLI, A., DAWSON, A. AND GARCIA, A., 2016. Thermal properties of asphalt pavements under dry and wet conditions. *Material and Design*, 91, 432-439.
- HENDEL, M., COLOMBERT, M., DIAB, Y. & ROYON, L. 2015. An analysis of pavement heat flux to optimize the water efficiency of a pavement-watering method. *Applied Thermal Engineering*, 78, 658-669.
- HERMANSSON, A. 2000. Simulation model for calculating pavement temperatures including maximum temperature. *Pavement Management and Monitoring, Transportation Research Record No. 1699*, 134-141.
- HERMANSSON, A. 2001. A Mathematical model for calculating pavement temperatures, comparisons between calculated and measured temperatures. Presented at Transportation Research Board 80 th Annual Meeting. Washington, DC, Jan.
- HERMANSSON, A. 2004. Mathematical model for paved surface summer and winter temperature: comparison of calculated and measured temperatures. *Cold Regions Science and Technology*, 40, 1-17.
- HILTON LTD, P. A. 1994. Experimental operating and maintenance manual. Thermal conductivity of building and insulating materials unit. Hampshire, P. A. Hilton Ltd.

Chapter 8. References

- HOGG, R. V. & CRAIG, A. T. 1995. Introduction to mathematical statistics.(5th edition), Upper Saddle River, New Jersey: Prentice Hall.
- THOMPSON, E., 2012. Interseasonal Heat Transfer. Energy World-Magazine of the Institute of Energy, (406), p.27
- INCROPERA, F. P., D. P. D., THEODORE L. BERGMAN & LAVINE, A. S. 2007. Fundamentals of Heat and Mass transfer. J. Wiley & sons.
- INCROPERA, F. P., LAVINE, A. S., BERGMAN, T. L. & DEWITT, D. P. 2013. Principles of heat and mass transfer. J. Wiley & sons.
- INPI 2011. Sustainable pavement for generation of electric energy from the movement of people and vehicles. Lisboa, Portugal: Instituto Nacional de Propriedade Industrial.
- JIANGBO, H., J., ZHOU, Z., 2013. Dynamics of Soil Water Evaporation during Soil Drying: Laboratory Experiment and Numerical Analysis. The Scientific World Journal, (2013), ID, 240280.
- KATUWAL, S., MOLDRUP, P., LAMANDE, M., TULLER, M. and De JONGE, L.W., 2015. Effects of CT number derived matrix density on preferential flow and transport in a macroporous agricultural soil. Vadose Zone Journal, 14(7).
- KATUWAL, S., NORGAARD, T., MOLDRUP, P., LAMANDE, M., WILDENSCHILD, D. & DE JONGE, L. W. 2015b. Linking air and water transport in intact soils to macropore characteristics inferred from X-ray computed tomography. Geoderma, 237, 9-20.
- KAZARIAN, E.A. and HALL, C.W., 1962. Thermal properties of grain (Doctoral dissertation, Michigan State University of Agriculture and Applied Science. Dept. of Agricultural Engineering).
- KIM, K.-H., JEON, S.-E., KIM., J.-K. & YANG, S. 2003. An experimental study on thermal conductivity of concrete. Cement and Concrete Research, 33(3), 363-371.
- KUVANDYKOVA, D. A. B., R., 2011. A new transient method to measure thermal conductivity of asphalt. C-Therm Technol, 2, 1-10.

Chapter 8. References

- LEHMANN, P., S. ASSOULINE, AND D. OR, 2008. Characteristic lengths affecting evaporative drying of porous media. *Physical Review E*, 77, ID, 056309.
- LEONG, W. H., TARNAWSKI, V.R., AITTOMÄKI, A. 1998. Effect of soil type and moisture content on ground heat pump performance. *International Journal of Refrigeration*, 21(8), 595-606.
- LIU, C., CHEN, P. AND LI, K., 2014. A 1 KW thermoelectric generator for low-temperature Geothermal resources. In 39th workshop on Geothermal Reservoir engineering.
- LIU, Z., PENG, C., XIANG, W., DEG, X., TIAN, D, ZHAO, M., YU, G., 2012. Simulations of runoff and evapotranspiration in Chinese fir plantation ecosystems using artificial neural net-works. *Ecological Modelling*, 226, 71-76.
- LOHMAN, S. W. 1972. Definitions of selected ground-water terms, revisions and conceptual refinements. US Govt. Print. Off.
- MALLICK, R. B., CHEN, B.-L. & BHOWMICK, S. 2009. Harvesting energy from asphalt pavements and reducing the heat island effect. *International Journal of Sustainable Engineering*, 2, 214-228.
- MALLICK, R. B., CHEN, B.-L., BHOWMICK, S. & HULEN, M. Capturing solar energy from asphalt pavements. International symposium on asphalt pavements and environment, international society for asphalt pavements, Zurich, Switzerland, 2008.
- MARSHALL, C., MEIER, R. W. & WELSH, M. 2001. Seasonal temperature effects on flexible pavements in tennessee. Presented at Transportation Research Board 80th Annual Meeting. Washington, DC, Jan.
- MARTIN, V., AUBERTIN, M., BUSSIÈRE, B. AND CHAPUIS, P.R., 2004. Evaluation of unsaturated flow in mine waste rock. In 57th Canadian Geotechnical Conference and the 5th joint CGS-IAH Conference, Canadian Geotechnical Society, 24-27.

Chapter 8. References

- MEHLING, H. & CABEZA, L. F. 2008. Heat and Cold Storage with PCM, Berlin, Springer.
- MINGYU, C., SHAOPEG, W., YUAN, Z. & HONG, W. 2010. Effects of conductive fillers on temperature distribution of asphalt pavements. *Physica Scripta*, 2010(T139), p.014046.
- MOHSENIN, N. N. 1980. Thermal properties of foods and agricultural materials. New York. USA.
- MORITA, K. and OGAWA, M., 1998. Geothermal and solar heat used to melt snow on roads. *GRC Bulletin*, 26(3), pp.83-85.
- MRAWIRA, D. M. & LUCA, J. 2002. Thermal properties and transient temperature responses of full-depth asphalt pavements. *Transportation Research Record: Journal of the Transportation Research Board*, (1809), pp.160-171.
- NOLAS, G. S., SHARP, J. & GOLDSMID, J. 2013. Thermoelectrics: basic principles and new materials developments, Springer Science & Business Media.
- NOVO, A. V., GOMEZ-ULLATE, E., BAYON, J. R., CASTRO-FRESNO, D. & RODRIGUEZ-HERNANDEZ, J. 2010. Monitoring and evaluation of thermal behaviour of permeable pavements under the northern Spain climate. *NOVATECH 2010*.
- O'FLAHERTY, C. A. 2002. Highways: The location, design, construction and maintenance of Pavements. Institution of Civil Engineering ICE.
- ONGEL, A. & HARVEY, J. 2004. Analysis of 30 years of pavement temperatures using the enhanced integrated climate model (EICM). Report, Pavement Research Centre, University of California Davis.
- PAN, P., WU, S., XIAO, Y., WANG, P. & LIU, X. 2014. Influence of graphite on the thermal characteristics and anti-ageing properties of asphalt binder. *Construction and Building Materials*, 68, 220-226.
- PARK, D., N. BUCH & CHATTI, K. 2001. Development of effective layer temperature prediction model and temperature correction using FWD

Chapter 8. References

- deflections. Presented at Transportation Research Board 80 th Annual Meeting. Washington, DC, Jan.
- PAVEGEN 2012. Pavegen systems-generating energy from footsteps. Pavegen Systems Ltd, UK.
- PAVEMENT-RESEARCH 2002. Albedo: A measure of pavement surface reflectance. American Concrete Pavement Association, 3.05.
- PERINI, K., OTTELÉ, M., FRAAIJ, E.M. H. A.L.A., RAITERI, R., 2011. Vertical greening systems and the effect on air flow and temperature on the building envelope. *Building and Environment*, 46, 2287-2294.
- PETH, S., HORN, R., BECKMANN, F., DONATH, T., FISCHER, J. AND SMUCKER, A.J.M., 2008. Three-Dimensional Quantification of Intra-Aggregate Pore-Space Features using Synchrotron-Radiation-Based Microtomography. *Soil Science Society of America Journal*, 72, 897-907.
- PHILLIPPS, P. 2007. Optimising pavement materials to collect the solar energy by asphalt. MSc dissertation, University of Nottingham.
- POWELL, R., HO, C. Y. & LILEY, P. E. 1966. Thermal conductivity of selected materials. DTIC Document.
- PTB. 2010. Comparing emissivity evaluation methods for infrared sources. [Online]. [Accessed].
- READ, J. & WHITEOAK, D. 2003. *The Shell Bitumen Handbook* London, Thomas Telford Publishing.
- RETSCREEN 2005. Clean Energy Project Analysis.
- ROWE, D. M. 1995. *CRC handbook of thermoelectrics*, CRC press.
- RUSSELL, R. 2007. Solar energy in Earth's atmosphere [Online]. [Accessed http://www.windows2universe.org/earth/Atmosphere/earth_atmosph_radiation_budget.html].
- SALVUCCI, G. D. 1997. Soil and moisture independent estimation of stage two evaporation from potential evaporation and albedo or surface temperature. *Water Resources Research*, 33(1), 111–122.

Chapter 8. References

- SHAKOURI, A. 2011. Recent developments in semiconductor thermoelectric physics and materials. 41, 399.
- SHAOPENG, W., MINGYU, C. & JIZHE, Z. 2011. Laboratory investigation into thermal response of asphalt pavements as solar collector by application of small-scale slabs. *Applied Thermal Engineering*, 31, 1582-1587.
- SHE, H. Y., SLEEP, E., B., 1998. The effect of temperature on capillary pressure-saturation relationships for air-water and perchloroethylene-water systems. *Water Resources Research*, 34(10), 2587-2597.
- SHOKRI, N., LEHMANN, P. & OR, D. 2008. Effects of hydrophobic layers on evaporation from porous media. *Geophysical Research Letters*, 35 (19).
- SHOKRI, N., LEHMANN, P. & OR, D. 2009. Characteristics of evaporation from partially wettable porous media. *Water Resources Research*, 45(2).
- SHOKRI, N., LEHMANN, P. & OR, D. 2009. Critical evaluation of enhancement factors for vapor transport through unsaturated porous media. *Water Resources Research*, 45(10).
- SHOKRI, N., LEHMANN, P. & OR, D. 2010. Evaporation from layered porous media. *Journal of Geophysical Research: Solid Earth*, 115(B6).
- SHOKRI, N. & OR, D. 2011. What determines drying rates at the onset of diffusion controlled stage-2 evaporation from porous media?. *Water Resources Research*, 47(9).
- SHORT, A. & KINNIBURG, W. 1978. *Lightweight concrete*. Great Britain: Galliard, Great Yarmouth.
- SNYDER, G. 2006. Thermoelectric power generation: efficiency and compatibility. *Thermoelectrics Handbook: Macro to Nano*, 9.1-9.26.
- SNYDER, G. J. 2008. Small thermoelectric generators. *The Electrochemical Society Interface*, , 54-56. doi: [http](http://).
- SOLAIMANIAN, M. & KENNEDY, T. W. 1993. Predicting maximum pavement surface temperature using maximum air temperature and hourly solar radiation. *Journal of the Transportation Research Board*, 1417, 1-11.

Chapter 8. References

- SOMERTON, W. H. 1992. Thermal properties and temperature-related behavior of rock/fluid systems, Elsevier.
- SR 2012. Solar Roadways. See <http://www.solarroadways.com/main.html> (accessed 04/05/2014).
- STEMPIHAR, J. J., POURSHAMS-MANZOURI, T., KALOUSH, K. E. & RODEZNO, M. C. 2012. Porous Asphalt Pavement Temperature Effects for Urban Heat Island Analysis. *Transportation Research Record*, 2293, 123-130.
- STEPHENS, R. B., CODY G.D. 1977. Optical reflectance and transmission of a textured surface. *Thin Solid Films*, 45(1), pp.19-29.
- SULLIVAN, C., BONDT, A. H. D., JANSEN, R. & VERWEIJMEREN, H. 2007. *Innovation in the production and commercial use of energy extracted from asphalt pavements*. 6th Annual International Conference on Sustainable Aggregates, Asphalt Technology and Pavement Engineering. Liverpool.
- SUNDBERG, J. 1988. Thermal properties of soils and rocks. Research Gate.
- TAKEBAYASI, H., MORIYAMA, M., 2012. Study on surface heat budget of various pavements for urban heat island mitigation. *Advances in Materials Science and Engineering*, 2012, ID, 523051.
- THE ENGINEERING TOOLBOX <http://www.engineeringtoolbox.com/>.
- THOM, N. 2008. *Principle of pavement engineering*., London, Thomas Telford Publishing.
- TRAFIKVERKET Database. Available from:
<http://www.trafikverket.se/>
- UYSAL, H., DEMIRBOGA, R., SAHIN, R. & GUL, R. 2004. The effects of different cement dosages, slumps, and pumice aggregate ratios on the thermal conductivity and density of concrete. *Cement and Concrete Research*, 34, 845-848.

Chapter 8. References

- VAN DER ZWAN, J. T., GOEMAN, T., GRUIS, H., SWART, J. & OLDENBURGER, R. 1990. Porous asphalt wearing courses in the Netherlands: State of the art review. *Transportation Research Record*.
- VOGEL, H.J., 1997. Morphological determination of pore connectivity as a function of pore size using serial sections. *European Journal of Soil Science*, 48(3), pp.365-377.
- VOGEL, H. J., ROTH, K., 2001. Quantitative morphology and network representation of soil pore structure. *Advances in Water Resources*, 24, 233-243.
- VORHAUER, N., T. METZGER, AND E. TSOTSAS., 2010. Empirical macroscopic model for drying of porous media based on pore networks and scaling theory. *Drying Technology*, 28, 991–1000.
- VOSTEEN, H.-D. & SCHELLSCHMIDT, R. 2003. Influence of temperature on thermal conductivity, thermal capacity and thermal diffusivity for different types of rock. *Physics and Chemistry of the Earth, Parts A/B/C*, 28, 499-509.
- WALUBITA, L. F., JAMISON, B., ALVAREZ, A.E., HU, X., MUSHOTA, C., (2012), 54, 1, . 2012. Air void characterisation of HMA gyratory laboratory-moulded samples and field cores using X-ray computed tomography (X-ray CT). *Journal of the South African Institution of Civil Engineering*, 54, 22-30.
- WANG, H., WU, S., CHEN, M. and ZHANG, Y., 2010. Numerical simulation on the thermal response of heat-conducting asphalt pavements. *Physical Script*, 2010(T139), p.014041.
- WAYDIP. 2012. Waynergy, Waydip – Energia e Ambiente, Lda, Covilha, Portugal, see <http://www.waydip.com/>(accessed 01/11/2015).
- WIPO. 2011. Pavement module for generating electric energy from the movement of people and vehicles [Online]. Geneva, Switzerland. Accessed online See:
<http://www.wipo.int/patentscope/search/en/WO2011145057> (accessed

Chapter 8. References

04/04/2014).

- WONG, N. H., Y. CHEN 2009. Tropical urban heat islands. Taylor & Francis, Abingdon, UK.
- WORLD-CLIMATE-MAP. 2007. Also available online at: <http://www.climate-charts.com/World-Climate-Maps.html> [Online]. [Accessed].
- WU, K. R., CHEN, B., YAO, W. & ZHANG, D. 2001. Effect of coarse aggregate type on mechanical properties of high-performance concrete. *Cement and Concrete Research*, 31, 1421-1425.
- XU, Y. & CHUNG, D. D. L. 2000. Effect of sand addition on the specific heat and thermal conductivity of cement. *Cement and Concrete Research*, 30(1), 59-61.
- YAMANAKA, T., A. TAKEDA, AND J. SHIMADA, 1998. Evaporation beneath the soil surface: some observational evidence and numerical experiments. *Hydrological Processes*, 12, 2193– 2203.
- YAVUZTURK, C., KSAIBATI K. and CHIASSON, A.D., 2005. Assessment of temperature fluctuations in asphalt pavement due to thermal environmental conditions using a two-dimensional-transient finite difference approach. *Journal of Materials in Civil Engineering*, 17(4), pp.465-475.
- YIOTIS, A. G., TSIMPANOGLIANNIS, I.N., STUBOS, A.K. AND YORTSOS, Y.C., 2006. Pore-network study of the characteristic periods in the drying of porous materials. *Journal of Colloid and Interface Science*, 297, 738–748.
- ZHENG, X. F., LIU, C.X., YAN, Y.Y. AND WANG, Q., 2014. A review of thermoelectrics research-Recent developments and potentials for sustainable and renewable energy applications. *Renewable and Sustainable Energy Reviews*, 32, 486-503.

9. Appendix A

BSEN 12697-5: 2009 Procedure C: Mathematical procedure

Aggregate Size	NTEC Sample ID	Percentage in mix %	Particle density of aggregate
		0	1.000
20mm	20	19.06	2.690
14mm	20	19.06	2.680
10mm	15	14.30	2.720
6mm	15	14.30	2.700
dust	30	28.59	2.660
filler	0	0.00	2.720
Bitumen	4.7	4.70	1.030
		100	
MAX DENSITY Pmc (Mg/m3)=	2.496		

14-895	
Target Air Voids	10 %
Maximum Density	2505 kg/m³
Target Density	2255 kg/m³
Asphalt Grade	pen 50
Binder Content	4.5 %
Volume of Mould	0.0046818 m³
Sample Type e.g. Slab/Gyro	Slab
No. of Samples	(Less than 25 kg) 5

Scaling factor to take into account mass loss on coating mixer: 1.005

Aggregate Size	Mass %	Mass (g)	Scaled up mass (g)	Mass for all samples (kg)
28 mm	-	0	0	0.000
20 mm	20.0	2016	2027	10.135
14 mm	23.0	2319	2331	11.655
10 mm	20.0	2016	2027	10.135
6.3 mm	11.0	1109	1115	5.575
Dust	26.0	2621	2635	13.175
Filler	0.0	0	0	0.000
Sum	100.0	10081	10135	50.675
Binder pen		475	477	2.385
Total Mass		10557	10610	

Total -binder mass

10082.000

Scaled up total -binder mass

10133

Designer	Abdudhsafi Hassn
Purpose	PhD
Project Name	Pavement Energy Harvesting
Date	08/04/2014
Requests	

BSEN 12697-5: 2009 Procedure C: Mathematical procedure

Aggregate Size	NTEC Sample ID	Percentage in mix %	Particle density of aggregate
		0	1.000
20mm	20	19.1	2.690
14mm	23	21.97	2.680
10mm	20	19.10	2.720
6mm	11	10.51	2.700
dust	26	24.83	2.660
filler	0	0.00	2.720
Bitumen	4.5	4.50	1.030
		100	
MAX DENSITY Pmc (Mg/m3)=	2.505		

14-900	
Target Air Voids	13 %
Maximum Density	2519 kg/m ³
Target Density	2192 kg/m ³
Asphalt Grade	pen 50
Binder Content	4.2 %
Volume of Mould	0.0046818 m ³
Sample Type e.g. Slab/Gyro	Slab
No. of Samples	(Less than 25 kg) 5

Scaling factor to take into account mass loss on coating mixer: 1.005

Aggregate Size	Mass %	Mass (g)	Scaled up mass (g)	Mass for all samples (kg)
28 mm	-	0	0	0.000
20 mm	20.0	1966	1976	9.880
14 mm	25.0	2458	2470	12.350
10 mm	26.0	2556	2569	12.845
6.3 mm	7.0	688	692	3.460
Dust	22.0	2163	2174	10.870
Filler	0.0	0	0	0.000
Sum	100.0	9831	9881	49.405
Binder pen		431	433	2.165
Total Mass		10263	10314	

Total -binder mass

9832.000

Scaled up total -binder mass

9881

Designer	Abdudhsafi Hassn
Purpose	PhD
Project Name	Pavement Energy Harvesting
Date	08/04/2014
Requests	

BSEN 12697-5: 2009 Procedure C: Mathematical procedure

Aggregate Size	NTEC Sample ID	Percentage in mix %	Particle density of aggregate
		0	1.000
20mm	20	19.16	2.690
14mm	25	23.95	2.680
10mm	26	24.91	2.720
6mm	7	6.71	2.700
dust	22	21.08	2.660
filler	0	0.00	2.720
Bitumen	4.2	4.20	1.030
		100	
MAX DENSITY Pmc (Mg/m3)=	2.519		

14-905	
Target Air Voids	17 %
Maximum Density	2534 kg/m ³
Target Density	2103 kg/m ³
Asphalt Grade	pen 50
Binder Content	3.8 %
Volume of Mould	0.0046818 m ³
Sample Type e.g. Slab/Gyro	Slab
No. of Samples	(Less than 25 kg) 5

Scaling factor to take into account mass loss on coating mixer: 1.005

Aggregate Size	Mass %	Mass (g)	Scaled up mass (g)	Mass for all samples (kg)
28 mm	-	0	0	0.000
20 mm	20.0	1894	1904	9.520
14 mm	31.0	2936	2951	14.755
10 mm	25.0	2368	2380	11.900
6.3 mm	5.0	474	476	2.380
Dust	19.0	1800	1809	9.045
Filler	0.0	0	0	0.000
Sum	100.0	9472	9520	47.600
Binder pen		374	376	1.880
Total Mass		9846	9895	

Total -binder mass

9472.000

Scaled up total -binder mass

9519

Designer	Abdudhsafi Hassn
Purpose	PhD
Project Name	Pavement Energy Harvesting
Date	08/04/2014
Requests	

BSEN 12697-5: 2009 Procedure C: Mathematical procedure

Aggregate Size	NTEC Sample ID	Percentage in mix %	Particle density of aggregate
		0	1.000
20mm	20	19.24	2.690
14mm	31	29.82	2.680
10mm	25	24.05	2.720
6mm	5	4.81	2.700
dust	19	18.28	2.660
filler	0	0.00	2.720
Bitumen	3.8	3.80	1.030
		100	
MAX DENSITY Pmc (Mg/m3)=	2.534		

Target Air Voids	23 %
Maximum Density	2552 kg/m³
Target Density	1965 kg/m³
Asphalt Grade	pen 50
Binder Content	3.3 %
Volume of Mould	0.0046818 m³
Sample Type e.g. Slab/Gyro	Slab
No. of Samples	(Less than 25 kg) 5

Scaling factor to take into account mass loss on coating mixer: 1.005

Aggregate Size	Mass %	Mass (g)	Scaled up mass (g)	Mass for all samples (kg)
28 mm	-	0	0	0.000
20 mm	20.0	1779	1788	8.940
14 mm	47.0	4181	4202	21.010
10 mm	20.0	1779	1788	8.940
6.3 mm	0.0	0	0	0.000
Dust	13.0	1156	1162	5.810
Filler	0.0	0	0	0.000
Sum	100.0	8895	8940	44.700
Binder pen		304	305	1.525
Total Mass		9200	9246	

Total -binder mass

8896.000

Scaled up total -binder mass

8941

Designer	Abdudhsafi Hassn
Purpose	PhD
Project Name	Pavement Energy Harvesting
Date	08/04/2014
Requests	

BSEN 12697-5: 2009 Procedure C: Mathematical procedure

Aggregate Size	NTEC Sample ID	Percentage in mix %	Particle density of aggregate
		0	1.000
20mm	20	19.34	2.690
14mm	47	45.45	2.680
10mm	20	19.34	2.720
6mm	0	0.00	2.700
dust	13	12.57	2.660
filler	0	0.00	2.720
Bitumen	3.3	3.30	1.030
		100	
MAX DENSITY Pmc (Mg/m3)=	2.552		

14-770-917

Target Air Voids	26 %
Maximum Density	2553 kg/m3
Target Density	1889 kg/m3
Asphalt Grade	pen 50
Binder Content	3.2 %
Volume of Mould	0.0046818 m³
Sample Type e.g. Slab/Gyro	Slab
No. of Samples	(Less than 25 kg) 5

Scaling factor to take into account mass loss on coating mixer: 1.005

Aggregate Size	Mass %	Mass (g)	Scaled up mass (g)	Mass for all samples (kg)
28 mm	-	0	0	0.000
20 mm	20.0	1712	1721	8.605
14 mm	60.0	5137	5162	25.810
10 mm	10.0	856	860	4.300
6.3 mm	0.0	0	0	0.000
Dust	10.0	856	860	4.300
Filler		0	0	0.000
Sum	100.0	8561	8603	43.015
Binder pen		283	284	1.420
Total Mass		8844	8888	

Total -binder mass

8561.000

Scaled up total -binder mass

8604

Designer	Abdudhsafi Hassn
Purpose	PhD
Project Name	Pavement Energy Harvesting
Date	08/04/2014
Requests	

BSEN 12697-5: 2009 Procedure C: Mathematical procedure

Aggregate Size	NTEC Sample ID	Percentage in mix %	Particle density of aggregate
		0	1.000
20mm	20	19.36	2.690
14mm	60	58.08	2.680
10mm	10	9.68	2.720
6mm	0	0.00	2.700
dust	10	9.68	2.660
filler	0	0.00	2.720
Bitumen	3.2	3.20	1.030
		100	
MAX DENSITY Pmc (Mg/m3)=	2.553		

	28mm 13-1455	20mm 13-1456	14mm 14-187	10mm 13-1458	6mm 13-1459	Dust
63.0	100	100	100	100	100	100
40.0	100	100	100	100	100	100
31.5	99.3	100	100	100	100	100
20.0	25.41	95.63	100	100	100	100
16.0	4.18	56.93	99.5	100	100	100
14.0	2.72	29.28	87.34	100	100	100
10.0	2.45	6.27	12.51	88.66	100	100
8.0	2.27	4.71	3.27	50.33	99.9	100
6.3	2.17	4.26	2.18	14.09	96.12	100
4.0	1.97	3.69	1.76	2.82	32.21	93.38
2.800	1.86	3.18	1.71	2.46	8.27	87.1
2.000	1.73	2.77	1.65	2.25	4.59	72.75
1.000	1.51	2.34	1.53	2.03	3.56	51.49
0.500	1.34	2.08	1.44	1.92	3.32	38.09
0.250	1.19	2.02	1.38	1.81	3.22	29.48
0.125	1.04	1.78	1.3	1.69	3.13	22.83
0.063	0.88	1.65	1.2	1.52	2.94	17.47
Rec	0.02	-0.01	-0.02	0	0.03	0.03

Dense Specimen 1st Mixture

		1st mixture. Objective (5%)	
28	0	63.0	100
20	20	40.0	100
14	20	31.5	100
10	15	20.0	99.126
6	15	16.0	91.286
Dust	30	14.0	83.324
		10.0	62.055
	100	8.0	54.1305
		6.3	47.8195
		4.0	34.3585
		2.800	28.7175
		2.000	23.735
		1.000	17.0595
		0.500	12.917
		0.250	10.2785
		0.125	8.188
Filler		0.063	6.48

10% Air Voids Targeted 4th Mixture

		4rd mixture. Objective (10%)	
28	0	63	100
20	20	40	100
14	23	31.5	100
10	20	20	99.126
6	11	16	91.271
Dust		26	82.9442
		10	58.8633
	100	8	48.7491
		6.3	40.7446
		4	29.5287
		2.8	25.077
		2	20.8034
		1	15.0049
		0.5	11.3998
		0.25	9.1024
		0.125	7.2731
Filler		0.063	5.7756

Porous Specimen 2nd Mixture

		2nd mixture. Objective (21%)	
28	0	63.0	100
20	10	40.0	100
14	38	31.5	100
10	35	20.0	99.563
6	0	16.0	95.503
Dust	17	14.0	88.1172
		10.0	53.4118
	100	8.0	36.3291
		6.3	23.1859
		4.0	17.8994
		2.800	16.6358
		2.000	14.059
		1.000	10.2792
		0.500	7.9025
		0.250	6.3715
		0.125	5.1446
Filler		0.063	4.1229

13% Air Voids Targeted 5th Mixture

		5th mixture. Objective (13%)	
28	0	63	100
20	20	40	100
14	25	31.5	100
10	26	20	99.126
6	7	16	91.261
Dust		22	82.691
		10	56.4331
	100	8	43.8383
		6.3	33.7888
		4	24.7095
		2.8	21.444
		2	17.8778
		1	12.9553
		0.5	9.8874
		0.25	7.9306
		0.125	6.3621
Filler		0.063	5.0744

Super Porous Specimen 3rd Mixture

		3rd mixture. Objective (26%)	
28	0	63.0	100
20	20	40.0	100
14	60	31.5	100
10	10	20.0	99.126
6	0	16.0	91.086
Dust	10	14.0	78.26
		10.0	27.626
	100	8.0	17.937
		6.3	13.569
		4.0	11.414
		2.800	10.618
		2.000	9.044
		1.000	6.738
		0.500	5.281
		0.250	4.361
		0.125	3.588
Filler		0.063	2.949

17% Air Voids Targeted 6th Mixture

		6th mixture. Objective (17%)	
28	0	63	100
20	20	40	100
14	31	31.5	100
10	25	20	99.126
6	5	16	91.231
Dust		19	81.9314
		10	51.2971
	100	8	38.5332
		6.3	28.8563
		4	21.3413
		2.8	18.7436
		2	15.68
		1	11.4109
		0.5	8.7455
		0.25	7.0465
		0.125	5.6757
Filler		0.063	4.5483

10. Appendix B



MFG Part Number : GM250-127-14-10

A thermoelectric power generating (TEG) module is one kind of power generating device which uses the Seebeck Effect in order to convert heat into electricity directly.

Characteristics:

- Compact structure (no moving parts)
- Reliable performance
- Maintenance-free
- Noise-free operation
- Low-carbon as it is a "green" technology

The selection of the heat source of the TEG is extensive. It is capable of generating DC electricity continuously as long as there is a temperature difference applied at the two sides of the module.

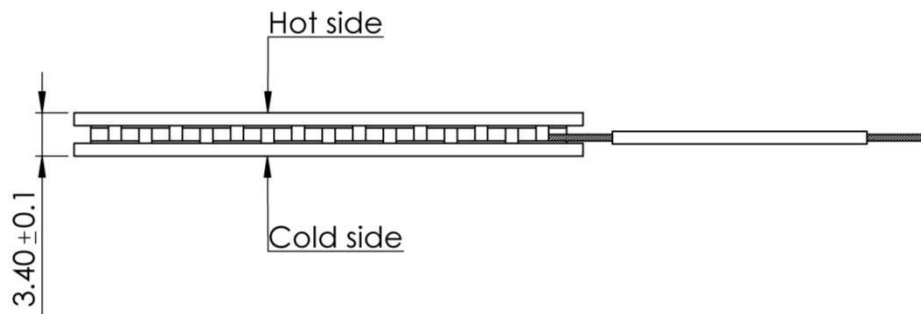
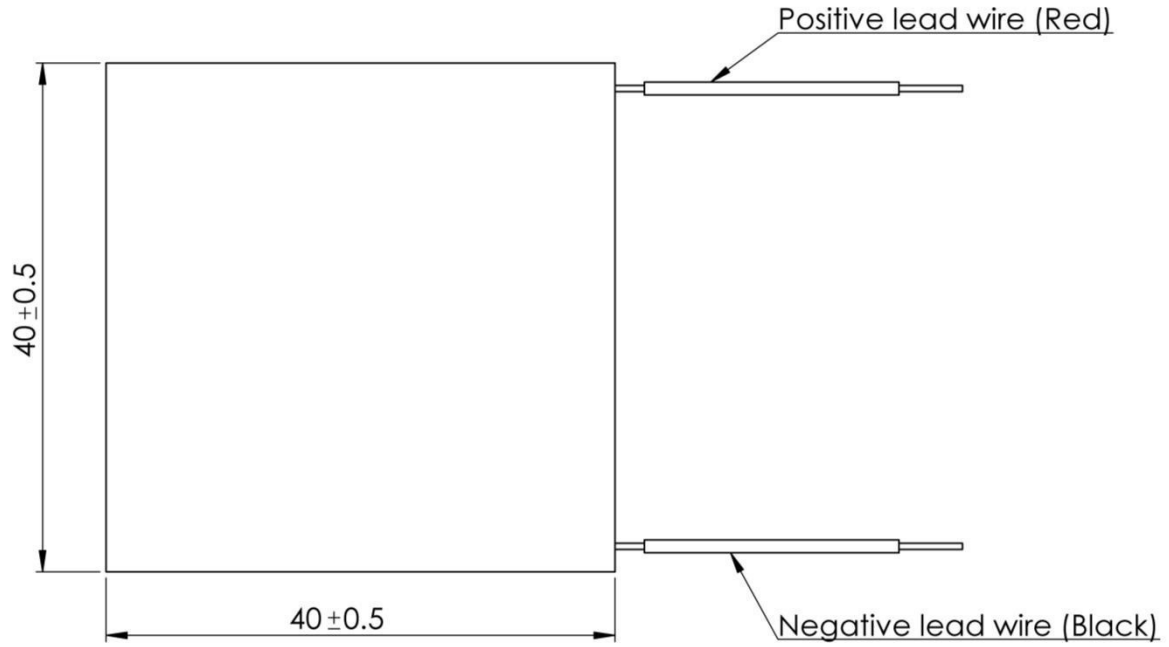
Except for the thermoelectric material, another important factor which affects the generating capacity and the conversion efficiency of the TEG module is the temperature difference. Increasing the temperature difference between the two sides of the module (the hot side and the cold side), increases both the generating capacity and hence the conversion efficiency of the module.

Performance Parameters

Parameters for Hot Side Temp 250°C and Cold Side 30°C	
Matched Load Output Power	11.6W
Matched Load Resistance	1.38Ω ± 15%
Open Circuit Voltage	8.0V
Matched Load Output Current	2.9A
Matched Load Output Voltage	4.0V
Heat Flow Through Module	~232W
Maximum. Compress. (non destructive)	1MPa
Max Operation Temperature	Hot side : 250°C
	Cold side: 175°C



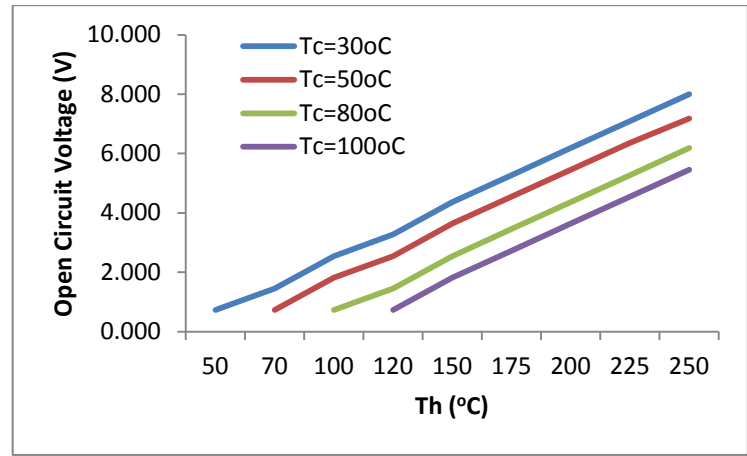
Dimensions: *Drawing



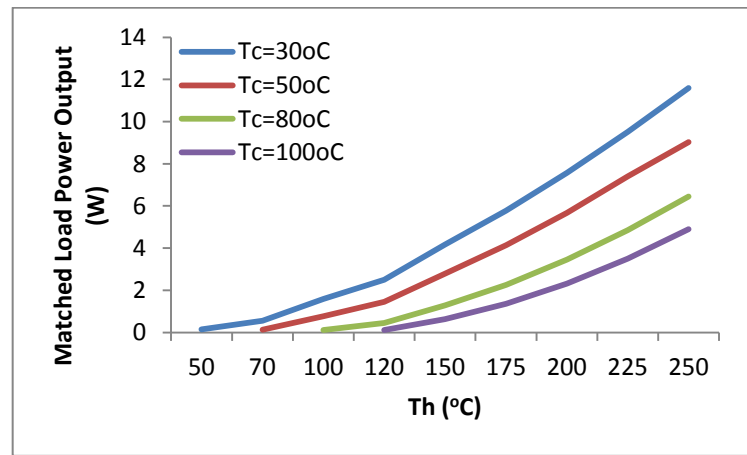


Performance Graphs:

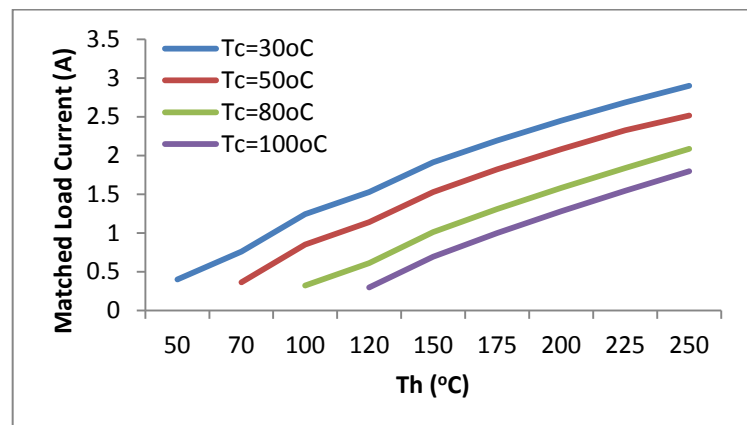
Graph indicating Open circuit voltage v. Hot side temperature with various fixed cold sides



Matched Load Output Power v. Hot side temperature for various fixed cold sides

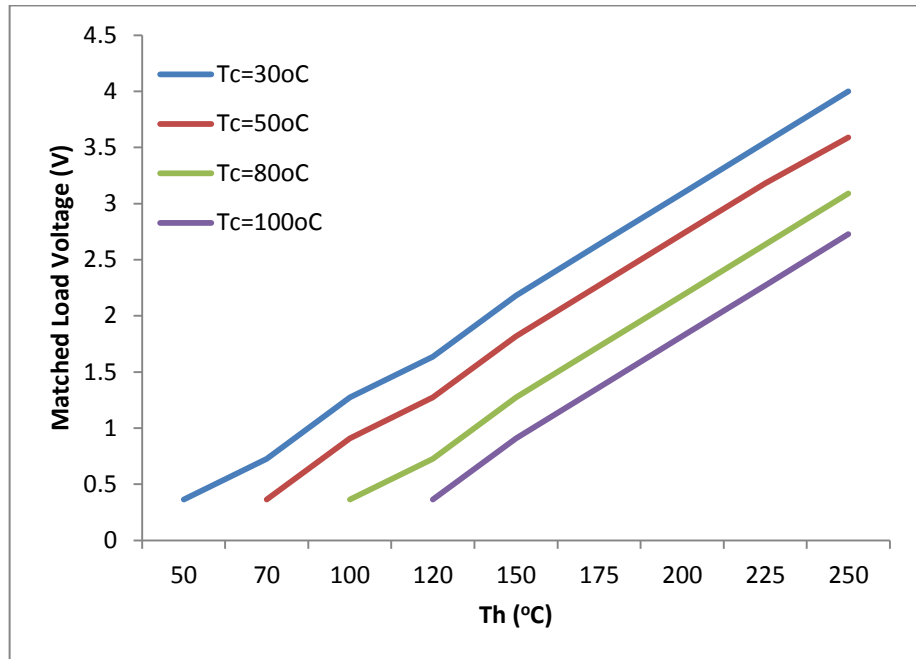


Matched Load Current v. Hot side temperature for various fixed cold sides





Matched Load Output Voltage v Hot side for various fixed cold sides



Matched Load Resistance v. Hot side for various fixed cold sides

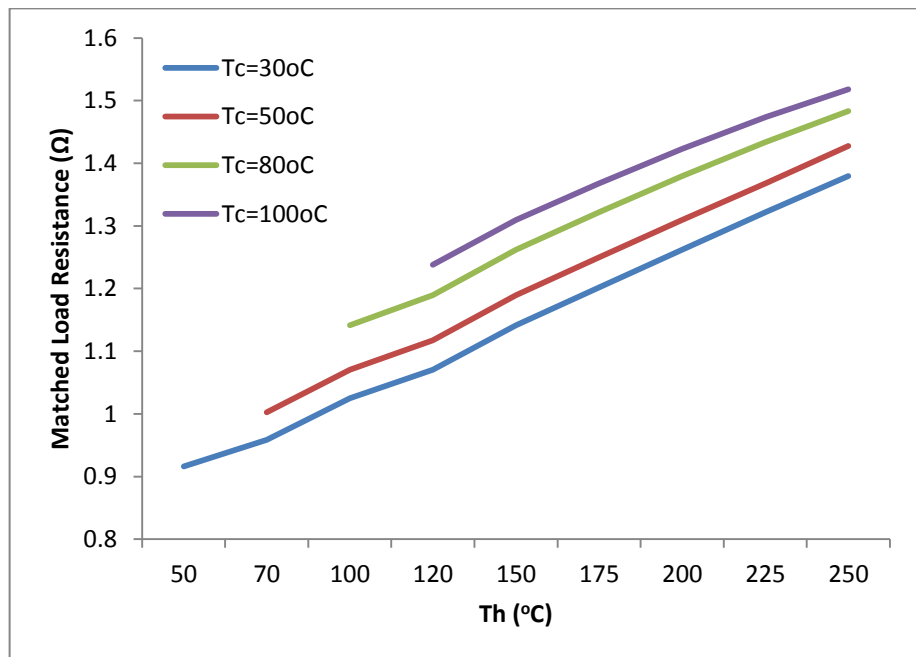
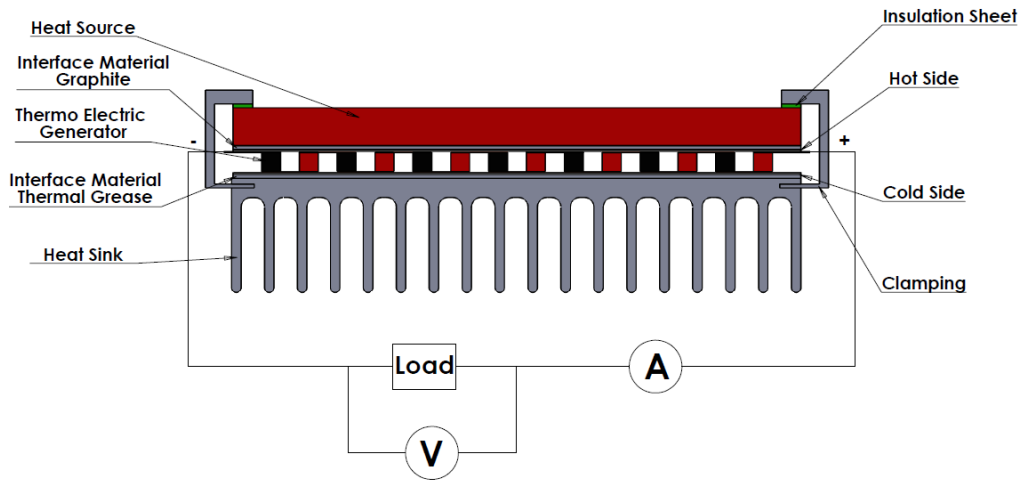




Diagram:



Formulae for calculating Thermoelectric Properties (Best Fit derived from measured material characteristics)

- Thermal conductivity

$$k_n = (0.0000334545 \times T^2 - 0.023350303 \times T + 5.606333) \frac{W}{mK}$$

$$k_p = (0.0000361558 \times T^2 - 0.026351342 \times T + 6.22162) W/mK$$

- Seebeck Coefficient

$$\alpha_n = (0.001530736 \times T^2 - 1.08058874 \times T - 28.338095) \times 10^{-6} \frac{V}{K}$$

$$\alpha_p = (-0.003638095 \times T^2 + 2.74380952 \times T - 296.214286) \times 10^{-6} \frac{V}{K}$$

- Electrical Conductivity

$$\sigma_p = (0.015601732 \times T^2 - 15.708052 \times T + 4466.38095) \times 10^2 S/m$$

$$\sigma_n = (0.01057143 \times T^2 - 10.16048 \times T + 3113.71429) \times 10^2 S/m$$

where the subscript n refers to the n-type thermoelement and the subscript p refers to the p-type thermoelement. It should be noted here that the electrical conductivity relates to the electrical resistivity as follows: $\rho = \frac{1}{\sigma}$

thus, where electrical resistivity is needed, one can calculate first the electrical conductivity through the aforementioned formulae and then reverse to calculate the electrical resistivity.



Scope

This specification is applied to thermoelectric generation module supplied under the European Thermodynamics brand.

Revision of these specifications may occur without consultation or notification, Issue number and date will be revised.



MFG Part Number : GM250-241-10-16

A thermoelectric power generating (TEG) module is one kind of power generating device which uses the Seebeck Effect in order to convert heat into electricity directly.

Characteristics:

- Compact structure (no moving parts)
- Reliable performance
- Maintenance-free
- Noise-free operation
- Low-carbon as it is a "green" technology

The selection of the heat source of the TEG is extensive. It is capable of generating DC electricity continuously as long as there is a temperature difference applied at the two sides of the module.

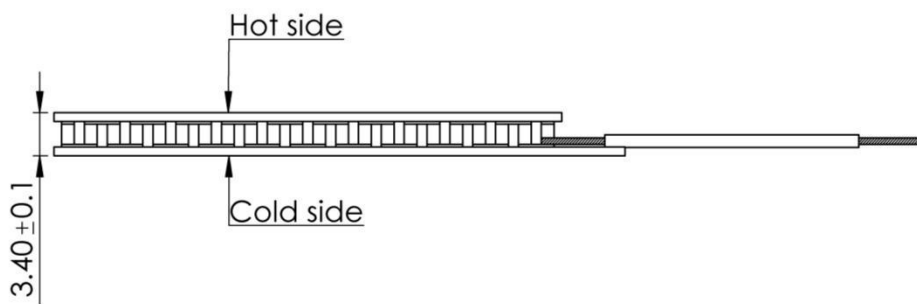
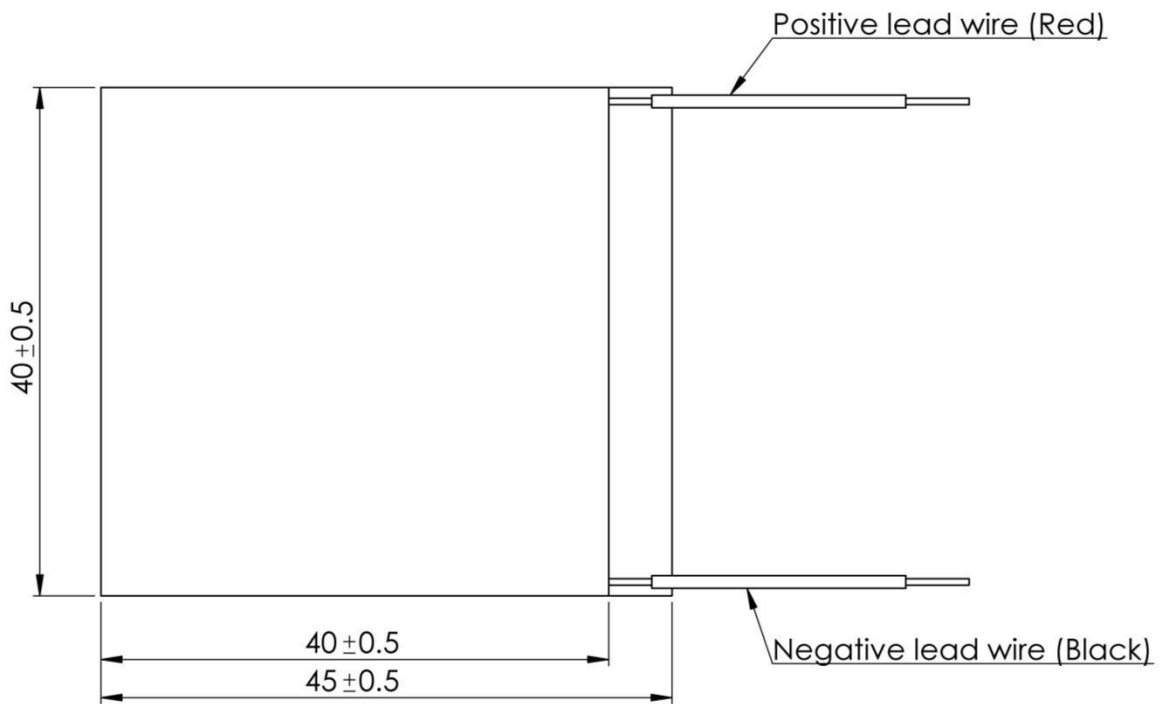
Except for the thermoelectric material, another important factor which affects the generating capacity and the conversion efficiency of the TEG module is the temperature difference. Increasing the temperature difference between the two sides of the module (the hot side and the cold side), increases both the generating capacity and hence the conversion efficiency of the module.

Performance Parameters

Parameters for Hot Side Temp 250°C and Cold Side 30°C	
Matched Load Output Power	9.1W
Matched Load Resistance	9.5Ω ± 15%
Open Circuit Voltage	18.6V
Matched Load Output Current	1.0A
Matched Load Output Voltage	9.3V
Heat Flow Through Module	~182W
Maximum. Compress. (non destructive)	1MPa
Max Operation Temperature	Hot side : 250°C
	Cold side: 175°C



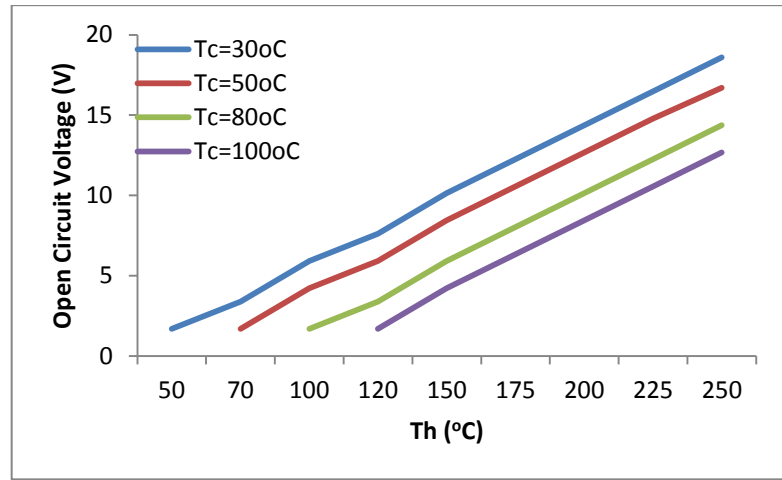
Dimensions: *Drawing



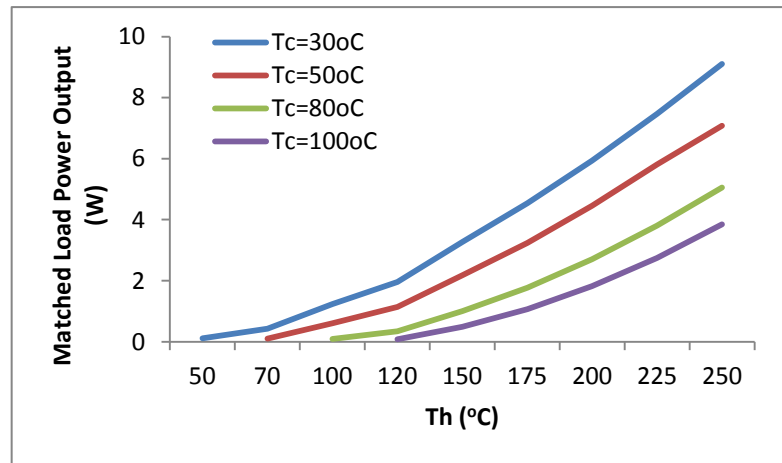


Performance Graphs:

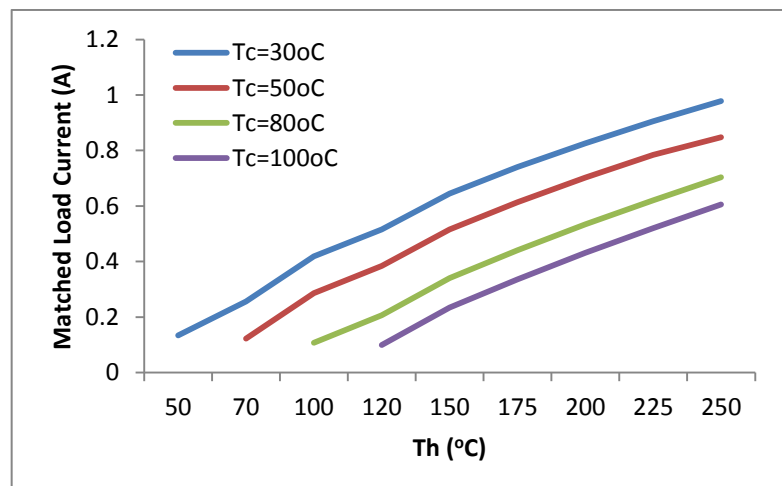
Graph indicating Open circuit voltage v. Hot side temperature with various fixed cold sides



Matched Load Output Power v. Hot side temperature for various fixed cold sides

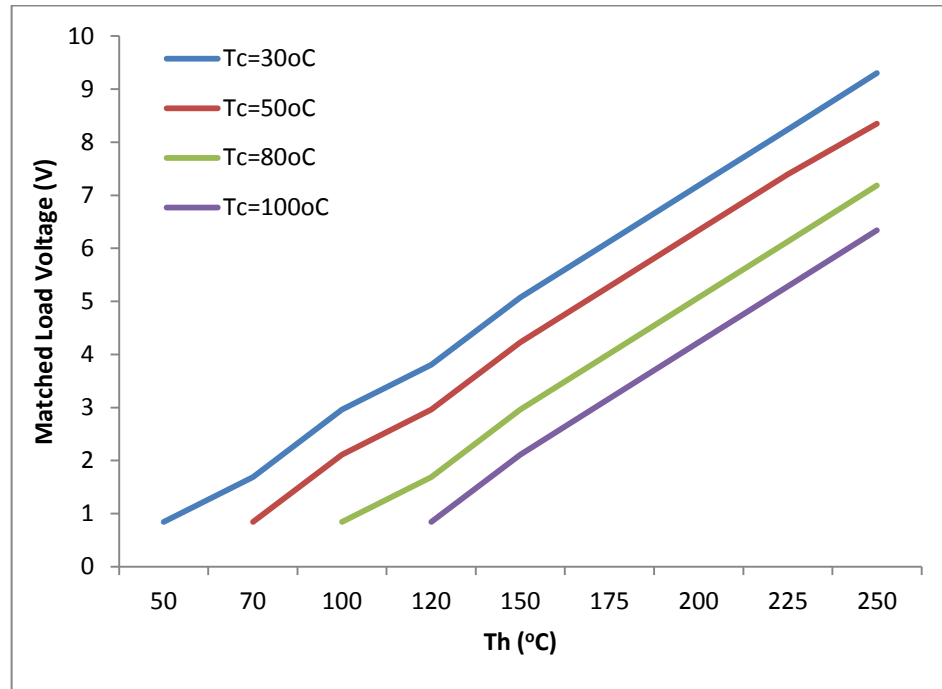


Matched Load Current v. Hot side temperature for various fixed cold sides





Matched Load Output Voltage v Hot side for various fixed cold sides



Matched Load Resistance v. Hot side for various fixed cold sides

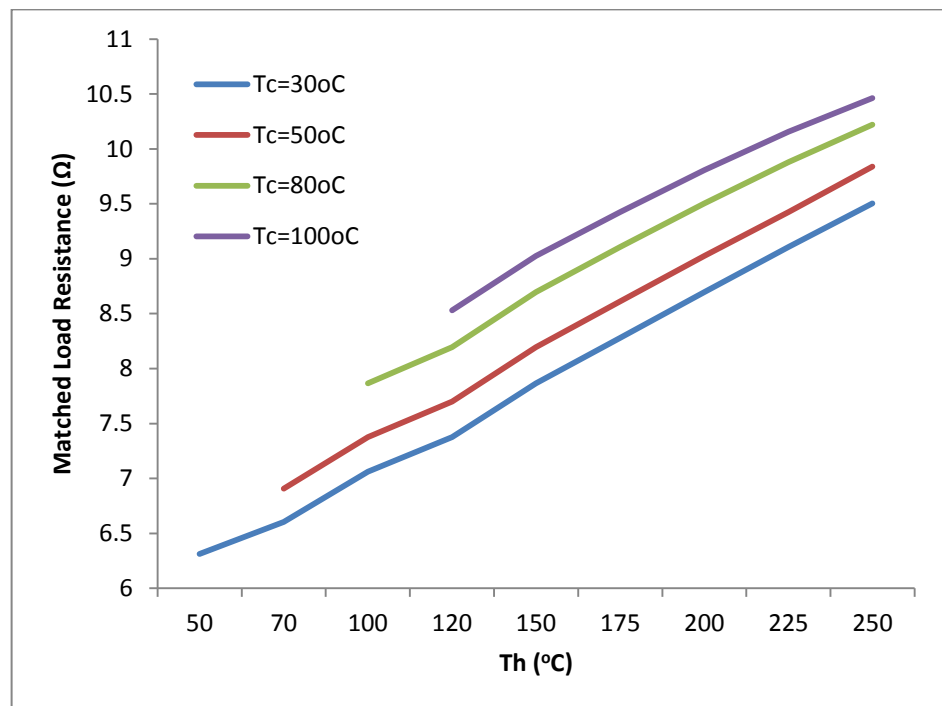
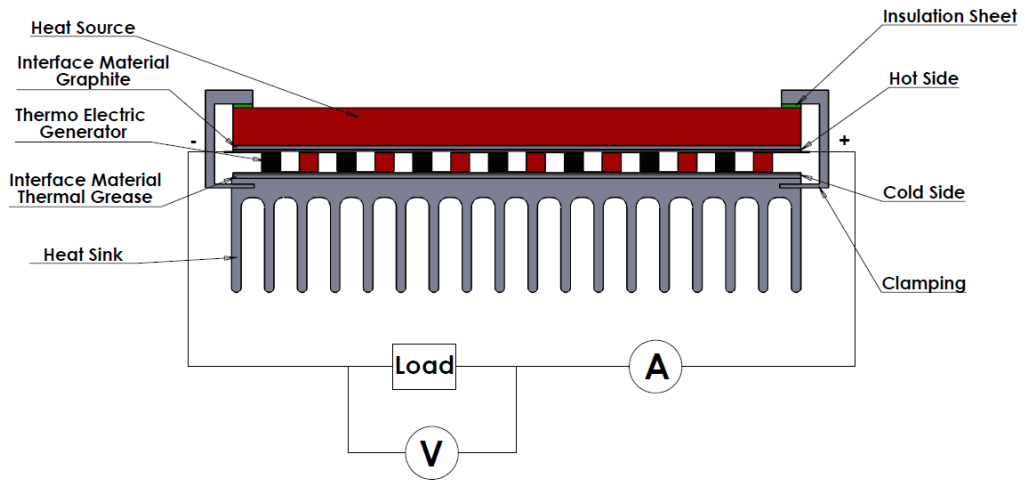




Diagram:



Formulae for calculating Thermoelectric Properties (Best Fit derived from measured material characteristics)

- Thermal conductivity

$$k_n = (0.0000334545 \times T^2 - 0.023350303 \times T + 5.606333) \frac{W}{mK}$$

$$k_p = (0.0000361558 \times T^2 - 0.026351342 \times T + 6.22162) W/mK$$

- Seebeck Coefficient

$$\alpha_n = (0.001530736 \times T^2 - 1.08058874 \times T - 28.338095) \times 10^{-6} \frac{V}{K}$$

$$\alpha_p = (-0.003638095 \times T^2 + 2.74380952 \times T - 296.214286) \times 10^{-6} \frac{V}{K}$$

- Electrical Conductivity

$$\sigma_p = (0.015601732 \times T^2 - 15.708052 \times T + 4466.38095) \times 10^2 S/m$$

$$\sigma_n = (0.01057143 \times T^2 - 10.16048 \times T + 3113.71429) \times 10^2 S/m$$

where the subscript n refers to the n-type thermoelement and the subscript p refers to the p-type thermoelement. It should be noted here that the electrical conductivity relates to the electrical resistivity as follows: $\rho = \frac{1}{\sigma}$

thus, where electrical resistivity is needed, one can calculate first the electrical conductivity through the aforementioned formulae and then reverse to calculate the electrical resistivity.



Scope

This specification is applied to thermoelectric generation module supplied under the European Thermodynamics brand.

Revision of these specifications may occur without consultation or notification, Issue number and date will be revised.